



VCU

Virginia Commonwealth University
VCU Scholars Compass

Theses and Dissertations


Graduate School

2019

Designing Biomimetic Implant Surfaces to Promote Osseointegration under Osteoporotic Conditions by Revitalizing Mechanisms Coupling Bone Resorption to Formation

Ethan M. Lotz
Virginia Commonwealth University

Follow this and additional works at: <https://scholarscompass.vcu.edu/etd>

 Part of the [Biomaterials Commons](#), [Dental Materials Commons](#), and the [Molecular, Cellular, and Tissue Engineering Commons](#)

© The Author

Downloaded from

<https://scholarscompass.vcu.edu/etd/5908>

This Dissertation is brought to you for free and open access by the Graduate School at VCU Scholars Compass. It has been accepted for inclusion in Theses and Dissertations by an authorized administrator of VCU Scholars Compass. For more information, please contact libcompass@vcu.edu.



VCU Biomedical Engineering

College of Engineering

Designing Biomimetic Implant Surfaces to Promote Osseointegration under Osteoporotic Conditions by Revitalizing Mechanisms Coupling Bone Resorption to Formation

By

Ethan Major Lotz

A dissertation submitted in partial fulfillment of the requirements for the degree of Doctor of Philosophy in Biomedical Engineering at Virginia Commonwealth University.

Approved May 10th, 2019 by:

Advisor

Barbara D. Boyan, Ph.D.

Alice T. and William H. Goodwin Jr. Dean, College of Engineering
Virginia Commonwealth University

Advisory Committee

¹Henry J. Donahue, Ph.D.; ²Ibrahim Guven, Ph.D.; ¹Zvi Schwartz, D.M.D., Ph.D.; ³Jolene J. Windle, Ph.D.;

¹Department of Biomedical Engineering, VCU College of Engineering; ²Department of Mechanical and Nuclear Engineering, VCU College of Engineering; ³Department of Molecular Biology and Genetics, VCU School of Medicine

Copyright © 2019 Ethan Major Lotz

Acknowledgements

First, I would like to thank my advisors, Dean Barbara Boyan and Dr. Zvi Schwartz. I have known them since 2010 when I began working as an undergraduate researcher in their laboratory during my final year at Georgia Institute of Technology. It is incredible to look back at the opportunity to work in their lab and realize how much it shaped my life. I even have Dean Boyan to thank for inadvertently introducing me to my girlfriend Kelly during the orientation for first year engineering graduate students. For the last decade, they have truly served as my second set of parents giving me just as much advice on my career and relationships as they did on science and research. Being included in events like Bar Mitzvahs and Thanksgiving Day celebrations were just some of the ways they would go out of their way to make me feel like part of their family. But the thing I most appreciated about our relationship was the respect and trust they showed me. It will be hard moving on from their lab, but I know they will serve as my lifelong mentors.

I am also grateful to the other members of my thesis committee. Dr. Hank Donahue for providing alternative views to dental and orthopaedic implant research; Dr. Ibrahim Guven for his expertise in materials and mechanical engineering and ensuring that these principles were emphasized in my project; and Dr. Jolene Windle for balancing the engineering approaches to research with traditional biological approaches as well as her wealth of knowledge in the area of animal models of bone disease.

Because of the success of Dean Boyan and Dr. Schwartz, their lab consists of some of the most intelligent and highest quality graduate students, post-doctoral fellows, and research clinicians. First, I would like to thank the many undergraduates that have been a critical part of my success including Regan Ellis, Irma Nalic, Andrew Phung, and especially Michael Berger, who has proven to be a great scientific researcher himself since deciding to pursue his own PhD under Dean Boyan and Dr. Schwartz. I am also grateful to Sharon Hyzy for not only maintaining

the day-to-day operations running as the lab manager for most of the time I was there, but also for giving me an interview and offering me the initial position of undergraduate researcher. Dr. Josh Cohen has also been an amazingly big help by seamlessly transitioning into the current lab manager while somehow finding the time to perform the animal surgeries for every project in the lab. I also want to congratulate Dr. Cohen as he will officially hold the title of longest active lab member once I leave. I am thankful to Dr. Michael McClure whose expertise in skeletal muscle tissue engineering has brought diversity into the research conducted by the lab as well as his advice and support for my individual research and overall career. My development as a researcher is also due to all the equally motivated and driven graduate students who have come and gone over the years. The collaboration and exchange of ideas promotes a higher quality research that is unmatched by other groups.

I would also like to thank the many collaborators, whom this project could never have been completed without. Dr. Simon Berner, Dr. Christoph Appert, and Heiner Bieli who served as my friends and mentors during my six-month internship at Institut Straumann AG in Switzerland; Dr. Jennifer Wayne for our collaborative efforts developing a system to measure implant removal torque values in our animal models; and Dr. Raphael Wagner and Alex Ostashko for continuing the collaboration between our lab and Institut Straumann AG.

Finally, I would like to thank my sister Sadie and her family, the many friends I have made in Richmond, and my girlfriend Kelly for being there whenever I needed them. I would also like to thank my parents Jeff and Kristin who have always been my personal heroes. My dad fostered my scientific curiosity starting at a young age, serving as my very first mentor by helping me with designing, conducting, and funding my first experiments which were accepted for poster presentations at the South Mississippi Regional Elementary Science Fair three years in a row. My mom is responsible for my strong work ethic and dedication to my passions as well as

teaching me to take pride in my work. I would also like to apologize to her for causing any anxiety in her life as I feel, at times, she was more stressed about my job than me.

This work was supported by the National Institute of Arthritis and Musculoskeletal and Skin Diseases of the National Institutes of Health under Award Numbers R01AR052102 and R01AR072500, the Elsbeth-Bonhoff-Stiftung (Berlin, Germany), ITI Foundation, Institut Straumann AG (Basel, Switzerland), as well as by the Georgia Tech/Emory Center for the Engineering of Living Tissues. Institut Straumann AG also provided all the surfaces and implants for my thesis work; however, none of the material characterization or biological assays were performed by their employees. The content is solely the responsibility of the authors and does not necessarily represent the official views of the National Institutes of Health.

Table of Contents

Acknowledgements	3
List of Symbols and Abbreviations.....	8
Thesis Abstract.....	10
Chapter 1. Introduction	11
Specific Aims.....	11
Significance.....	13
Chapter 2. Background.....	16
Stages of Osseointegration	17
Biomimetic Implant Surfaces: Lessons from Bone Remodeling	19
Coupling of Bone Resorption to Formation: Implications for Osteoporosis	22
Chapter 3. Comparable Responses of Osteoblast Lineage Cells to Microstructured Hydrophilic Titanium-Zirconium and Microstructured Hydrophilic Titanium	29
Abstract	29
Introduction.....	30
Materials and Methods	32
Results	36
Discussion.....	41
Conclusions.....	47
Chapter 4. Osteogenic Response of Human MSCs and Osteoblasts to Hydrophilic and Hydrophobic Nanostructured Titanium Implant Surfaces.....	48
Abstract	48
Introduction.....	48
Materials and Methods	50
Results	54
Discussion.....	59
Conclusions.....	67
Chapter 5. Regulation of Osteoclasts by Osteoblast Lineage Cells Depends on Titanium Implant Surface Properties	68
Abstract	68
Introduction.....	69
Materials and Methods	72
Results	77
Discussion.....	84
Conclusions.....	90



Chapter 6. Bisphosphonates Inhibit Surface Mediated Osteogenesis	91
Abstract	91
Introduction.....	91
Materials and Methods	93
Results	97
Discussion.....	102
Conclusions.....	107
Chapter 7. Ibandronate Treatment Before and After Implant Insertion Impairs Osseointegration in Aged Rats with Ovariectomy Induced Osteoporosis	109
Abstract	109
Introduction.....	110
Materials and Methods	112
Results	121
Discussion.....	129
Conclusions.....	133
Chapter 8. Titanium Implant Surface Properties Enhance Osseointegration in Aged Osteoporotic Rats without Pharmacologic Intervention	135
Abstract	135
Introduction.....	135
Materials and Methods	138
Results	145
Discussion.....	151
Conclusions.....	155
Chapter 9. Conclusions and Future Perspectives.....	157
Vita	163
References	164

List of Symbols and Abbreviations

1 α ,25(OH) ₂ D ₃	1 α ,25-Dihydroxy vitamin D3
BIC	Bone to implant contact
BIS / BP	Bisphosphonate
BMD	Bone mineral density
BMP	Bone morphogenetic protein
BRU	Bone remodeling unit
BSA	Bovine serum albumin
BV	Bone volume
BV/TV	Bone volume over total volume
CM	Conditioned media
COX	Cyclooxygenase
cpTi	Commercially pure titanium
DBM	Demineralized bone matrix
DMEM	Dulbecco's modified Eagle's medium
E ₂	17 β -estradiol
ECM	Extracellular matrix
ELISA	Enzyme linked immunosorbent assay
ER α	Estrogen receptor α
FBS	Fetal bovine serum
FGF	Fibroblast growth factor
GAPDH	Glyceraldehyde 3-phosphate dehydrogenase
H ₂ SO ₄	Sulfuric acid
HCl	Hydrochloric acid
HSC	Hematopoietic stem cell
IGF	Insulin-like growth factor
IL	Interleukin
ITG	Integrin
M-CSF	Macrophage colony stimulating factor
modSLA / mSLA	Modified sand blasted large grit acid etched surface
MSC	Mesenchymal stem cell
MSCGM	Mesenchymal stem cell growth medium
NHOst	Normal human osteoblast
NRP	Neuropilin
OB	Osteoblast
OC	Osteoclast
OCGM	Osteoclast precursor growth medium

OCN	Osteocalcin
OCP	Osteoclast precursor
ONJ	Osteonecrosis of the jaw
OPG	Osteoprotegerin
OPN	Osteopontin
OVX	Ovariectomized
PBS	Phosphate buffered saline
PGE	Prostaglandin E
PLXN	Plexin
pNPP	P-nitrophenyl phosphate
PRP	Platelet rich plasma
PT	Pretreatment surface
PTH	Parathyroid hormone
RANK	Receptor activator of nuclear factor kappa B
RANKL	Receptor activator of nuclear factor kappa B ligand
rOB	Rat osteoblast
RT-PCR	Reverse transcription polymerase chain reaction
RTV	Removal torque value
SEM	Scanning electron microscopy
SEMA3A	Semaphorin
SHAM	Sham-operated
SHOVX	Sham-ovariectomy-operated
SLA	Sand blasted large grit acid etched surface
SLAnano	Sand blasted large grit acid etched nano surface
TCPS	Tissue culture polystyrene
TGF β	Transforming growth factor β
Ti	Titanium
Ti6Al4V	Titanium–aluminum–vanadium
TiZr	Titanium-zirconium
TNF α	Tumor necrosis factor α
TRAP	Tartrate-resistant acid phosphatase
VEGF	Vascular endothelial growth factor
XPS	X-ray photoelectron spectroscopy

Thesis Abstract

In cases of compromised bone remodeling like osteoporosis, insufficient osseointegration occurs and results in implant failure. Implant retention relies on proper secondary fixation, which is developed during bone remodeling. This process is disrupted in metastatic bone diseases like osteoporosis. Osteoporosis is characterized low bone mass and bone strength resulting from either accelerated osteoclast-mediated bone resorption or impaired osteoblast-mediated bone formation. These two processes are not independent phenomena. In fact, osteoporosis can be viewed as a breakdown of the cellular communication connecting bone resorption to bone formation. Because bone remodeling occurs at temporally generated specific anatomical sites and at different times, local regulators that control cross-talk among the cells of the BRU are important. Previous studies show Ti implant surface characteristics like roughness, hydrophilicity, and chemistry influence the osteoblastic differentiation of human MSCs and maturation of OBs. Furthermore, microstructured Ti surfaces modulate the production of factors shown to be important in the reciprocal communication necessary for the maintenance of healthy bone remodeling. Semaphorin signaling proteins are known to couple the communication of osteoblasts to osteoclasts and are capable of stimulating bone formation or bone resorption depending on certain cues. Implant surface properties can be optimized to exploit these effects to favor rapid osseointegration in patients with osteoporosis.

Chapter 1. Introduction

Specific Aims

Successful osseointegration of dental and orthopaedic implants is determined by the degree of bone apposition to the surface of the implant material. This complex cascade of biological events involves primary bone formation, ultimately leading to the development of mature lamellar bone via bone remodeling. In cases of compromised bone remodeling, like osteoporosis, insufficient osseointegration occurs, which can result in implant failure.

In addition to its role in osseointegration, bone remodeling provides the mechanism for adaptation to mechanical stress and repair of micro-damage. The versatility of bone remodeling implies its ubiquity within the skeleton and its initiation highlights the importance of locally generated and regulated factors ensuring appropriate coupling mechanisms among bone forming osteoblasts (OBs), bone resorbing osteoclasts (OCs), and their respective mesenchymal (MSC) or hematopoietic (HSC) stem cell lineage precursors. These cells comprise the bone remodeling unit (BRU), and their contemporaneous and multidirectional communication balances bone formation with bone resorption. Any defects in this coupling process may lead to the dysregulation of bone homeostasis leading to low bone mass and strength resulting in osteoporosis. Thus, the continuous loss of bone that occurs in osteoporosis implies a defect in the coupling process. Although age-related mechanisms contributing to osteoporosis may originate from accelerated bone resorption or impaired bone formation, these processes are not independent phenomena. Therapeutic interventions targeting either half of this process will inevitably affect its counterpart.

Implant surfaces made from titanium (Ti) or its alloys, including commercially pure Ti (cpTi), titanium – aluminum – vanadium (Ti6Al4V), and titanium – zirconium (TiZr), can be modified to stimulate osteogenesis, resulting in enhanced osseointegration, eliminating the need for exogenous biologics such as bone morphogenetic proteins (BMPs). Surface microroughness,

hydrophilicity, and chemistry influence the osteoblastic differentiation of human mesenchymal stem cells (MSCs). When grown on Ti surfaces that are microstructured and hydrophilic, these cells produce factors that create an osteogenic environment by: stimulating osteoblastic differentiation in progenitor cells distal to the implant; promoting vasculogenesis; reducing inflammation; and regulating osteoclastic resorption to achieve net new bone formation. These *in vitro* findings are correlated with preclinical studies in animal models and with human clinical studies. However, this research was limited to healthy animals and did not focus on compromised conditions.

The **overall goal** of this research project addresses the clinical need for materials that enable rapid and sufficient implant osseointegration for patients with osteoporosis. The **central hypothesis** is that microstructured Ti and TiZr surfaces regulate the remodeling phase of osseointegration through direct actions on the coupling of cells in the BRU. Furthermore, we can tailor Ti implant design to exploit these effects to favor rapid osseointegration in patients with osteoporosis. However, to optimize osteoporotic osseointegration, we need a more complete understanding of cellular and molecular coupling events within the BRU and how modified Ti implants exert their regulatory control on bone remodeling. The objectives of this research project were completed by pursuing the following three specific aims.

Aim 1: Determine the effects of microstructured titanium and titanium-zirconium surfaces on production of factors that regulate OC activity by cells of the osteoblast lineage. We will investigate how Ti and TiZr surface properties control local factor production responsible for the communication occurring within the BRU. The **working hypothesis** is that the microtopography and hydrophilicity of Ti and TiZr surfaces regulate production of factors associated with the reciprocal communication between MSCs, OBs, and OCs, specifically factors associated with Eph/Ephrin and semaphorin signaling. Smooth, rough, and hydrophilic-rough Ti and TiZr disks will be used to assess changes in MSC and OB gene expression and

protein production of this signaling pathway.

Aim 2: Determine the mechanisms through which implant surface properties influence cellular communication in bone remodeling. We have established that MSC differentiation and OB maturation are very different when cultured on microstructured surfaces vs. TCPS. MSCs and OBs primarily express the $\alpha 5\beta 1$ integrin complex when grown on TCPS but shift to $\alpha 1\beta 1$ and $\alpha 2\beta 1$ when grown on microstructured substrates. Furthermore, microstructured implant surfaces facilitate osteogenesis through the non-canonical Wnt5a pathway, in contrast to the canonical Wnt3a pathway seen on TCPS. Semaphorins not only mediate BRU crosstalk but also stimulate osteoblastic differentiation and bone growth through β -catenin, bypassing canonical Wnt3a signaling, suggesting they are involved. The **working hypothesis** is that microstructured, hydrophilic surfaces regulate the BRU through semaphorin signaling inducing OB differentiation. We have developed a system that allows us to focus on surface-dependent mechanisms that control BRU reciprocal communication.

Aim 3: Examine whether Ti implant surface properties can impact osseointegration in an *in vivo* model of compromised bone remodeling. Using an osteoporotic aged rat model, the *in vivo* effectiveness of surface modified Ti implants to influence bone formation will be examined as a function of surface-dependent regulation of OB/OC coupling mechanisms. The **working hypothesis** is that modified Ti implants can reinvigorate locally compromised bone remodeling without use of additional therapeutics. Osseointegration of modified Ti implants will be compared between aged osteoporotic rats with or without medications commonly used to combat osteoporosis. MSCs and OBs isolated from these rats will be used to correlate *in vitro* and *in vivo* results.

Significance

Aging of the population is currently a topic of public health concern. The number of people aged 60 or older is projected to grow to nearly 2 billion by 2050, with most of the increase seen

in developing countries.¹ Consequently, the increasing occurrence of disorders and morbidities associated with aging is driving the necessity to develop technologies addressing the needs of this demographic.

Currently, 18.1% of American adults over the age of 65 are completely edentulous and an estimated 37.9 million adults in the United States will have no natural teeth by 2020.² Historically, edentulous patients have been treated with removable dentures. However, decreased dietary adequacy has been observed in these patients compared to dentate patients. Implant-supported dentures significantly improve quality of life in comparison to removable dentures, but many prosthetic and surgical problems and complications are still present. In a systematic review of data pooled from maxillary and mandibular fixed implant prostheses, only 29% of prostheses remained complication free after 5 years, which decreased to 9% after 10 years.³ These complications were attributed to the effects of aging on metabolic and endocrine processes, making implant osseointegration difficult to predict accurately.

Sufficient bone volume (BV) and bone mineral density (BMD) are two of the most important patient factors for predicting implant success. These factors significantly diminish with age and their reduction is exacerbated by menopause. Patients experiencing excessive decreases in BMD are at risk of developing osteoporosis. Osteoporosis is a metabolic bone disease characterized by low BMD and BV, impairing bone strength and healing. An estimated 53.6 million U.S. adults over the age of 50 were affected by osteoporosis or osteopenia in 2010.⁴ By 2030, its prevalence is projected to increase to 71.4 million people.⁴ Furthermore, 80% of those affected by osteoporosis were postmenopausal women.⁴

Countless research efforts have focused on developing new methods of altering biomaterial surfaces and characterizing their effects on early stage osteogenesis. No efforts, however, have sought to investigate how implant surfaces modulate the bone remodeling phase of osseointegration. By investigating the extent to which microstructured surfaces orchestrate the

dynamic cellular interplay of the BRU, this research shifts the paradigm of contemporary biomaterial surface research. An understanding of bone remodeling regulation will allow us to address the clinical need for implants capable of osseointegration in patients with a multitude of disorders compromising bone remodeling. The aim is not to cure these disorders, but rather determine whether microstructured implant surfaces can locally mitigate their effects and reinvigorate bone remodeling to promote rapid and sufficient osseointegration.

Chapter 2. Background

Implants are used in orthopaedics and dentistry to improve the quality of life for patients who suffer from chronic back pain, degenerative joints, or edentulism. Titanium (Ti) and its alloys, including commercially pure Ti (cpTi), titanium–aluminum–vanadium (Ti6Al4V), and titanium–zirconium (TiZr), are commonly used to restore structure and function of musculoskeletal tissues because of their high biocompatibility, corrosion resistance, and favorable weight-to-strength ratio. These attributes of Ti are due to its ability to form a passive oxide layer making it stable in biological systems. Since bone has a high composition of inorganic calcium phosphates, many have speculated that the passive oxide layer of Ti mimics the ceramic nature of bone. Ti and Ti alloy implants support stable osseointegration, the biological phenomenon providing a direct structural and functional connection between surfaces of load-bearing implant and living bone.

The modern use of metallic implants for orthopaedic and dental applications has been evolving over the last 60 years.^{5–7} Early efforts in biomaterial design were primarily concerned with the biocompatibility of the material with the host tissue. Materials that limited the development of foreign body giant cells, provided no evidence of local toxicity, and mitigated fibrous encapsulation were deemed acceptable. Implants made from these materials were viewed as biologically inert fixtures, anchored in place either using cement or via mechanical interlocking between the implant and the surrounding bone tissue. However, failure to achieve mechanical stability led to micromotion of the implant and localized inflammation, and frequently ending with osteolysis and implant failure.

Over the last few decades, research has made it clear that implant materials should go beyond compatibility and actively promote bone formation. One approach has been to induce peri-implant bone formation through the use of osteoinductive agents like demineralized bone matrix (DBM)^{8,9} and bone morphogenetic protein-2 (BMP2).^{10,11} Alternative approaches have included the use of bone graft substitutes that are designed to be osteogenic via the use of a

variety of factors, including platelet rich plasma (PRP),¹²⁻¹⁴ platelet derived growth factor (PDGF),^{15,16} and insulin-like growth factor-1 (IGF1),^{17,18} as well as vasculogenic factors like vascular endothelial growth factor (VEGF),^{17,19} and fibroblast growth factor-2 (FGF2).^{20,21} However, many of these biologics are temporary solutions designed to stimulate initial bone formation. Long-term stability of an implant requires solutions that not only result in net bone formation but also provide continued osteogenic signals throughout the entire process of osseointegration. Physical modifications to the implant material surface, which will be present long after the exogenous bioactive agents are gone, provide the best options to achieve this.

Stages of Osseointegration

Bone is a dynamic tissue making it obvious that coordinated and sequentially organized cellular communication and biomechanical cues are needed to initiate and maintain the events responsible for osseointegration (**Fig.1**). Osseointegration begins with surgical trauma followed by the insertion of an implant. After implant insertion, blood vessels rupture and release proteins, ions, sugars, and lipids, important for blood clot formation (**Fig.1A**). Following formation of the blood clot, initial inflammatory response is controlled via immunomodulatory cells such as neutrophils, dendritic cells, and macrophages (**Fig.1B**). These immune cells produce chemokines that clean and disinfect the microenvironment, guide MSC recruitment or additional immune cells, and initiate tissue repair.

The blood clot spans the gap between the injured bone and the implant. Formation of the blood clot is an important step in implant osseointegration, as it serves as a provisional matrix and scaffold for the migration of MSCs to the implant surface (**Fig.1B**). Surface design that facilitates this contact osteogenesis has been shown to control the fundamental processes that drive the osteoblastic differentiation of MSCs.^{22,23} Differentiating MSCs and mature OBs produce factors that create an osteogenic microenvironment, promote angiogenesis, reduce inflammation, and regulate osteoclast-mediated bone resorption. A cell-rich, immature bone

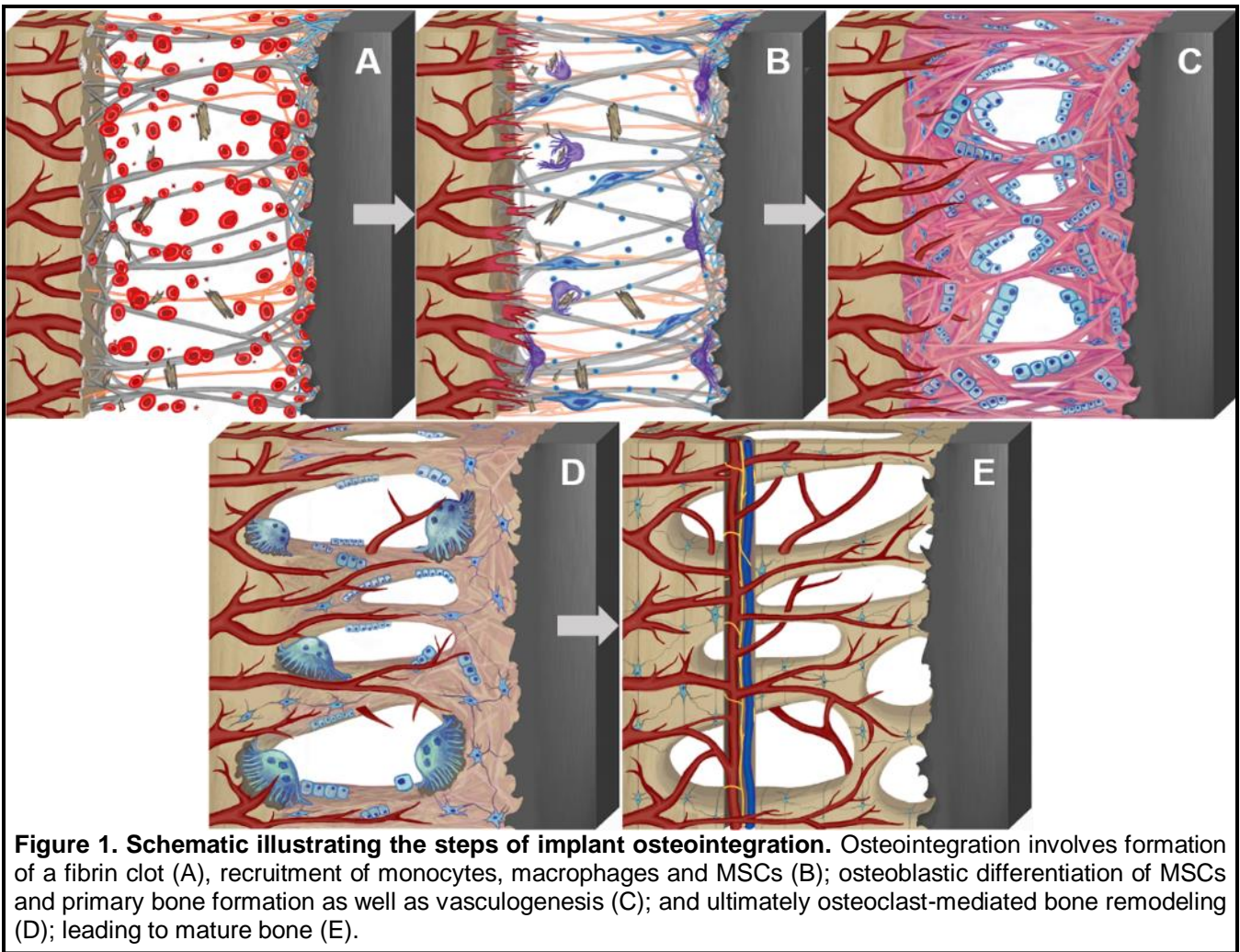


Figure 1. Schematic illustrating the steps of implant osseointegration. Osseointegration involves formation of a fibrin clot (A), recruitment of monocytes, macrophages and MSCs (B); osteoblastic differentiation of MSCs and primary bone formation as well as vasculogenesis (C); and ultimately osteoclast-mediated bone remodeling (D); leading to mature bone (E).

(primary bone) forms in direct contact with the surface of the Ti implant (**Fig.1C**). Following the formation of the primary bone, OCs begin to form (**Fig.1D**). Their formation marks the beginning of the bone remodeling phase of osseointegration and with it comes the progressive removal of the primary bone, creating space for new lamellar bone formation and replacing passive primary stability with active secondary fixation through biological bonding (**Fig.1E**).

In vivo, bone is formed by OBs on areas of the bone surfaces that have been prepared by OCs. It is unclear as to how resorption sites are selected, but the process is initiated by the retraction of bone-lining cells to uncover osteoid. After removal of the osteoid, the OC attaches to the mineralized surface and forms a sealing zone. Beneath the OC, the formation of a closed compartment called the resorption lacunae occurs where the OC membrane is folded forming the ruffled border. The OC is able to release hydrogen ions through the ruffled border via activity

of carbonic anhydrase, thereby reducing the pH and dissolving the mineralized portion of the extracellular matrix.^{24,25} Other enzymes like lysosomal cysteine proteinases and matrix metalloproteinases are then secreted to degrade the organic matrix.^{26,27}

The resorption pit created by the osteoclast has been shown to be chemotactic for osteoprogenitor cells,²⁸ which migrate onto the surface and differentiate into mature osteoblasts. These cells produce growth factors like BMPs together with their regulatory apparatus, which induce osteoblast differentiation of MSCs and osteoprogenitor cells. The secretory osteoblasts produce osteoid consisting of extracellular matrix proteins such as type I collagen as well as osteocalcin and osteonectin. Mineralization of the osteoid is then promoted through the regulation of local concentrations of calcium and phosphate and tailoring of the extracellular matrix components.

Biomimetic Implant Surfaces: Lessons from Bone Remodeling

Based on the research from our group and others,²⁹ biologically inspired dental and orthopaedic implant surfaces are now being produced that mimic the features of an OC resorption pit. Studies using model Ti surfaces fabricated using photolithography and micromachining show that 30 – 100 μ m diameter craters are preferentially colonized by osteoblasts,^{30,31} which are similar in size to OC resorption pits.^{32,33} Moreover, OCs do not uniformly degrade the mineralized portion of bone and are unable to completely degrade all the extracellular matrix components leaving debris such as collagen and hydroxyapatite fragments in the wake of their resorption. Hydroxyl ions also remain in the resorption pit as a result of the dissolution of hydroxyapatite crystals.³⁴ Once the OC detaches from the bone, a resorption pit remains that has a unique surface with a particular chemistry and complex hierarchical structure that contains micro-, meso-, and nano features. Thus, native bone has physical features capable of altering the mechanical environment experienced by osteoblast lineage cells, and the inherent chemistry, roughness, and hydrophilicity of the bone surface can influence cell attachment and

cell shape, which can dictate cell proliferation and differentiation *in vitro* as well as osseointegration *in vivo*.

Surface Chemistry

Surface chemistry of an implant is determined by the properties of the bulk material as well as its method of fabrication. As stated previously, Ti is the choice material for both dental and orthopedic implant materials because of favorable bulk properties its high biocompatibility, increased resistance to corrosion, and favorable weight-to-strength ratio. Ti-based alloys, like Ti-6Al-4V and TiZr, are also used because of their improved material properties, particularly mechanical strength. Because of the altered bone turnover, many osteoporotic/osteopenic patients have severely limited bucco-lingual and/or mesiodistal dimensions, which further complicate dental implant interventions. Reduced diameter implants (1.8 – 3.0mm) have become a common alternative for these patients.³⁵ Although Ti is the dominant material for dental implant applications, its mechanical properties can be inadequate following reductions in its diameter, increasing incidences of fatigue fracture and deformation from masticatory forces. Research investigating TiZr and Ti-6Al-4V substrates has shown increasing support for their use as an alternative biomaterial.

Traditionally, Ti implants are produced by machining Ti or alloyed rods. The machining process results in a smooth surface with some microscopic irregularities;^{36–38} however, these irregularities have not been shown to be clinically significant.³⁷ Using this machined surface as a base, additive or subtractive post-processing methods are employed to further alter the surface of the implant to generate a surface topography with features similar to OC resorption pits.

Additive layering of Ti particles onto existing machined surfaces is frequently used to create bulk structures from computer aided designs.³⁹ Ti plasma spraying applies layers of Ti particles onto the surface of machined rod implants using a plasma torch. Local melting typically occurs during this process, which can generate a patchwork surface containing irregular regions of

depressions and protrusions as well as relatively smooth areas. Bulk structures can also be produced by additive manufacturing reducing cost, time, and material waste. Metallic implants fabricated bottom-up can possess irregular geometries. Selective laser melting and electron beam melting are two methods in which powder layers of micron sized metallic particles are fused using a high energy beam, in a layer-by-layer fashion following a computer aided design.

Surface Topography

The positive influence of surface topography on osseointegration, achieved through subtractive methods like grit-blasting and acid-etching, has been a topic of investigation for several decades. It has been understood for some time that macro- and micro-rough implants outperform their smooth counterparts.^{40–44} Today, microrough surfaces dominate the market as they have been shown to achieve faster bone integration, a higher percentage of bone to implant contact (BIC), and a higher resistance to shear, as determined by removal torque values (RTVs), when compared to smooth implant surfaces.³⁵

Recently, studies have suggested features at the submicron and nanoscale have a direct effect on the biological response of bone.^{45–48} Type I collagen, the primary organic component of bone, consists of fibers ~300nm in length and ~0.5nm in width while the hydroxyapatite crystals in bone are generally ~50nm in length and ~5nm in diameter.⁴⁹ In order to mimic these features, nanomodifications have been developed to directly restructure the oxide layer formed on the implant surface using coatings,⁵⁰ hydrothermal reactions treatments,⁵¹ and surface oxidation.^{52,53} Reorganization of the oxide layer leads to a disordered nanostructure orientation, which has been shown to be more favorable compared to a highly ordered pattern.⁵⁴

Hydrophilicity

Hydrophilicity is related to the wettability of the implant surface and is generally regarded as a result of the surface chemistry.⁵⁵ The hydrophilicity of an osteoclast resorption pit surface is not known, making it difficult to mimic this property, but hydrophilic surfaces are known to

promote an environment conducive for bone formation.^{56,57} This has been attributed to rapid spreading of serum on the surface providing an overall coating of bioactive factors⁵⁸ that can influence early cell adhesion,⁵⁹ proliferation,⁶⁰ and differentiation^{23,61} by modulating the bonding strength, total amount, and conformation of adsorbed proteins.⁶² One method commonly used to retain surface hydrophilicity of a biomaterial is to reduce atmospheric hydrocarbon contamination.⁶³ Post-processing saline storage or plasma cleaning before implantation are two commonly used methods to either prevent the deposition of hydrocarbons or rid the surface of deposited hydrocarbons. Both processes indirectly increase the presence of hydroxyl ions on the implant surface, which could be the reason for the increased performance of hydrophilic compared to hydrophobic implants.

Coupling of Bone Resorption to Formation: Implications for Osteoporosis

In a healthy adult skeleton, the amount of resorbed bone is generally equal to the amount of new bone formation, thus maintaining skeletal integrity. This coordination, referred to as coupling, could play a significant role in the pathophysiology of osteoporosis. If the acceleration of bone resorption were matched by an equal or greater increase in bone formation there might be transient bone loss, but ultimately the removed bone would be replaced by new bone. Hence, the continuous loss of bone that occurs in osteoporosis implies a defect in the coupling process. Thus, it is of great importance to determine which factors regulate coupling and the influence implant surfaces have on these mechanisms.

Regulation of Estrogen

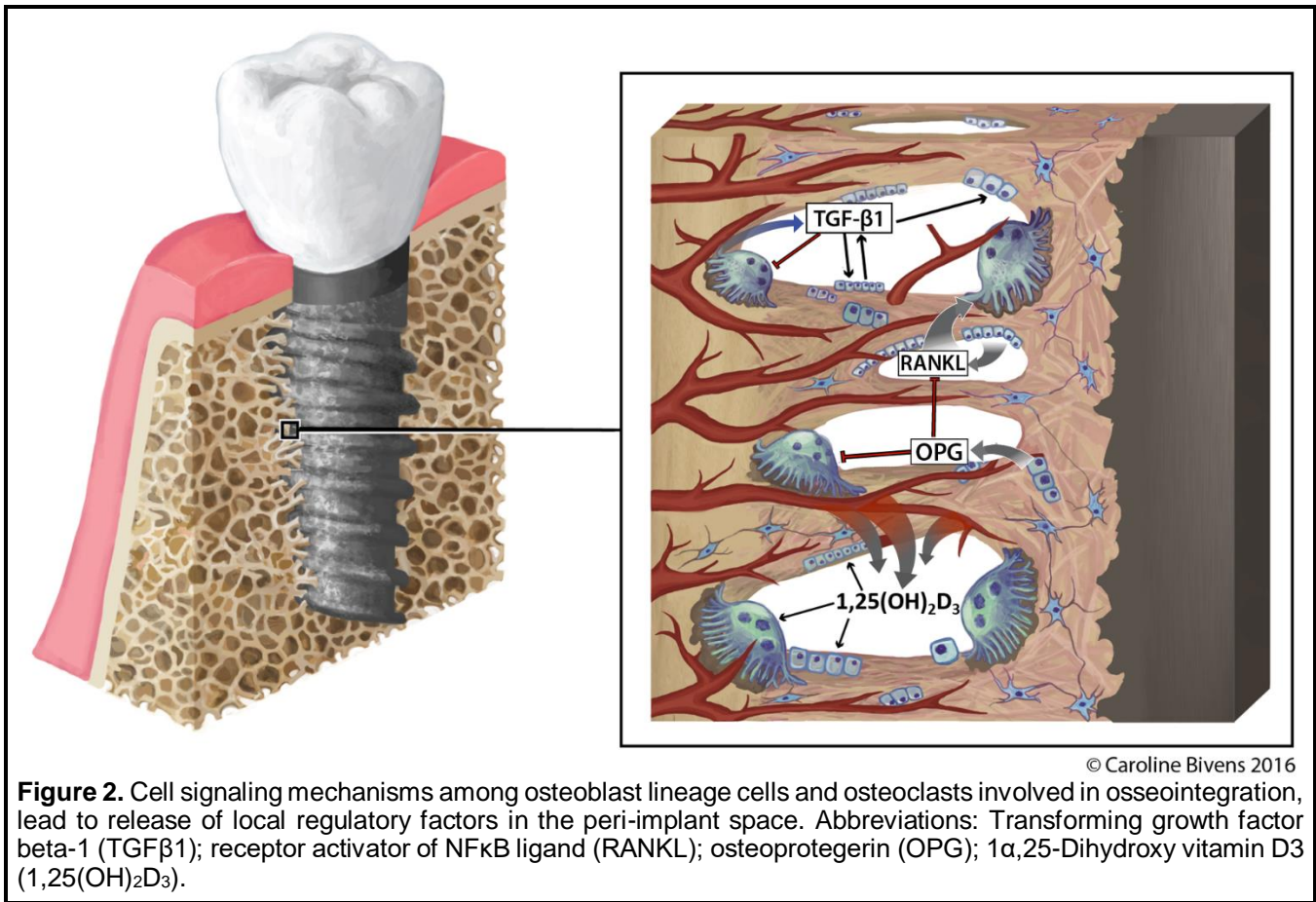
The rate at which bone remodeling occurs varies when an implant is present and depends on the type of implant used and its surface properties.^{64–66} Cells on microstructured surfaces exhibit an osteoblastic phenotype within the first 4 days of culture and produce factors that act via autocrine/paracrine signaling to regulate peri-implant bone remodeling.⁶¹ On TCPS, MSC differentiation occurs through the canonical Wnt3A pathway, causing an accumulation of β -

catenin in the cytoplasm and its translocation into the nucleus to serve as a transcriptional activator.^{67–69} Previous studies have demonstrated surface mediated MSC differentiation downregulates genes associated with the Wnt3A pathway while upregulating genes of the Wnt11 and non-canonical calcium-dependent Wnt5a pathway.^{70–72} Expression of Wnt5a and Wnt11 signaling pathway components are also induced in mature female OBs when treated with 17 β -estradiol (E2),^{73,74} the primary sex hormone responsible for the development of post-menopausal osteoporosis. Moreover, sensitivity to E2 treatment is increased when these cells are cultured on microrough and/or hydrophilic Ti implant surfaces compared to smooth Ti or TCPS.^{74–76} Estrogen deficiency may play a role in the impaired formation response during remodeling, because animals lacking ER α showed decreased formation responses to mechanical loading by a mechanisms that involves the Wnt signaling pathway.

Estrogen is an osteoprotective hormone, and its deficiency leads to an elevated rate of bone turnover culminating in osteoporosis in females and, in some cases, older males. A hallmark of E2 deficiency is an elevated rate of bone turnover in which the rate of OC-mediated bone resorption increases and, secondarily, OB-mediated bone formation decreases. In osteoporotic patients, MSCs and OBs produce factors favoring osteoclastogenesis unfettered by any regulatory feedback mechanisms. Increased levels of pro-inflammatory IL-6 and decreased levels of TGF β 1 are produced by bone cells isolated from osteoporotic patients compared to healthy patients.^{77–79} Interestingly, both E2 treatment and microstructured Ti substrates are known to inhibit IL-6 production while enhancing production of TGF β 1 and OPG.^{75,80,81}

Communication from Osteoblasts

Many of the factors produced by osteoblasts cultured on microrough Ti surfaces regulate bone remodeling by favoring osteogenesis over osteoclastic resorption, promoting net new bone formation (**Fig.2**). TGF β 1-dependent regulation of OPG production is one of the classic



mechanisms controlling localized bone remodeling.⁸⁰ TGFβ₁ enhances the proliferation of MSCs and OBs and stimulates extracellular matrix production of proteins like type I collagen. Latent TGFβ₁ and latent TGFβ binding protein are synthesized and stored in the extracellular matrix. Most of the TGFβ₁ produced by OBs cultured on Ti is in latent form,⁸² and the amount incorporated into the matrix is increased on rougher surfaces. Once the bone remodeling phase of osseointegration begins, the OCs degrade the newly synthesized matrix releasing the stored, latent TGFβ₁ and convert it into active TGFβ₁. Once activated, TGFβ₁ acts on osteoclasts and downregulate their activity, in part by regulating production of OPG.⁸⁰

OPG serves as a decoy receptor for receptor activator of NFκB ligand (RANKL).⁸³ By binding to RANKL, it prevents osteoclast differentiation by preventing its interaction with receptor activator of NFκB (RANK) on the OCP surface, an interaction required for the fusion and subsequent maturation of differentiated OCs. A feedback mechanism is in place that allows

osteoblasts to produce soluble RANKL in order to deplete excess OPG if the regulatory stimulus favors new osteoclast formation. Microrough Ti substrates facilitate increased production of OPG by osteoblasts; however, levels of RANKL do not change.⁸⁴ Thus, the net effect is bone formation without bone resorption.

Local regulatory factor production has also been shown to be sensitive to microstructured Ti implants. In addition to the high production of negative regulators of osteoclast activity, cells produce high levels of osteocalcin and osteopontin.^{22,53,85} Osteocalcin has been shown to promote the chemotaxis, adhesion, and spreading of osteoclasts^{86,87} while osteopontin plays a role in anchoring osteoclasts to the mineralized bone matrix.⁸⁸ The sequential production of these factors suggests microstructured Ti facilitates the production of a cascade of factors by MSCs and osteoblasts to mediate osteoclast recruitment while preventing their premature fusion and activity. Although PGE₂ stimulates osteoclastic activity at high levels, it is required at low levels for osteoblast activity.^{89,90} Osteoblast production of PGE₁ and PGE₂ is markedly increased when cells are cultured on microrough surfaces.⁸² Blocking the production of prostaglandins by the cyclooxygenase (Cox) inhibitor, indomethacin, also blocks the increase in other osteoblastic markers when cells are cultured on these surfaces, suggesting that they are necessary for enhanced osteogenesis.^{91,92}

BMP signaling is also tightly regulated during surface mediated osteogenesis, and that modulation of these signals can enhance or inhibit bone remodeling.⁹³ Autocrine and paracrine actions of BMPs are known to be involved in cell proliferation, differentiation, and apoptosis.⁹⁴ Among these proteins, BMPs 2, 4, and 7 have shown to be the most important in bone formation and healing.^{95,96} Modulation of these osteogenic factors by implant surfaces provide molecular evidence of the increased osteoblastogenesis seen *in vitro* and increased healing times seen clinically. MSCs cultured on microstructured Ti substrates, display temporal upregulation of BMPs with increases of BMP2 and BMP4 occurring as early as 4 days, suggesting that they are

early regulators of surface-mediated osteogenesis.⁹³ Their presence could also serve as the impetus for the commitment of MSCs to the osteoblast lineage when cultured on microstructured Ti, as they are known to regulate embryonic skeletal development.¹¹ Furthermore, they also provide a mechanism for the differentiation of MSCs distal to the implant surface, as they are capable of multidirectional signaling. When MSCs were silenced for BMP2, production of OPG decreased suggesting that BMP2 effects impacts bone remodeling.⁹³

Axon Guidance Molecules

Axon guidance molecules were originally identified as instructive cues for the navigation of axons, allowing axons to migrate to their targets during nervous system development. These molecules that guide growing axons towards and away from specific brain regions have been classified as attractive and repulsive, respectively.⁹⁷ Besides their roles in neural circuit formation, axon guidance molecules have been implicated in various other biological processes, including cell motility, proliferation, differentiation, angiogenesis, cardiogenesis, tumor growth, tissue development, immune response, and, more recently, the coupling of osteoblasts and osteoclasts during bone remodeling.^{98–104}

Interactions of Eph family proteins with membrane bound Ephrin ligands on adjacent cells activate Eph receptor kinase-dependent pathways. Interestingly, the ephrins can also trigger tyrosine phosphorylation-dependent and independent signals, making bidirectional cell contact-dependent communications possible.¹⁰⁰ Loss- and gain-of-function experiments showed that osteoclast-derived EphrinB2 can act through a contact-dependent mechanism through its receptor, EphB4, expressed on the surface of osteoblasts.^{105,106} Forward signaling of EphrinB2 through EphB4 has been shown to enhance osteogenic differentiation, while reverse signaling of EphB4 through EphrinB2 into OCPs can inhibit osteoclastogenesis by suppressing the c-Fos-NFATc1 cascade.^{105,106} Overexpression of EphB4 in osteoblasts increases bone mass in transgenic mice, while high levels of EphrinB2 over-expression induce the committal of MSCs

to an osteoblastic lineage.^{106–108} Another possible ephrin/Eph mechanism within the osteoblast lineage arises from the finding that PTH and PTHrP promote production by osteoblasts of ephrinB2, and that blockade of the interaction between EphrinB2 and receptor EphB4 impairs late-stage differentiation of osteoblasts, indicating a role for this pathway in promoting osteoblast differentiation and bone formation.¹⁰⁹

Control of bone remodeling can also occur through the semaphorin signaling system, including their receptors, PLXNs and NRPs. Of the eight classes of semaphorin family proteins categorized by structure and sequence similarities, SEMA4D and SEMA3A have shown particularly convincing and intriguing control over bone remodeling.¹¹⁰ Sema4D is a transmembrane protein that is highly expressed at the cell membrane of both OCPs and mature OCs, whereas its expression in OBs is undetectable.^{111,112} Of the three receptors to which SEMA4D can bind, its highest affinity is for the PLXNB1 receptor, which is strongly increased during OB differentiation but not osteoclastogenesis.¹¹³ The binding of SEMA4D to PLXNB1 impairs bone formation by inhibiting IGF-1 signals.¹¹² Treatment of OBs with recombinant SEMA4D enhances motility and impairs cell – cell interaction, suggesting that OC-derived SEMA4D is required for the proper positioning of OBs within the bone microenvironment.¹¹² Genetic deletion of SEMA4D or PLXNB1 or blocking SEMA4D signaling with neutralizing antibodies in mice causes increased trabecular bone volume.¹¹² Moreover, when SEMA4D was neutralized in OVX mice, bone formation was promoted without affecting bone resorption. Similar results were observed in a preclinical osteoporotic model when SEMA4D-targeting siRNA interfering molecules were specifically delivered to the bone using polymeric nanoparticles.¹¹⁴ Potent increases in trabecular bone volume are seen with SEMA4D silencing by enhancing OB number and activity, as indicated by the elevated mineral apposition rate.¹¹⁴ Interestingly, the number of OCs are unchanged suggesting SEMA4D regulates the activity of mature OCs rather than their maturation.¹¹⁴

The class III semaphorin, SEMA3A, is a secreted protein which exerts its biological activity through interactions with NRP1 and its subsequent complex formation with PLXNA1.^{115,116} NRP1 deficient mice display features of osteoporosis, which was reflected by both an increase in OC number and decrease in OB number.¹¹⁶ Interestingly, SEMA3A binding to NRP1 also disrupts the interaction between PLXNA1 and TREM2-DAP12, which is responsible for RANKL-induced osteoclastogenesis.¹¹⁶ Therefore, NRP1 is thought to compete with TREM2 for the PLXNA1 complex formation. When NRP1 expression is low, binding of PLXNA1 to TREM2 is favored, stimulating osteoclastogenesis; however, in the presence of SEMA3A, generation of the SEMA3A-NRP1-PLXNA1 complex is favored, inhibiting osteoclastogenesis. These findings suggested that SEM3A secreted by osteoblast lineage cells synchronously affects both osteoclasts and osteoblasts in paracrine and autocrine manners, respectively.

Like the effects of estrogen, SEMA3A is osteoprotective. The osteoprotective potential of SEMA3A is supported by some *in vitro* and preclinical studies. Treatment of OBs with recombinant SEMA3A activates Rac1 through FARP2, which facilitates the translocation of β -catenin into the nucleus bypassing the need for any canonical Wnt3A initiating signals.^{116–118} SEMA3A was also able to enhance bone regeneration in a cortical defect mouse model. Moreover, in a postmenopausal osteoporosis mouse model, SEMA3A treatment decreases bone loss after ovariectomy. These observations demonstrate that SEMA3A plays a crucial role in bone protection, yet no clear evidence that SEMA3A has similar bone protective effects in humans exists. To date, one cross-sectional study among postmenopausal women indicates that serum SEMA3A levels are positively with bone turnover as determined by serum osteocalcin levels. However, this association did not exist with BMD.¹¹⁹

Chapter 3. Comparable Responses of Osteoblast Lineage Cells to Microstructured Hydrophilic Titanium-Zirconium and Microstructured Hydrophilic Titanium

Abstract

Although titanium (Ti) is commonly used for dental implants, Ti alloy materials are being developed in order to improve their physical material properties. Studies indicate that osteoblast differentiation and maturation of human mesenchymal stem cells (MSCs) and normal human osteoblasts (NHOs) respond to microstructured Ti and titanium-aluminum-vanadium (Ti6Al4V) surfaces in a similar manner. The goal of this study was to determine whether this is the case for osteoblast lineage cells grown on microstructured TiZr surfaces and whether their response is affected by surface nanotexture and hydrophilicity. Grade 4 Ti and TiZr (13-17% Zr) discs were modified by large grit sand-blasting and acid-etching with storage in saline solution, resulting in a complex microstructured and hydrophilic surface corresponding to the commercially available implants SLActive® and Roxolid® SLActive® (Institut Straumann AG, Basel, Switzerland). The subsequent Ti modSLA and TiZr modSLA surfaces were characterized and osteogenic markers were measured. Evaluation of physical parameters revealed that the fabrication method was capable of inducing a microstructured and hydrophilic surface on both the Ti and TiZr discs. Overall the surfaces were similar, but differences in nanostructure morphology/density and surface chemistry were detected. On Ti modSLA and TiZr modSLA, osteoblastic differentiation and maturation markers were enhanced in both MSCs and NHOs while inflammatory markers decreased compared to TCPS. These results indicate a similar positive cell response of MSCs and NHOs when cultured on Ti modSLA and TiZr modSLA. Both surfaces were hydrophilic, indicating the importance of this property to osteoblast lineage cells.

Introduction

For the past two decades, titanium (Ti) has been the dominant material for dental implant applications due to its ability to form a passive oxide layer that makes it stable in biological systems.¹²⁰ Ti exhibits superior biocompatibility and corrosion resistance as a result of this passive layer when compared to other implant materials and contributes to its functional osseointegration with the surrounding bone tissue.¹²¹

Despite their high success rate, significant bone resorption in patients with Ti implants placed in close proximity to adjacent teeth as well as insufficient formation of peri-implant bone have been observed, particularly in patients with reduced or limited bucco-lingual and/or mesiodistal dimensions.¹²² Implants with reduced diameter (1.8 – 3.0 mm) have been used to prevent bone loss in these patients.¹²² While reduced diameter implants have reported retention rates of up to 100%, reducing the diameter of grade 4, commercially pure Ti (cpTi) implants compromises their mechanical properties, thereby increasing incidences of fatigue fracture and deformation from masticatory forces.^{123–128}

Alloying titanium is a common method used to increase the inherent strength of the implant material; however, the corrosion characteristics and toxicity of certain alloying components must be considered when selecting the appropriate material for surgical applications. Titanium-aluminum-vanadium alloy (Ti6Al4V) is frequently used for dental and orthopaedic implants and has shown good biocompatibility, stability, corrosion resistance, and mechanical properties. Recent studies have reported that components of Ti6Al4V may be gradually released over time.^{129–131} These ions, particularly vanadium, have been shown to cause adverse cells responses *in vitro*,^{131–137} although it is unclear whether a sufficient quantity of these ions will leach from an implant and cause a similar adverse reaction *in vivo*.

Using other alloying components that have elicited no adverse reactions *in vitro*, like zirconium (Zr), would avoid this outcome entirely.¹³⁸ An implant consisting of Ti alloyed with 13

to 17% Zr was developed by Institut Straumann AG (Basel, Switzerland). An analysis of the material properties of the TiZr alloy demonstrated a 40% increase in tensile strength and a 60% greater yield strength compared to the lower limit of the standard for cold worked grade 4 Ti, and 13 to 42% higher endurance levels when compared to cpTi of similar dimensions, while retaining superior corrosion resistance.^{35,139} The enhanced mechanical properties of the TiZr alloy make it an excellent candidate for small diameter implants.

Surface modifications that produce a complex micro-topography and increase hydrophilicity of dental implants have been shown to increase osteoblast differentiation, suggesting that they might also improve osseointegration, stability and retention of TiZr dental implants.^{23,29,55,61,140–145} One such surface modification involves sand-blasting and acid-etching cpTi with immediate storage in saline solution, used by Straumann for fabrication of their commercially available Ti SLActive® and Roxolid® (13 – 17% TiZr alloy) SLActive implants. Clinical studies have shown that the Roxolid® implant meets established dental implant survival criteria and has a high success rate in patients (ranging from 95.2 to 100%), acceptable bone-level changes, probing pocket depth, plaque and sulcus bleeding.^{146–148} Although both preclinical *in vivo* and clinical studies have concluded that cpTi and TiZr dental implants behave similarly,^{146,149–151} there are few *in vitro* data supporting these findings. Additionally, the available *in vitro* studies have been limited to characterizing the molecular level cellular response of the osteoblast-like MG63 cell line.³⁵ No study has directly compared the biological response of two key cell types important for osseointegration (progenitor cells and cells committed to an osteoblast phenotype) to cpTi and TiZr.

The method used to modify the surface of the SLActive® and Roxolid® implants is the same, but the differences in chemical composition result in varying surface characteristics, potentially influencing cell response in different ways.⁵² Therefore, the purpose of this study was to assess the osteoblastic differentiation and maturation of human mesenchymal stem cells (MSCs) and

normal human osteoblast (NH₄Ost) cells in response to grit-blasted, acid-etched and hydrophilic titanium-zirconium (TiZr modSLA) surfaces, and determine the similarity of these responses to those seen on grit-blasted, acid-etched, hydrophilic Ti (Ti modSLA).

Materials and Methods

Surfaces and Modifications

Grade 4 Ti and TiZr (13 – 17wt% Zr) discs, 5mm in diameter and 1mm in thickness, were provided by Institut Straumann AG (Basel, Switzerland). Discs were modified by the same protocol used to produce commercially available Ti SLActive® and Roxolid® SLActive® implants. Disc surfaces were first treated by large grit sand-blasting (250 – 500µm) followed by acid-etching in a boiling mixture of HCl and H₂SO₄ with immediate storage in 0.9% NaCl solution. The subsequent Ti modSLA and TiZr modSLA discs were sterilized using γ-irradiation.

Surface Characterization

Scanning Electron Microscopy (SEM)

Qualitative and quantitative characterization of the disc surface topography was evaluated using SEM (Ultra 60 FEG-SEM, Carl Zeiss SMT Ltd., Cambridge, UK). Secondary electron images were recorded at varying magnifications using an acceleration voltage of 5kV for three different samples (n=3). Morphometric quantification of nanostructure size and peak-to-peak distance was measured using ImageJ software (National Institutes of Health, USA). A grid composed of 20 evenly spaced squares arranged into a 4x5 matrix was superimposed onto the highest magnification SEM images. The diameter and peak distance to its closest neighbor were obtained for the centermost nanostructure within each square for a total of 60 measurements per material.

X-Ray Photoelectron Spectroscopy (XPS)

Chemical composition of the surface of the samples (n=3) was obtained by XPS (Thermo K-Alpha XPS, Thermo Fisher Scientific, Waltham, Massachusetts). Spectra were collected using

a 400 μ m X-ray spot size at three different locations on each individual sample.

Contact Angle Measurement

Measurements were obtained using a goniometer (CAM 250, Ramé-Hart, Mountain Lakes, NJ). Samples (n=3) were measured in three different locations and dried with nitrogen between each measurement. A drop size of 2 μ L was used per individual measurement and a contact angle was calculated every 5s for 20s. The four measurements were then averaged to obtain one of the three measurements per disc.

Confocal Laser Microscopy

Surface roughness of the samples (n=3) was evaluated using a confocal laser microscope (Lext, Olympus, Shinjuku, Tokyo, Japan). Three measurements per sample were taken over an area of 644 μ m x 644 μ m with a 20x objective and a scanning pitch of 50nm. A cutoff wavelength of 100 μ m was used when calculating surface roughness (S_a) and peak-to-valley height (S_z).

Cell Culture

We used two different cell cultured models to examine cell response. Normal human osteoblasts (NHOst cells) (Lonza Biosciences, Walkersville, MD), a non-transformed cell line obtained from normal human bone, were cultured using Dulbecco's modified Eagle medium (DMEM CellGro[®], Mediatech, Inc., VA) supplemented with 10% fetal bovine serum (FBS, Life Technologies, Carlsbad, CA) and 1% penicillin-streptomycin (Life Technologies). Human MSCs (Lonza Biosciences), originally isolated from normal human bone marrow and demonstrated to be multipotent, were cultured in MSC growth medium (Lonza Biosciences). All cells were cultured at 37°C in 5% CO₂ and 100% humidity. NHOst cells and MSCs were cultured on tissue culture polystyrene (TCPS) to facilitate determination of confluence. Test surfaces were Ti modSLA or TiZr modSLA. Cells were seeded on all groups at a density of 10,000 cells/cm² in a 96-well plate. After 24h, discs were transferred to a new 96-well plate with fresh medium and subsequently fed every 48h until confluence.

Cell Morphology

MSCs or NHOst cells were plated on Ti modSLA or TiZr modSLA at a density of 5,000 cells/cm² in a 96-well plate and media were changed after 24h. Cells were cultured for 72h, washed in PBS, and then fixed in 3.7% paraformaldehyde. After a 10min fixation, surfaces were washed with PBS, and permeabilized with 0.05% Triton X-100 for 10min. Surfaces were washed again with PBS, and incubated in a staining solution consisting of 0.165 μ M AlexaFluor 488 phalloidin (Life Technologies) and 2 μ g/mL Hoechst 33342 (Life Technologies) to visualize actin filaments and nucleic acids respectively. After staining, surfaces were mounted on glass cover slips using SlowFade (Life Technologies) and images were captured with a laser scanning microscope (Zeiss LSM 710, Carl Zeiss SMT Ltd., Cambridge, UK) at an excitation of 488nm for actin filaments and an excitation of 405nm for nucleic acids using a 40x objective.

Biological Response

At confluence, cells were incubated with fresh media for 24h. Media were collected and ELISAs used to measure levels of osteocalcin (Biomedical Technologies Inc., Stoughton, MA) osteoprotegerin (OPG, R&D Systems, Minneapolis, MN), vascular endothelial growth factor (VEGF, R&D Systems), bone morphogenetic protein-2 (BMP2, PeproTech, Rocky Hill, NJ), interleukin-6 (IL6, R&D Systems), and interleukin-10 (IL10, R&D Systems) following manufacturer's instructions. Cells attached to surfaces were washed twice with 0.2ml PBS. Three discs were combined in 0.5ml of 0.05% TritonX-100 for each individual sample in a total sample size of six (n=6). Cells were lysed by sonication at amplitude 40 using an ultrasonicator (Vibra-Cell, Sonics, Newtown, CT).

DNA content in the cell lysate was measured (QuantiFluor™ dsDNA system, Promega, Madison, WI) using a fluorescence detector (Synergy H1 Hybrid Reader, BioTek, Winooski, VT) at an excitation of 485nm and emission of 538nm. Immunoassay levels were normalized to DNA content. Cell lysate was also analyzed for alkaline phosphatase specific activity as the release

of *p*-nitrophenol from *p*-nitrophenylphosphate (Sigma-Aldrich, St. Louis, MO) at a pH of 10.25 and a temperature of 37°C. Absorbance was measured at 405nm and alkaline phosphatase activity was quantified using a standard curve. Activity was normalized to total protein content in the cell lysates, as determined by bicinchoninic acid protein assay kit (Thermo Fisher Scientific).

To quantify mRNA, cells were plated as described above. At confluence on TCPS, cells on all surfaces were incubated with fresh media for 12h. Samples were harvested using a TRIzol® (Invitrogen, Carlsbad, CA) extraction method. Six 5mm discs were combined in TRIzol® for each individual sample in a total sample size of six (n=6). RNA was quantified using a NanoDrop spectrophotometer (Thermo Fisher Scientific) and then reverse transcribed into 250 ng/μL cDNA. Real-time PCR was performed using a fluorescent dye (Power SYBR Green, Applied Biosystems, Foster City, CA) to quantify starting mRNA levels for integrin subunits alpha-1, alpha-2, alpha-5 and beta-1 (ITGA1, ITGA2, ITGA5, and ITGB1) and members of the bone morphogenetic protein (BMP) family: BMP4 and BMP7, BMP receptor-2 (BMPR2) and the BMP inhibitor Noggin (Nog). Levels of mRNA are normalized to glyceraldehyde phosphate dehydrogenase (GAPDH). Primer sequences are listed in **Table 1**.

Statistical Analysis

Surface characterization experiments and assessments of cell morphology were done using 3 discs per material. Data for surface analysis represent 3 measurements per disc, resulting in an n=9 per variable. Data are presented as the mean ± standard error (SE).

Table 1: Human Primers Used in Real-Time PCR Analysis

Gene	Primer Sequence
ITGα1	F CACTCGTAAATGCCAAGAAAAG
	R TAGAACCCAACACAAAGATGC
ITGα2	F ACTGTTCAAGGAGGAGAC
	R GGTCAAAGGCTTGTTTAGG
ITGα5	F ATCTGTGTGCCTGACCTG
	R AAGTTCCTGGGTGTCTG
ITGβ1	F ATTACTCAGATCCAACCAC
	R TCCTCCTCATTTTCATTCATC
BMP4	F ACGGTGGGAAACTTTTGATGTG
	R CGAGTCTGATGGAGGTGAGTC
BMP7	F AGCAGCAGCGACCCAGAGG
	R ACAGTAGTAGGCGGCGTAGC
BMPR1A	F CAAGAGGCATCTCAAGCAGCAG
	R CAGACCCACTACCAGACCTTTG
BMPR2	F TCTTTGCCCTCCTGATTCTTG
	R CATAGCCGTTCTTGATTCTGC
NOG	F QuantiTect primer assay,
	R QT00210833
GAPDH	F GCTCTCCAGAACATCATCC
	R TGCTTACCACCTTCTTG

For cell morphology, no quantitative analyses were performed. *In vitro* assays (n=6 cultures per variable) are presented as the mean \pm SE. All cell culture experiments were repeated at least three times to ensure validity of the results. Data shown in the figures are from representative experiments. Expression of mRNAs for BMPs, receptors, inhibitors and integrins are represented as treatment over control using the fold increase of Ti modSLA and TiZr modSLA compared to TCPS as an internal control for the experiment. QQ-plots (not reported) showed the data were normally distributed, and the Brown-Forsythe test indicated the data were homoscedastic. A parametric one-way analysis of variance was performed with a Bonferroni post-hoc correction and $\alpha = 0.05$ for the analysis of protein production. A Student's t-test was used to compare gene expression on the two test surfaces using an alpha of 0.05. All statistical analyses were performed using JMP statistical software (SAS, Cary, NC).

Results

Material Characterization

At low magnification, SEM images showed that the macroscale and microscale topography were similar for both surfaces (data not shown). However, SEM imaging at high magnification (**Fig.3A, B, C**) revealed larger and more exaggerated micro-scale surface features on Ti modSLA compared to TiZr modSLA (**Fig.3D, E, F**). Small, high density nanostructures were detected on Ti modSLA while large nanostructures at a lower density were observed on TiZr modSLA. Mean surface roughness (S_a) was greater on Ti modSLA compared to TiZr modSLA with no significant differences detected in mean peak-to-valley height (S_z) (**Fig.3G**). Morphometric analysis of the surface nanostructures (**Fig.3H**) reinforced the qualitative observations indicated by the SEM images. The mean nanostructure separation distance and nanostructure diameter were greater on TiZr modSLA when compared to Ti modSLA.

XPS (**Table 2**) indicated similar oxygen and carbon levels between Ti modSLA and TiZr modSLA. Unalloyed Ti modSLA had only Ti while TiZr modSLA displayed appreciable

percentages of Ti and Zr. Contact angle measured 0° for both surfaces.

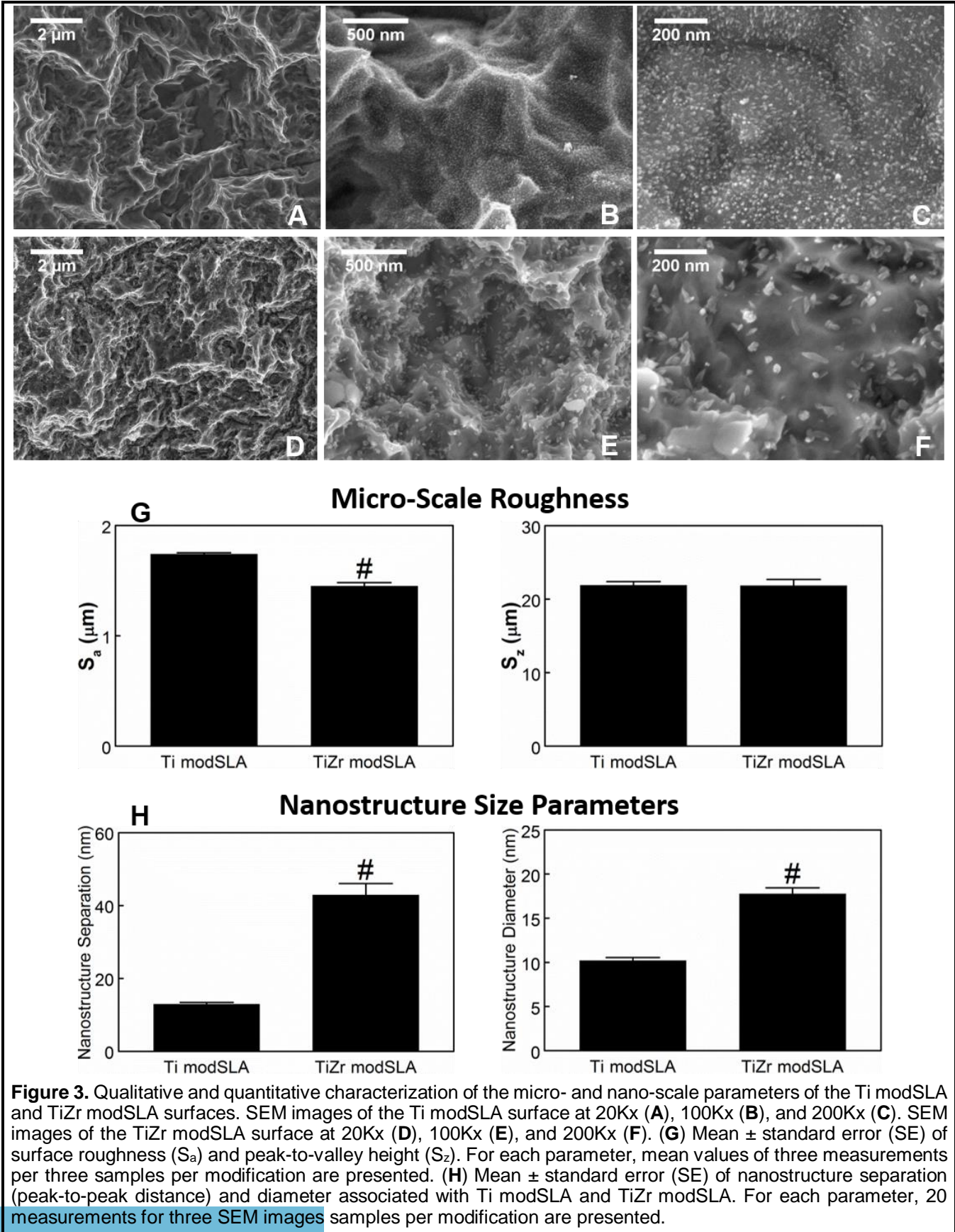


Table 2: Mean \pm standard deviation (SD) and median with interquartile range (IQR) of surface atomic concentration (%)

Surface	%O		%C		%Ti		%Zr	
	Mean	Median	Mean	Median	Mean	Median	Mean	Median
Ti modSLA	63.3 \pm 0.5	63.2 (62.2, 64.7)	14.8 \pm 0.6	14.7 (13.3, 16.4)	21.5 \pm 0.4	21.3 (20.7, 22.7)	0	0
TiZr modSLA	60.3 \pm 1.4	59.5 (57.1, 63.8)	17.4 \pm 1.3	15.9 (15.2, 20.2)	17.1 \pm 0.3	17.2 (16.2, 17.7)	3.6 \pm 0.2	3.6 (3.2, 3.8)

Cell Morphology

Figure 4 shows MSCs and NHOst cells superimposed on the rough metallic surfaces of Ti modSLA or TiZr modSLA (actin – green, DNA – blue). Parallel striations of the actin filaments could be seen surrounding the nucleus of each cell. The nuclei and actin filaments around the nucleus were localized to area of the cell that did not overlay the valleys (dark regions) of the substrate. In contrast, distal actin filaments spanned valleys, and many appeared to associate with rough peaks (light areas) of the surface.

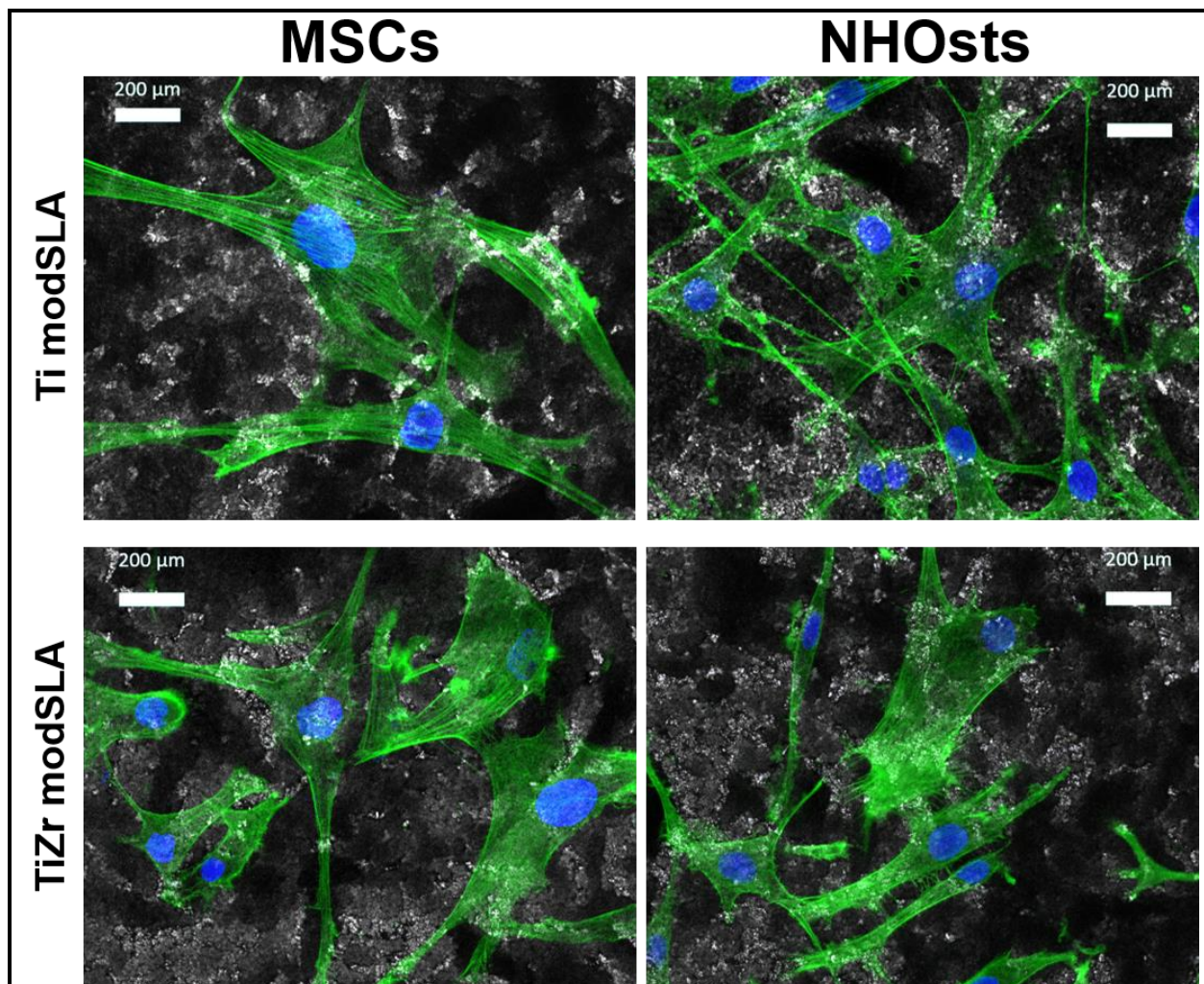


Figure 4. Cell staining of MSCs (left) and NHOst cells (right) on Ti modSLA or TiZr modSLA 72h after cell seeding. Actin filaments are stained green and nucleic acids are stained blue. Each image was taken using a 40x objective.

Biological Response

Cells grown on TiZr modSLA exhibited similar responses to those grown on Ti modSLA when compared to behavior on TCPS. DNA content was significantly lower on Ti modSLA and TiZr modSLA compared to TCPS for both MSCs (**Fig.5A**) and NHOst cells (**Fig.5B**), but DNA content of both MSC and NHOst cultures was greater on TiZr modSLA compared to Ti modSLA. Alkaline phosphatase specific activity was significantly higher on Ti modSLA and TiZr modSLA when compared to TCPS for both MSCs (**Fig.5C**) and NHOst cells (**Fig.5D**) (MSCs: Ti modSLA < TiZr modSLA; NHOst cells: Ti modSLA = TiZr modSLA). Production of osteocalcin (**Fig.5E, F**), osteoprotegerin (**Fig.5G, H**), VEGF (**Fig.6A, B**), and BMP2 (**Fig.6C, D**) was comparable in MSC and NHOst cultures grown on both Ti modSLA and TiZr modSLA and was greater than production on TCPS. IL6 production by MSCs (**Fig.6E**) and NHOst cells (**Fig.6F**) was significantly lower on Ti modSLA and TiZr modSLA compared to TCPS. No significant difference in MSC production of IL6 was detected between Ti modSLA and TiZr modSLA; however, IL6 production by NHOst cells was significantly lower on TiZr modSLA compared to Ti modSLA. IL10 was produced in greater amounts by both MSCs (**Fig.6G**) and NHOst cells (**Fig.6H**) on Ti modSLA and TiZr modSLA compared to TCPS. MSCs produced less IL10 on TiZr modSLA compared to Ti modSLA, but no significant difference was detected in NHOst cell IL10 production on these surfaces.

Compared to TCPS, significantly higher mRNA for BMP4, BMP7, BMPR2, and NOG were detected for MSCs and NHOst cells on Ti modSLA and TiZr modSLA (data not shown). There were some differences noted in gene expression in MSCs (**Fig.7A**) and NHOst cells (**Fig.7B**) grown on the test surfaces. BMP4 mRNA levels were higher for MSCs on TiZr modSLA compared to Ti modSLA; however, BMP4 mRNA levels were significantly lower for NHOst cells on TiZr modSLA compared to Ti modSLA. No significant differences were detected in MSC or NHOst cell BMP7, BMPR2, and NOG expression for cells cultured on either Ti modSLA or TiZr

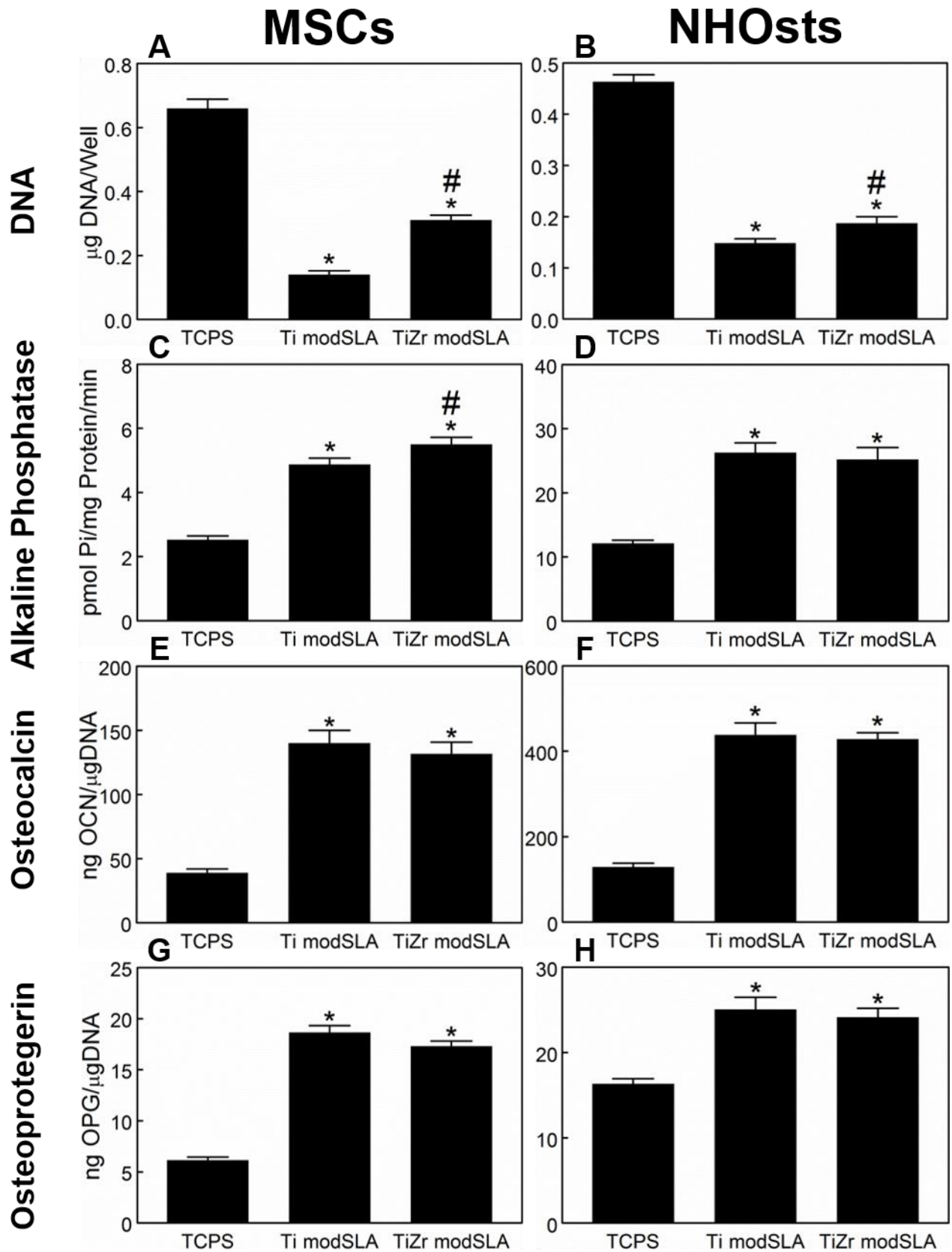


Figure 5. Effects of Ti modSLA and TiZr modSLA on the maturation of MSCs (left) and NHOst cells (right). MSCs and NHOst cells were plated separately on TCPS, Ti modSLA, or TiZr modSLA. At confluence on TCPS, cells were incubated in fresh media for 24h, collected, and measured for (A, B) DNA content, (C, D) alkaline phosphatase specific activity, (E, F) osteocalcin, and (G, H) osteoprotegerin. Data shown are the mean \pm standard error (SE) of six independent samples. * $p < 0.05$ vs. TCPS; # $p < 0.05$ vs. Ti modSLA.

modSLA. mRNA levels of ITG α 1, ITG α 2, and ITG β 1 were significantly higher on Ti modSLA and TiZr modSLA compared to TCPS, while mRNA levels of ITG α 5 were significantly lower for both MSCs and NHOst cells (data not shown). No significant differences in integrin expression were detected between MSCs plated on Ti modSLA or TiZr modSLA (**Fig.8A**); however, NHOst cell expression of ITG α 2 was significantly lower on TiZr modSLA compared to Ti modSLA (**Fig.8B**).

Discussion

This study examined the response of cells involved in implant osseointegration of clinically available TiZr implant surfaces in order to assess whether there are differences with their response to commercially pure Ti surfaces processed in an identical manner. This is important because TiZr alloy provides the mechanical strength needed for small diameter implants that are designed for patients with limited mandibular bone dimensions,³⁵ but less is known concerning the biological responses of osteoblast lineage cells to TiZr modSLA surfaces than is known concerning cell responses to Ti modSLA. Our results show that the surfaces are similar at the microscale but differ at the nanoscale. Cell number was higher on the hydrophilic TiZr surface than on hydrophilic cpTi, but osteoblastic differentiation of MSCs and osteoblastic maturation of NHOst cells were comparable. Moreover, production of factors that promote osteogenesis and vasculogenesis were comparable. MSCs and NHOst cells on both surfaces produced increased levels of the anti-inflammatory cytokine IL10 and reduced levels of the pro-inflammatory cytokine IL6. While responses to both surfaces were similar, the expression of mRNAs for BMP4, BMP7, and the BMP-inhibitor Noggin differed between the two cell types. MSCs expressed higher levels of BMP4 whereas NHOst cells expressed higher BMP7.

The morphology of the Ti modSLA and TiZr modSLA surfaces was not identical. Average roughness (S_a) of Ti modSLA was greater than was achieved on TiZr modSLA, although peak-to-valley height (S_z) was identical. SEM revealed the formation of nanostructures on the Ti modSLA and TiZr modSLA surfaces similar to those described in previous studies.^{52,63} There

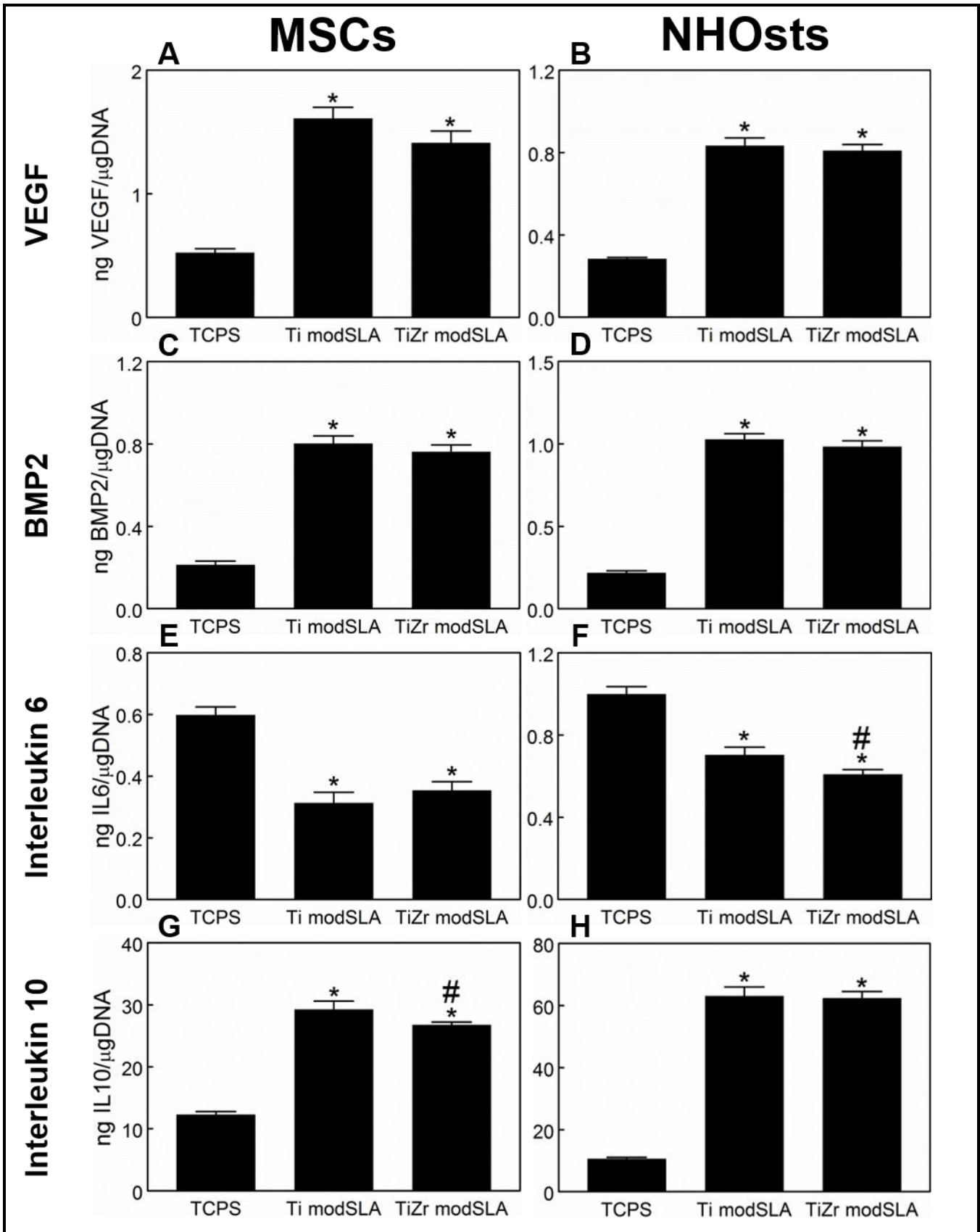


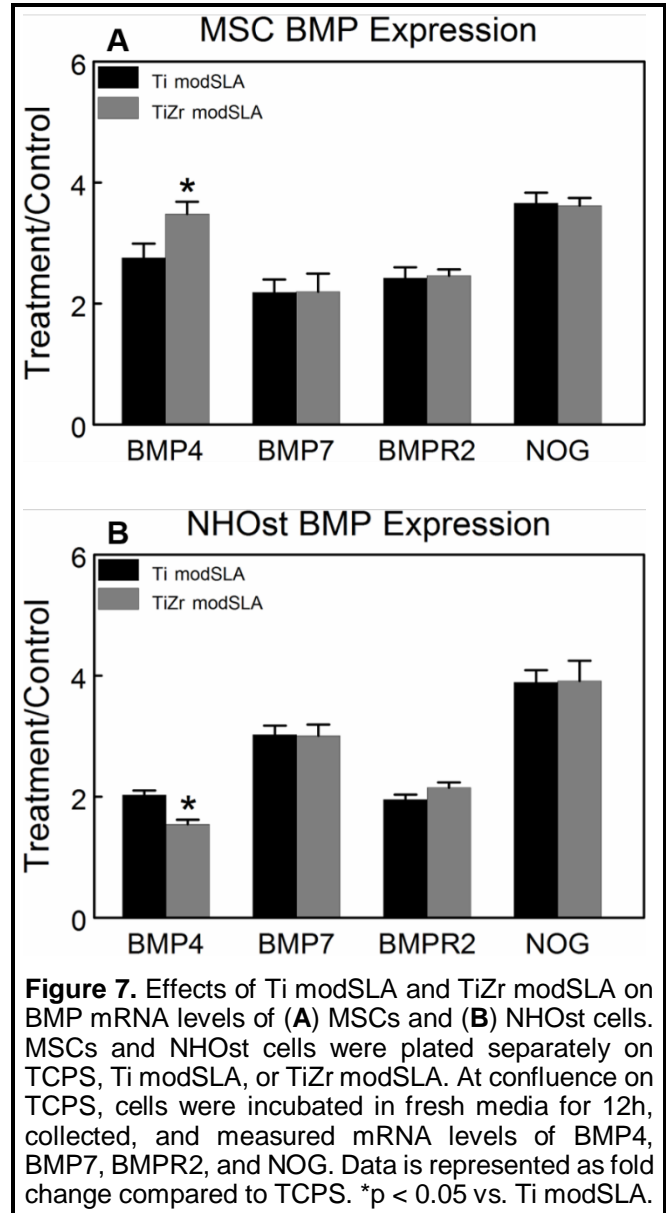
Figure 6. Effects of Ti modSLA and TiZr modSLA on the soluble factor production of MSCs (left) and NHOst cells (right). MSCs and NHOst cells were plated separately on TCPS, Ti modSLA, or TiZr modSLA. At confluence on TCPS, cells were incubated in fresh media for 24h, collected, and measured for (A, B) VEGF, (C, D) BMP2, (E, F) interleukin 6, and (G, H) interleukin 10. Data shown are the mean \pm standard error (SE) of six independent samples. * $p < 0.05$ vs. TCPS; # $p < 0.05$ vs. Ti modSLA.

were distinct differences in the size and distribution of the nanostructures, with diameters and distances between nanostructures being greater on TiZr modSLA.

The exact mechanism by which these nanostructures spontaneously generate is not known. Differences in the micro and nanoscale features of the Ti modSLA and TiZr modSLA surfaces following grit-blasting, acid-etching and storage in saline solution probably reflect differences in the Ti oxidation layer due to the underlying bulk material. The nanostructure is part of the oxide layer and grows as a result of the storage in saline solution (aqueous solution). The underlying bulk directly influences the oxide layer and thus the nanostructures depend on the bulk material.

Wennerberg et al. speculated that the different corrosion properties and thus different diffusion energies/behavior are responsible for the differences in nanostructures.⁵² Furthermore, they suggest that the hydride layer resulting from acid-etching might act as nucleation centers. We did not examine the underlying mechanisms that resulted in the differences in nanostructures, but our data indicate that they contributed to the overall biological response of the MSCs and NHOst cells. That nanoscale features can impact cell response has been noted by us as well as others.^{51,142,152–154}

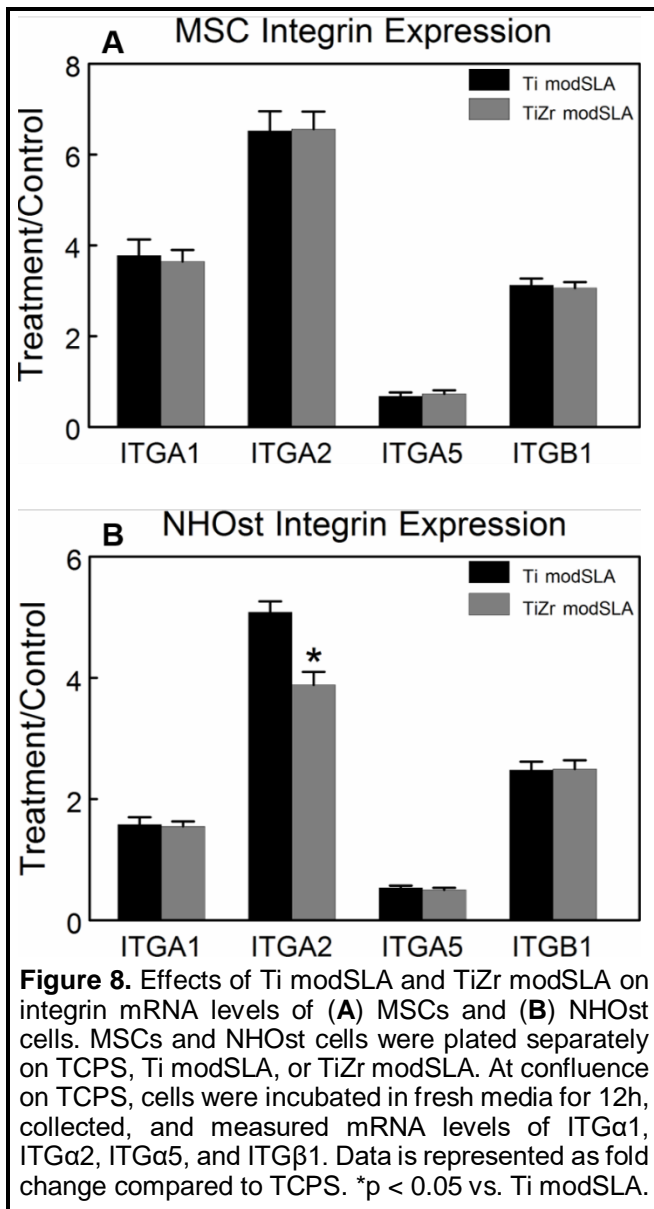
The surface energy of the two metals used in this study was indirectly measured using contact angle measurements to assess the surface hydrophilicity and XPS to determine the amount of surface carbon contamination.



These measurements confirmed that the sand-blasting/acid-etching procedure with subsequent storage in saline solution induced a comparable surface energy between the two metals. In addition to detecting differences in bulk material using the presence or absence of zirconium, XPS showed increased oxygen and decreased carbon content and thus low level of carbon contamination. Contact angles measured 0° , demonstrating the surfaces of Ti modSLA and TiZr modSLA to be super-hydrophilic, consistent with the results of XPS and previous studies.^{52,71,155}

These results also suggest that the retention of a clean surface via prevention of hydrocarbon adsorption was a critical processing step. Variations in surface topography at the microscale and nanoscale can cause patterning of hydrophobic and hydrophilic regions,¹⁵⁶ which can impact protein adsorption and ultimately integrin signaling. We did not compare dry microstructured Ti and TiZr to determine if such patterning had occurred, but our results indicate that the aqueous storage mitigated this occurring. Moreover, there were no visible differences in cell morphology or actin filament alignment to indicate a difference in attachment by either cell type on either surface. Our results indicate that both surfaces supported osteoblast differentiation of MSCs. The cells adopted a branched and elongated phenotype on the surface consistent with commitment to an osteogenic lineage rather than to adipogenic differentiation. As noted previously the cells tended to attach to the peaks via filopodia and suspend the cell body over valleys.¹⁵⁷

The qualitative capacity for Ti modSLA and TiZr modSLA to support a healthy osteoblastic phenotype is supported quantitatively using measurements of osteoblastic markers of differentiation and maturation. For both cell types, DNA content was decreased on both surfaces compared to TCPS, a trend described previously in studies comparing TCPS to Ti modSLA^{61,144,158} and TiZr modSLA.³⁵ DNA content was greater on TiZr modSLA compared to Ti modSLA supporting the report that MC3T3-E1 osteoblasts exhibited greater attachment to a smooth TiZr (50% Zr) alloy compared to smooth cpTi.¹⁴⁵ Together, these results suggest the



possibility that cells can attach or proliferate more readily on the surface of a TiZr alloy compared to cpTi. Overall, however, osteoblast differentiation on the two surfaces was comparable with respect to alkaline phosphatase specific activity and production of osteocalcin, osteoprotegerin, VEGF, and BMP2. Moreover, MSCs and NHOst cells exhibited comparable production of immune mediators on both surfaces. As noted previously for cells grown on Ti modSLA,¹⁵⁸ production of the pro-inflammatory cytokine IL6 was reduced and production of the anti-inflammatory cytokine IL10 was increased by cells grown on TiZr modSLA.

Expression of genes encoding for additional osteoblastic proteins by MSCs and NHOst cells

were similarly enhanced on Ti modSLA and TiZr modSLA. mRNA levels of BMPs (BMP4, BMP7), BMPR2 receptor, and NOG antagonist were increased to comparable levels by both cell types on modified surfaces compared to TCPS. Studies have demonstrated that BMPs are important factors for stimulating an osteogenic environment, which facilitates osteoblastic differentiation and maturation,^{159,160} and the signaling of BMPs is mediated by activation of their receptors and modulated by their antagonists. Promotion of the optimal osteogenic environment requires a delicate balance among these factors. As seen previously, the expression of BMP complexes was sensitive to microrough, nanostructured, and hydrophilic Ti;^{71,158} a result that

was not altered on TiZr modSLA. The small differences detected in BMP4 production were attributed to the intricate nature of the BMP system and do not reflect a preference toward either surface material.

A similar result was also observed for the expression of integrin subunits. The α and β integrin subunit combinations determine which extracellular matrix proteins will be recognized by a cell, thus dictating cellular interactions with implanted materials by sending important information to the cell in order to maintain a healthy osteoblastic phenotype.¹⁶¹ Ti modSLA and TiZr modSLA were able to similarly enhance the expression of osteoblastic integrin subunits ITG α 1, ITG α 2, and ITG β 1 while decreasing the expression of ITG α 5 by both MSCs and NHOst cells when compared to TCPS. Osteoblasts primarily express α 5 β 1 when grown on TCPS but shift to the production of α 1 β 1 and α 2 β 1 when grown on rough Ti substrates.¹⁶¹ α 2 β 1 is further increased on surfaces exhibiting high surface energy in the presence of nanostructures,^{155,161–163} a trend that remains consistent when the bulk material of the surface is altered.

It is evident that MSC and NHOst osteoblastic differentiation and maturation have no significant preference to either Ti modSLA or TiZr modSLA, confirming the results observed both *in vivo* and clinically.^{146,149–151} Interestingly, this result was achieved despite differences in bulk material composition and surface roughnesses at both the micro- and nanoscale. This alludes to the possibility that a super-hydrophilic surface can conceal any modulatory effects the surface nanostructures may have had on the osteoblastic differentiation and maturation of MSCs and NHOst cells. Previous studies have reported the positive effects nanostructures have on osteoblastic differentiation and maturation over a range of varying morphologies.^{51,142,164} However, these surfaces were not considered to be super-hydrophilic leaving unanswered questions regarding the degree to which a super-hydrophilic surface is able to overpower the effects of nanostructures. Because of the similar cellular response between the two materials it can be assumed that implants composed of either cpTi or 13 – 17% TiZr subjected to a similar

sandblasting and acid-etching procedure will achieve similar levels of osseointegration when used clinically.

Overall, these results indicate that the in vitro outcomes observed with Ti modSLA, which have been shown to have a positive correlation with clinical outcomes,¹⁶⁵ are also demonstrated in MSC and NHOst cells grown on TiZr modSLA. Many other cell types are involved in osseointegration and subsequent remodeling of the peri-implant bone, which were not examined in this study. Moreover, we used commercially available MSCs and NHOst cells, which were from single donors. Thus, our results do not consider variability inherent to the human population, or the health status of the donors themselves. Despite these caveats, our data support the hypothesis that osteoblastic differentiation and maturation in response to the modSLA surface contribute to the clinical performance of TiZr implants.^{146,148,166}

Conclusions

Ti and TiZr were successfully modified to enhance surface hydrophilicity, create micro-roughness, and induce nanostructure formation. The surfaces at the micron scale achieved by grit-blasting and acid-etching were similar and similar degrees of surface energy were obtained for both materials. Differences in bulk material led to variations in surface nanostructure morphology and density, osteoblastic differentiation and maturation of MSCs and NHOst cells were enhanced on both Ti modSLA and TiZr modSLA to a comparable extent. It can be indirectly concluded that the clinical use of 13 – 17% TiZr alloyed metals for dental implants will lead to a successful outcome comparable to those observed with cpTi.

Chapter 4. Osteogenic Response of Human MSCs and Osteoblasts to Hydrophilic and Hydrophobic Nanostructured Titanium Implant Surfaces

Abstract

Microstructured implant surfaces created by grit blasting and acid etching titanium (Ti) support osseointegration. This effect is further enhanced by storing in aqueous solution to retain hydrophilicity, but this also leads to surface nanostructure formation. The purpose of this study was to assess the contributions of nanostructures on the improved osteogenic response of osteoblast lineage cells to hydrophilic microstructured Ti. Human mesenchymal stem cells (MSCs) and normal human osteoblasts (NHOs) were cultured separately on non-nanostructured/hydrophobic (SLA), nanostructured/hydrophilic (modSLA), or nanostructured/hydrophobic (SLAnano) Ti surfaces. XPS showed elevated carbon levels on SLA and SLAnano compared to modSLA. Contact angle measurements indicated only modSLA was hydrophilic. Confocal laser microscopy revealed minor differences in mean surface roughness. SEM showed the presence of nanostructures on modSLA and SLAnano. MSCs and NHOs cells exhibited similar morphology on the substrates and osteoblastic differentiation and maturation were greatest on modSLA. These results suggest that when the appropriate microstructure is present, hydrophilicity may play a greater role in stimulating MSC and NHOs osteoblastic differentiation and maturation than the presence of nanostructures generated during storage in an aqueous environment.

Introduction

Successful dental implantation is measured by the degree of osseointegration between the surface of the implant material and bone tissue.^{167,168} Surface modifications altering implant topography^{140,169} and energy^{23,144} on titanium (Ti) and Ti-based alloys^{141,145} have been heavily emphasized in current research efforts in order to overcome problems associated with

osseointegration. Surface roughness at the micro-level enhances osteoblast differentiation and local factor production^{30,31,61,142,170,171} by mimicking resorption pit structural features¹⁷². Microscale and submicroscale features are sensed by osteoblast lineage cells via integrin alpha-1,beta-1 ($\alpha1\beta1$) and alpha-2,beta-1 ($\alpha2\beta1$) signaling,^{155,157,161,173} leading to osteoblast differentiation of mesenchymal stem cells (MSCs) and maturation of committed osteoblasts (NHOst cells)¹⁷³ and osteoblast-like MG63 cells.¹⁶¹

Recent studies have suggested that nanostructured topography provides a surface structure much more analogous to that of natural bone.^{142,164,174–177} Nanoscale surface features mimic the extracellular matrix with which cells normally interact, thereby influencing the type, quantity, and adsorbed protein conformation, integrin signaling, and signaling pathways that work together to control cellular adhesion, proliferation, and differentiation.¹⁷⁸ However, many studies examining the role of nanotopography have used patterned tissue culture polystyrene (TCPS) as the substrate,^{154,179,180} which is very different from materials used clinically such as Ti. Thus, it is difficult to extrapolate the reported findings to implant surface effects.

Hydrophilic (high energy) implant surfaces have also been shown to improve clinical outcomes,^{23,144} particularly when the surface is microtextured.¹⁵⁵ Recently it was shown that when grit blasted/acid etched Ti implants were stored in water or saline to retain their hydrophilic surface post-processing, nanostructures formed on the surface due to reorganization of the outermost oxide layer.⁵² It is not clear what contribution the nanostructures make to the improved osseointegration seen with hydrophilic, microtextured Ti implants.¹⁸¹ Nonetheless, many studies have suggested the importance of a nanostructured surface for facilitating osteoblast differentiation and maturation *in vitro*.^{51,61,182} Furthermore, an *in vivo* rabbit study by Wennerberg et al., which used disc implants, suggests that the presence of nanostructures is beneficial for new bone formation.¹⁸³

The hypothesis of the present study is that nanostructures generated by storage in saline will

impact the overall biological response to hydrophilic, microstructured Ti. To do this, we cultured human MSCs and NHOst cells on Ti surfaces that were fabricated using the same methods employed for production of commercially available implants. Ti discs were grit blasted and acid etched, then stored in air (SLA); grit blasted, acid etched, and stored in saline (modSLA); or grit blasted, acid etched, stored in saline to generate nanostructures, then dried and stored in air (SLAnano). This experimental design enabled comparison of hydrophilicity + nanostructures; hydrophobicity + nanostructures; and hydrophobicity without nanostructures.

Materials and Methods

Ti Disc Preparation

5 mm diameter and 1 mm thick discs were fabricated from Grade 4 Ti and subjected to one of the following modifications.

SLA

Sand-blasted with large grit particulate (250 – 500 μm corundum) followed by acid etching in a boiling mixture of HCl and H₂SO₄. Discs were cleaned in HNO₃, rinsed in ultrapure water, packed in aluminum foil, and γ -irradiated before use.

modSLA

Same initial sandblasting and acid etching procedure as used for SLA samples, but subsequent steps took place under nitrogen to prevent exposure to air. The discs were rinsed, stored in 0.9% NaCl solution, and γ -irradiated before use.

SLAnano

modSLA samples that were removed from 0.9% NaCl solution after aging 5 weeks, a procedure outlined by Wennerberg et al. Once removed from solution, samples were rinsed in ultrapure water, packed in aluminum foil, and γ -irradiated before use.

Surface Characterization

Scanning Electron Microscopy (SEM)

Surface topography was qualitatively evaluated using SEM (Ultra60 FE-SEM, Zeiss). Six images at varying magnifications were captured on each of n=3 discs per surface modification using 5 kV accelerating voltage for a total of 18 images per modification.

X-ray Photoelectron Spectroscopy (XPS)

Chemical composition of the samples (n=3) was obtained from the sample surfaces by XPS (Thermo K-Alpha XPS, Thermo Fisher Scientific). Spectra were collected using a 400 μm X-ray spot size at three different locations on each individual sample.

Contact Angle Measurement

Measurements were obtained using a goniometer (CAM 250, Ramé-Hart). Samples (n=3) were measured in three different locations and dried with nitrogen between each measurement. A drop volume of 2 μL was used per individual measurement and a contact angle was calculated every 5 seconds for 20 seconds. The four measurements were then averaged together to obtain one of the three measurements per disc.

Confocal Laser Microscopy (CLM)

Surface roughness of the samples (n=3) was evaluated using a confocal laser microscope (Lext, Olympus). Three measurements per sample were taken over an area of 644 μm x 644 μm with a 20x objective and a scanning pitch of 50 nm. A cutoff wavelength of 100 μm was used when calculating surface roughness (S_a) and peak-to-valley height (S_z).

Cell Culture

Human MSCs (Lonza Biosciences, Walkersville, MD) were cultured in MSC growth medium (MSCGM; Lonza Biosciences). NHOst cells (Lonza Biosciences) were cultured using Dulbecco's modified Eagle medium (DMEM CellGro[®]; Mediatech, Inc., VA) supplemented with 10% fetal bovine serum (FBS, Life Technologies, Carlsbad, CA) and 1% penicillin-streptomycin (Life Technologies). All cells were 4th passage and cultured at 37°C in 5% CO₂ and 100% humidity. MSCs and NHOst cells were cultured on unmodified/non-patterned tissue culture polystyrene

(TCPS), SLA, SLAnano, or modSLA at a density of 10,000 cells/cm² in a 96-well plate. After 24 h, discs were transferred to a new 96-well plate with fresh medium and subsequently fed every 48 h until confluence.

Cell Morphology

MSCs and NHOst cells were plated on SLA, SLAnano, or modSLA at a density of 5,000 cells/cm² in a 96-well plate and media were changed after 24 h. Cells were cultured for 72 h, washed in PBS, and then fixed in 3.7% paraformaldehyde. After a 10 min fixation, surfaces were washed with PBS, and permeabilized with 0.05% Triton X-100 for 10 min. Surfaces were washed again with PBS, and incubated in a staining solution consisting of 0.165 μ M AlexaFluor 488 phalloidin (Life Technologies) and 2 μ g/mL Hoechst 33342 (Life Technologies) to visualize actin filaments and nucleic acids respectively. After staining, surfaces were mounted on glass cover slips using SlowFade (Life Technologies) and images were captured with a Laser Scanning Microscope (Zeiss LSM 710, Carl Zeiss SMT Ltd., Cambridge, UK) at an excitation of 488 nm for actin filaments and an excitation of 405 nm for nucleic acids using a 40x objective.

Biological Response

At confluence, cells were incubated with fresh media for 24 h. Media were collected and ELISAs were used to measure levels of osteocalcin (Biomedical Technologies Inc., Stoughton, MA), osteoprotegerin (R&D Systems, Minneapolis, MN), vascular endothelial growth factor-A (VEGF, R&D Systems), bone morphogenetic protein-2 (BMP2, PeproTech, Rocky Hill, NJ), interleukin 6 (IL6, R&D Systems), and interleukin 10 (IL10, R&D Systems) following manufacturer's instructions. Cells attached to surfaces were washed twice with 0.2 ml PBS. Three 5 mm discs were combined in 0.5 ml of 0.05% TritonX-100 for each individual sample in a total sample size of six (n=6). Cells were lysed by sonication at amplitude 40 using an ultrasonicator (Vibra-Cell, Sonics, Newtown, CT).

DNA content in the cell lysate was measured (QuantiFluor™ dsDNA system, Promega,

Madison, WI) using a fluorescence detector (Synergy H1 Hybrid Reader, BioTek, Winooski, VT) at an excitation of 485 nm and emission of 538 nm. Immunoassay levels were normalized to DNA content. Cell lysate was also analyzed for alkaline phosphatase specific activity as the release of *p*-nitrophenol from *p*-nitrophenylphosphate (Sigma-Aldrich, St. Louis, MO) at a pH of 10.25 and a temperature of 37°C. Absorbance was measured at 405 nm and alkaline phosphatase activity was quantified using a standard curve. Activity was normalized to total protein content in the cell lysates, as determined by bicinchoninic acid protein assay kit (Thermo Fisher Scientific).

To quantify mRNA, cells were plated as described above. At confluence on TCPS, cells were incubated with fresh media for 12 h. Samples were harvested using a TRIzol® (Invitrogen, Carlsbad, California) extraction method. Six 5 mm discs were combined in TRIzol® for each individual sample in a total sample size of six (n=6). RNA was quantified using a NanoDrop spectrophotometer (Thermo Fisher Scientific) and then reverse transcribed into 250 ng/μL cDNA. Real-time PCR was performed using a fluorescent dye (Power SYBR Green, Applied Biosystems, Foster City, CA) and StepOnePlus™ Real-Time PCR system (Applied Biosystems) to quantify starting mRNA levels using gene specific primers (**Table 1**). Specific genes were amplified for 40 cycles and levels of mRNA were normalized to GAPDH.

Statistical Analysis

Data from surface characterization experiments are presented as the mean ± standard error (SE). Data for surface analyses represent 3 measurements per disc, resulting in an n=9 per variable. For cell morphology, no quantitative analyses were performed. All cell culture experiments had an N=6 independent cultures for each variable. Experiments were repeated at least three times to ensure validity of the results. Data from individual experiments were not combined and data shown in the figures are from representative experiments. A one-way analysis of variance was performed followed by a Bonferroni correction to maintain an

experiment-wise error rate (α) of 0.05. All statistical analyses were performed using JMP statistical software.

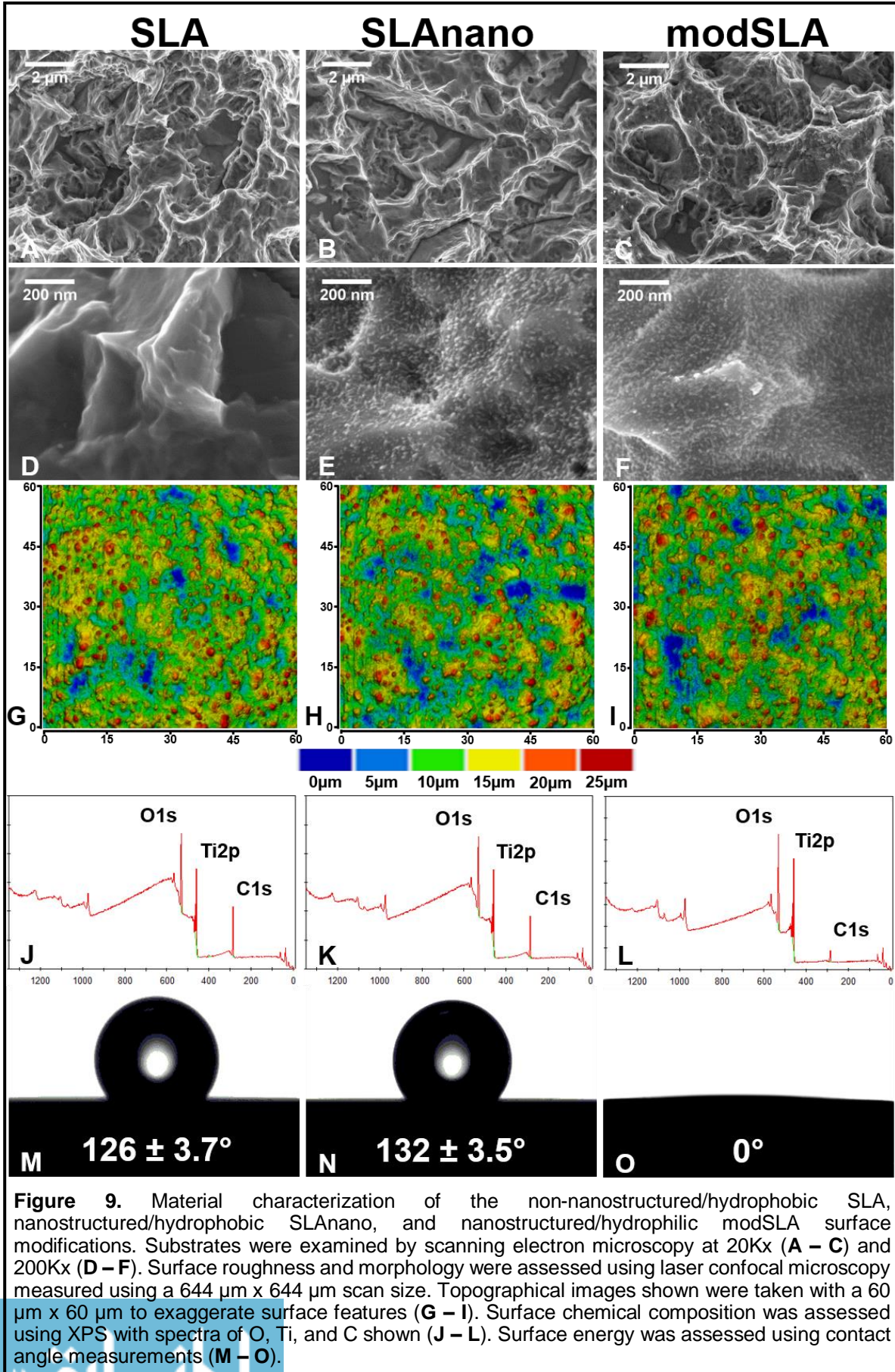
Results

Material Characterization

Low magnification SEM imaging (**Fig.9A – C**) revealed a similar topography among SLA, SLAnano, and modSLA. Confocal microscopy confirmed these qualitative observations (**Fig.9G – I**), resulting in no significant differences among the mean surface roughness's (S_a) or the mean peak-to-valley height (S_z) of the SLA ($S_a = 1.65 \pm 0.01 \mu\text{m}$; $S_z = 23.17 \pm 0.82 \mu\text{m}$), SLAnano ($S_a = 1.79 \pm 0.03 \mu\text{m}$; $S_z = 25.55 \pm 0.80 \mu\text{m}$), and modSLA ($S_a = 1.74 \pm 0.01 \mu\text{m}$; $S_z = 21.88 \pm 0.51 \mu\text{m}$). At a higher SEM magnification, no nanostructures were observed on SLA (**Fig.9D**) while similar needle-like nanostructures were observed on SLAnano (**Fig.9E**) and modSLA (**Fig.9F**). Using ImageJ software (National Institutes of Health, USA), a morphometric analysis was conducted by superimposing a grid composed of 20 evenly spaced squares arranged into a 4x5 matrix onto the highest magnification SEM images. The diameter and peak distance to its closest neighbor were obtained for the centermost nanostructure within each square for a total of 60 measurements per material. Differences between SLAnano and modSLA mean nanostructure diameter ($11.44 \pm 0.38 \text{ nm}$; $10.21 \pm 0.34 \text{ nm}$, respectively) and mean nanostructure separation ($18.87 \pm 0.7 \text{ nm}$; $12.95 \pm 0.5 \text{ nm}$, respectively) were observed.

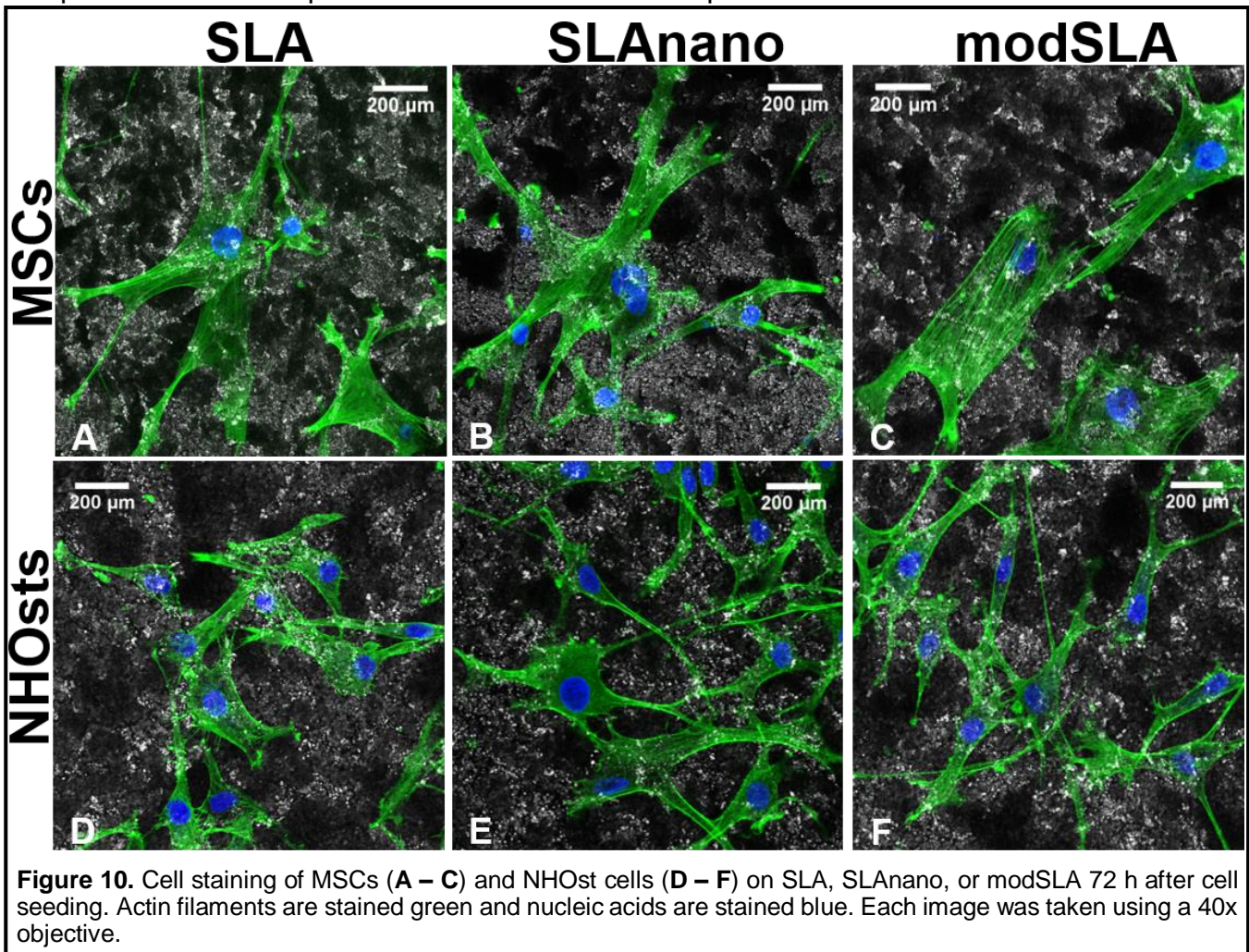
XPS survey spectra displayed titanium (Ti), oxygen (O), and carbon (C) as the main atomic components of the SLA, SLAnano, and modSLA surfaces (**Fig.9J – L**). The chemical composition was almost identical between SLA and SLAnano with spectral analyses indicating a high presence of Ti, O, and C. The spectral analysis for modSLA revealed a lower quantity of C compared to that detected on SLA and SLAnano. Measured contact angles are also shown in **Figure 9**. SLA (**Fig.9M**) and SLAnano (**Fig.9N**) had hydrophobic surfaces with contact angles of $126 \pm 4^\circ$ and $132 \pm 4^\circ$ respectively while modSLA (**Fig.9O**) had a hydrophilic surface with 0°

contact angle.



Cell Morphology

Figure 10 shows both the stained components of the MSCs and NHOst cells superimposed with the rough metallic surfaces of the SLA, SLAnano, and modSLA (actin – green; DNA – blue). Striations of the actin filaments and the nucleus can be visualized in each of the images. The actin filaments in both cell types adopted a parallel orientation that did not exhibit a preference for any particular structure. Nuclei and the immediate surrounding actin filaments mostly avoid the valleys (dark areas) of the rough surfaces; however, the more distal actin filaments can be seen spanning valleys. MSCs and NHOst cells cultured on TCPS exhibited morphologies comparable to those reported in the literature for non-patterned TCPS.



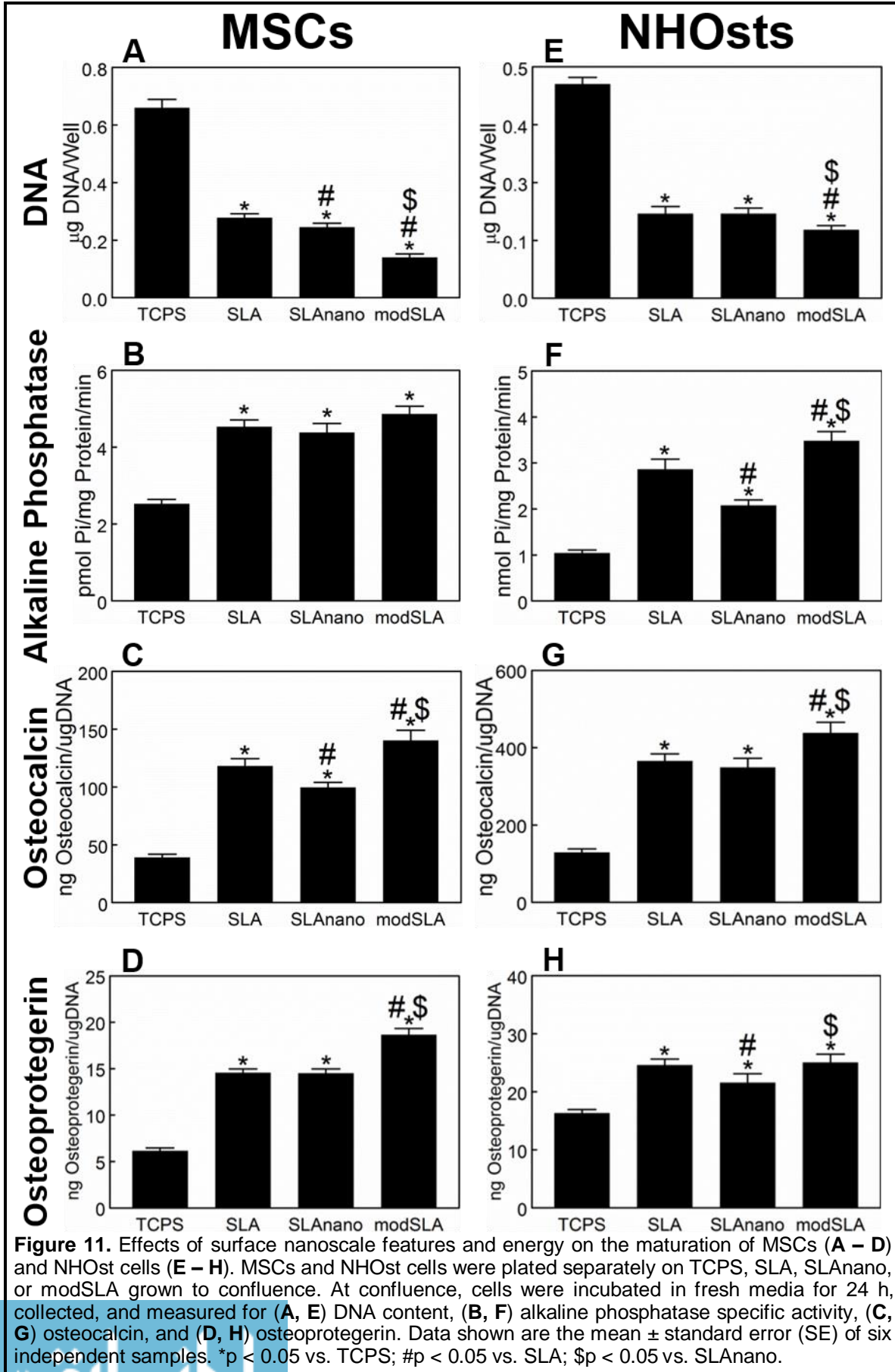
Biological Response

DNA content was significantly lower on SLA, SLAnano, and modSLA compared to TCPS for both MSCs (**Fig.11A**) and NHOst cells (**Fig.11E**) with modSLA exhibiting significantly lower DNA

compared to SLA and SLAnano. Compared to TCPS, MSCs and NHOst cells cultured on SLA, SLAnano, and modSLA had significantly higher alkaline phosphatase specific activities (**Fig.11B, F**) and production of osteocalcin (**Fig.11C, G**) and osteoprotegerin (**Fig.11D, H**). Alkaline phosphatase specific activity in the MSC cultures was comparable on the modified surfaces. MSCs cultured on modSLA produced significantly higher osteocalcin and osteoprotegerin compared to SLA and SLAnano with SLAnano producing significantly lower osteocalcin compared to SLA. Alkaline phosphatase specific activity and osteocalcin production by NHOst cells were significantly higher compared to SLA and SLAnano with significantly lower alkaline phosphatase specific activity detected on SLAnano compared to SLA. No significant differences in NHOst osteoprotegerin production were detected between modSLA and SLA; however, production on both was significantly greater compared to SLAnano.

MSCs and NHOst cells cultured on modified surfaces produced significantly higher quantities of VEGF (**Fig.12A, E**), BMP2 (**Fig.12B, F**), and the anti-inflammatory cytokine IL10 (**Fig.12C, G**) compared to those cultured on TCPS. The opposite effect was observed for the production of the pro-inflammatory cytokine IL6 (**Fig.12D, H**) where significantly lower quantities were detected on modified surfaces compared to TCPS. VEGF, BMP2, and IL10 production by MSCs was significantly greater on modSLA compared to SLA and SLAnano with a significantly lower production detected on SLAnano compared to SLA. No significant differences were detected in NHOst VEGF production among modified surface. NHOst cells cultured on SLAnano produced significantly lower quantities of BMP2 compared to SLA and modSLA which were not significantly different from each other. IL10 production by NHOst cells was significantly higher on modSLA compared to SLA and SLAnano with a significantly lower production detected on SLAnano compared to SLA. Both MSCs and NHOst cells cultured on modSLA exhibited significantly lower productions of IL6 compared to SLA and SLAnano. No significant differences were detected between MSC IL6 production between SLA and SLAnano while NHOsts produced

a significantly lower amount of IL6 on SLAnano compared to SLA.



BMPs, receptor, and antagonist expression are shown in **Figure 13**. Compared to TCPS, significantly higher mRNA expressions of BMP4, BMP7, BMPR1A, and NOG were detected for MSCs (**Fig.13A – D**) and NHOst cells (**Fig.13E – H**) on SLA, SLAnano, and modSLA. MSCs cultured on modSLA had significantly higher expressions of each gene with significantly lower BMP4 and NOG expressions detected on SLAnano compared to SLA. NHOst cells cultured on modSLA exhibited significantly higher expressions of BMP4, BMP7, and NOG compared to SLA and SLAnano. SLAnano significantly upregulated NHOst BMPR1A expression compared to SLA and modSLA. NHOst NOG expression was significantly greater on SLAnano compared to SLA.

mRNA levels of ITG α 1 (**Fig.14A, E**), ITG α 2 (**Fig.14B, F**) and ITG β 1 (**Fig.14D, H**) were significantly higher on modified surfaces compared to TCPS for both cell types. Additionally, MSC and NHOst ITG α 5 (**Fig.14C, G**) expression was significantly lower on modified surfaces compared to TCPS except for MSCs cultured on SLAnano which was significantly greater. MSCs cultured on modSLA exhibited significantly higher mRNA levels of ITG α 1, ITG α 2, and ITG β 1 compared to SLA and SLAnano with significantly lower mRNA levels of ITG α 1 and ITG β 1 on SLAnano compared to SLA. No significant difference was detected in MSC ITG α 2 mRNA levels between SLA and SLAnano. Among modified surfaces, NHOst expression of ITG α 1 was not significantly different. NHOst cells cultured on modSLA had significantly higher ITG α 2 and ITG β 1 mRNA levels compared to SLA and SLAnano. MSCs and NHOst cells cultured on SLAnano exhibited significantly higher ITG α 5 expression compared to SLA and modSLA. No significant differences were detected between SLA and modSLA MSC ITG α 5 expression while NHOst ITG α 5 expression was significantly lower on modSLA compared to SLA.

Discussion

Implant surface properties dictate the resulting molecular events that take place at the cell-material interface. Studies have highlighted the importance of surface properties such as roughness, topography, chemistry, and energy in the modulation of cell proliferation and

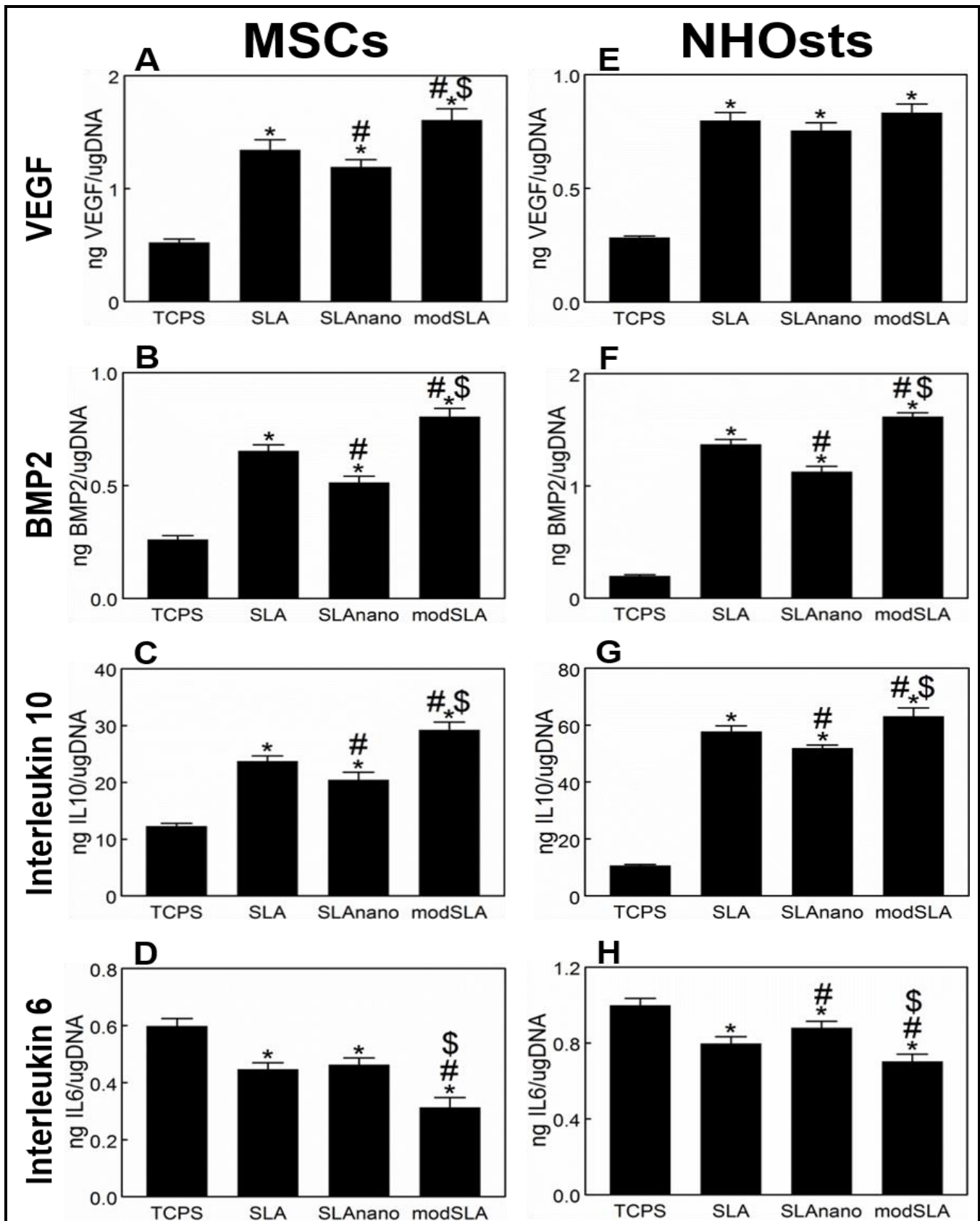


Figure 12. Effects of surface nanoscale features and energy on the soluble factor production of MSCs (A – D) and NHOst cells (E – H). MSCs and NHOst cells were plated separately on TCPS, SLA, SLAnano, or modSLA grown to confluence. At confluence, cells were incubated in fresh media for 24 h, collected, and measured for (A, E) VEGF, (B, F) BMP2, (C, G) interleukin 10, and (D, H) interleukin 6. Data shown are the mean \pm standard error (SE) of six independent samples. * $p < 0.05$ vs. TCPS; # $p < 0.05$ vs. SLA; \$ $p < 0.05$ vs. SLAnano.

differentiation.^{23,61,140–142,144,145,167–170} In the present study, Ti metal was treated to exhibit either a hydrophilic or hydrophobic nanostructured surface in order to distinguish between the effects these parameters have on osteogenic responses of MSCs and NHOst cells. Using a hydrophobic, non-nanostructured surface (SLA) as a control, cells at two different stages in the osteoblast lineage were grown separately to confluence on the modified surfaces. Subsequent examination of mRNA expression and protein production showed that a hydrophilic nanostructured surface facilitated the greatest increase in osteogenic markers. Interestingly, our data suggest that a hydrophobic nanostructured surface may stunt or delay the osteogenic capacity of MSC and NHOst cells compared to a hydrophobic non-nanostructured surface.

Although many other cell types are involved in osseointegration and the subsequent remodeling of peri-implant bone, MSCs and NHOst cells are critical for the process of bone mineralization. We used commercially available MSCs and NHOst cells from single donors, which limits the scope of our results since it does not consider variability inherent to the human population, or the health of the donors themselves. Despite these limitations, our results indicate that the positive osteogenic effects nanostructures have on MSC and NHOst cells are dependent on the inclusion of hydrophilicity.

Scanning electron microscopy confirmed the presence or absence of nanostructures on the modified Ti surfaces. In accordance with previous studies, sand blasting and acid etching techniques generated submicron scale roughness but did not induce nanostructure formation.^{52,63} Instead, nanostructure formation was dependent upon the reorganization of the oxide layer facilitated by the aqueous NaCl solution. Consistent with this idea, nanostructures with a similar size were present on SLAnano and modSLA but not SLA. The exact process of nanostructure formation is unknown; however, many studies have fabricated nanostructures on metallic surfaces using a variety of methods involving changes in temperature, pressure, and chemical treatments. The modification process used in this study also provided a consistent

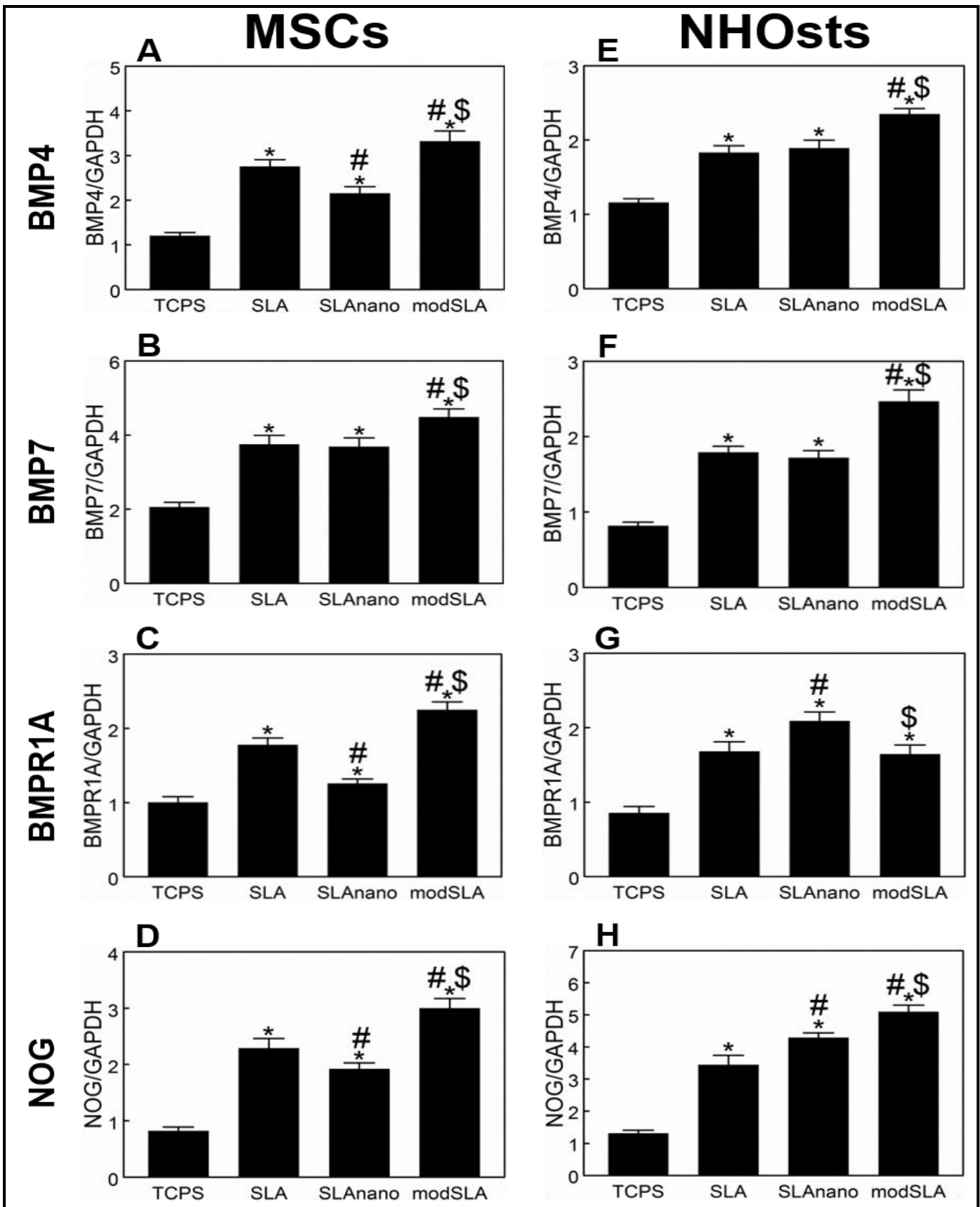


Figure 13. Effects of surface nanoscale features and energy on BMP mRNA levels of MSCs and NHOst cells. MSCs and NHOst cells were plated separately on TCPS, SLA, SLAnano, or modSLA grown to confluence. At confluence, cells were incubated in fresh media for 12 h, collected, and measured mRNA levels of BMP4, BMP7, BMPR1A, and NOG. * $p < 0.05$ vs. TCPS; # $p < 0.05$ vs. SLA; \$ $p < 0.05$ vs. SLAnano.

micro-roughness among SLA, SLAnano, and modSLA, allowing for an accurate separation between the effects of the nanostructures and the surface hydrophilicity.

The hydrophilicity of the surfaces was validated using x-ray photoelectron spectroscopy and contact angle measurements. The XPS spectra revealed that the thin Ti oxide layer consists mainly of TiO₂. Additionally, the presence of C(1s) is indicative of aliphatic carbons due to the adsorption of carbon-containing molecules from the air.⁷¹ Exposure to air increased the value of the peak corresponding to the presence of C(1s) carbon which was detected on SLA and SLAnano surfaces similar to previous studies.^{52,71} Immediate storage in saline without any exposure to air was an effective method for preventing organic impurity deposition resulting in a very low C(1s) peak on the surface of modSLA.^{52,71,184} Consistent with the XPS results, contact angle measurements demonstrated SLA and SLAnano to be hydrophobic and modSLA to be super-hydrophilic.

Cytoskeleton staining revealed that SLA, SLAnano, and modSLA surfaces were able to support a normal osteoblastic morphology as demonstrated by the clear, branched morphology adopted by MSCs¹⁸⁵ and NHOst cells.¹⁸⁶ Cytoskeleton organization of the cell is essential for focal adhesion, stress fiber formation, and spreading, and is dependent on the spatial distribution of both micro- and nanostructured topographies.^{164,187} Cell morphology influences gene expression,¹⁸⁸ and MSC differentiation relies in part on extracellular mechanical cues inherent to the underlying structure of the cytoskeleton.¹⁸⁵ It has been shown previously that MSC adipogenesis is preceded by round cell morphology while MSC osteoblastogenesis is preceded by a branched cell morphology when cultured on titanium substrates.¹⁸⁵ The branched morphology displayed by MSCs undergoing osteoblastogenesis is like that observed in mature osteoblasts grown on titanium substrates.¹⁸⁶ Moreover, the production and expression of osteoblastic markers further support enhanced osteoblastogenesis on the SLA, SLAnano, and modSLA.

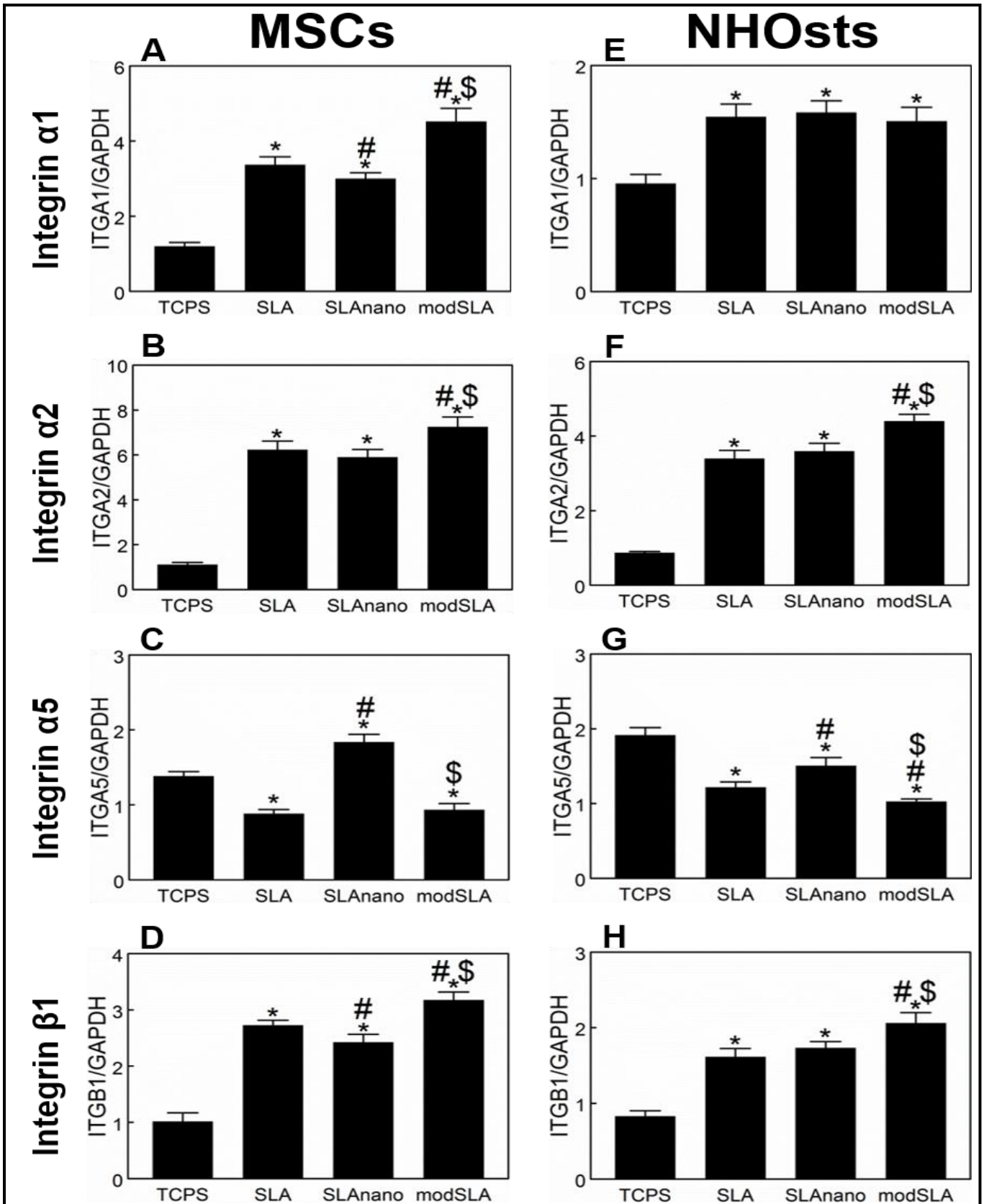


Figure 14. Effects of surface nanoscale features and energy on integrin mRNA levels of MSCs and NHOst cells. MSCs and NHOst cells were plated separately on TCPS, SLA, SLAnano, or modSLA grown to confluence. At confluence, cells were incubated in fresh media for 12 h, collected, and measured mRNA levels of ITG α 1, ITG α 2, ITG α 5, and ITG β 1. * $p < 0.05$ vs. TCPS; # $p < 0.05$ vs. SLA; \$ $p < 0.05$ vs. SLAnano.

A decrease in DNA compared to TCPS was accompanied by an increase of osteoblastic markers of differentiation and maturation on SLA, SLAnano, and modSLA for both cell types. Previous studies have shown that MSCs and NHOst cells grown on microstructured Ti surfaces produce an osteogenic environment facilitating their differentiation and maturation with the highest being produced on modSLA followed by SLA.^{70,158} These include the early marker of osteoblastic differentiation, alkaline phosphatase specific activity; the late marker of osteoblastic differentiation, osteocalcin; the osteoclast inhibitory factor, osteoprotegerin; the angiogenic factor, VEGF; and the osteogenic factor, BMP2. Additionally, modified surfaces had the ability to mitigate the inflammatory response compared to TCPS as indicated by the increased production of the anti-inflammatory cytokine interleukin 10 (IL10) and the decreased production of the pro-inflammatory cytokine interleukin 6 (IL6) in accordance with previous reports.¹⁵⁸ Interestingly, the inflammatory response was highest on SLAnano among modified surfaces. Additionally, MSC osteocalcin, VEGF, BMP2, and NHOst alkaline phosphatase specific activity, osteoprotegerin, and BMP2 on SLAnano were lowest among modified surfaces. Although each modification was able to support a healthy osteoblastic phenotype, it was frequently observed that SLAnano had a comparatively diminished capacity to enhance production of osteoblastic markers.

MSC and NHOst gene expression was less upregulated by SLAnano compared to SLA and modSLA. In general, for both cell types, the expression of BMPs (BMP4, BMP7), receptors (BMPR1A), and antagonists (NOG) was highest on modSLA followed by SLA as seen previously.^{61,71,158} Additionally, both cell types primarily expressed $\alpha 5\beta 1$ subunits when grown on TCPS but shifted to the production of $\alpha 1\beta 1$ and $\alpha 2\beta 1$ subunits when grown on rough titanium substrates. A further increase was observed for $\alpha 2\beta 1$ subunits on hydrophilic and nanostructured substrates as previously described.¹⁶¹⁻¹⁶³ However, removal of the hydrophilicity while retaining nanostructures resulted in fluctuations in osteoblastic gene expression. MSC

expression of BMP4, its receptor BMPR1A,¹⁸⁹ and its specific antagonist NOG^{159,190} decreased on SLAnano suggesting a lessened capacity to stimulate an osteogenic environment by nanostructures in the absence of hydrophilicity. SLAnano also altered the expression of BMP complexes in NHOst cells. NOG expression was increased compared to SLA without a similar increase in BMP4; furthermore, BMPR1A expression was highest on SLAnano.

Alterations in the balance of BMPs, their receptors, and antagonist results in altered bone remodeling, a potential outcome indicated by the *in vitro* gene expression modulated by SLAnano. Integrins are also important for both cell attachment and maintenance of the osteoblastic phenotype, and an altered expression of integrin subunits was observed on SLAnano. Although pro-osteoblastic integrin subunits increased on SLAnano, $\alpha 1$ and $\beta 1$ were decreased compared to SLA. Moreover, an increase of the non-osteoblastic subunit $\alpha 5$ was observed for both MSCs and NHOst cells cultured on SLAnano with its expression being greater than TCPS. Together, the expression of BMP and integrin complexes suggests that the bone remodeling process is somewhat diminished on a hydrophobic and nanostructured surface. However, this is capable of being recovered with the addition of surface hydrophilicity.

Previous studies analyzing the biological response to a hydrophobic and nanostructured surface determined favorable effects of nanostructures on osteoblastic differentiation and maturation. This contrasts with other studies comparing SLA to a hydrophobic, nanostructured surface.¹⁹¹ Using thermally nanomodified hydrophobic Ti (NMSLA) and Ti-6Al-4V alloy surfaces, it was shown that the osteoblastic differentiation of MG63 cells was enhanced compared to a microrough and hydrophobic SLA. Interestingly, human MSC response to the NMSLA modification suggested that differentiation was suppressed by the superposition of nanostructures.¹⁹¹ In these studies, nanostructures were classified as submicron, reporting a size range from 40 to 200 nm, while the nanostructure size range produced on surfaces used in this study was between 10 and 11 nm. It is possible that osteoblastic differentiation and

maturation can be altered by varying the size and shape of the nanostructures, an idea previously suggested.¹⁶⁴

Our results may be partially explained by a recent study investigating the influence of nanostructures and hydrophilic Ti substrates on fibrinogen and fibronectin protein adsorption and the degree of blood coagulation.¹⁹² It was shown that a hydrophilic and nanostructured surface led to the highest protein adsorption levels and the most pronounced degree of blood coagulation whereas the effects of a hydrophobic nanostructured surface on these outcomes were weak.¹⁹² This suggests that the effects the surface parameters have on early protein adsorption may dictate the rate of MSC osteoblastic differentiation or NHOst maturation. The effect of the nanostructures can be recovered and improved through the addition of the hydrophilicity providing the optimum conditions of osteoblastic differentiation and maturation.

Conclusions

Clinical grade Ti was successfully modified to fabricate microrough surfaces exhibiting hydrophobic or hydrophilic nanostructured surfaces. Although modified surfaces were able to support osteoblastic morphology in MSCs, indicated by staining of the cytoskeleton, production and expression of markers of osteoblastic differentiation and maturation suggest that an average nanostructure size of approximately 11 nm may delay the process of osteoblastogenesis. The effect of the nanostructures can be recovered with the addition of hydrophilicity. In order to promote enhanced osteoblastic differentiation of MSCs and maturation of NHOst cells, a nanostructured Ti surface will be dependent on an increased surface hydrophilicity.

Chapter 5. Regulation of Osteoclasts by Osteoblast Lineage Cells Depends on Titanium Implant Surface Properties

Abstract

A critical stage during osseointegration of a titanium (Ti) implant is primary bone remodeling, which involves cross talk among osteoclast precursors, osteoclasts, mesenchymal stem cells (MSCs), and osteoblasts. This phase couples the processes of bone formation and resorption. During remodeling, osteoclasts produce factors capable of regulating MSC migration and osteogenesis. Furthermore, they degrade primary bone, creating a foundation with a specific chemistry, stiffness, and morphology for osteoblasts to synthesize and calcify their matrix. MSCs and osteoblasts receiving cues from the implant surface produce factors capable of regulating osteoclasts in order to promote net new bone formation. The purpose of this study was to determine the effects Ti implant surfaces have on bone remodeling. Human MSCs and normal human osteoblasts (NHOst) were cultured separately on 15mm grade 2 smooth PT, hydrophobic-microrough SLA, hydrophilic-microrough Ti (mSLA) (Institut Straumann AG, Basel, Switzerland), or tissue culture polystyrene (TCPS). After 7d, conditioned media from surface cultures were used to treat human osteoclasts for 2d. Activity was measured by fluorescence of released collagen followed by mRNA quantification. This study demonstrates that MSC and NHOst cultures can suppress osteoclast activity in a surface dependent manner and osteoclast mRNA levels are selectively regulated by surface treatments. The substrate-dependent regulatory effect was mitigated when MSCs were silenced for integrin subunits and when conditioned media were denatured. These results indicate that MSCs and NHOst regulate at least two aspects of remodeling: reduced fusion of new osteoclasts and reduced activity of existing osteoclasts.

Introduction

Osseointegration is a complex cascade of biological events responsible for providing a direct structural and functional connection between the surface of a load-bearing implant and living bone. Greater bone apposition to implant materials results in functional stability, reducing the risk of failure while maintaining implant longevity. In addition to various intrinsic factors that enhance or inhibit osseointegration, the implant surface directly contacts the biological tissues and influences the outcome.

Titanium (Ti) and its alloys are choice materials for both dental and orthopaedic implants because of their ability to form a passive oxide layer bestowing high biocompatibility and corrosion resistance.¹²¹ Because of its stability in biological systems, Ti has been used extensively to investigate the process of osseous wound healing and osseointegration. Our previous studies have identified several important surface characteristics including microroughness, hydrophilicity, and chemistry that stimulate osteogenesis, resulting in enhanced osseointegration. When grown on Ti surfaces that are microstructured and hydrophilic, mesenchymal stem cells (MSCs) and osteoblasts (OBs) produce factors that create an osteogenic environment by stimulating osteoblastic differentiation in progenitor cells distal to the implant; promoting vasculogenesis; reducing inflammation; and regulating osteoclastic resorption to achieve net new bone formation.^{61,70,71,80,161,193}

Much of the research regarding osseointegration revolves around bone-forming OBs and MSCs due in part to the necessity to achieve net new bone formation. Materials that do not promote osteogenesis, such as polymers like polyether-ether-ketone, result in a fibrous connective tissue interface.¹⁹⁴ Although implant materials should actively promote bone formation, long-term stability requires solutions that not only result in net new primary bone formation but also provide continued osteogenic signals to maintain healthy bone remodeling. Bone-resorbing osteoclasts (OCs) are present during peri-implant healing, significantly

influencing implant outcomes by playing an important role during the initial and late phases of osseointegration.¹⁹⁵ Bone is continuously remodeled through a finely balanced equilibrium of cell mediated extracellular matrix (ECM) degradation and formation. Bone remodeling is a versatile and ubiquitous process providing the mechanism for adaptation to mechanical stress, repair of micro-damage, and replacement of primary bone during osseointegration of implanted materials.³² Because it can occur in separate areas asynchronously, locally generated regulatory factors and environmental cues ensure the appropriate balance among OCs, OBs, and their precursors. Although it seems counterintuitive, implant materials for dental and orthopaedic applications should not inhibit OC-mediated bone resorption to promote net new bone formation, but instead promote a healthy communication among these cells to achieve osseointegration and maintain its longevity.

Achieving implant stability is critical for successful osseointegration; however, insertion of a dental or orthopaedic implant influences the nature of bone healing.¹⁹⁶ Immediately after insertion, implant stability depends on the initial mechanical interlock with the surrounding bone. Unless primary fixation is achieved via new bone formation between the implant surface and the existing bone bed, micromotion of the implant and localized inflammation may occur, frequently ending with osteolysis and implant failure. In addition, the trauma of implant placement ruptures blood vessels and releases growth factors and proteins,^{62,197} which provide the local environment with a provisional ECM important for blood clot formation.¹⁹⁸ The adsorption of these early proteins is dependent upon the surface topography with superior anchorage occurring on micro-roughened implant surfaces compared to smooth surfaces.^{199,200} Moreover, this protein layer serves as a scaffold for the migration of MSCs to the implant surface.^{201,202}

Surface design that facilitates this contact osteogenesis has been shown to control the fundamental processes that drive the osteoblastic differentiation of MSCs.^{22,203} A cell-rich immature bone (woven bone) is seen in the provisional connective tissue that surrounds newly

formed blood vessels.²⁰⁴ Woven bone forms in direct contact with the surface of the Ti implant and continues to form over 2 weeks.²⁰⁵ Although OCs are present in the peri-implant tissues as early as 1 week following implantation, it is not until after formation of the woven bone that OC activity in relation to osseointegration begins.¹⁹⁵ This marks the beginning of the progressive removal of woven bone, creating space for new lamellar bone formation and replacing passive primary stability with active secondary fixation through biological bonding.²⁰⁶

Modifications to the implant surface topography, chemistry, and hydrophilicity are employed as a means of controlling bone–implant interactions and shortening the time of bone fixation. Furthermore, it is known that the communication among OCs, MSCs, and OBs is coupled to provide control of bone mass and healing. Commitment of OC precursors to mature OCs is dependent on production of RANKL (receptor activator of the NFκB ligand)²⁰⁷ and its physiologic inhibitor OPG (osteoprotegerin)²⁰⁸ by OBs and MSCs. Implant surface microstructure and hydrophilicity facilitate increased production of OPG by MSCs and OBs, leading to increased bone formation. In this regard, much attention has been given to the anabolic aspects of osseointegration. In contrast, there is little information regarding the OC-mediated catabolic processes associated with bone remodeling. It remains unclear as to whether implant surface topography can affect the process of osteoclastogenesis or OC function. A thorough understanding of healing, repair, modeling, and remodeling of bone is critical for the establishment and maintenance of osseointegration of dental and orthopaedic implants. Given that the process of bone adaptation and maturation are critical features for the long-term success of osseointegration, continued attention to the molecular processes underlying these events may create new biological design criteria for implant surface design. This insight is critical to optimize an implant surface capable of simultaneously enhancing peri-implant osteogenesis while also positively influencing the later stages of osseointegration. Therefore, the objective of this study was to determine the effects microrough and hydrophilic Ti surfaces have on a novel *in vitro*

model of bone remodeling by studying their distal influence on OC formation and activity and the mechanisms responsible for the influence.

Materials and Methods

Ti disk preparation

Grade 2 Ti disks, 15mm in diameter and 1mm in thickness, were provided by Institut Straumann AG (Basel, Switzerland). Disks were degreased in acetone and processed for 30s in a 55°C 2% ammonium fluoride/2% hydrofluoric acid/10% nitric acid solution to produce pretreatment Ti disks (PT). SLA substrates were prepared by subjecting PT substrates to sand blasting (250 – 500µm corundum) and acid etching (HCl/H₂SO₄). Disks were cleaned in HNO₃, rinsed in deionized water, air dried, and packed in aluminum foil. mSLA substrates were produced using the same sandblasting and acid etching procedure as used for SLA, but subsequent steps took place under nitrogen gas to prevent exposure to air. mSLA disks were rinsed and stored in 0.9% NaCl solution. The methods used to characterize the surface microroughness, contact angle, and carbon contamination of the surfaces (PT [$S_A=0.59\mu\text{m}$; $\theta_{CA}=93.6^\circ$; %C=31], SLA [$S_A=3.58\mu\text{m}$; $\theta_{CA}=120.9^\circ$; %C=35], mSLA [$S_A=3.64\mu\text{m}$; $\theta_{CA}=0^\circ$; %C=17]) have been reported previously.²⁰⁹ All disks were γ -irradiated prior to use.

OC Cell Culture

Human OC precursors (OCPs; Lonza Biosciences, Walkersville, MD) were cultured on a human type I collagen coated, 96-well OsteoLyse™ Assay Kit (Lonza Biosciences). OCPs were differentiated into mature OCs using osteoclast precursor growth medium (OCGM, Lonza Biosciences) supplemented with 33ng/ml macrophage colony stimulating factor (M-CSF, Lonza Biosciences) and 66ng/ml receptor activator of nuclear factor kappa-B ligand (RANKL, Lonza Biosciences). OCPs were also cultured in OCGM supplemented with 33ng/ml M-CSF without RANKL for use as a negative control.

Establishment of Osteoclast Phenotype and Treatment Period

In order to establish the OC phenotype and treatment period, OCPs were harvested at 3d, 7d, 9d, and 14d and subjected to the following assays.

OC Activity

OC activity was measured by the release of the europium conjugated human type I collagen coated on the bottom of the OsteoLyse™ Assay Kit at each time point. 200µl of a fluorophore releasing reagent (Lonza Biosciences) was placed in each well of a 96-well black, clear-bottom assay plate (Corning Inc., Corning, NY). 10µl of cell culture supernatant was transferred to each well of the assay plate containing the fluorophore releasing reagent. Fluorescence of each well of the assay plate was measured with an excitation wavelength of 340nm and an emission wavelength of 615nm over a 400µs period after an initial delay of 400µs.

Gene Expression

To quantify mRNA, cells were plated as described above. At each time point, mRNA was isolated from cells using a TRIzol® (Invitrogen, Carlsbad, California) extraction method. RNA was quantified using a NanoDrop spectrophotometer (Thermo Fisher Scientific, Waltham, MA) and then reverse transcribed into 250 ng/µL cDNA. Real-time PCR was performed using a fluorescent dye (Power SYBR Green, Applied Biosystems, Foster City, CA) to quantify starting mRNA levels using gene specific primers (**Table 3**). Levels of mRNA are normalized to GAPDH.

Table 1. Human Primers Used in Real-Time PCR Analysis

Name	Gene		Primer Sequence
Carbonic Anhydrase II	CA2	F	CACTCGTAAATGCCAAGAAAAG
		R	TAGAACCCAACACAAAGATGC
Cystatin B	CSTB	F	ACTGTTCAAGGAGGAGAC
		R	GGTCAAAGGCTTGTTTAGG
Cathepsin K	CTSK	F	ATCTGTGTGCCTGACCTG
		R	AAGTTCCTGGGTGTCTG
Osteoclast Stimulatory Transmembrane Protein	OCSTAMP	F	ATTACTCAGATCCAACCAC
		R	TCCTCCTCATTTCATTCATC
Integrin β3	ITGβ3	F	ACGGTGGGAAACTTTTGATGTG
		R	CGAGTCTGATGGAGGTGAGTC
Integrin αV	ITGαV	F	AGCAGCAGCGACCAGAGG
		R	ACAGTAGTAGGCCGGCGTAGC
Glyceraldehyde 3-phosphate dehydrogenase	GAPDH	F	GCTCTCCAGAACATCATCC
		R	TGCTTACCACCTTCTTG

Scanning Electron Microscopy (SEM) Imaging

OCs were qualitatively evaluated using SEM (Hitachi FE-SEM Su-70, Tokyo, Japan) at each time point. In addition, the collagen coating of the OsteoLyse™ Assay Kit was assessed before and after OC treatment. For assessment of the collagen coating, OCs were trypsinized for 5min. All samples were then fixed in 4% paraformaldehyde for 15min after three rinses in 1x PBS. Samples were then dehydrated stepwise in increasing ethanol concentrations of 15%, 30%, and 45% for two hours, followed by 60%, 75%, 90% and 100% (x3) for at least 1 hour. The samples were then critically dried using a 1:1 exchange of 100% ethanol and hexamethyldisilazane (HMDS, Sigma-Aldrich, St. Louis, MO) for 30min in a chemical safety hood, then twice with 100% HMDS for 30min. Sample wells were trimmed to allow even sputter coating, then dried in a desiccator for 24hrs prior to platinum sputter coating. Samples were imaged with 56µA ion current, 5kV accelerating voltage and 8mm working distance. Representative images were selected from 18 images per well and n=4 per group.

Tartrate-Resistant Acid Phosphatase (TRAP) Staining

OCs were stained for tartrate-resistant acid phosphatase (TRAP) and were analyzed using light microscopy. OC groups (n=4) were prepared based on a modified manufacture's protocol (Sigma-Aldrich). Briefly, OCs were rinsed three times with 1x PBS, fixed in a fixative solution comprising of 25mL citrate solution, 65mL acetone, and 8mL of 37% formaldehyde for 15min. Followed by 3 rinses in deionized water. Staining solution consisting of 45mL of deionized water at 37°C, 1mL diazotized Fast Garnet GBC solution, 0.5mL Naphthol AS-BI Phosphate Solution, 2mL Acetate solution, and 1mL Tartrate solution was prepared and 200µL of staining solution was added to each well and allowed to incubate for 1hr at 37°C. Samples were counterstained with 200µL hematoxylin solution for 2min and rinsed in deionized water prior to imaging with a Carl Zeiss Primo Vert™ Inverted Microscope (Zeiss, Oberkochen, Germany). Representative images were selected from 18 images per well and n=4 per group.

MSC and NHOst Cell Culture

Human MSCs (Lonza Biosciences) were cultured in MSC growth medium (MSCGM; Lonza Biosciences). Normal human osteoblasts (NHOsts, Lonza Biosciences) were cultured using Dulbecco's modified Eagle medium (DMEM, CellGro®; Mediatech, Inc., VA) supplemented with 10% fetal bovine serum (FBS, Life Technologies, Carlsbad, CA) and 1% penicillin-streptomycin (Life Technologies). MSCs and NHOsts were separately cultured on tissue culture polystyrene (TCPS), PT, SLA, or mSLA at a density of 10,000 cells/cm² at 37°C in 5% CO₂ and 100% humidity. Media were changed 24h after plating and every 48h thereafter for 7d. At 7d, cells were incubated with fresh media for 24h, which was used for subsequent experiments.

Indirect Effects of MSC/NHOst Conditioned Media on OCs

MSCs, NHOsts, and OCPs were separately cultured as described previously. After culture for each cell type, 200µl media from MSCs or NHOsts were transferred to wells of the OsteoLyse™ Assay Kit containing differentiated OCs. In order to control for the initial concentrations of M-CSF and RANKL used to differentiate the OCs, an additional group of differentiated OCs was incubated with 200µl of MSC or NHOst media supplemented with 33ng/ml M-CSF and 66ng/ml RANKL. For each experiment, positive (differentiated OCs receiving OCGM supplemented with 33ng/ml M-CSF and 66ng/ml RANKL) and negative (undifferentiated OCPs receiving OCGM supplemented with 33ng/ml M-CSF) controls were used. Differentiated OCs were treated for 2d, followed by quantification of activity and gene expression.

Cell Presence and Conditioned Media Effects on OCs

In order to determine whether the observed indirect effects of conditioned media were dependent on the presence of cells, MSCs were cultured on TCPS or mSLA and compared to conditioned media collected from TCPS and mSLA without seeded cells. Both the cellular and acellular TCPS and mSLA were incubated and received media changes in the exact same

manner for 7d followed by treatment with MSCGM for 24hr. After treatment, conditioned media were supplemented with 33ng/mL M-CSF and 66ng/mL RANKL and used to treat differentiated OCS for 2d. Positive and negative controls were also used.

Proteins and Conditioned Media Effects on OCS

Whether proteins were the primary factor for the observed effects of conditioned media on OCS was determined by two methods of denaturation: 1) proteinase K or 2) heat. For proteinase K denaturation, MSCs were cultured on either TCPS or mSLA as described previously. After treatment with MSCGM, conditioned media were collected and treated with 200µg/ml proteinase K (Sigma-Aldrich) for 1h at 37°C. Proteinase K activity was then neutralized with 5mM Pefabloc® SC (Sigma-Aldrich) for 2h at 37°C. For heat treatment, conditioned media were placed in an 80°C water bath for 2h. Heat treated media were then cooled to room temperature by placing samples on ice for 10 min. Denatured conditioned media were then supplemented with 33ng/mL M-CSF and 66ng/mL RANKL prior to treating differentiated OCS for 2d using positive and negative controls.

ITGA2 and ITGB1 Silencing

MISSION® shRNA lentiviral transduction particles (Sigma-Aldrich) were used to silence human MSCs for either ITGA2 (SHCLNV-NM_002203) or ITGB1 (SHCLNV-NM_002211). MSCs were plated at 20,000 cells/cm² and cultured overnight at 37°C in 5% CO₂ and 100% humidity. Particles were added to the cells at a multiplicity of infection of 2 in culture media supplemented with 8µg/ml hexadimethrine bromide for 18h. Transduced cells were selected using MSCGM supplemented with 0.5 µg/ml of puromycin. Silencing of ITGB1 and ITGA2 were confirmed using real-time qPCR and maintained over the period of culture (data not shown). A 70% reduction in mRNA levels compared to the wild-type control was considered the minimum acceptable decrease.

Effects of ITGA2 and ITGB1 Silencing on Indirect Effects of MSC Conditioned Media

To determine if signaling via the $\alpha 2$ or $\beta 1$ integrin subunit was required for the indirect effects of conditioned media on OCs, wild type (WT) and silenced MSCs were cultured on TCPS or mSLA for 7d in MSCGM followed by a 24hr treatment with MSCGM. Conditioned media were supplemented with 33ng/ml M-CSF and 66ng/mL RANKL and used to treat differentiated OCS for 2d. Positive and negative controls were also used.

Paracrine Effects of OPG and TGF β 1 in Conditioned Media

The contribution of osteoprotegerin (OPG) and transforming growth factor $\beta 1$ (TGF β 1), two known regulators of OC activity and function, to the indirect effects of conditioned media on OCs were also evaluated. Conditioned media were collected from cultures of MSCs on TCPS or mSLA as previously described. Conditioned media were supplemented with either 2 μ g/ml or 0.5 μ g/ml anti-TGF β 1 type II receptor antibody (R&D Systems, Minneapolis, MN); 1 μ g/ml or 0.1 μ g/ml soluble type II receptor (R&D Systems); or 2 μ g/ml or 0.5 μ g/ml anti-OPG antibody (R&D Systems, Minneapolis, MN). All conditioned media were then supplemented with 33ng/ml M-CSF and 66ng/mL RANKL and used to treat differentiated OCs for 2d. Positive controls supplemented with each treatment were also used.

Statistical Analysis

Data from surface characterization experiments and *in vitro* assays are presented as the mean \pm standard error (SE) per variable (n=6). A one-way analysis of variance was performed with a two-tailed Tukey correction and $\alpha = 0.05$. All statistical analyses were performed using JMP statistical software.

Results

Initial studies established the OC phenotype and treatment period (**Fig.15**). Activity of OCs is shown as differentiated OCs (OCPs receiving M-CSF and RANKL) per undifferentiated OCs (OCPs receiving M-CSF) within the same time point. A significant increase in OC activity was

observed at each time point (**Fig.15A**). Gene expression data are shown by indicating the source of the media (OCGM) and the presence (+) or absence (-) of RANKL. No difference in OCP CA2 mRNA was detected at 3d, 7d, and 9d (**Fig.15B**). At 14d, CA2 mRNA increased to levels comparable to 3d OC cultures. CA2 mRNA further increased in OCs 7d post-culture then decreased at 14d. Similar CTSK expression was observed among OCPs and 3d OC cultures

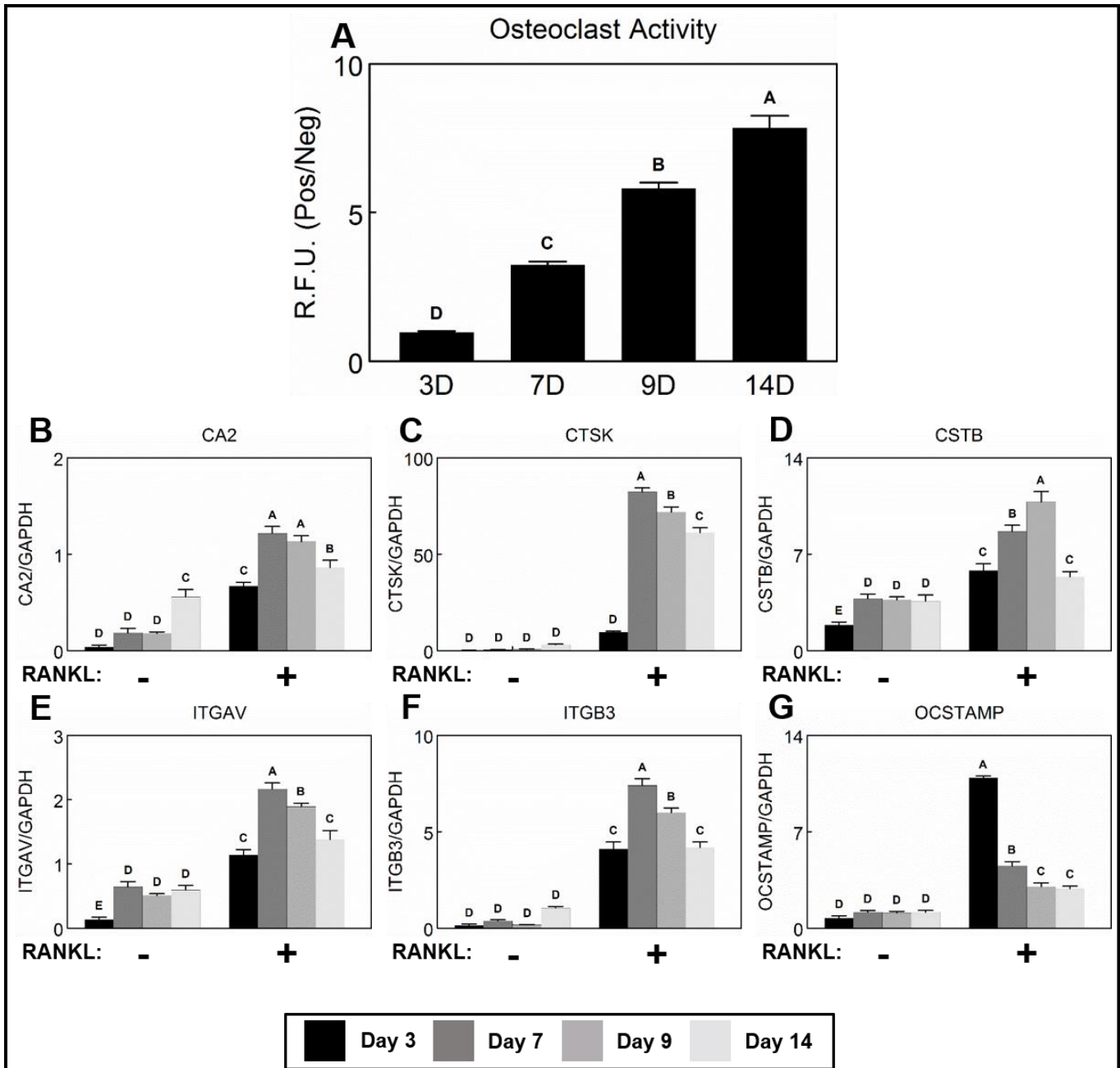
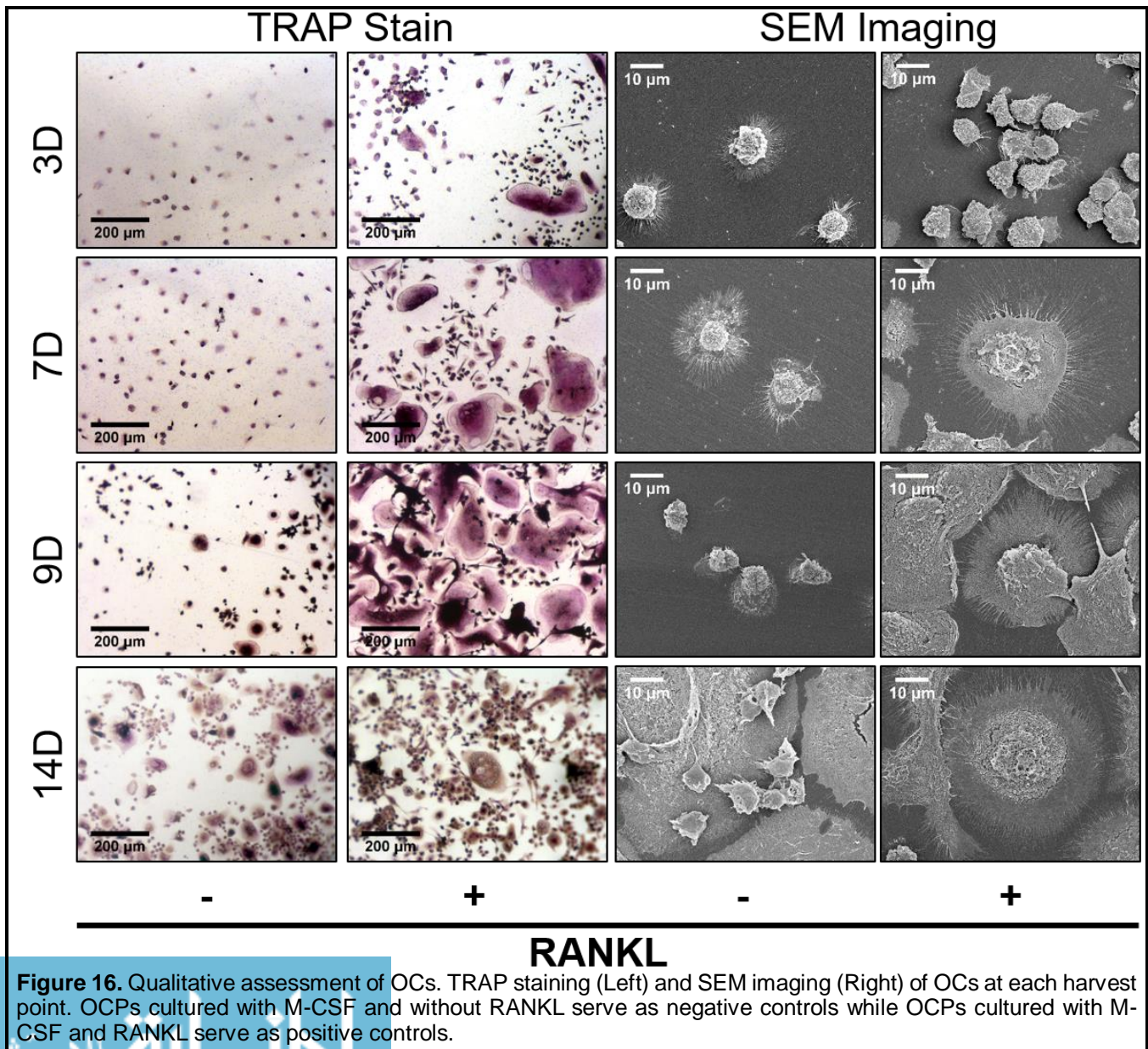


Figure 15. Establishment of OC phenotype and treatment period. OCPs were differentiated with M-CSF (negative control) or M-CSF and RANKL (positive control) on an OsteoLyse Kit. After 3d, 7d, 9d, and 14d OC activity was measured by absorbance following the addition of 10 μ l of media to 200 μ l of a fluorophore releasing agent. Afterwards, mRNA was isolated from OCs and CA2, CTSK, CSTB, ITGAV, ITGB3, and OCSTAMP were measured. Data shown are the mean \pm standard error (SE) of six independent samples. Groups not sharing a letter are statistically significant at an $\alpha=0.05$.

(Fig.15C). CTSK expression in 7d OCs was highest and subsequently decreased at 9d and 14d. OCP expression of CSTB (Fig.15D), ITGAV (Fig.15E), ITGB3 (Fig.15F), and OCSTAMP (Fig.15G) was lower compared to OCs. CSTB and ITGAV expression increased to similar levels on 7d, 9d, and 14d OCP cultures compared to 3d. No differences were detected in OCP ITGB3 and OCSTAMP expression. For OCs, similar levels of CSTB, ITGAV, and ITGB3 mRNA were detected at 3d and 14d cultures; however, CSTB was highest in 9d OC cultures while ITGAV and ITGB3 were highest in 7d OC cultures. Peak OCSTAMP expression was observed in 3d OC cultures. OCSTAMP expression declined at 7d and further decreased to similar levels at 9d and 14d.



Qualitative assessment of the OC phenotype at each time point is shown in **Figure 16**. As early as three days, RANKL supplemented OCPs began to aggregate and fuse into multinucleated OCs as indicated by TRAP stain. At 7d, increased TRAP stain multi-nucleation as well as ruffled border formation in SEM images was seen. This phenotype continued to develop through 9d. The 9d RANKL negative cultures had larger cells attributed to the actions of M-CSF; however, they lacked the magnitude of surface area, TRAP stain intensity, and multi-nucleation compared to OCs. Interestingly, TRAP stain intensity and multi-nucleated cell density decreased in the 14d RANKL positive cells while both increased in the 14d RANKL negative cells suggesting that the phenotypic integrity of OCPs and OCs was lost by 14d. Although the collagen coating is slightly altered by trypsin, differentiated OCs degrade much of the collagen coating by 9d of culture and only a few fragments of protein are left by 14d.

Figure 17 shows the indirect effects microstructured Ti substrates have on OC activity via MSCs (**Fig.17A, B**) and NHOsts (**Fig.17C, D**) after treatment for 2d. The sources of the treatment media (OCGM or MSCs/NHOsts cultured on TCPS or PT, SLA, or mSLA disks) are shown below each group. Furthermore, indications of whether treatment media were supplemented with (+) or without (-) RANKL are shown below each group. For each cell type, the OC activity was highest in the positive control and lowest in the negative control. Compared to the positive control, OC activity was reduced following treatment with media collected from cultures of MSCs (**Fig.17A**) and NHOsts (**Fig.17C**) grown on TCPS and microstructured Ti. Similar effects were seen when media collected from MSCs and NHOsts were supplemented with RANKL and M-CSF (**Fig.17B, D** respectively). OC activity was reduced to comparable levels in groups treated with media collected from MSCs and NHOsts cultured on TCPS and PT with or without RANKL and M-CSF supplementation. A further reduction in OC activity was observed after treatment with media from SLA cultured MSCs followed by mSLA cultured MSCs. Supplementing MSC treatment media with RANKL and M-CSF abrogated this effect. OCs

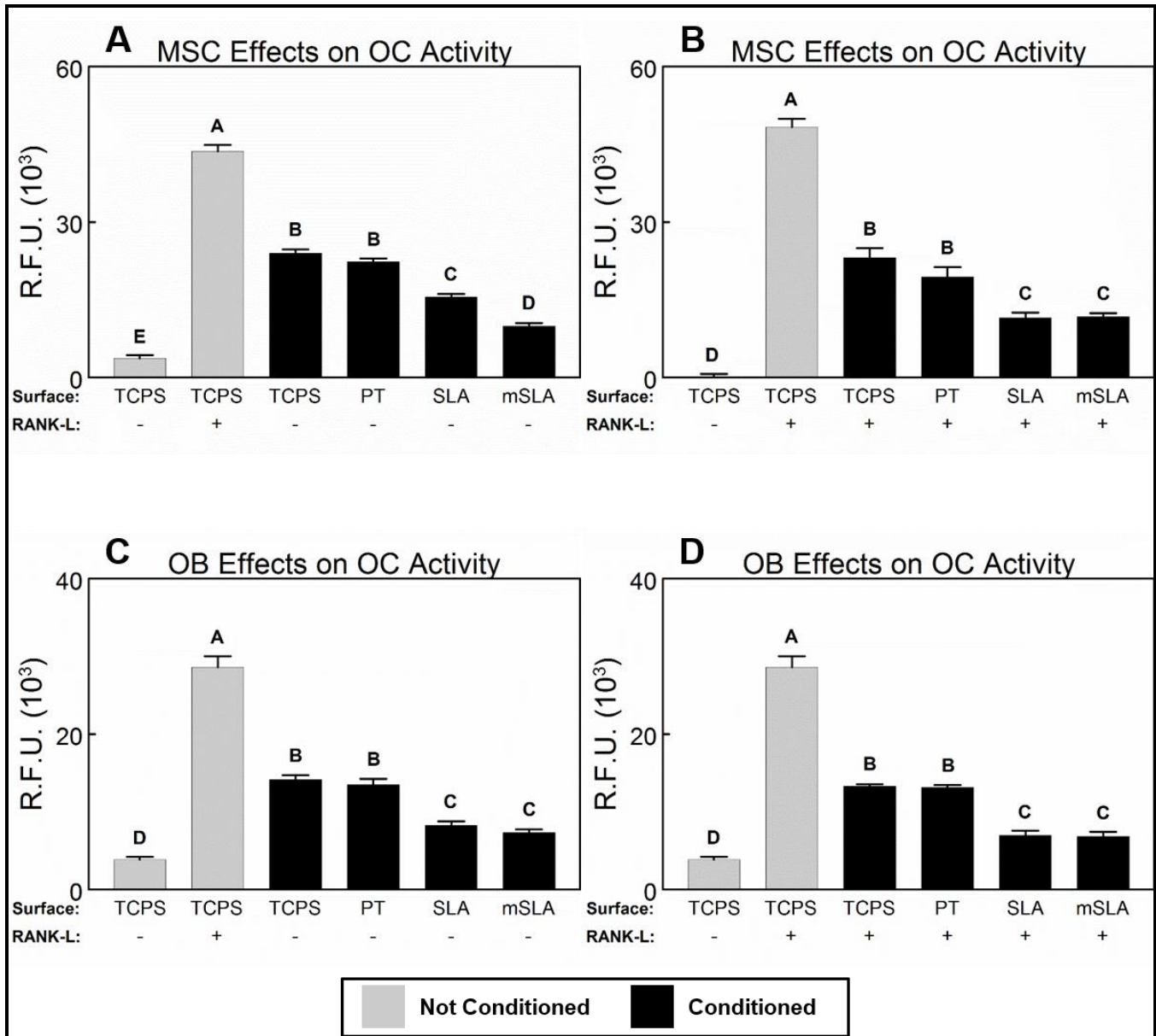


Figure 17. The indirect effects of Ti surface cultured osteoblast lineage cell conditioned media on osteoclast activity. OCPs were differentiated on an OsteoLyse Kit with M-CSF and RANKL. MSCs and NHOsts were separately cultured on TCPS, PT, SLA, or mSLA. After 7d, MSC and NHOst media were collected, supplemented with or without M-CSF and RANKL, and used to treat OCs, leaving a negative (OCPs + M-CSF) and positive (OCPs + M-CSF + RANKL) control. After treatment for 2d, 10 μ l of media was placed into 200 μ l of a fluorophore releasing agent and absorbance measured. Data shown are the mean \pm standard error (SE) of six independent samples. Groups not sharing a letter are statistically significant at an $\alpha=0.05$.

treated with media collected from SLA and mSLA cultured NHOsts were not sensitive to the effects of RANKL and M-CSF supplementation observed with MSC treatment.

Data regarding gene expression following treatment with MSC and NHOst conditioned media (CM) supplemented with M-CSF and RANKL are shown in **Figure 18**. For all genes, expression was higher in the positive control compared to the negative control. MSC-CM treatment reduced OC CA2 (**Fig.18A**) and CSTB (**Fig.18B**) expression compared to the positive control. CA2

expression further decreased when OCs were treated with SLA and mSLA MSC-CM. CSTB expression decreased after MSC-CM treatment and continued to decrease in a surface dependent manner with no differences detected between SLA and mSLA MSC-CM. OCSTAMP (**Fig.18C**) was reduced to similar levels for all MSC-CM treatments. CTSK (**Fig.18D**) mRNA levels decreased when treated with mSLA MSC-CM. Although not different from the positive control, OC CTSK expression decreased when treated with SLA MSC-CM compared to TCPS and PT MSC-CM. No differences in OC ITGAV (**Fig.18E**) expression were detected between the positive control and OCs treated with SLA and mSLA MSC-CM; however, OCs treated with TCPS and PT MSC-CM had significantly higher ITGAV expression compared to the positive control and mSLA MSC-CM. OC ITGB3 expression (**Fig.18F**) increased compared to the positive control following treatment.

Treatment with NHOst-CM reduced CA2 (**Fig.18G**) expression to similar levels. OC CSTB (**Fig.18H**) mRNA levels decreased when treated with TCPS and PT NHOst-CM and further decreased when treated with SLA and mSLA NHOst-CM. OCSTAMP (**Fig.18I**) mRNA levels were reduced in OCs to similar levels; however, OCs treated with TCPS NHOst-CM had significantly higher OCSTAMP mRNA levels compared to those treated with mSLA NHOst-CM. CTSK (**Fig.18J**) expression was reduced in OCs treated with TCPS, PT, and SLA NHOst-CM and further reduced in OCs treated with mSLA NHOst-CM. No differences in ITGAV (**Fig.18K**) expression were detected in OCs treated with NHOst-CM compared to the positive control. However, mSLA NHOst-CM reduced ITGAV expression compared to other treatments. ITGB3 (**Fig.18L**) mRNA levels were highest in OCs treated with TCPS and PT NHOst-CM. ITGB3 mRNA remained unchanged compared to the positive control in OCs treated with SLA and mSLA NHOst-CM.

For experiments to determine the mechanisms responsible for the indirect regulation of OCs, a simplified model was used that included only MSCs cultured on either TCPS or mSLA. **Figure**

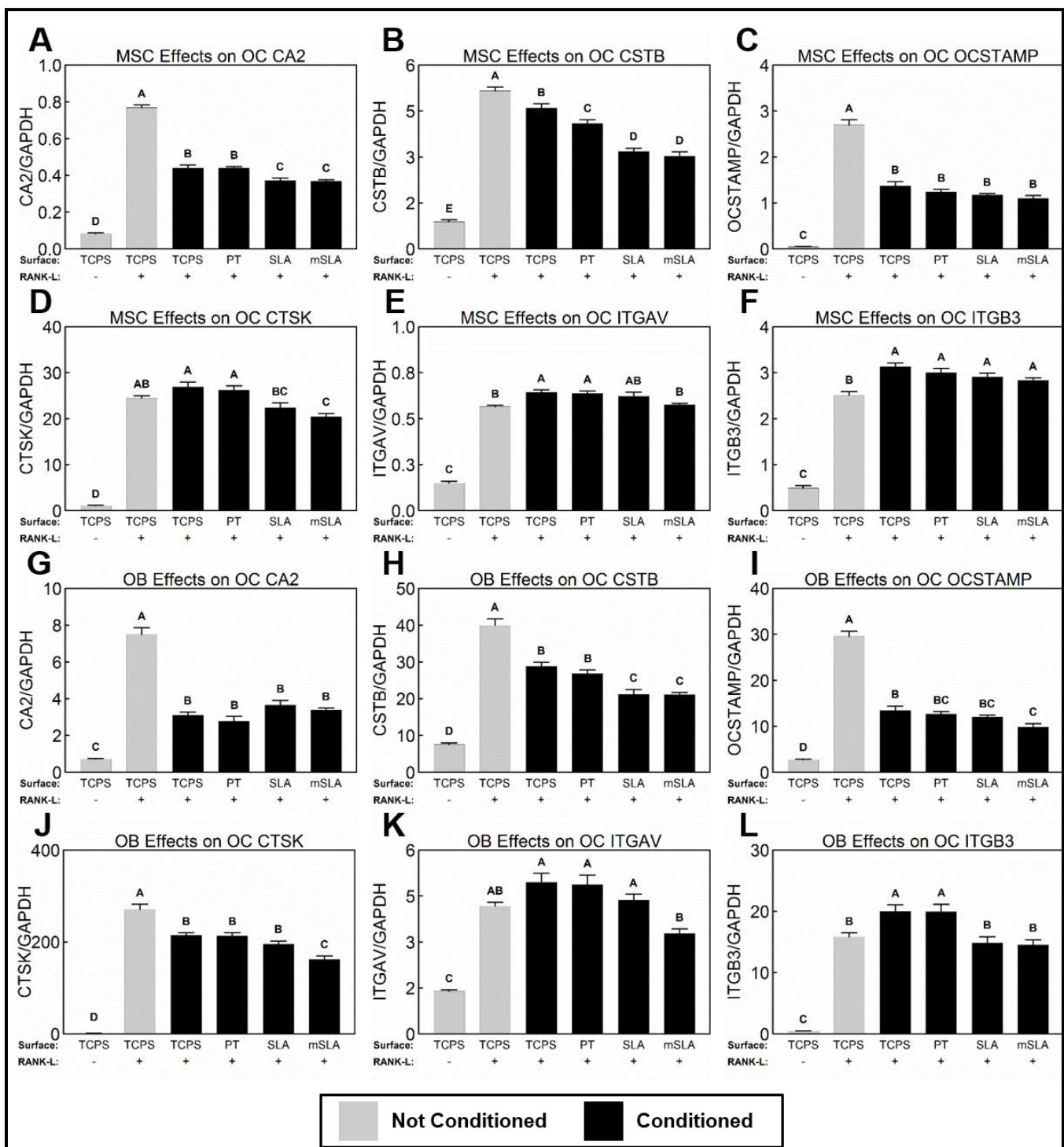


Figure 18. The indirect effects of Ti surface cultured osteoblast lineage cell conditioned media on osteoclast gene expression. OCPs were differentiated on an OsteoLyse Kit with M-CSF and RANKL. MSCs and NHOsts were cultured on TCPS, PT, SLA, or mSLA. After 7d, MSC and NHOst media were collected, supplemented with M-CSF and RANKL, and used to treat OCs, leaving a negative (OCPs + M-CSF) and positive (OCPs + M-CSF + RANKL) control. After treatment for 2d, OCs were harvested and mRNA levels of CA2, CSTB, OCSTAMP, CTSK, ITGAV, and ITGB3 quantified. Data shown are the mean \pm standard error (SE) of six independent samples. Groups not sharing a letter are statistically significant at $\alpha=0.05$.

19A demonstrates that the observed inhibitory effect is dependent on the presence of cells conditioning the media prior to treatment, although there is an equal inhibitory effect on OCs due

to treatment with acellular MSCGM. ITGA2 silenced MSCs (**Fig.19B**) and ITGB1 silenced MSCs (**Fig.19C**) decreased OC activity compared to the positive control. shITGA2 MSCs cultured on TCPS decreased OC activity compared to WT. The decrease in OC activity by mSLA MSC-CM was attenuated by silencing ITGA2. Similar results were observed for shITGB1 MSCs; however, no difference in OC activity was detected between TCPS WT MSC-CM and TCPS shITGB1 MSC-CM. In order to determine whether the inhibitory effect was due to proteins, two methods of protein denaturation were employed. Treatments subjected to proteinase K digestion (**Fig.19D**) decreased OC activity to levels comparable to the negative control regardless of the initial surface. Interestingly, heat denaturation of proteins (**Fig.19E**) increased OC activity compared to the intact protein treatments, although the activity was significantly lower than the positive control.

The addition of an antibody against TGF β type 2 receptor (**Fig.20A**) or soluble TGF β type 2 receptor (**Fig.20B**) decreased OC activity when added to TCPS MSC-CM to levels like mSLA MSC-CM. OC activity was unchanged when these factors were added to mSLA MSC-CM. Furthermore, no effects on OC activity were detected when an antibody against osteoprotegerin was added to either TCPS or mSLA MSC-CM, although the activity was significantly lower in mSLA MSC-CM compared to TCPS MSC-CM (**Fig.20C**). In all instances, addition of either antibody or soluble protein had no effect on the positive control.

Discussion

Implant design that promotes both early bone formation while maintaining healthy cellular signaling throughout the remaining stages of osseointegration will achieve long-term implant stability. It is now understood that surface properties modulate immune cell function and factors produced by macrophages influence osteogenesis.^{209,210} Others have shown that osteocytes make direct contact with the implant surface, suggesting their importance in maintaining healthy bone remodeling as well as the longevity of implant osseointegration.^{211,212} However, no studies

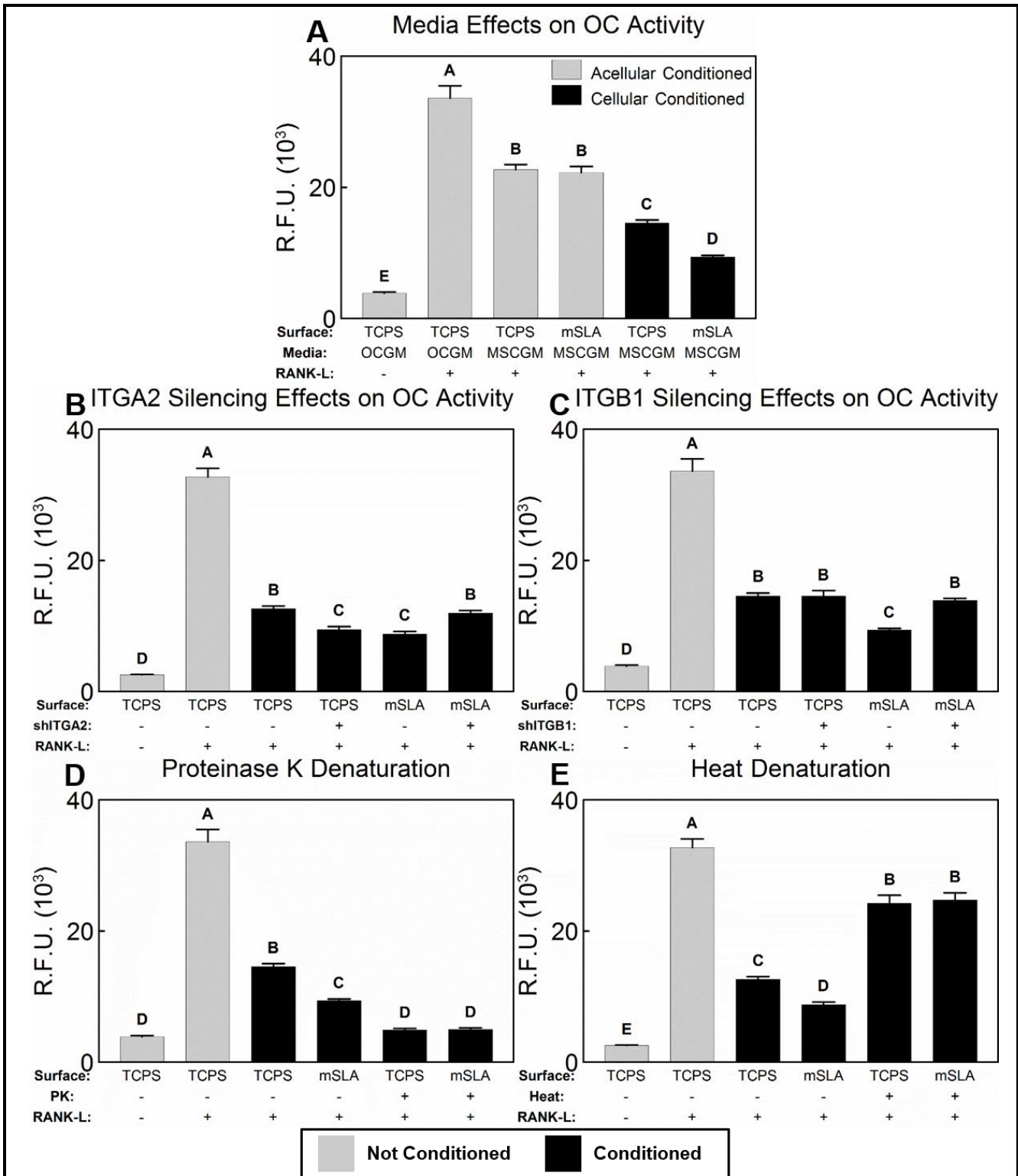
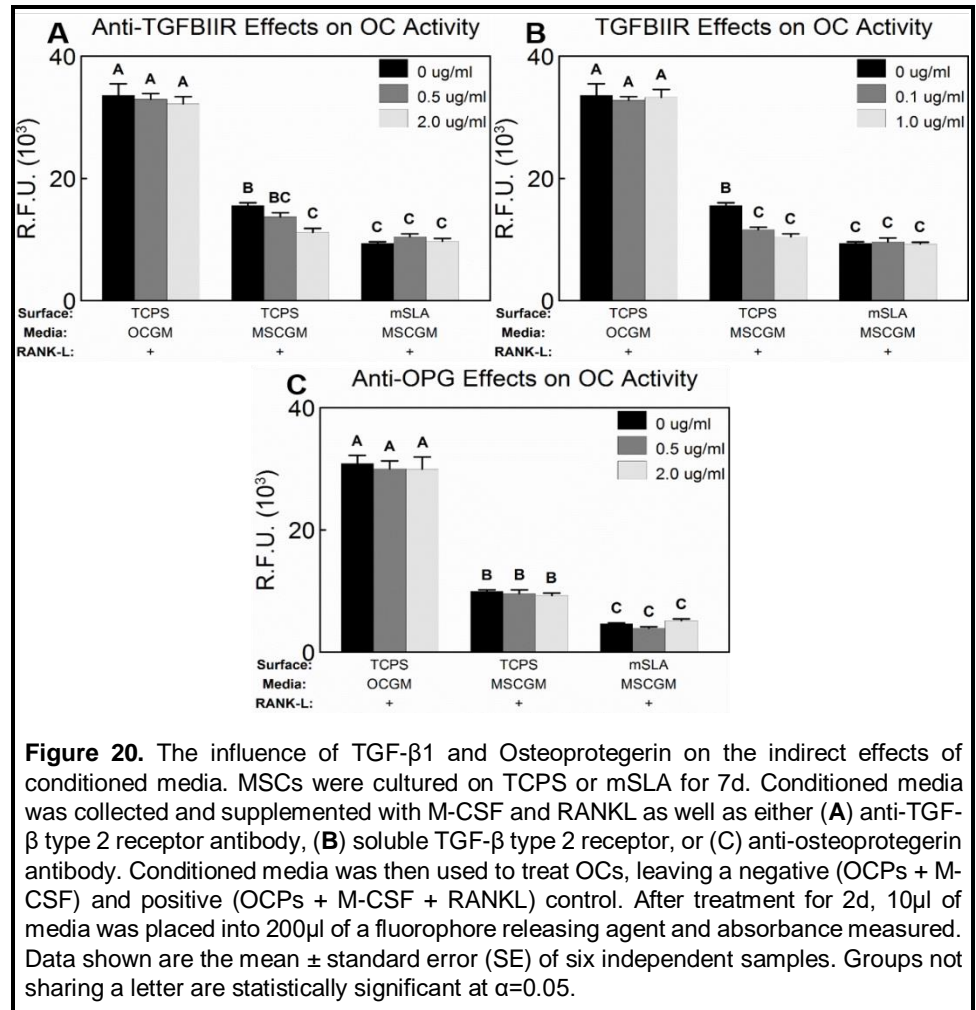


Figure 19. The indirect effects of conditioned media are mediated through integrin signaling and dependent on cells and proteins. (A) MSCs were cultured on TCPS or mSLA and compared to their acellular counterparts. TCPS and mSLA containing no cells were incubated with MSCGM and received media changes identical to MSC cultured TCPS or mSLA. MSCs silenced for either ITGA2 (B) or ITGB1 (C) were cultured on TCPS or mSLA and compared to their WT controls. Conditioned media were subjected to protein denaturation via proteinase K (D) or heat (E) and compared to non-denatured controls. After 7d, conditioned media were collected, supplemented with M-CSF and RANKL, and used to treat OCs, leaving a negative (OCPs + M-CSF) and positive (OCPs + M-CSF + RANKL) control. After treatment for 2d, 10 μ l of media was placed into 200 μ l of a fluorophore releasing agent and absorbance measured. Data shown are the mean \pm standard error (SE) of six independent samples. Groups not sharing a letter are statistically significant at $\alpha=0.05$.

have sought to investigate how implant surface properties modulate MSC and NHOst communication with OCs, an integral part of the bone remodeling phase of osseointegration. The results of this study demonstrate that implant surface properties can impact downstream events during



osseointegration. A novel *in vitro* model of bone remodeling was developed and used to assess the influence commercially available Ti implant surfaces have on osteoclastogenesis and OC activity. CM collected from MSCs and NHOsts cultured on smooth, microrough, and/or hydrophilic Ti surfaces decreased OC activity with NHOst cultures having a more robust effect. Gene expression was selectively regulated rather than completely shut down suggesting that the OCs have the capacity to return once the regulatory stimulus favors bone resorption.

The OsteoLyse™ assay kit is a cell culture plate coated with europium-conjugated human type I collagen used in experiments of OC differentiation and activity.^{213–215} OC resorptive activity is directly proportional to the release of Eu-labeled collagen fragments. Although type I collagen is the most abundant protein in bone, the assay lacks the complexity of native bone, including the presence of bone mineral. Furthermore, ITGAV and ITGB3 complex binding can occur on

multiple bone matrix proteins not present in the assay substrate. Shifting to bone or dentine may alter the expression patterns observed in the present study and may be necessary to confirm our results. Lastly, the assay does not allow cell culture beyond 14d as indicated by the phenotypic changes in both the OCPs and OCs. This could be due to the complete resorption of the collagen coating leading to cell death or foreign body giant cell (FBGC) fusion. Because OCs and OCPs are from the hematopoietic lineage,²¹⁶ they are sensitive to many chemokines including interleukin 4 (IL-4). IL-4 is the driving factor for FBGC fusion and is produced by OCs and OCPs.^{217,218} As a result, the chosen period of our model permits only 9d of total OC culture.

Despite these limitations, our model proved to be a practical *in vitro* tool for studying bone remodeling. Our results confirm countless observations that MSCs and NHOs release factors capable of limiting the degree and extent to which OCs resorb bone. However, for the first time we have shown that the attenuating effect is enhanced when cultured on microstructured and/or hydrophilic Ti surfaces. CM were supplemented with RANKL and M-CSF to ensure that their abrupt removal was not the cause of the decreased OC activity. The observed effect went largely unchanged, although differences were detected between SLA and mSLA MSC-CM without supplementation. Despite this observation, our results suggest that surface microroughness may play a larger role in mitigating OCs than hydrophilicity. Furthermore, these observed effects are not due to the influence Ti surfaces have on cell attachment, proliferation, or death. Previously we have shown that cell proliferation is reduced on Ti surfaces compared to TCPS, but osteogenic differentiation is increased.^{61,71,93} Although, SLA and mSLA have the fewest number of cells attached, CM from these surface cultures resulted in the greatest decrease in OC activity.

Differential gene expression in osteoclasts following treatment with CM suggests that pathways in OCs are selectively targeted. The fusion marker, OCSTAMP, was markedly reduced in OCs following treatment with CM from both cell types suggesting that a portion of the regulatory influence acts to prevent OC fusion. In order to initiate resorption, mature OCs attach

to the mineralized bone matrix, forming a sealing zone. Their initial attachment and subsequent activation are mediated by integrins, specifically, the osteopontin/vitronectin receptor, $\alpha V\beta 3$.²¹⁹⁻²²¹ Attachment of $\alpha V\beta 3$ induces signaling mechanisms that control cytoskeletal reorganization, which is important for the spreading, motility, and sealing zone organization.²²²⁻²²⁴ Interestingly, expression of either subunit did not decrease, suggesting that this signaling complex maintains its activity after treatment with MSC or NHOst CM. Following formation of the sealing zone by $\alpha V\beta 3$ signaling, the resorption lacuna beneath the OC forms where its membrane is folded forming the ruffled border. The OC can release hydrogen ions through the ruffled border via activity of carbonic anhydrase II (CA2), thereby reducing the pH and dissolving the mineralized portion of the ECM. In humans, CA2 deficiency causes non-functional osteoclasts and osteopetrosis.²²⁵ Its expression is induced through RANKL dependent pathways so its reduction would reduce the ability of the osteoclast to maintain optimal pH gradients, thus decreasing activity.²²⁶

In addition to regulating pH in the resorption lacunae, osteoclasts secrete enzymes like lysosomal cysteine proteinases and matrix metalloproteinases are then secreted to degrade the organic matrix.^{26,27} Cathepsin K (CTSK) is one of the main cysteine proteinases secreted into the resorption lacuna.^{26,227} CTSK has been shown to degrade insoluble type I collagen, and inhibition of its enzymatic activity *in vitro* and *in vivo* models prevents matrix degradation.^{228,229} Osteoclasts are also rich in cystatin B (CSTB), a natural inhibitor of cysteine proteinases. A balance between CTSK and CSTB is important for regulating cell survival as addition of CSTB to osteoclasts protects them from experimentally induced apoptosis.²³⁰ The decreased CTSK and CSTB accompanying CM treatment suggests that organic matrix degradation is subsiding, and OCs may be attempting to regulate their survival. Interestingly, NHOsts had a more robust effect on CTSK expression compared to MSCs. In general, NHOsts produce higher quantities of regulatory factors compared to MSCs, suggesting that regulation may be dependent on the

cell type.

The potential regulatory difference between cell types was the impetus for choosing MSCs to study mechanisms mediating OCs. In addition, we focused on the modulating effects of mSLA. Microroughness was the more important surface feature in terms of reducing OC activity, but our previous studies indicated that mSLA is superior at facilitating MSC differentiation.^{53,70,71,93,158} MSCs are attachment dependent and interact with their underlying substrate via integrins such as $\alpha 2\beta 1$. Silencing of both the ITGA2 and ITGB1 subunits in MSCs attenuated the inhibitory effect on OCs. Interestingly, TCPS shITGA2 MSC-CM decreased OC activity suggesting a unique signaling through the $\alpha 2$ integrin subunit.

Proteins produced by MSCs cultured on Ti surfaces are crucial to the observed phenomena in the present study. Although there is an inhibitory effect on OCs due to factors present in the basal growth media, MSC-CM decreased OC activity, which further declined with mSLA MSC-CM treatment. Heat denaturation of the CM mitigated the inhibition of OC activity. Interestingly, proteinase K digestion inhibited OC activity more. Proteinase K cleaves peptide bonds adjacent to the carboxylic group of aliphatic and aromatic amino acids.²³¹ If proteins have complicated secondary, tertiary, and/or quaternary structures, proteinase K may be unable to access certain amino acids preventing their complete degradation. This could lead to selective degradation and exacerbate the effect if antagonistic proteins are denatured over agonistic proteins. Moreover, susceptible proteins could be digested in a way that leaves the residual fragments active. Alternatively, addition of proteinase K and its neutralizer may have diluted the CM preventing OCs from receiving sufficient nutrients to stay healthy.

There is a myriad of signals capable of regulating OCs. One mechanism by which MSCs control OCs is mediated by TGF β 1-dependent regulation of OPG production.⁸⁰ TGF β 1 enhances the proliferation of MSCs and osteoblasts and stimulates ECM protein production like type I collagen. Latent TGF β 1 and latent TGF β binding protein are synthesized and stored in the ECM.

Most of the TGF β 1 produced by OBs cultured on Ti is in latent form, and the amount incorporated into the matrix is increased on rougher surfaces.⁸² Once the bone remodeling phase of osseointegration begins, OCs degrade the newly synthesized matrix releasing the stored, latent TGF β 1 and convert it into active TGF β 1. Once activated, TGF β 1 regulates OCs, in part, by regulating production of OPG. OPG serves as a decoy receptor for RANKL, which prevents RANKL-RANK binding on the OCP surface inhibiting OC differentiation.⁸³ A feedback mechanism is in place that allows osteoblasts to produce soluble RANKL in order to deplete excess OPG if the regulatory stimulus favors new osteoclast formation. Microrough Ti substrates facilitate increased production of OPG by osteoblasts; however, levels of RANKL do not change. Thus, the net effect is bone formation without bone resorption. Soluble TGF β type 2 receptor and anti-TGF β type 2 receptor antibody will compete with endogenous TGF β . Addition of these factors to TCPS MSC-CM but not mSLA MSC-CM decreased OC activity, suggesting that TGF β signaling is an important regulatory protein produced by MSCs cultured on TCPS. However, TGF β was not a contributing factor to the regulation of OCs by surfaces. This could be due to the overwhelming presence of other factors. Furthermore, the addition of anti-OPG antibody to both the TCPS and mSLA MSC-CM did not mitigate the decreased OC activity confirming the importance of OPG as a regulator of OC fusion rather than a regulator of OC activity.

Conclusions

We have shown that microstructured Ti surfaces indirectly regulate OC activity and gene expression. After surface recognition by integrins, MSC and NHOst protein production is modulated and responsible for the decreased activity of existing OCs and reduced fusion of new OCs. In addition, OC gene expression is selectively regulate suggesting more than one pathway of control may be involved. Of the proteins responsible, TGF β and OPG do not contribute to the surface dependent regulation *in vitro*.

Chapter 6. Bisphosphonates Inhibit Surface Mediated Osteogenesis

Abstract

Bisphosphonates target osteoclasts, slowing bone resorption and providing rationale to support osseointegration. However, bisphosphonates may negatively affect osteoblasts, impairing peri-implant bone formation. The goal of this study was to assess the effects bisphosphonates have on surface mediated osteogenesis of osteoblasts. MG63 cells were cultured on 15mm grade 2 titanium disks: smooth PT, hydrophobic-microrough SLA, or hydrophilic-microrough mSLA (Institut Straumann AG, Basel, Switzerland). Tissue culture polystyrene (TCPS) was used as a control. At confluence, cells were treated with 0M, 10^{-8} M, 10^{-7} M, and 10^{-6} M of alendronate, zoledronate, or ibandronate for 24h. Sprague Dawley rats were also treated with $1\mu\text{g}/\text{kg}/\text{day}$ ibandronate or phosphate buffered saline control for 5wk. Calvarial osteoblasts (rOBs) were isolated, characterized, and cultured on surfaces. Osteogenic markers in the media were quantified using ELISAs. Bisphosphonate treatment reduced osteocalcin, osteoprotegerin, osteopontin, BMP2, PGE2, TGF β 1, IL10, and VEGF in MG63 cells. The effect was more robust on rough surfaces, and higher concentrations of bisphosphonates stunted production to TCPS/PT levels. Ibandronate conditioned rOBs produced less osteogenic markers similar to direct bisphosphonate treatment. These results suggest bisphosphonate exposure jeopardizes the pro-osteogenic response osteoblasts have to microstructured surfaces. Their effects persist *in vivo* and negatively condition osteoblast response *in vitro*. Clinically, bisphosphonates could compromise osseointegration.

Introduction

Bisphosphonates (BPs) are synthetic compounds characterized by two C–P bonds sharing a carbon atom (P–C–P), making them chemically stable analogues of pyrophosphates (P–O–P). Substitution of oxygen with carbon makes BPs completely resistant to enzymatic hydrolysis

while maintaining their affinity for bone mineral.²³² Differences in side chain moieties at the R¹ and R² positions of the P–C–P bond explain the wide variance in the physiochemical properties and physiological effects among BPs.²³² Substitutions of a hydroxyl and a nitrogen containing group have proven to greatly increase affinity and adherence to the hydroxyapatite surface as well as their anti-resorptive potency. As a result, the molecular mechanisms of action and tissue distribution of these aminobisphosphonates are restricted to the skeleton making them widely used to treat diseases of calcium metabolism.²³³ These anti-resorptive effects have also led to their use to positively influence osseointegration of titanium (Ti) dental and orthopaedic implants.

The primary mechanism by which BPs prevent bone loss is through actions on bone resorbing osteoclasts. BPs preferentially bind to exposed bone mineral at surfaces undergoing resorption where they are then internalized by osteoclasts, disrupting their resorptive ability.²³⁴ While these actions on osteoclasts are well known, their effects on other bone cells like osteocytes, osteoblasts, and mesenchymal stem cells (MSCs) are less understood. Low concentrations of BPs were shown to prevent apoptosis of osteocytes and osteoblasts.²³⁵ This effect is mediated by hexameric connexin-43 hemichannels, calcium influx, and activation of the extracellular signal-regulated kinases, suggesting that intracellular uptake is not required.²³⁶ BPs were also shown to stimulate the proliferation of osteoblasts and their progenitors as well as enhance alkaline phosphatase activity, mineral formation, and expression of bone morphogenetic protein (BMP)-2, collagenase-3, osteocalcin, and osteoclast inhibitory factors.²³⁷

Other studies, however, have reported adverse effects of BP treatment. Calcium deposition,²³⁸ collagen production,²³⁹ mineralized bone nodule formation,²⁴⁰ and response to parathyroid hormone (PTH)²⁴¹ are impaired by BPs. Furthermore, BPs can impede angiogenesis,²⁴² cause microfracture accumulation,²⁴³ and are associated with osteonecrosis of the jaw (ONJ),²⁴⁴ all of which can be detrimental to the formation of healthy bone tissue especially during implant osseointegration. Much controversy as to the efficacy of BP therapy

on implant osseointegration stems from these contrasting observations.

Despite these discrepancies, current research does reveal that BPs modulate osteoblast biosynthesis; however, the current knowledge has been limited to osteoblasts cultured on tissue culture polystyrene (TCPS). Osteoblast differentiation and maturation are very different when cultured on implant surfaces compared to TCPS.^{70,71} Surface microtopography and hydrophilicity enhance the production of osteoblast markers in MG63 osteoblast-like cells,²⁴⁵ primary human osteoblasts and MSCs,²² and fetal rat calvarial cells,²⁴⁶ without supplements typically used to induce osteoblast differentiation. The increased osteogenic potential of these implant surfaces *in vitro* correlates with a more rapid and sufficient osseointegration in preclinical and clinical studies. It is unknown whether BPs affect the surface mediated osteogenesis of osteoblasts, but other osteotropic agents such as $1\alpha,25\text{-dihydroxy vitamin D}_3$ ($1\alpha,25(\text{OH})_2\text{D}_3$)²⁴⁷ and $17\beta\text{-estradiol}$ ⁷⁵ are known to modulate the cellular response and work synergistically with implant surface characteristics.

As the population of patients receiving BPs continues to grow, it is imperative to determine these effects as they could directly influence the ability of implants to osseointegrate and maintain their longevity clinically. Unravelling these molecular mechanisms may help expand the utility of BPs, ensure their overall safety, and limit their contraindications. The goal of this study was to test the hypothesis that clinically used, nitrogen-containing bisphosphonates (alendronate, zoledronate, and ibandronate) modulate the pro-osteogenic response osteoblasts have to implant surface roughness and hydrophilicity.

Materials and Methods

MG63 Cell Culture

Human MG63 cells (ATCC, Manassas, VA) were separately cultured on tissue culture polystyrene (TCPS) or 15mm diameter, 1mm thick, grade 2 Ti disks modified as described previously to be smooth/hydrophobic (PT), microrough/hydrophobic (SLA), or

microrough/hydrophilic (mSLA). Disks were provided as a gift from Institut Straumann AG (Basel, Switzerland). Cells were seeded at a density of 10,000 cells/cm² and incubated at 37°C in an atmosphere of 5% CO₂ and 100% humidity using Dulbecco's modified Eagle medium (DMEM; Mediatech, Manassas, VA) supplemented with 10% fetal bovine serum (FBS; Life Technologies, Carlsbad, CA) + 1% penicillin-streptomycin (Life Technologies). Media were changed 24h after plating and every 48h thereafter until cells reached confluence on TCPS.

Biological Response

Confluent cultures were incubated with fresh media supplemented with either 0M, 10⁻⁸M, 10⁻⁷M, or 10⁻⁶M alendronate (C₄H₁₂NNaO₇P₂•3H₂O; Merck Sharp & Dohme, Kenilworth, NJ), zoledronate (C₅H₁₀N₂O₇P₂•H₂O; Novartis AG, Basel, Switzerland) or ibandronate (C₉H₂₂NNaO₇P₂•H₂O; AuroMedics, East Windsor, NJ) for 24h. Radioimmunoassay kits were used to measure intact osteocalcin (Biomedical Technologies, Stoughton, MA) and prostaglandin E₂ (PGE₂; Perkin Elmer, Wellesley, MA) levels in alendronate and zoledronate treated cultures. Active transforming growth factor β1 (TGFβ1) was measured prior to acidification of the conditioned media, using an ELISA kit specific for human TGFβ1 (Promega Corp., Madison, WI). Total TGFβ1 was measured after acidifying the media and latent TGFβ1 was defined as total TGFβ1 minus active TGFβ1. For ibandronate treated MG63 cultures, ELISAs were used to measure levels of intact osteocalcin (Alfa Aesar, Haverhill, MA), human/mouse/rat BMP2 (PeproTech, Rocky Hill, NJ), osteopontin (R&D Systems, Minneapolis, MN), interleukin 6 (IL6; R&D Systems), and interleukin 10 (IL10; R&D Systems) following manufacturer's instructions. ELISAs for osteoprotegerin (R&D Systems) and vascular endothelial growth factor VEGF-A (VEGF-A; R&D Systems) were used for all MG63 cultures. Experiments treating MG63 cells with either alendronate or zoledronate were normalized to cell number, while ibandronate treated cultures were normalized to DNA content.

Cell number or DNA content was determined in all cultures 24h after BP treatment. For cell

number, cells were released from the surfaces by two sequential incubations in 0.25% trypsin for 10min at 37°C. Released cells were counted using an automatic Z1 Coulter Cell Particle Counter (Beckman Coulter, Fullerton, CA). Cell lysates were then collected by centrifuging the cells after counting. For DNA content, cell monolayers were washed twice with 0.2ml phosphate-buffered saline (PBS), lysed in 0.05% Triton X-100, and homogenized by sonication at 40A using a Vibra-Cell ultrasonicator (Sonics & Materials Inc., Newtown, CT). DNA content in the cell lysate was measured with PicoGreen (Promega, Madison, WI) using a Synergy H1 Hybrid Reader fluorescence detector (BioTek, Winooski, VT) at an excitation of 485nm and emission of 538nm. Alkaline phosphatase specific activity [orthophosphoric monoester phosphohydrolase, alkaline; E.C. 3.1.3.1] was assayed in cell lysates by measuring the conversion of *p*-nitrophenylphosphate to *p*-nitrophenol at pH 10.25 and a temperature of 37°C. Absorbance was measured at 405nm. Activity was normalized to total protein content in the cell lysates as determined by a bicinchoninic acid protein assay kit (Thermo Fisher Scientific, Waltham, MA).

Rat Calvarial Osteoblast Isolation and Biological Response

All subsequent experiments were carried out under an Institutional Animal Care and Use Committee approved protocol at Virginia Commonwealth University (protocol AD10000675) and reported according to ARRIVE guidelines. All animals were treated humanely per the guidelines outlined in the Guide for the Care and Use of Laboratory Animals by the National Institutes of Health. CD Sprague Dawley rats were single-housed in an individually ventilated, solid-bottomed polysulfone cage and kept at a temperature of 17-28°C with a humidity of 40-70% and a 12/12 h light/dark cycle. All rats were given ad libitum access to standard pellet and water and received fresh food daily.

Six, 9mo old, virgin, female CD Sprague Dawley rats (Charles River Laboratories, Wilmington, MA) were injected subcutaneously with 25µg/kg ibandronate (n=3) or PBS (n=3) on day 0 and on day 25. Rats were euthanized 5wk after the first injection (day 35), so each animal

received a total of two injections of ibandronate or PBS. After euthanasia via CO₂ inhalation, the heads were cleaned with 70% ethanol and betadine solution and the frontal and parietal bones excised. Connective tissue was then removed, and the remaining bone was minced into pieces approximately 1mm x 1mm. Explants from each animal in the same group were pooled together into a 100mm x 20mm Petri dish with DMEM + 10% FBS + 1% penicillin-streptomycin. Petri dishes were incubated at 37°C in an atmosphere of 5% CO₂ and 100% humidity until cells reached confluence. Cells were passaged and explants were placed into a new Petri dish. This process was repeated until migration of osteoblasts from the explants stopped.

The osteoblastic phenotype of primary rat osteoblasts (rOBs) was confirmed by treating confluent cultures of rOBs with either 0M or 10⁻⁸M 1 α ,25(OH)₂D₃ (Enzo Biochem, Farmingdale, NY) for 24h. Conditioned media were measured for intact rat osteocalcin (Alfa Aesar) and alkaline phosphatase specific activity was quantified in cell lysates. Verified rOBs (passage<4) were cultured on modified Ti substrates as described for the MG63 cells (Section 2.2). At confluence, cells were incubated with fresh DMEM for 24h. Responses were assessed using ELISAs measuring osteocalcin, rat/mouse osteopontin (R&D Systems), mouse osteoprotegerin (R&D Systems), human/mouse/rat BMP2 (PeproTech), mouse receptor activator of nuclear kappa-B ligand (RANKL; R&D Systems), and rat VEGF-A (R&D Systems). Alkaline phosphatase specific activity was measured in cell lysates and normalized to total protein content. Immunoassays were normalized to DNA content.

Statistical Analysis

Data are presented as the mean \pm standard error (SE) of n=6 cultures per variable. All experiments were repeated at least three times to ensure validity of the results. Data shown in the figures are from representative experiments. A *t*-test was used was used to determine significant differences for experiments assessing the osteoblastic phenotype of rOBs. A two-way analysis of variance (ANOVA) was used to model the mean production of biological variables by

MG63 cells or rOBs cultured on four different surfaces (TCPS, PT, SLA, mSLA) and treated with four different BP concentrations (0M, 10^{-8} M, 10^{-7} M, 10^{-6} M). The model included main effects for surface and BP concentration, as well as a surface by BP concentration interaction. If a significant interaction was identified between variables, mean differences between the levels of surface were compared at specific levels of BP concentration (and vice versa). If no significant interaction was present, mean differences were compared separately within each variable. A two-tailed Tukey correction was used to adjust for multiple comparisons to maintain an experiment-wise error rate (α) of 0.05. All statistical analyses were performed using JMP statistical software (SAS Institute Inc., Cary, North Carolina).

Results

MG63 Cell Response

Alendronate

Control (0M) MG63 cultures had reduced cell numbers (**Fig.21A**) on Ti surfaces compared to TCPS and further reduced on SLA and mSLA compared to PT. When treated with alendronate, cell number remained similar on PT and TCPS but was reduced on SLA except when treated with 10^{-6} M alendronate. mSLA cultures had reduced cell numbers similar to SLA. Within each surface cell number increased when treated with 10^{-6} M alendronate compared to 10^{-8} M. 10^{-6} M treated PT and SLA cultures saw increased cell numbers compared to other concentrations. Alkaline phosphatase specific activity (**Fig.21B**) was reduced on all surfaces. Treatment with 10^{-6} M alendronate increased activity compared to no treatment for TCPS, PT, and SLA cultures. Osteocalcin levels (**Fig.21C**) significantly increased on mSLA compared to PT and TCPS. Treatment with 10^{-6} M alendronate decreased osteocalcin levels within surface cultures compared to non-treated controls for mSLA. On other surfaces, the decrease was significant to the 10^{-8} M treatment. Osteoprotegerin (**Fig.21D**) and latent TGF β 1 (**Fig.21E**) levels increased on SLA and mSLA cultures compared to TCPS and PT cultures. 10^{-6} M alendronate

treatment decreased MG63 osteoprotegerin production on all surfaces and decreased latent TGFβ1 levels in SLA and mSLA cultures. PGE₂ (Fig.21F) levels were increased on SLA and mSLA compared to TCPS and PT across all concentrations. TCPS, SLA, and mSLA cultures treated with 10⁻⁶M alendronate had significant reductions in VEGF (Fig.21G) production compared to untreated controls.

Zoledronate

Cell number (Fig.22A) significantly decreased on SLA compared to PT and TCPS and further decreased on mSLA for untreated MG63 cultures. Treatment with 10⁻⁷M zoledronate resulted in increased cell numbers compared to non-treated controls on each surface. These numbers were

similar to 10⁻⁶M treatment for SLA and mSLA cultures. Few differences were detected with alkaline phosphatase specific activity (Fig.22B); however, none of these differences were due to treatment with zoledronate. Surface topography significantly increased osteocalcin levels (Fig.22C) while treatment with zoledronate decreased its production to similar levels across all

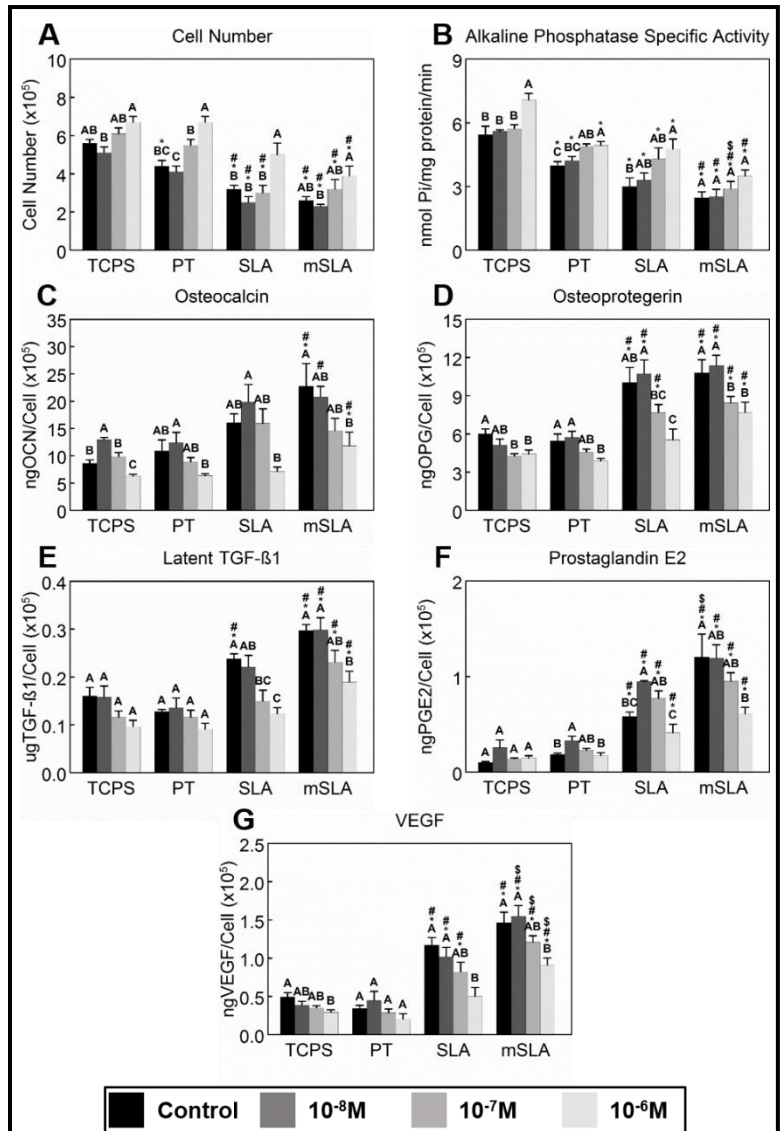


Figure 21. Effects of alendronate treatment on MG63 cells cultured on microstructured and hydrophilic Ti substrates. MG63 cells were cultured separately on TCPS, PT, SLA, or mSLA. At confluence, cells were treated with 0M (control), 10⁻⁸M, 10⁻⁷M, or 10⁻⁶M alendronate for 24h. After 24h, cells were counted (A) and alkaline phosphatase (B) specific activity was quantified in lysates. Media were assayed for osteocalcin (C), osteoprotegerin (D), latent TGFβ1 (E), PGE₂ (F), and VEGF (G). Data shown are the mean ± standard error (SE) of six independent samples. Letters denote significance among alendronate treatments within the same substrate culture. Groups not sharing a letter are statistically significant at α=0.05. Symbols denote significance among surface cultures within the same alendronate treatment. *p < 0.05 vs. TCPS; #p < 0.05 vs. PT; \$p < 0.05 vs. SLA.

surfaces. Osteoprotegerin (Fig.22D) production was similar to osteocalcin, although mSLA production after treatment remained higher compared to PT and TCPS. Furthermore, treatment decreased production on all surfaces compared to non-treated controls. Increased latent TGFβ1 (Fig.22E) levels were detected in mSLA cultures. Treatment with high concentrations of zoledronate decreased latent TGFβ1 production compared to non-treated controls or lower concentrations. PGE₂ (Fig.22F) and VEGF (Fig.22G) increased in a surface dependent manner. Treatment with 10⁻⁷M or 10⁻⁶M zoledronate reduced the production of PGE₂ in SLA and mSLA cultures and the production of VEGF in PT and mSLA cultures. VEGF was reduced in SLA cultures when treated with 10⁻⁶M zoledronate.

Ibandronate

Compared to TCPS, DNA content (Fig.23A) was reduced on all surfaces. A further reduction was observed on SLA and mSLA compared to PT. Treatment with ibandronate increased the

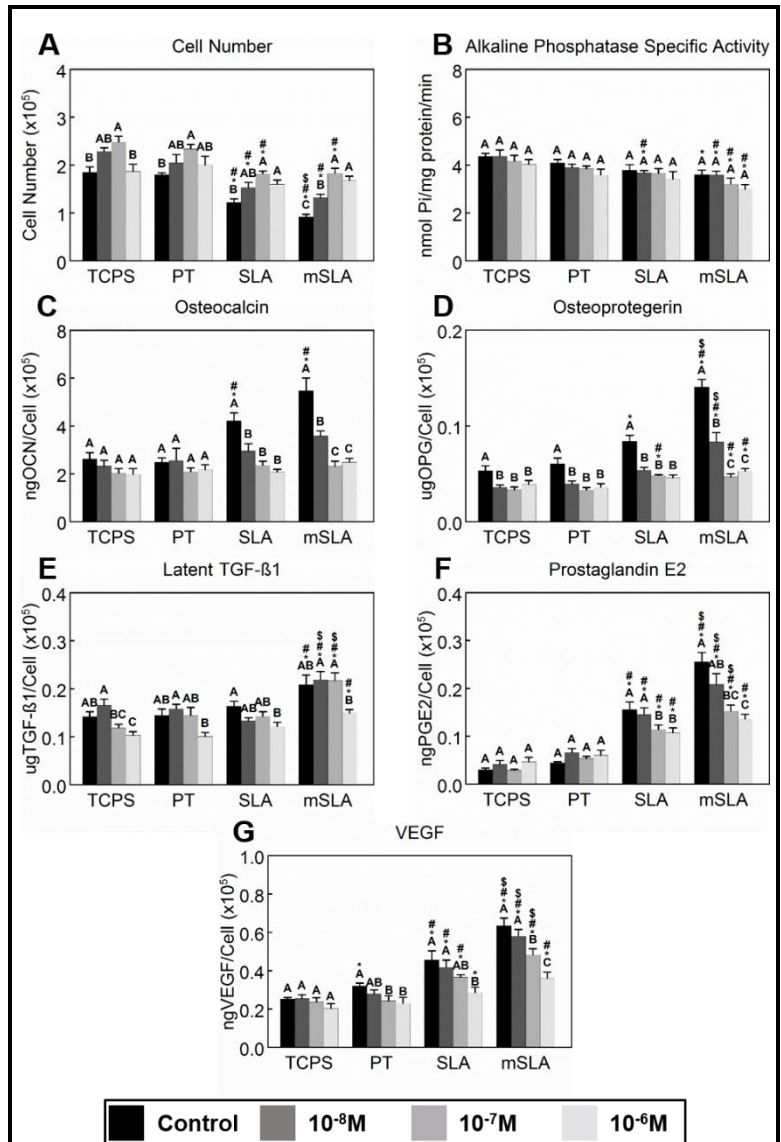


Figure 22. Effects of zoledronate treatment on MG63 cells cultured on microstructured and hydrophilic Ti substrates. MG63 cells were cultured separately on TCPS, PT, SLA, or mSLA. At confluence, cells were treated with 0M (control), 10⁻⁸M, 10⁻⁷M, or 10⁻⁶M zoledronate for 24h. After 24h, cells were counted (A) and alkaline phosphatase specific activity (B) was quantified in lysates. Media were assayed for osteocalcin (C), osteoprotegerin (D), latent TGFβ1 (E), PGE₂ (F), and VEGF (G). Data shown are the mean ± standard error (SE) of six independent samples. Letters denote significance among zoledronate treatments within the same substrate culture. Groups not sharing a letter are statistically significant at α=0.05. Symbols denote significance among surface cultures within the same zoledronate treatment. *p < 0.05 vs. TCPS; #p < 0.05 vs. PT; \$p < 0.05 vs. SLA.

DNA content within surface cultures.

Alkaline phosphatase specific activity (Fig.23B) was reduced in response to surface topography. Treatment with 10^{-7} M or 10^{-6} M ibandronate reduced activity further on Ti substrates while

10^{-6} M ibandronate treatment reduced the activity on TCPS. Production of osteocalcin (Fig.23C), osteoprotegerin (Fig.23D), BMP2 (Fig.23E), and VEGF (Fig.23G) were significantly increased on SLA compared to TCPS and PT and mSLA compared to TCPS, PT, and

SLA. MG63s cultured on TCPS or Ti substrates produced less osteocalcin, BMP2, osteopontin, and VEGF when treated with ibandronate. Osteoprotegerin production was reduced in SLA cultures when treated with ibandronate; however, mSLA

cultures were not sensitive to the 10^{-8} M concentration. Ti substrates facilitated the decreased production of IL6 (Fig.24A) and the increased production of IL10 (Fig.24B). Treatment with ibandronate decreased production of IL6 in TCPS and PT cultures while stimulating production in SLA and mSLA at 10^{-6} M and 10^{-7} M/ 10^{-6} M concentrations respectively. Ibandronate treatment

reduced in SLA cultures when treated with ibandronate; however, mSLA

cultures were not sensitive to the 10^{-8} M concentration. Ti substrates facilitated the decreased production of IL6 (Fig.24A) and the increased production of IL10 (Fig.24B). Treatment with ibandronate decreased production of IL6 in TCPS and PT cultures while stimulating production in SLA and mSLA at 10^{-6} M and 10^{-7} M/ 10^{-6} M concentrations respectively. Ibandronate treatment

reduced in SLA cultures when treated with ibandronate; however, mSLA

cultures were not sensitive to the 10^{-8} M concentration. Ti substrates facilitated the decreased production of IL6 (Fig.24A) and the increased production of IL10 (Fig.24B). Treatment with ibandronate decreased production of IL6 in TCPS and PT cultures while stimulating production in SLA and mSLA at 10^{-6} M and 10^{-7} M/ 10^{-6} M concentrations respectively. Ibandronate treatment

reduced in SLA cultures when treated with ibandronate; however, mSLA

cultures were not sensitive to the 10^{-8} M concentration. Ti substrates facilitated the decreased production of IL6 (Fig.24A) and the increased production of IL10 (Fig.24B). Treatment with ibandronate decreased production of IL6 in TCPS and PT cultures while stimulating production in SLA and mSLA at 10^{-6} M and 10^{-7} M/ 10^{-6} M concentrations respectively. Ibandronate treatment

reduced in SLA cultures when treated with ibandronate; however, mSLA

cultures were not sensitive to the 10^{-8} M concentration. Ti substrates facilitated the decreased production of IL6 (Fig.24A) and the increased production of IL10 (Fig.24B). Treatment with ibandronate decreased production of IL6 in TCPS and PT cultures while stimulating production in SLA and mSLA at 10^{-6} M and 10^{-7} M/ 10^{-6} M concentrations respectively. Ibandronate treatment

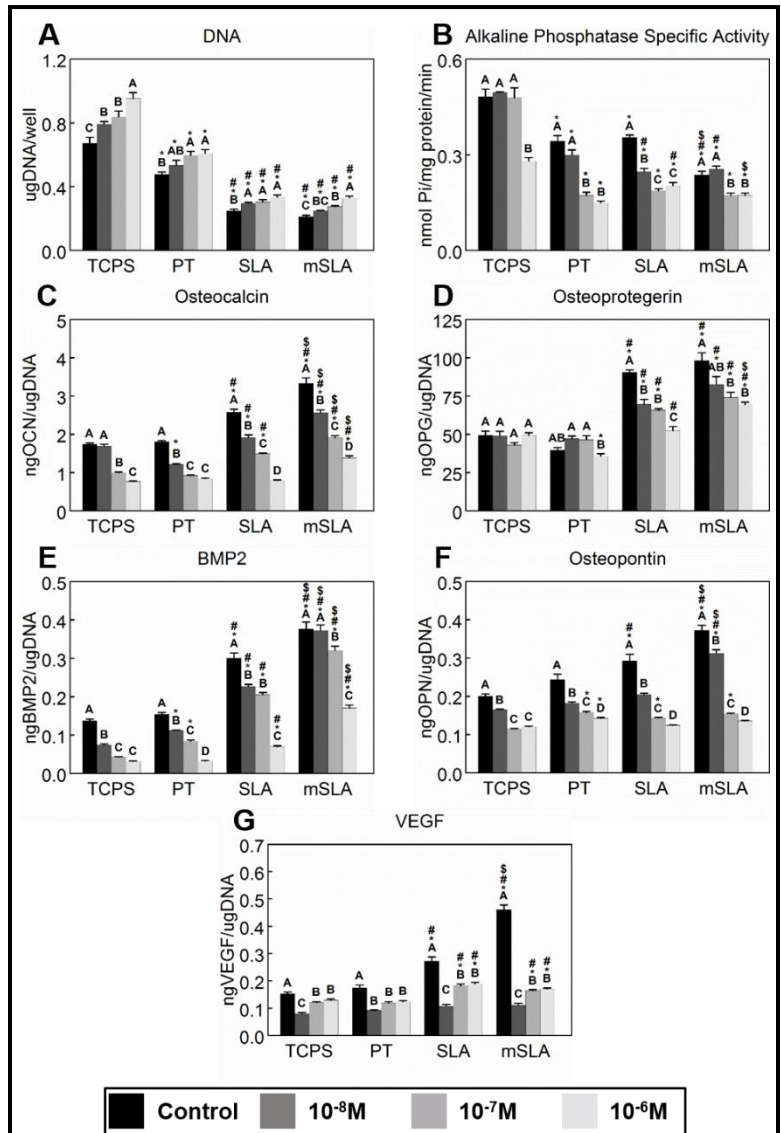
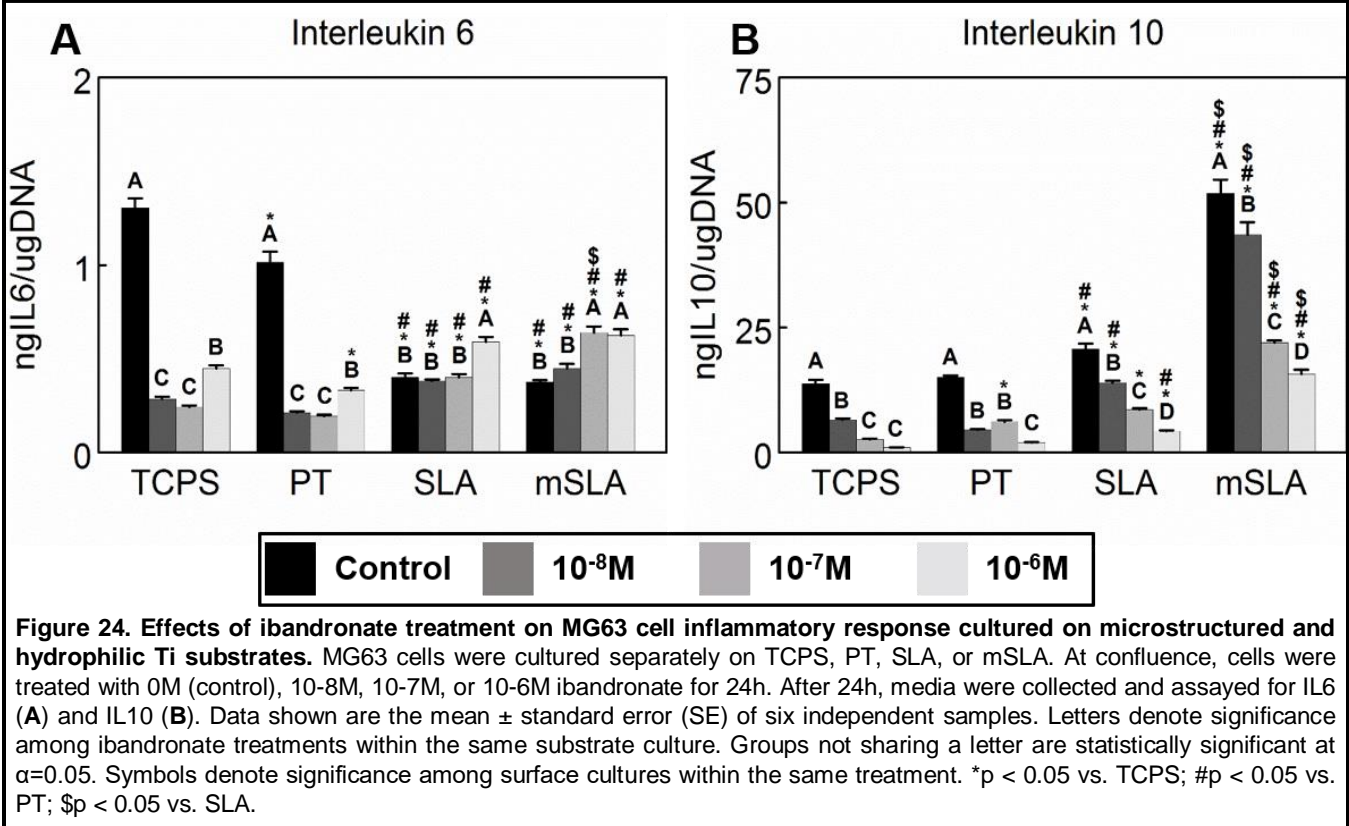


Figure 23. Effects of ibandronate treatment on MG63 cells cultured on microstructured and hydrophilic Ti substrates. MG63 cells were cultured separately on TCPS, PT, SLA, or mSLA. At confluence, cells were treated with OM (control), 10^{-8} M, 10^{-7} M, or 10^{-6} M ibandronate for 24h. After 24h, cell lysates were assayed for DNA content (A) and alkaline phosphatase specific activity (B). Media were assayed for osteocalcin (C), osteoprotegerin (D), BMP2 (E), osteopontin (F), and VEGF (G). Data shown are the mean \pm standard error (SE) of six independent samples. Letters denote significance among ibandronate treatments within the same substrate culture. Groups not sharing a letter are statistically significant at $\alpha=0.05$. Symbols denote significance among surface cultures within the same ibandronate treatment. * $p < 0.05$ vs. TCPS; # $p < 0.05$ vs. PT; \$ $p < 0.05$ vs. SLA.

decreased production of IL10 in all cultures.



Rat Calvarial Osteoblast Response

Addition of 10^{-8} M $1\alpha,25(\text{OH})_2\text{D}_3$ to confluent cultures of rOBs increased osteocalcin and alkaline phosphatase specific activity, confirming their successful isolation and expansion. DNA content of rOBs (**Fig.25A**) was reduced on Ti surfaces compared to TCPS for both treatment groups. When cultured on the same surface, ibandronate rOBs had decreased DNA content compared to PBS rOBs. Similarly, decreased levels of alkaline phosphatase specific activity (**Fig.25B**) were observed on Ti surfaces with the lowest levels occurring on SLA and mSLA for both groups of osteoblasts. Ibandronate treatment decreased alkaline phosphatase specific activity in rOBs cultured on TCPS and PT compared to PBS rOBs. Osteocalcin production (**Fig.25C**) was increased in a surface dependent manner (mSLA>SLA>PT>TCPS) for all rOBs; however, ibandronate rOBs had decreased productions when cultured on SLA and mSLA compared to PBS rOBs. Osteoprotegerin levels (**Fig.25D**) decreased on Ti surfaces compared to TCPS while ibandronate treatment was able to stimulate its production compared to PBS.

Production of BMP2 (Fig.25E), osteopontin (Fig.25F), VEGF (Fig.25G), and RANKL (Fig.25H) was increased in rOBs cultured on Ti surfaces compared to TCPS. When cultured on the same surface, ibandronate rOBs had decreased production compared to PBS rOBs.

Discussion

Bisphosphonates are commonly used to treat metabolic bone disorders due to their high affinity for bone and their antiresorptive effects via actions on osteoclasts. Because BPs slow the rate and severity of bone resorption, it is reasonable to assume that they could significantly impact the osseointegration of dental and orthopaedic implants, particularly during the bone modeling and remodeling phases. This suggests that BPs could affect bone formation as well as bone resorption. The results of the

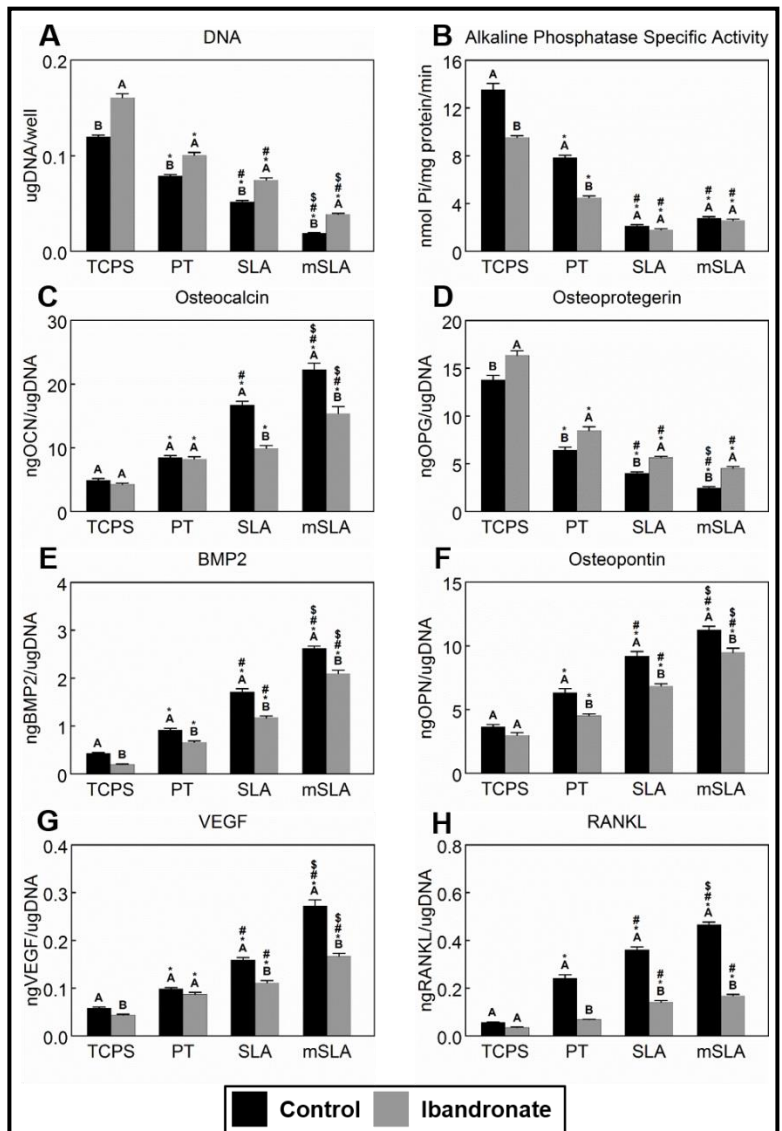


Figure 25. Response of calvarial osteoblasts isolated from aged rats treated with ibandronate to microstructured and hydrophilic Ti substrates. Six 9-month-old, female, virgin, CD Sprague-Dawley rats were treated with either 25 μ g/kg ibandronate (n=3) or PBS (n=3) on day 0 and again on day 25. Rats were euthanized on day 35. Calvarial osteoblasts were isolated and cultured separately on TCPS, PT, SLA, or mSLA in DMEM. At confluence, cells were treated with fresh DMEM for 24h. After 24h, media were collected, and cell lysates were assayed for DNA content (A) and alkaline phosphatase specific activity (B). Media were assayed for osteocalcin (C), osteoprotegerin (D), BMP2 (E), osteopontin (F), VEGF (G), and RANKL (H). All osteoblasts used were of passage 3 or less. Data shown are the mean \pm standard error (SE) of six independent samples. Letters denote significance between ibandronate and PBS (control) treatments within the same substrate culture. Groups not sharing a letter are statistically significant at $\alpha=0.05$. Symbols denote significance among surface cultures within the treatment. *p < 0.05 vs. TCPS; #p < 0.05 vs. PT; \$p < 0.05 vs. SLA.

present study confirm that osteoblasts respond to nitrogen-containing BPs and demonstrate that implant surface properties modulate their response.

The physicochemical and biological profile of clinically available BPs are dose-dependent and vary with the chemistry of the compound making it difficult to extrapolate findings from one BP to another with respect to its actions. Differences in pharmacokinetics, pharmacodynamics, affinity to bone, cell permeability, and intracellular protein binding between mechanistically similar BPs contribute significantly to their potency. For these reasons, the response of MG63 cells to three different nitrogen-containing BPs at three different concentrations was assessed to determine whether the observed effects were similar. This study shows for the first time that the surface mediated osteogenesis of MG63 cells and rOBs is impaired by BP treatment. These results support previous observations in our lab^{75,84,93,247,248} and others^{249,250} showing that the response of cells to osteotropic agents is surface-dependent. The observed effects were dose dependent and were more robust in SLA and mSLA cultures compared to PT and TCPS cultures, indicating that BPs could affect cells differently depending on their specific state of differentiation and/or maturation.

Typically, microrough and/or hydrophilic SLA and mSLA cultures of osteoblasts exhibit a more differentiated and mature phenotype compared to smooth PT and TCPS cultures.⁸² Late stage modulators of differentiation and mineralization, osteocalcin, BMP2, and osteopontin, as well as the angiogenic factor, VEGF, were increased on microstructured surfaces while the early differentiation marker, alkaline phosphatase specific activity was decreased. Moreover, osteoblasts on microstructured substrates produce factors that favor osteogenesis over osteoclastic resorption by producing increased TGF β 1 and osteoprotegerin, which inhibit osteoclast activation.⁸⁰ The effects of alendronate, zoledronate, or ibandronate on confluent cultures of MG63 cells are consistent with studies showing that BPs enhance the proliferation of osteoblasts,^{251,252} as indicated by the increased cell number or DNA content. BP treatment was also able to reduce production of VEGF suggesting impeded angiogenesis as described previously.²⁴² However, our results are inconsistent with studies describing their ability to

increase production of osteogenic markers.²³⁷ With the exception of alkaline phosphatase specific activity, BP treatment decreased all pro-osteogenic markers as well as the anti-inflammatory cytokine IL10. Many of the markers measured in this study were more susceptible to BP treatment in SLA and mSLA cultures compared to TCPS and PT cultures, and, for IL6 production, had opposite effects between TCPS/PT and SLA/mSLA cultures. These results along with findings suggesting BPs both increase²⁵³ and decrease²⁵⁴ IL6 production by osteoblast-like cells, indicate that BPs could affect cells differently depending on the specific state of differentiation and/or maturation.

The inconsistencies among studies could also be influenced by the alternate pathways through which Ti surface topography facilitates osteogenesis compared to TCPS. On TCPS, osteoblastic differentiation occurs through the canonical Wnt3A pathway while also primarily expressing the $\alpha5\beta1$ integrin complex.^{70,161} Surface mediated differentiation occurs through the calcium-dependent Wnt5A pathway and shift to the production of $\alpha1\beta1$ and $\alpha2\beta1$ integrin complexes.^{70,161} In addition, this occurs with media supplements typically used to induce osteoblastic differentiation. Very few studies have investigated the effects BPs have on surface mediated differentiation and maturation of osteoblasts, and many are concerned with the effects BP coated Ti substrates have on osteogenesis.²⁵⁵ rOBs isolated from 1d old Sprague Dawley rats saw no changes in osteoblastic markers when cultured on Ti substrates coated with immobilized pamidronate.²⁵⁶ Another study reported positive osteogenic effects of Ti surfaces coated with immobilized alendronate on human osteoblasts and MSCs.²⁵⁷ However, the chemical process used to coat the substrates could easily distort the already highly variable chemical effects of the BPs. Many of these studies also used osteogenic media to induce differentiation.^{257,258} Since the differentiation of cells driven by surface topography and osteogenic media are divergent,⁷¹ BPs could alter downstream signalling mechanisms differently.

Differences in BP chemistries were also evident when comparing their biological effects. Alendronate was most inhibitory at the highest concentration, 10^{-6} M, and occasionally elicited pro-osteogenic effects at the lowest concentrations by increasing osteocalcin and PGE_2 on certain surfaces. Zoledronate was effective at all concentrations; however, its effects were mostly limited to the more differentiated SLA and mSLA cultures. Ibandronate had the greatest impact on the production of osteogenic factors on all surface cultures as well as at all concentrations. Interestingly, each BP had a different effect on alkaline phosphatase specific activity as it was increased by alendronate, not affected by zoledronate, and impaired by ibandronate. Despite these differences, high concentrations of each BP were able to reduce the osteogenic potential of SLA and mSLA to similar levels as TCPS and PT. This has significant clinical implications suggesting BP usage impairs the osteoblast response to microstructured surfaces and potentially slowing the rate of osseointegration.

Because the effects of BPs have shown to be dependent on cell type, we obtained primary cell cultures from a clinically relevant animal model in order to verify our findings. Moreover, we were interested in whether the effects of BP treatment *in vivo* could persist well after administration. Relatively lower-affinity BPs have demonstrated extended bone mineral density maintenance for up to a year despite a resolution of turnover markers with that time frame. This indicates that the primary determinant of the antiresorptive potency for bisphosphonates is more likely to be the biochemical and cellular effects of BPs on bone cells, as illustrated by correlations between potency for effects at the molecular/cellular level and antiresorptive potency in animal models.²⁵⁹ 9-month old female rats were used in the present study because they closely match the age when human patients would likely begin receiving BPs as a first line therapy for metabolic bone disorders.²⁶⁰

Ibandronate was selected for the animal study out of the three tested BPs since it has an average inhibitory potency compared to other nitrogen containing BPs.²⁵⁹ Ibandronate

conditioned rOBs displayed decreased markers of osteogenesis compared to PBS conditioned rOBs. Unlike MG63 cells, however, BP treatment decreased osteoprotegerin production and increased RANKL production on microstructured surfaces. Previously, it was shown that the osteoblast-specific production of osteoprotegerin decreases while RANKL increases with age in humans²⁶¹ and rodents.⁷⁹ Perhaps the maturation of aged osteoblasts facilitated by microstructured Ti surfaces accelerates this senescent-like phenotype. Additionally, BPs have been shown to increase serum osteoprotegerin *in vivo*, which correlates with increased bone mineral density.²⁶² It is unknown if the increased osteoprotegerin reflects a direct effect of BPs on osteoblasts or an indirect effect by altering osteoclastogenesis and thereby altering the catabolism of osteoprotegerin. Regardless, our data suggest that the effects of BP treatment persists well after administration *in vivo*, and negatively influences the ability of osteoblasts isolated from BP-treated animals to undergo osteogenesis on microstructured surfaces *in vitro*.

The present study is not without its limitations. First, the correlation between BP potency *in vitro* and *in vivo* is rather poor, which may be due to the lack of consideration of the relative affinity of BPs for bone when establishing *in vitro* models. Moreover, there is little information on the concentrations that osteoblasts, osteocytes, or osteoclasts are exposed to *in vivo*, so our experiment was designed to mimic clinical treatment.^{233,263–265} Treatment method, dose, and frequency were determined based on findings that total amount, not frequency, of ibandronate injections is important for drug efficacy and the optimal dose was 1.0 μ g/kg.^{263–265} Subcutaneous injection was chosen instead of oral administration to ensure total dosage delivery to each rat. 25 days was chosen to mimic monthly injections used clinically while also minimizing distress arising from frequent injections. It should be noted that 1.0 μ g/kg of ibandronate is approximately 83.5 μ M, which is roughly 8 times higher than the highest concentration used for *in vitro* experiments.

Perhaps the most important limitation to our study is that the main cell type investigated was

the MG63 cell line, which are immature osteoblast-like cells originally isolated from a male human osteosarcoma and most recipients of BPs are post-menopausal females. BPs have been frequently demonstrated to elicit antitumor effects including inhibition of proliferation and induction of apoptosis in human myeloma cells^{266,267} and osteosarcoma cells^{268,269} *in vitro*. The exact mechanisms for the observed antitumor effects are unclear, although studies suggest BPs may act by decreasing certain tumor-stimulating cytokines like TGF β 1²⁷⁰ or by decreasing angiogenic factors like VEGF.^{271,272} Production of both latent TGF β 1 and VEGF were inhibited by BPs when MG63 cells were cultured on SLA and mSLA surfaces but not in TCPS or PT cultures. Although ibandronate inhibited VEGF production in TCPS and PT cultures at all concentrations, alendronate inhibited production of VEGF on TCPS at 10⁻⁶M compared to no treatment, while zoledronate inhibited production of latent TGF β 1 in TCPS cultures and VEGF on PT cultures compared to no treatment. Moreover, certain concentrations of BPs favored proliferation over apoptosis as indicated by cell number and DNA content. In general, much higher concentrations (>10 μ M) of BPs than what was used for the present experiments are needed to affect tumor cell proliferation and survival.^{273,274} Furthermore, confirmation of the effects in primary rOBs also serves to eliminate any possible tumor specific effects.

Conclusions

We have shown that MG63 cells and rOBs are sensitive to surface roughness and hydrophilicity and their response to nitrogen containing BPs is modified by this topography. Since BP treatment was more robust in cells cultured on rough and/or hydrophilic surfaces compared to smooth substrates, this effect may be dependent on cell maturation state, as well as donor sex and age. These results suggest that bisphosphonate exposure may jeopardized the pro-osteogenic response osteoblasts have to microstructured surfaces. Their effects persist *in vivo* and condition osteoblasts to negatively influence their *in vitro* response. Clinically, bisphosphonates could compromise peri-implant bone formation slowing the rate and quality of

implant osseointegration. Although our results were observed in both MG63 cells and rOBs, confirmation of our findings *in vivo* need to be conducted.

Chapter 7. Ibandronate Treatment Before and After Implant Insertion Impairs Osseointegration in Aged Rats with Ovariectomy Induced Osteoporosis

Abstract

Excessive decreases in bone volume (BV) and bone mineral density (BMD) can lead to osteoporosis, potentially hindering implant osseointegration. Bisphosphonates are commonly used to combat osteoporosis by slowing osteoclast-mediated resorption; however, functional osteoclasts are integral to bone remodeling and, thus, implant osseointegration, potentially contraindicating bisphosphonate use during implantation. To optimize the use of implant technologies in patients with compromised bone structure and metabolism, we need a more complete understanding of the biological response to surface design. The goal of this study was to assess the effects of osteoporosis and bisphosphonates on osseointegration of titanium (Ti) implants with microstructured surfaces, which have been shown to support osteoblast differentiation *in vitro* and rapid osseointegration *in vivo*. Forty, 8-month-old, virgin, female CD Sprague Dawley rats underwent ovariectomy (OVX) or sham (SHOVX) surgery. After 5 weeks, animals were injected subcutaneously with either the bisphosphonate (BIS), Ibandronate (25µg/kg), or phosphate-buffered saline (PBS) every 25 days. 1 week after the initial injection, Ø2.5mm x 3.5mm microrough (SLA; grit-blasted/acid etched) implants were placed transcortically in the distal metaphysis of each femur resulting in four groups: 1) SHOVX+PBS; 2) SHOVX+BIS; 3) OVX+PBS; and 4) OVX+BIS. After 28d, qualitative properties of the bone and implant osseointegration were assessed using micro-computed tomography (microCT), calcified histomorphometry (Van Gieson's stain), and removal torque testing. microCT revealed decreased bone volume in OVX rats, which was slowed by bisphosphonate treatment. Reduced bone-to-implant contact (BIC) was evident in OVX+PBS compared to SHOVX+PBS. Although BV/TV was increased in OVX+BIS compared to OVX+PBS, bisphosphonate treatment had no

effect on BIC. Removal torque testing revealed a higher maximum torque, torsional stiffness, and torsional energy in SHO VX compared to OVX with no effects due to bisphosphonate treatment. Our results show that osseointegration is decreased in osteoporotic animals. Ibandronate halts the progression of osteoporosis but does not enhance osseointegration.

Introduction

Sufficient bone volume (BV) and bone mineral density (BMD) are two of the most important patient factors for predicting the long-term success of dental and orthopaedic implant osseointegration, which is defined as the direct anchorage of an implant to mature bone tissue without the growth of fibrous tissue.^{275–277} These factors significantly diminish with age and their reduction is exacerbated by certain factors including postmenopausal estrogen deficiency. Osteoporosis is also characterized by excessive decreases in BMD and BV as a result of increased rates of bone turnover. An estimated 53.6 million U.S. adults over the age of 50 were affected by osteoporosis or osteopenia in 2010.⁴ By 2030, its prevalence is projected to increase to 71.4 million people.⁴ Furthermore, 80% of those affected by osteoporosis were postmenopausal women.⁴ Although data on the outcomes of dental and orthopaedic implants in osteoporotic patients are very limited, the compromised qualitative properties of the bone, strength, and healing associated with osteoporosis suggest these patients experience lower rates of implant success.

Healthy osseointegration is critically dependent on bone remodeling, which involves the reciprocal communication among osteoblasts, osteoclasts, mesenchymal stem cells (MSCs), and osteoclast precursors (OCPs).^{195,196,278} During remodeling, osteoclasts resorb a volume of bone leaving behind a foundation with a specific chemistry,⁵⁵ stiffness,¹⁵³ and morphology²⁰⁶ for osteoblasts to synthesize and calcify their matrix. Osteoclasts produce factors (both independent and as a byproduct of matrix resorption) capable of regulating MSC and osteoblast migration and their subsequent osteogenesis.³² In turn, MSCs and osteoblasts release factors capable of

limiting the degree and extent to which osteoclasts resorb bone. Any defects in the coupling of bone resorption to bone formation has not only been implicated in impaired healing and osseointegration but also the onset and progression of osteoporosis. Although age-related mechanisms contributing to osteoporosis may originate from accelerated bone resorption or impaired bone formation,²⁷⁹ these processes are not independent.

Bisphosphonates are commonly used to combat osteoporosis by targeting osteoclasts, slowing the rate and severity of bone resorption. These events translate to decreased bone turnover and increased BV and BMD.²⁸⁰ Bisphosphonates have also been reported to exert anabolic effects on osteoblasts *in vitro* by stimulating proliferation^{236,237}, preventing apoptosis,^{235,281} and enhancing production of alkaline phosphatase, bone morphogenetic protein (BMP)-2, type-I collagen, and osteocalcin,^{237,282–284} The positive effects bisphosphonates have on osteoblasts has provided some rationale for their use to enhance osseointegration. Other studies, however, have reported impaired mineralized bone nodule formation^{238,240} and responses to parathyroid hormone (PTH) with bisphosphonates.^{241,285–288} Furthermore, bisphosphonates can impede angiogenesis^{242,289,290} and are associated with osteonecrosis of the jaw (ONJ) at high doses,^{244,291} both of which can be detrimental to peri-implant bone formation and osseointegration. Moreover, functional osteoclasts are integral to healthy bone remodeling. Therapeutic interventions targeting either half of this process will inevitably affect its counterpart, contraindicating the use of bisphosphonates when bone remodeling is of the utmost importance like implant osseointegration.

Considering the growing number of osteoporotic patients²⁹² and high rate of bisphosphonate prescriptions,²⁹³ the success of implant outcomes and osseointegration in this demographic has turned into a significant dental and orthopaedic challenge. To optimize the use of implant technologies in patients with compromised bone structure and metabolism, a more complete understanding of the biological response to surface design and the impact of bisphosphonate

treatments on osseointegration are needed. The goal of this study was to assess the effects post-menopausal osteoporosis and bisphosphonate treatment have on the osseointegration of clinically used microstructured titanium (Ti) implants.

Materials and Methods

This study was conducted under approval of the Institutional Animal Care and Use Committee at Virginia Commonwealth University. All experiments were carried out in accordance with approved procedures and reported according to ARRIVE guidelines. All animals were treated humanely per the guidelines outlined in the Guide for the Care and Use of Laboratory Animals by the National Institutes of Health. Animals were single-housed in an individually ventilated, solid-bottomed polysulfone cage and kept at a temperature of 17-28°C with a humidity of 40-70% and a 12/12 h light/dark cycle.

Implant Preparation

Ti implants were designed to fit a rat femur and provided by Institut Straumann AG (Basel, Switzerland). 3.5mm long implants with a 2.5mm outer diameter and a 0.8mm pitch were initially machined from a rod of grade 4 Ti. They were then processed for 30s in a 55°C 2% ammonium fluoride/2% hydrofluoric acid/10% nitric acid solution. Implants were sand-blasted with large grit particulate (250 – 500 μm corundum) followed by acid etching in a boiling mixture of HCl and H₂SO₄ to generate implant with a surface similar to the clinically used SLA implant.⁵² Implants were cleaned in HNO₃, rinsed in ultrapure water, packed in aluminum foil, and γ -irradiated before use.

Implant Characterization

Scanning Electron Microscopy (SEM)

Scanning electron microscopy (SEM; Hitachi SU-70 FE-SEM, Hitachi, Tokyo, Japan) was used to qualitatively evaluate implant surface structure and roughness. Six images at varying magnifications were captured on 3 implants per surface modification using 5 kV accelerating

voltage for a total of 18 images.

Laser Confocal Microscopy

Laser confocal microscopy (LCM, Zeiss LSM 710, Zeiss, Oberkochen, Germany) was used to quantitatively evaluate surface micro-roughness. Measurements on each implant (n=3) were taken over an area of 106.2 μ m x 106.2 μ m with a 20x objective and a scanning pitch of 50nm. A Gaussian high-pass filter with a cutoff wavelength of 100 μ m was used when calculating average surface roughness (S_a) over three scans per implant (total n=9).

X-Ray Photoelectron Spectroscopy (XPS)

Chemical composition of the samples (n=3) was obtained from the sample surfaces by XPS (Thermo K-Alpha XPS, Thermo Fisher Scientific, Waltham, MA, USA). Spectra were collected using a 500 μ m spot size, using an XR5 gun and Al K α x-ray source at 15kV. Scans were taken with a 20ms dwell time and 1eV step size. Three different locations on each sample (total n=9) were analyzed.

Animals and Surgical Procedures

A schematic detailing the timing of surgical procedures and treatments is shown in **Figure 26**. All surgical procedures were performed at the same session under isoflurane inhalation anesthesia. 40, 8-month-old, skeletally mature, virgin, female CD Sprague-Dawley rats (Charles River Laboratories, Wilmington, MA) underwent ovariectomy (OVX; n=20) or sham OVX (SHOVX; n=20) surgery. The OVX and SHOVX surgeries were performed by Charles River Laboratories. Development of the osteoporotic phenotype occurred over the next 5 weeks.

Bisphosphonate Treatment

Animals received two bisphosphonate injections. The first injection was at 5wk post-OVX; animals received subcutaneous injections of either the bisphosphonate (BIS), ibandronate (AuroMedics Pharma LLC, Dayton, NJ, USA) (25 μ g/kg), or phosphate buffered saline (PBS) resulting in four groups: 1) SHOVX + PBS (n=10 animals); 2) SHOVX + BIS (n=10 animals); 3)

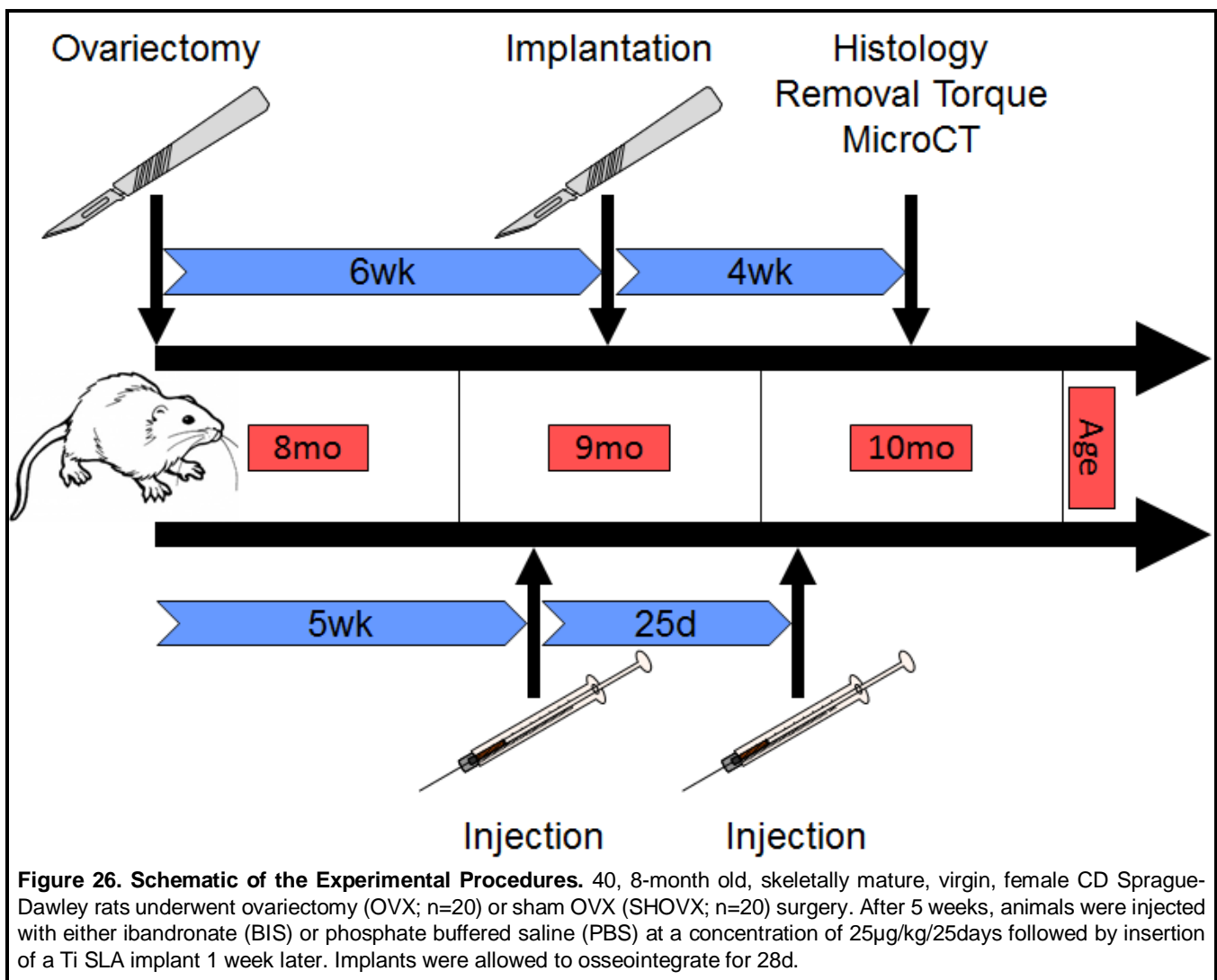


Figure 26. Schematic of the Experimental Procedures. 40, 8-month old, skeletally mature, virgin, female CD Sprague-Dawley rats underwent ovariectomy (OVX; n=20) or sham OVX (SHOVX; n=20) surgery. After 5 weeks, animals were injected with either ibandronate (BIS) or phosphate buffered saline (PBS) at a concentration of 25 μ g/kg/25days followed by insertion of a Ti SLA implant 1 week later. Implants were allowed to osseointegrate for 28d.

OVX + PBS (n=10 animals); 4) OVX + BIS (n=10 animals). One week after the first injection, the implants were placed (described below). Animals received a second injection of ibandronate or PBS 25 days after the first injection; thus, animals had bisphosphonate treatment before and after the placement of the implants. Treatment method, dose, and frequency were based on previous reports detailing that total amount, not frequency, of ibandronate injections is important for drug efficacy with an optimal dose of 1.0 μ g/kg/day.²⁹⁴ A subcutaneous injection was chosen over oral administration to ensure total dosage delivery to each rat. 25 days was chosen to mimic monthly injections used clinically while also minimizing distress arising from frequent injections. This timing has also been successfully employed previously.²⁹⁵

Transcortical Implant Surgeries

One week after the first injections, SLA modified implants were placed transcortically into the

distal metaphysis of both femurs. Animals were anesthetized with 5% isoflurane gas inhalation. The hind limbs were prepared by shaving and cleaning using ethanol and chlorohexidine. Anesthesia was maintained at 4% isoflurane in O₂ gas inhalation for the duration of the surgical procedure. Cleaned, anesthetized animals were placed in a supine position and covered with a sterile surgical drape. An 8mm incision was made over the medial side of the right knee. Overlying muscle was separated, and the distal femur was exposed using blunt dissection to a point immediately above the articular capsule. A high-speed dental hand-piece was used to create a progressively larger pilot hole in the distal femur using a series of increasing diameter drill bits (Ø1.0mm, Ø1.6mm, Ø2.0mm, and Ø2.2mm) with a 3.5mm drill stop. Ti SLA implants were then screwed into place by hand using a custom-made driver. Following implant placement, custom-made stainless-steel cover screws were placed on the end of the implant to prevent bone from growing into the internal threading of the implant. The periosteum and muscle were reapposed and sutured in place using resorbable sutures and the skin was closed with 9mm wound clips. These steps were then repeated for the left femur. Animals recovered from anesthesia on a water-circulating warming pad and were injected subcutaneously with 1mg/kg buprenorphine SR LAB. All animals had access to water *ad libitum* for the duration of the study; however, food access was regulated.

Diet and Pair Feeding

The diet of ovariectomized animals is a potential source of at least two confounding variables. The first is the tendency of rats to have increased appetites following OVX. This can lead to excessive weight gain potentially altering the mechanical loading on the implant thus affecting the osseointegration.²⁹⁶ In order to eliminate weight gain as a confounding variable, the animals in this study were pair fed. Each week SHOVS+PBS animals had their food intake monitored by calculating the difference in available food weight in a 24-hour period. The average difference across the four SHOVS+PBS animals was given to each animal in the three remaining groups

daily. The success of the pair feeding regimen was verified by weekly weighing of all animals for the duration of the study.

The content of the food can also confound the results studies involving ovariectomized animals. Many rodent feeds are made from products known to contain phytoestrogens. Phytoestrogens are structurally similar with 17β -estradiol causing them to have estrogenic and/or anti-estrogenic effects potentially preventing bone loss.²⁹⁷ Because the dietary estrogenic activity is a concern, all animals were given a phytoestrogen-free diet (Advanced Protocol Verified Casein Diet 10 IF, LabDiet, St. Louis, MO, USA).

Tissue Analysis

Transcortical implants were allowed to osseointegrate for 28d, after which rats were euthanized via CO₂ inhalation. The hind limbs from each animal were isolated for removal torque testing (n=5 animals/group) or micro-computed tomography (microCT) and histological analysis (n=5 animals/group). Each limb was treated as a separate sample providing an effective sample size of 10 per group for both the removal torque testing and microCT/histological analysis.

MicroCT

MicroCT (SkyScan 1173, Bruker, Kontich, Belgium) was used to assess the osteoporotic phenotype in the femoral head as well as evaluate peri-implant bone growth and bone-to-implant contact (BIC) in the distal femur. Femurs used for microCT were stored and fixed in 10% neutral buffered formalin for at least 24hr prior to imaging. The femoral heads of fixed samples were scanned at a resolution of 1120x1120 pixels (image pixel size of 12.94 μ m) over 360° using a 1.0mm aluminum filter, 85kV voltage, 94 μ A current, and 270ms exposure time. 5 x-ray projections were acquired every 0.2° and averaged. A standard Feldkamp reconstruction was done using NRecon Software (Bruker) with a beam hardening correction of 20% and a Gaussian smoothing kernel of 0. To calibrate for cortical tissue mineral density and trabecular bone mineral density, 4mm epoxy resin rods containing concentrations of 0.25 and 0.75gcm⁻³ calcium

hydroxyapatite (CaHA). Cortical and trabecular bone were isolated, and densities determined separately using CTAn analysis software (Bruker). Total porosity and trabecular number were also quantified from the isolated trabecular bone.

The distal femoral metaphysis was scanned at a resolution of 1120x1120 pixels (image pixel size of 13.66 μ m) over 360° using a 0.25mm brass filter, 120kV voltage, 66 μ A current, and 420ms exposure time. 5 x-ray projections were acquired every 0.2° and averaged. After reconstruction, a uniform volume of interest (VOI) was isolated. The VOI began at the base of the implant and extended 3mm towards its apex to eliminate any variability arising from the implant not being exactly at bone level for every sample. The VOI was shrink-wrapped, dilated 2 pixels around the implant, and subtracted from the original VOI. The remaining bone and implant were thresholded and quantified as the total bone volume (BV) and then normalized to the total uniform VOI (TV) to get bone volume over total volume (BV/TV). The BIC was calculated using a separate BV that encompassed only the bone in direct contact with the implant. The same VOI was dilated 10 pixels around the implant, rethresholded, further dilated by 3 pixels, and subtracted from the original VOI. After eroding the remaining VOI by 3 pixels, the remaining BV was normalized to the implant volume.

Histology

Following imaging with microCT, samples were placed in fresh 10% neutral buffered formalin and sent to be commercially processed for calcified histological staining (Histon, Everett, WA, USA). Femurs were embedded in methyl methacrylate, sectioned longitudinally relative to the implant and transaxially relative to the femur (transcortical), and stained with Stevenel's blue and van Gieson. Sections were imaged using bright field light microscopy with an AxioCam MRc5 camera and Axio Observer Z1 and analyzed using ZEN 2012 Blue Edition software (Zeiss). Histomorphometry was then used to evaluate peri-implant bone growth and BIC.

New peri-implant bone growth was quantified within a uniform rectangular region of interest (ROI) for all samples that was 3.56mm in width by 3.0mm in length with an area of 10.7mm². The ROI was drawn 0.3mm beneath the distal portion of the implant and centered. The area of all bone within the ROI was then quantified (BV) and normalized to the area of the ROI (TV). The area of bone contained within the ROI divided by the area of the ROI was defined as the histological BV/TV. In addition, the perimeter of the implant contained within both the trabecular region and the cortical region of the bone was measured. The trabecular BIC and cortical BIC were determined by dividing the length of bone in direct contact with the implant by the trabecular and cortical perimeter length respectively. The total BIC was calculated by summing both lengths of contact and dividing by the total perimeter of the implant.

Removal Torque

Removal torque testing was performed on fresh, non-fixed samples using an ElectroForce 3200 Series III test instrument (TA Instruments, New Castle, DE, USA). Because of their asymmetrical shape, femurs were mounted in 1cm diameter flexible polyurethane tubing to ensure no movement of the femur during analysis (**Fig.31A**). The tubing was cut into 5cm segments and halved longitudinally to provide access to the transcortical implant. Femurs were secured to the tubing with polyurethane adhesive and allowed to cure overnight at 4°C prior to testing. The transcortical implant in each hind limb was then fit to a custom-made driver and aligned to the testing machine axis to ensure no initial torque was present on the implant (0Nm). A clamp was then carefully tightened, securing each sample in place with no initial compressive load present on the implant (0Nm). A 0Nm compressive load was critical to guarantee no axial mismatch between the implant and the testing apparatus, which could greatly alter our results. Torque was then applied to each sample with a rotational speed of 0.1°s⁻¹ with an axial displacement of 0.8mm/360° to ensure no compressive load was applied to the sample during the duration of each test. Torque vs. degree graphs were generated for each sample and fit to

a bilinear model in order to distinguish the toe-region from the linear region using an open-source least squares spline modeling package (SLM - Shape Language Modeling version 1.14) for MATLAB (MathWorks, Natick, MA, USA). The linear region of each graph was then evaluated for the maximum torque, torsional energy (area below linear region), and torsional stiffness (slope of linear region).

Osteoblast Response In Vitro

To further assess the effects of bisphosphonate treatment, following euthanasia, calvarial osteoblasts were isolated from the frontal and parietal bones of rats in each of the four experimental groups. After removal of the periosteum and soft tissue, bone fragments were digested for 15min at 37°C with 0.25% trypsin-EDTA (Life Technologies, Carlsbad, CA). Bones were minced into pieces approximately 1mm x 1mm and placed into a 100mm x 20mm Petri dish with Dulbecco's modified Eagle medium (DMEM; Mediatech, Manassas, VA) + 10% fetal bovine serum (FBS) + 1% penicillin-streptomycin (Life Technologies). At confluence, cells were subpassaged and cultured as above. The osteoblast phenotype of each of the four groups of isolated cells was confirmed by measuring alkaline phosphatase specific activity and osteocalcin production after treatment of confluent cultures with either 0M or 10⁻⁸M 1 α ,25-dihydroxy vitamin D₃ (1 α ,25(OH)₂D₃; Enzo Biochem, Farmingdale, NY) for 24hrs on tissue culture polystyrene (TCPS).

Validated rat osteoblasts (rOBs) from each experimental group were cultured on TCPS or 15mm Ti SLA disks. Disks were prepared from Ti sheets but subjected to the same sand-blasting and acid etching procedure as described above. Cells were plated at a density of 10,000 cells/cm² and incubated at 37°C in an atmosphere of 5% CO₂ and 100% humidity. Media were changed 24h after plating and every 48h thereafter for 7d. At 7d, cells were incubated with fresh DMEM for 24h. Media were collected and immunoassays were used to measure levels of intact rat osteocalcin (Alfa Aesar, Haverhill, MA) rat/mouse osteopontin (R&D Systems, Minneapolis,

MN), mouse osteoprotegerin (R&D Systems), human/mouse/rat BMP2 (PeproTech), mouse receptor activator of nuclear kappa-B ligand (RANKL; R&D Systems), and rat vascular endothelial growth factor-A (VEGF; R&D Systems).

After collection of media, cell monolayers were washed twice with 0.2ml PBS, lysed in 0.05% Triton X-100, and homogenized by sonication at 40 amplitude using a Vibra-Cell ultrasonicator (Sonics & Materials Inc., Newtown, CT). DNA content in the cell layer lysate was measured with PicoGreen (Promega, Madison, WI) using a Synergy H1 Hybrid Reader fluorescence detector (BioTek, Winooski, VT) at an excitation of 485 nm and emission of 538 nm. Alkaline phosphatase specific activity [orthophosphoric monoester phosphohydrolase, alkaline; E.C. 3.1.3.1] was assayed by measuring the conversion of *p*-nitrophenylphosphate to *p*-nitrophenol at pH 10.25 and temperature of 37°C. Absorbance was measured at 405nm. Activity was normalized to total protein content in the cell lysates as determined by bicinchoninic acid protein assay kit (Thermo Fisher Scientific, Waltham, MA). Immunoassay data were normalized to DNA content.

Statistical Analysis

Based on previous studies,^{193,296} in order to detect a 30% mean difference with 20% variance and a type I error rate of 0.05, a two-tailed one-way ANOVA power analysis determined a sample size of 10 per group is necessary to maintain 80% power. In order to ensure that differences in mechanical loading would not affect the results, identical implants were placed in the right and left hind limbs. In addition, animals received the same systemic treatment (e.g. OVX/SHOVX or ibandronate/PBS), which prevents any potential carry-over effects between legs. Since both legs were treated identically, it is safe to assume that movement or loading in one limb will not affect the movement or loading experienced by the other limb. The design of our study permits the assumption that implants from individual limbs can be treated as independent data points rather than dependent. Data are presented as the mean \pm standard error (SE) for each analysis. All cell culture experiments had a sample size of six (n=6) and repeated at least three times to

ensure validity of the results. Data shown in the figures are from representative experiments. A one-way analysis of variance with a two-tailed Tukey correction was performed to adjust for multiple comparisons to maintain an experiment-wise error rate (α) of 0.05. All statistical analyses were performed using JMP statistical software (SAS Institute, Cary, NC, USA).

Results

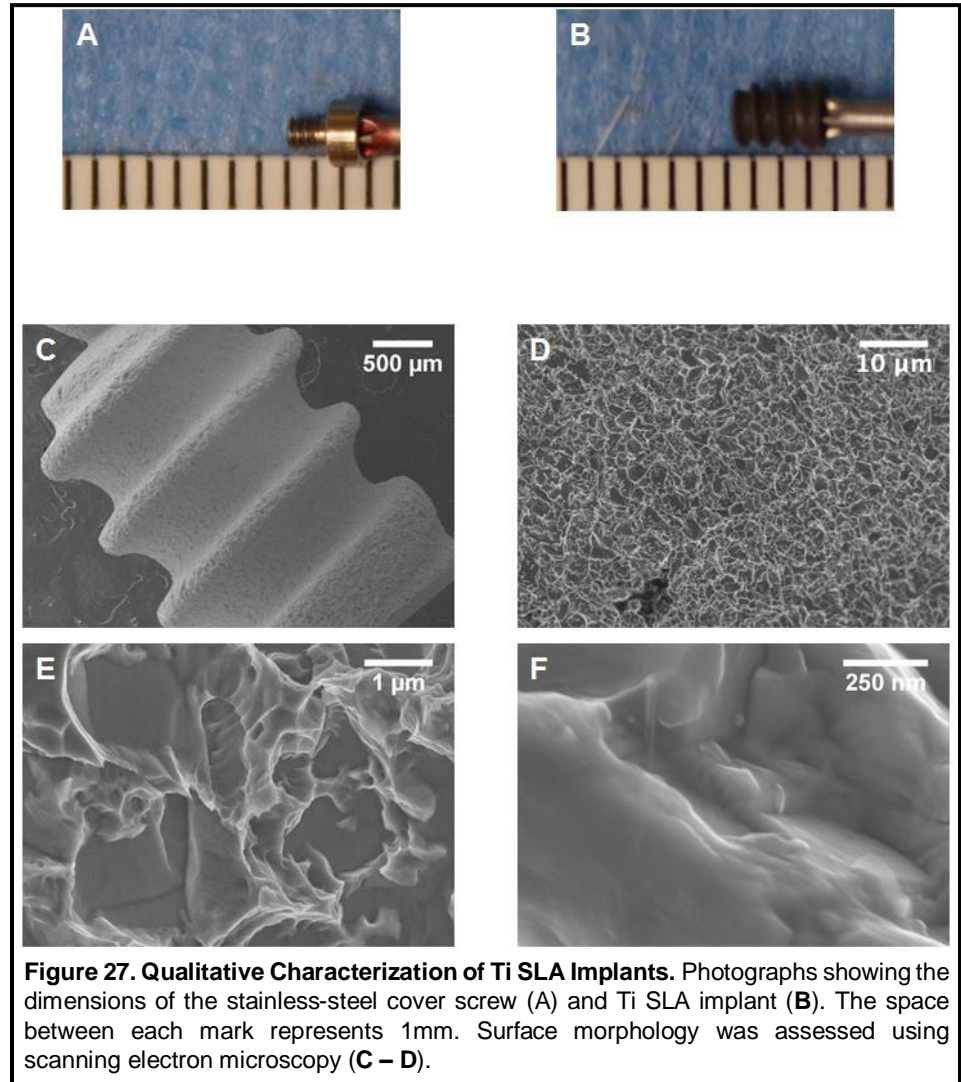
Transcortical Implant

Characterization

Qualitative images of the transcortical Ti SLA implants as well as the cover screw are shown in

Figure 27. Gross morphology of the stainless-steel cover screw and Ti SLA implant can be seen in **Figure 27A** and **Figure 27B** respectively.

SEM images of the transcortical Ti SLA



implants (**Fig.27C – F**) reveal the rough surface induced by the sand-blasting and acid etching procedure, resulting in a combination of microscale and submicron-scale surface features. These complex features were also strewn with unmodified areas characterized by flat and smooth sections. Together the sand-blasting and acid etching procedure led to an average surface roughness (S_a) of $3.91 \pm 0.09 \mu\text{m}$ as measured by confocal microscopy (**Table 4**). XPS survey spectra (**Table 4**) displayed titanium (Ti), oxygen (O), and carbon (C) as the main atomic

components of the SLA implant.

Table 4. Mean \pm standard deviation (SD) of surface roughness (Sa) and atomic concentration (%)

	Confocal Microscopy	X-Ray Photoelectron Spectroscopy		
	Mean Roughness (S _a) \pm [μ m]	O (%)	C (%)	Ti (%)
SLA	3.91 \pm 0.09	38.19 \pm 1.37	51.83 \pm 1.01	9.89 \pm 0.21

Evaluation of Pair Feeding and Osteoporotic Phenotype

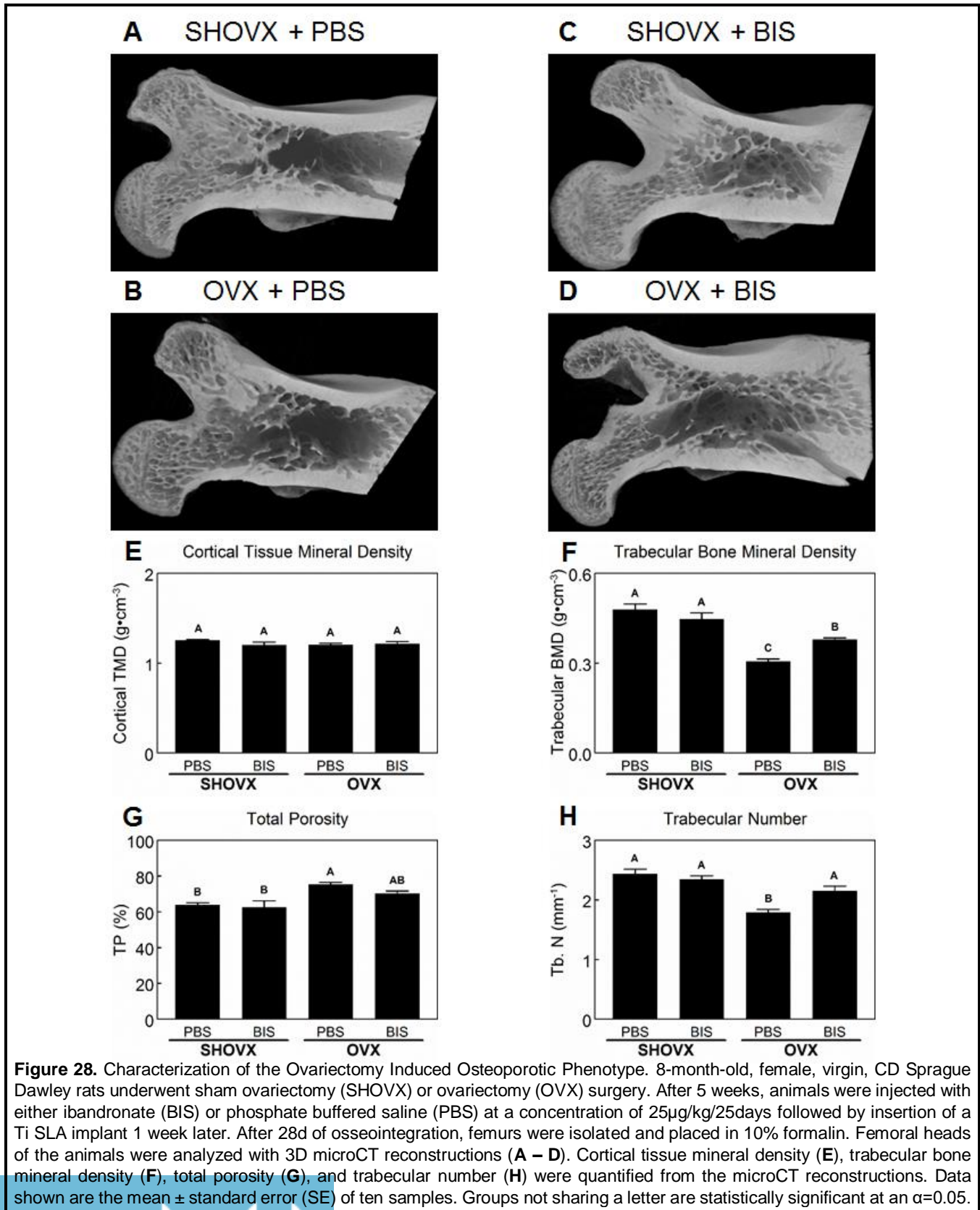
Animals from the four groups maintained similar weights and levels of activity throughout the duration of the study. Select week results from the overall ANOVA F-test (Week 1: $F_{3,36} = 1.5$, $p = 0.2376$; Week 4: $F_{3,36} = 1.1$, $p = 0.3467$; Week 8: $F_{3,36} = 0.6$, $p = 0.6041$; Week 10: $F_{3,36} = 0.2$, $p = 0.8946$) indicate a successful pair feeding regimen.

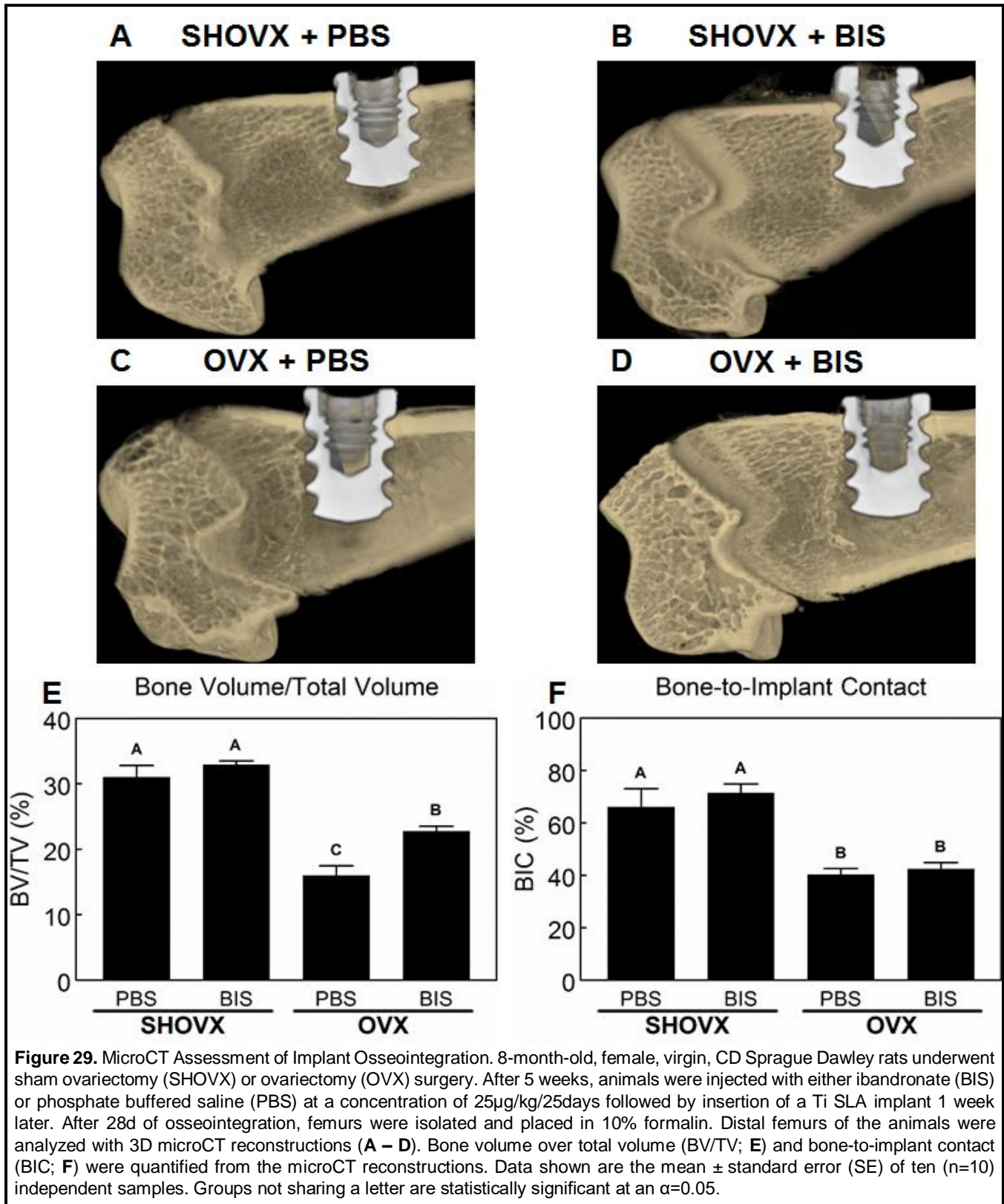
MicroCT was used to evaluate the osteoporotic phenotype of the femoral head with representative images shown in **Figure 28A – D**. The cortical tissue mineral density (**Fig.28E**) was not affected by the OVX nor treatment with ibandronate. However, the trabecular bone mineral density (**Fig.28F**) was significantly reduced in OVX animals compared to SHO VX animals. Treatment with ibandronate mitigated the loss of the trabecular bone mineral density. Total porosity (**Fig.28G**) was increased in OVX animals receiving PBS compared to SHO VX animals. OVX animals receiving ibandronate had a total porosity similar to both SHO VX animals and OVX animals receiving ibandronate. Trabecular number (**Fig.28H**) decreased in OVX animals receiving PBS compared to the other groups.

MicroCT

3D reconstructions of microCT scans (**Fig.29A – D**) showed peri-implant bone formation in all animal groups. Furthermore, the transcortical implants did not contact the growth plate eliminating any potential influence on the bone formation in our defined VOI. The BV/TV (**Fig.29E**) decreased in OVX animals compared to SHO VX, and the severity of the reduction was lessened in OVX animals receiving ibandronate. Osseointegration was achieved in all animal groups as well. BIC values (**Fig.29F**) obtained through microCT analysis were reduced

in OVX animals compared to SHO VX animals after 4 weeks. Ibandronate treatment of both SHO VX and OVX animals did not influence BIC values.





Histology

Histological sections of transcortical implants from each animal group (**Fig.30A – D**) confirmed the results seen from the microCT analysis. More trabecular bone can be seen in the SHO VX groups (**Fig.30A, B**) compared to the OVX groups (**Fig.30C, D**). Quantification of the total bone area with a fixed region of interest (**Fig.30E**) was significantly higher in SHO VX animals compared to OVX animals. Administration of ibandronate mitigated some of the loss in OVX animals. BIC (**Fig.30F**) was higher in SHO VX compared to OVX animals and were not influenced by ibandronate treatment.

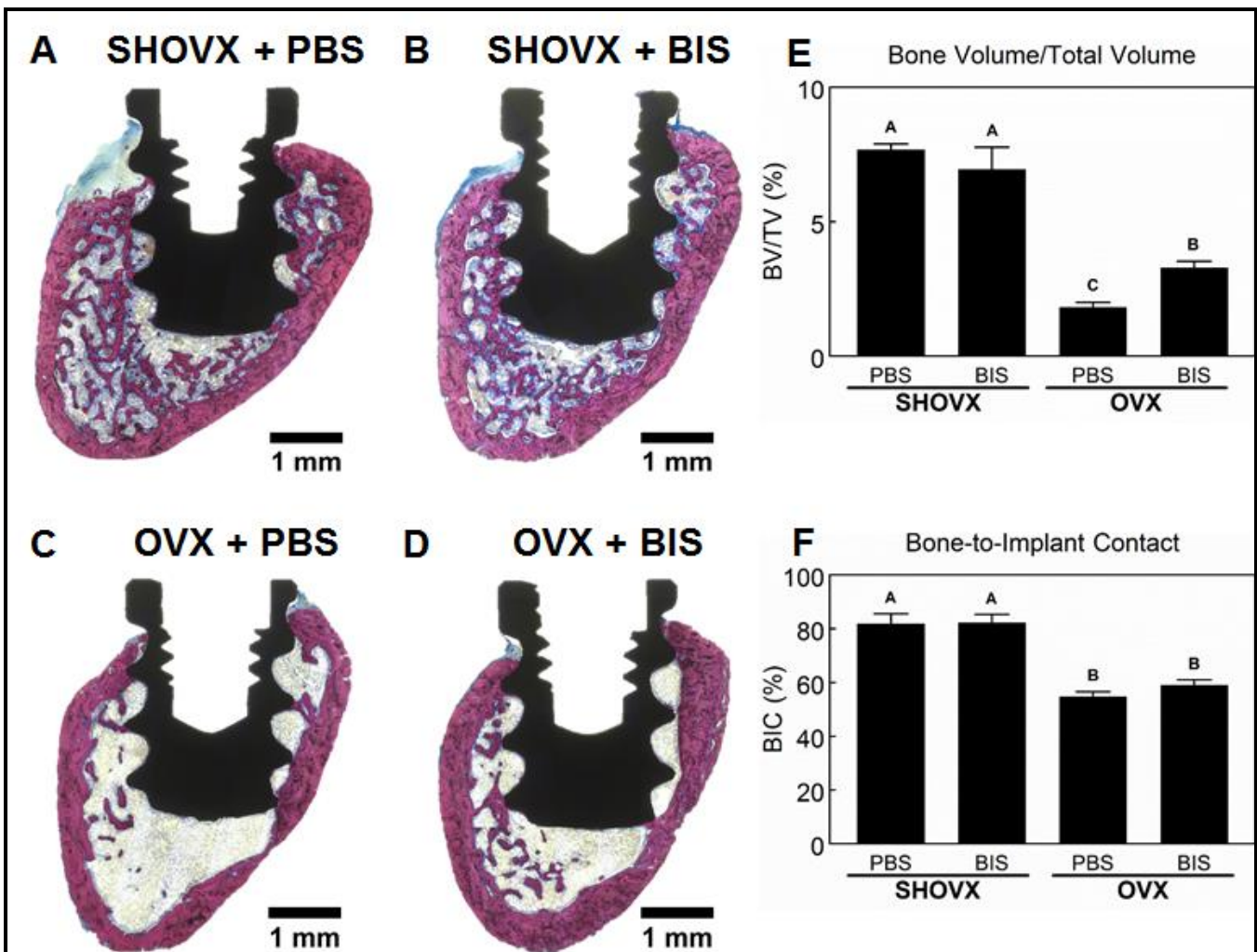
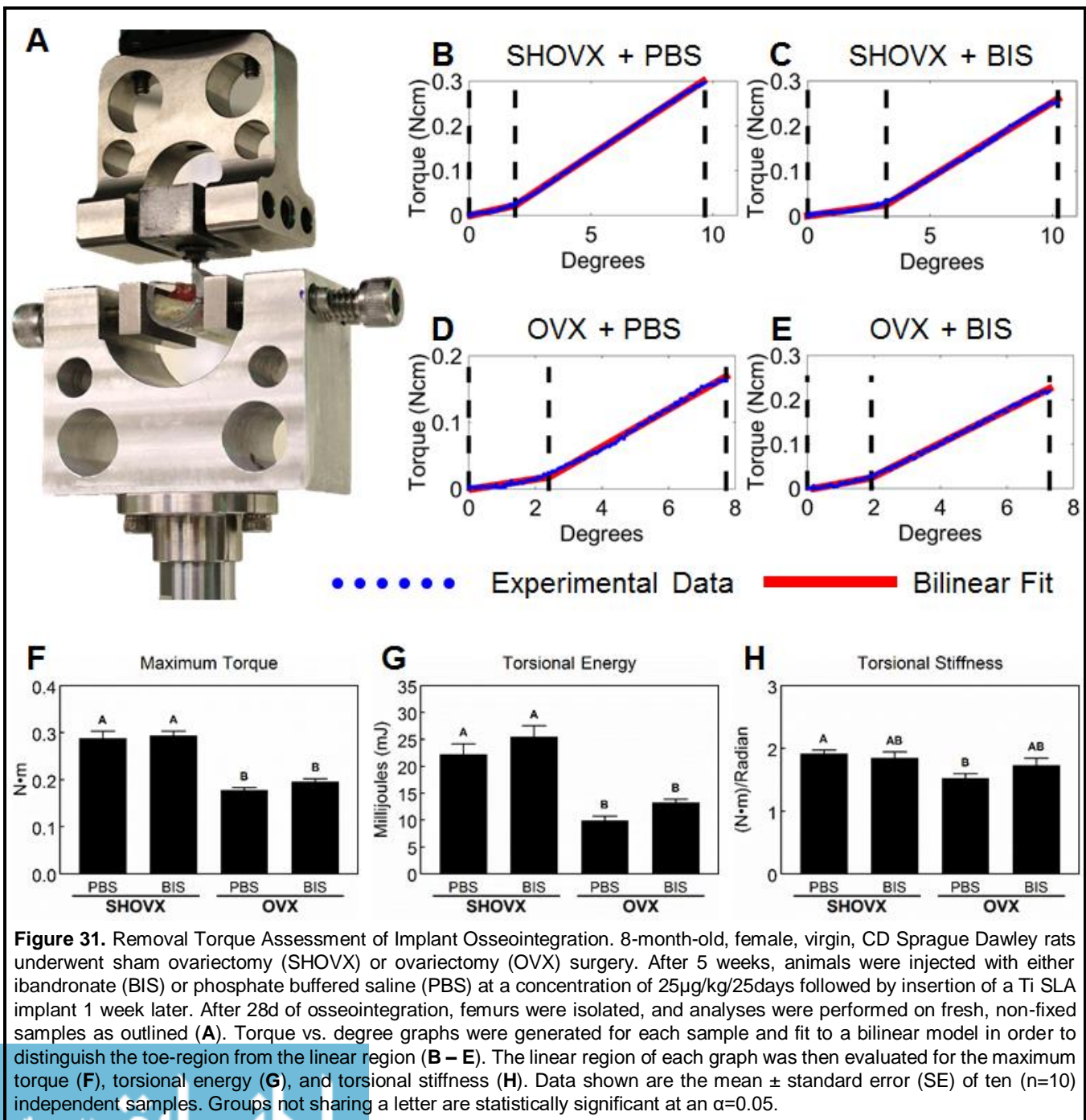


Figure 30. Histological Assessment of Implant Osseointegration. 8-month-old, female, virgin, CD Sprague Dawley rats underwent sham ovariectomy (SHO VX) or ovariectomy (OVX) surgery. After 5 weeks, animals were injected with either ibandronate (BIS) or phosphate buffered saline (PBS) at a concentration of 25 μ g/kg/25days followed by insertion of a Ti SLA implant 1 week later. After 28d of osseointegration, femurs were isolated and placed in 10% formalin. Distal femurs of the animals were embedded in methyl methacrylate, sectioned longitudinally relative to the implant and transaxially relative to the femur (transcortical), and stained with Stevenel's blue and van Gieson (**A – D**). Bone volume over total volume (BV/TV; **E**) and bone-to-implant contact (BIC; **F**) were quantified using histomorphometrics. Data shown are the mean \pm standard error (SE) of six ten (n=10) independent samples. Groups not sharing a letter are statistically significant at an $\alpha=0.05$.

Mechanical Testing

Isolated femurs were secured in polyurethane tubing and aligned to the machine axis in a custom-fabricated sample holder to ensure no movement was created during the test (**Fig.31A**). Representative torque vs. degree graphs for each group (**Fig.31B – E**) display the bilinear model (red) fit to the experimental data (blue). The end of each curve identifies failure, and no secondary peaks were observed for any sample. The middle vertical dashed line (black)



separates the toe region (left section) and the linear region (right section) as determined by the least squares spline modeling package in MATLAB. The maximum torque (**Fig.31F**) and torsional energy (**Fig.31G**) was greatest in SHO VX animals and significantly reduced in OVX animals. Ibandronate treatment had no effect on either parameter. Torsional stiffness (**Fig.31H**) was greatest in SHO VX animals treated with PBS and lowest in OVX animals treated with PBS. SHO VX+BIS and OVX+BIS animal torsional stiffness values were not different from either SHO VX+PBS or OVX+PBS.

In Vitro Response of Calvarial Osteoblasts

$1\alpha,25(\text{OH})_2\text{D}_3$ stimulated osteocalcin production and alkaline phosphatase specific activity in confluent cultures of rOBs from all four experimental groups, confirming their successful isolation and expansion. DNA content (**Fig.32A**) and alkaline phosphatase specific activity (**Fig.32B**) in cultures grown on SLA were lower than in cultures grown on TCPS. DNA content was higher in cultures of osteoblasts isolated from ibandronate treated animals grown on TCPS compared to the other treatment groups. Among SLA cultures, DNA content was highest in SHAM+BIS osteoblasts. Ibandronate treatment decreased alkaline phosphatase specific activity among TCPS cultures, but no effect was observed in SLA cultures. SLA increased osteoblast osteocalcin (**Fig.32C**) production in all groups except SHAM+BIS, which remained like TCPS cultures. Furthermore, OVX+BIS osteoblasts had decreased osteocalcin production compared to OVX+PBS osteoblasts. Osteoprotegerin (**Fig.32D**) levels decreased in SLA cultures compared to TCPS. Osteoblasts isolated from OVX animals had decreased osteoprotegerin levels in TCPS cultures, although ibandronate treatment did stimulate its production. Production of BMP2 (**Fig.32E**), osteopontin (**Fig.32F**), VEGF (**Fig.32G**), and RANKL (**Fig.32H**) was increased on SLA compared to TCPS with the highest levels of BMP2, osteopontin, and RANKL occurring in OVX+PBS osteoblasts. The highest levels of VEGF were observed in SHAM+PBS osteoblasts. Ibandronate treatment led to decreased productions of these proteins in SLA

cultures compared to their respective PBS controls with SHAM+BIS osteoblasts producing amounts of osteopontin and VEGF to levels similar to those observed in TCPS cultures.

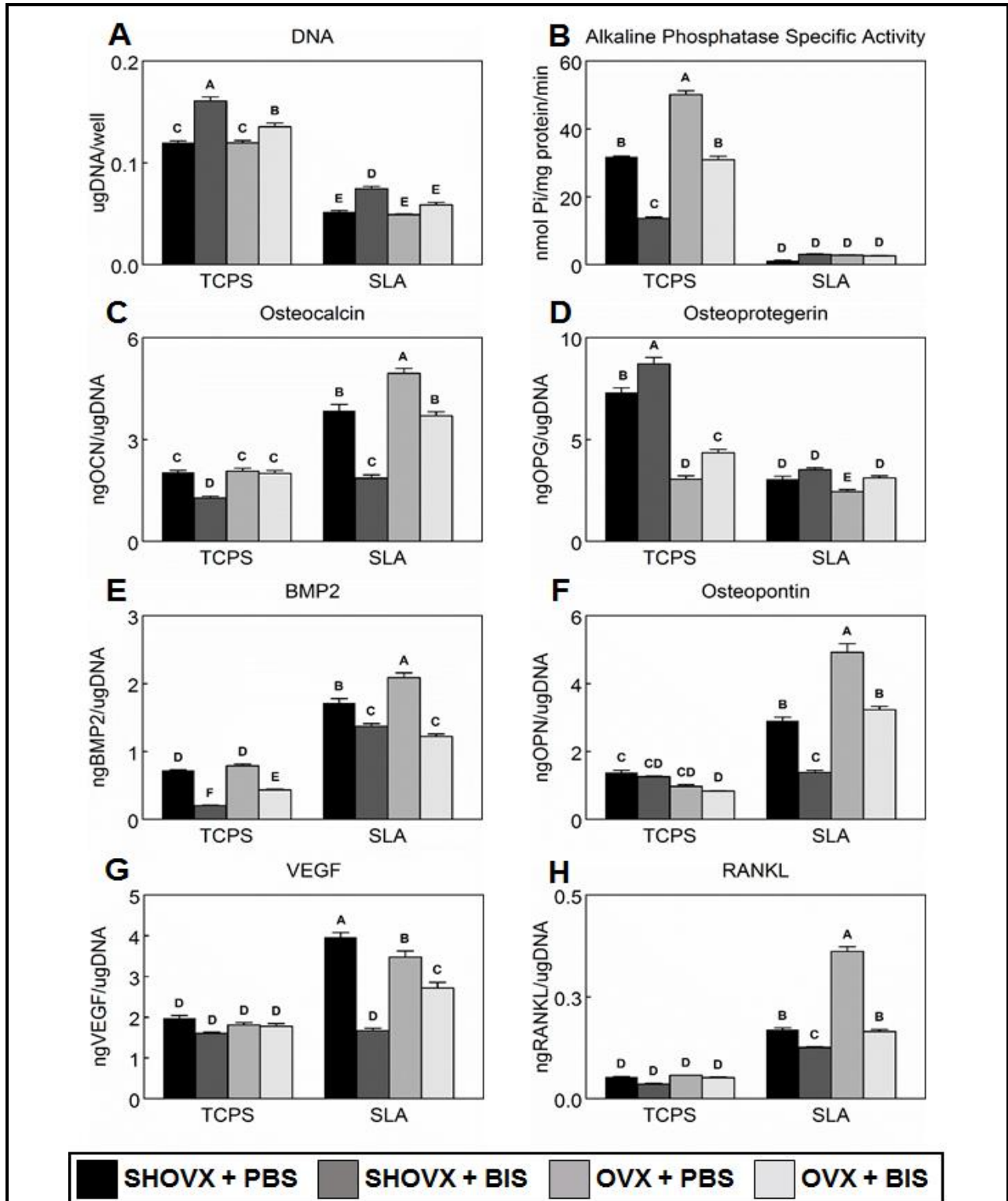


Figure 32. In Vitro Response of Primary Calvarial Osteoblasts. Calvarial osteoblasts were isolated from each of the four groups of animals and cultured separately on either TCPS or SLA in DMEM. After 7d, cells were treated with fresh DMEM for 24h. After 24h, media were collected, and cell lysates were assayed for DNA content (A) and alkaline phosphatase specific activity (B). Media were assayed for osteocalcin (C), osteoprotegerin (D), BMP2 (E), osteopontin (F), VEGF (G), and RANKL (H). Data shown are the mean \pm standard error (SE) of six (n=6) independent samples. Groups not sharing a letter are statistically significant at $\alpha=0.05$.

Discussion

Osseointegration involves a complex cascade of biological events, ultimately leading to the structural and functional connection between mature, lamellar bone and the inserted implant.²⁷⁷ The cellular miscommunication associated with osteoporosis leads to excessive bone resorption and impaired bone remodeling, which challenges successful osseointegration and implant outcomes. Although bisphosphonates are known to increase BV and BMD by mitigating the resorptive damage caused by overactive osteoclasts, their continued disruption of bone remodeling may contribute to greater risks of compromised implant osseointegration. In order to improve osseointegration and long-term stability of implants in osteoporotic patients, we sought to determine the effects ibandronate treatment has on the osseointegration of microrough Ti implants in an aged, OVX-induced osteoporotic rat model.

In the present study, microCT analyses, calcified histomorphometrics, and removal torque testing revealed decreased osseointegration in ovariectomized animals compared to SHAM operated controls. Moreover, ibandronate treatment did not affect BIC and removal torque values, although it was able to halt the progression of the osteoporotic phenotype as observed through increased BV/TV in ovariectomized animals. The physiological consequences of osteoporosis are known to alter cellular communication leading to lower qualitative properties of the bone and impaired healing.²⁹⁸ It is clear from this study and others that the estrogen deficient osteoporotic phenotype negatively impacts implant osseointegration.^{299–302} Previous studies, however, have lauded the use of bisphosphonates to reverse the negative effects of osteoporosis on implant osseointegration.^{303–309} On the other hand, BIC and removal torque values were either unaffected^{308,310} or decreased³¹¹ by bisphosphonate therapy in healthy animals. Despite the inhibitory effect bisphosphonates have on bone remodeling, the precise mechanism of action is not fully understood, which has led to many studies with variations in experimental methods. Selection of the appropriate animal model, development of the

osteoporotic phenotype, timing of both the bisphosphonate treatment and implant insertion as well as the route of bisphosphonate administration and location of implant placement are important factors. Conflicting results between these studies and ours can be largely explained through these differences. It should also be noted that the femoral implant model is not an exact replica of bone turnover in the oral cavity, which could limit the translation of our results to clinical outcomes for patients receiving dental implants rather than orthopaedic implants.

An ovariectomized rat is a well-characterized model that closely mimics postmenopausal osteoporosis in humans. Basic multicellular unit-based endocortical and cancellous bone remodeling occurs in both rats and humans.^{312,313} Estrogen deficiency in both humans and rats leads to an increased presence of osteoclasts on the endocortical bone surface causing cancellous and endocortical bone loss by altering the balance between bone formation and bone resorption.^{314–316} In contrast, there is increased bone formation at the periosteal surface.^{314,317} As a result of the opposing changes in radial growth and endocortical remodeling, cortical bone volume generally remains unchanged in ovariectomized rats, similar to what was observed in this study. However, trabecular bone turnover is known to be elevated in ovariectomized rats,^{318,319} which explains the increased total porosity as well as the decreased trabecular number in PBS treated ovariectomized rats.

Evidence also suggests that both the age of the animal during OVX and implant insertion could significantly influence the results. While rats reach skeletal maturity around 3 months, their growth rate changes continuously for the first 6 months of life.³²⁰ In some instances, bone elongation in rats may persist up to their first 8 months.³²⁰ OVX of growing rats results in cancellous osteopenia due to increased resorption of growth plate calcified cartilage.³¹⁵ The amount of primary spongiosa that serves as a template for future bone apposition is subsequently decreased.³¹⁵ As bone growth slows with age, the contribution of altered endochondral ossification to the skeletal effects of OVX diminishes, and the contribution of

altered bone remodeling increases and eventually becomes the predominant mechanism for the alteration of cancellous bone mass.

Further methodological complications arise when bone remodeling targeting therapies and implant osseointegration are introduced to the ovariectomized rat model. Many previous reports using this model to investigate implant osseointegration and bisphosphonate therapy perform the OVX surgery in rats under the age of 6 months.^{303–309} In spite of not approximating the relative timing of the onset of menopause in humans, it is difficult to attribute the impaired osseointegration to altered bone remodeling. A few of these studies do refer to the ovariectomized skeletal phenotype as estrogen-deficient osteoporosis rather than postmenopausal; however, no attempt was made to control for the number of phytoestrogens present in the animal diet, potentially altering the results. Another study using ovariectomized 6 – 9 month old retired breeders found that osseointegration of implants was enhanced by bisphosphonate therapy.³²¹ The multiple pregnancies and lactations incurred by the retired breeders has been shown to result in osteopenia.³²² Compared to age-matched virgins, OVX of retired breeders results in less bone loss and more variable indices of bone mass and turnover.³²²

Regardless of the age at OVX, the osteoporotic phenotype needs sufficient time to develop as the combination of rat age and skeletal site used influence the resulting temporal pattern of bone loss.³²³ Studies treating animals with bisphosphonates³⁰⁶ or inserting implants³⁰⁵ on the same day as the OVX surgery do not fully capture the impact the physiological changes the osteoporotic phenotype has on implant osseointegration. Furthermore, studies treating animals with bisphosphonates either on the same day of the implant surgery or immediately after are not appropriate models to study the effects postmenopausal osteoporosis have on the osseointegration of implants. Clinically, patients diagnosed with osteoporosis will not remain untreated until after a surgical intervention.

The effects of bisphosphonates have also been shown to be dose-dependent and vary with the chemistry of the compound being tested. Daily and weekly treatment regimens are available for many of these bisphosphonates, but it is predicted that novel and simplified regimens with bisphosphonates given at intervals between doses of longer than 1 week will be more convenient for patients and improve adherence to therapy. Ibandronate has the potential to be effective when administered less frequently than once weekly. Preclinical studies using OVX rats found that the lowest dose of ibandronate that completely prevented bone loss was 1 $\mu\text{g}/\text{kg}/\text{day}$. Although the bone turnover in skeletally mature rats is approximately 3 – 5 times higher compared to humans, it decreases with age and OVX.^{316,324} Considering the age at OVX (8 months), the bone turnover of the rats used in this study closely reflects that of adult human bone. In addition, intermittent and continuous dosing of ibandronate produced similar results, so administration of 25 $\mu\text{g}/\text{kg}/25$ days was selected to mimic monthly injections patients would receive clinically as well as minimizing animal distress.³²⁵

3.5mm long and 2.5mm wide, grade 4, Ti implants were custom made for this study. This design allowed for a transcortical insertion, which more closely mimics clinical procedures as opposed to intramedullary canal insertion commonly performed on mice. The SLA surface modification is clinically used, and no studies have investigated this topography in response to either OVX induced osteoporosis and/or ibandronate treatment. Furthermore, this is the first reported use of these transcortical implants custom-made to fit rat femurs. Scanning electron microscopy, laser confocal microscopy, and x-ray photoelectron spectroscopy revealed a surface morphology, average surface roughness, and surface composition similar to what has been previously reported for implants processed in the same manner.^{209,210,326}

Primary calvarial osteoblasts were obtained from the osteoporotic animals and were used to evaluate potential phenotypic and/or proliferative changes. rOBs were cultured on 15mm diameter and 1mm thick Ti disks that were processed to have the same surface microstructural

features as those seen on the implants used *in vivo*. Both OVX and ibandronate treatment were able to condition rOBs *in vivo* to alter their response *in vitro*. Typically, cells cultured on rough surfaces display attributes of more differentiated and mature osteoblasts with decreased proliferative capacity and cell number than those on TCPS.³²⁷ While this was true for all groups, rOBs isolated from untreated OVX animals had higher productions of osteogenic markers compared to SHO VX, while bisphosphonate treatment decreased osteogenic and angiogenic markers compared to PBS treated cells. This suggests that the altered bone remodeling in OVX animals may be reinvigorated with implant surface properties, and bisphosphonate exposure may jeopardize the pro-osteogenic response osteoblasts have to microstructured surfaces. Furthermore, components of the osteoprotegerin/RANKL/RANK system, a critical pathway for the regulation of bone remodeling, were affected differently. In this study, rOBs displayed a decreased production of osteoprotegerin and an increased production of RANKL compared to TCPS. Previous studies have shown that aging in humans^{261,328} and rodents^{78,79} leads to increased RANKL and decreased osteoprotegerin production by osteoblasts, which could be exacerbated by the enhanced maturation that Ti surfaces facilitate in osteoblasts. Interestingly, ibandronate treatment facilitated an increased osteoprotegerin and decreased RANKL productions indicating bisphosphonate treatment can influence and condition a shift from bone resorption to bone formation at the cellular level. Bisphosphonates have been shown to increase serum osteoprotegerin levels and that increases of osteoprotegerin correlate with increases in BMD.²⁶² It is unclear if the increased osteoprotegerin reflects a direct effect of bisphosphonates on osteoblasts or an indirect effect by altering osteoclastogenesis and thereby altering the catabolism of osteoprotegerin.

Conclusions

In conclusion, our results show that osseointegration is decreased in osteoporotic animals.

Clinically relevant doses of ibandronate were able to halt the progression of the osteoporotic

phenotype. However, these doses were unable to enhance the osseointegration of microrough titanium implants. These *in vivo* results were supported by *in vitro* studies examining the biological response of primary rat osteoblasts to SLA disks.

Chapter 8. Titanium Implant Surface Properties Enhance Osseointegration in Aged Osteoporotic Rats without Pharmacologic Intervention

Abstract

Successful osseointegration involves resorption of primary bone and its replacement with mature bone. Osteoporosis compromises bone remodeling, increasing rates of implant failure. Anti-osteocatabolic drugs can treat osteoporosis but continue to suppress bone remodeling, contraindicating their use during osseointegration. This study determined whether implant surfaces that promote osseointegration in normal rats can promote osseointegration in osteoporotic rats without pharmacologic intervention. Virgin female 8-month-old CD Sprague Dawley rats (N=25) were ovariectomized. At 6 weeks, microstructured/non-nanostructured/hydrophobic (SLA), microstructured/nanostructured/hydrophobic (SLAnano), or microstructured/nanostructured/hydrophilic (mSLA) Ti implants ($\text{\O}2.5\text{mm} \times 3.5\text{mm}$; Institut Straumann AG, Basel, Switzerland) were placed in the distal metaphysis of each femur. At 28 days, bone quality and implant osseointegration were assessed using microCT, histomorphometrics, and removal torque values (RTVs). Calvarial osteoblasts were isolated and cultured on $\text{\O}15\text{mm}$ SLA, SLAnano, or mSLA discs for 7 days. mSLA promoted increased bone-to-implant contact and RTVs *in vivo* and facilitated increased osteoblastic marker production *in vitro* compared to SLA and SLAnano, suggesting that osseointegration occurs in osteoporotic animals, and implant surface properties improve its rate. When appropriate microstructure is present, hydrophilicity has a greater influence than nanostructures. These results provide critical insight for developing implants with improved osseointegration in patients with metabolic disorders of bone remodeling.

Introduction

Osteoporosis is a systemic disease characterized by the microarchitectural deterioration of bone tissue leading to low bone mass and strength. It is one of the most common metabolic diseases and has become a significant topic of public health around the world as many countries begin to encounter the morbidities of an aging population. In 2010, the number of U.S. adults with osteoporosis or low bone mass (osteopenia) was estimated to be 53.6 million, representing 54% of the U.S. population over the age of 50 years.⁴ Moreover, osteoporosis is more prevalent in postmenopausal women, affecting over 80% of the total estimated U.S. population with osteoporosis.⁴ The prevalence of the disease will continue to increase as the number of people aged 60 or older is expected to grow to nearly 2 billion by 2050.³²⁹ The comorbidities of edentulism and fracture risk with osteoporosis are driving the necessity to develop more permanent, predictable, and complication-free dental and orthopaedic implants for this demographic.³³⁰

Osseointegration is important for determining the success of dental and orthopaedic implant outcomes as it results in the direct structural and functional connection between the surface of a load-bearing implant and living bone.¹⁹⁶ This complex biological process involves the modeling of primary bone followed by its subsequent remodeling into mature bone, which is achieved through a locally regulated communication between bone resorbing osteoclasts and bone forming osteoblasts.¹⁹⁶ The communication between osteoclasts and osteoblasts is also important for maintaining bone homeostasis, and any defects in the coupling of bone resorption to formation can lead to osteoporosis.³³¹ Evidence suggests age-related osteoporosis develops from a combination of accelerated bone loss owing to excessive resorption and impaired bone formation during remodeling.³³¹ Metabolic disorders like osteoporosis could jeopardize the bone healing process and thus the predictability of implant osseointegration.³³²

Multiple cellular mechanisms that contribute to the dysfunctional coupling in osteoporosis have been identified. During osteoporosis development, the proliferation and recruitment of

mesenchymal stem cells (MSCs) to the site of resorption is hindered.^{333–336} MSCs also exhibit a reduced capacity to differentiate into osteoblasts and an increased capacity to differentiate into adipocytes.^{337–339} This shift from osteoblastogenesis to adipogenesis has been shown to contribute to the development of osteoporosis by reducing bone formation and increasing marrow fat accumulation.^{340,341} Those MSCs that do differentiate into mature osteoblasts suffer from a decreased life-span as well as an impaired bone-forming capacity with alterations in collagen stability, alignment, and composition.^{342–346}

Osteoporotic bone cells also have a decreased capacity to regulate osteoclasts as evident by their decreased production of transforming growth factor β 1 (TGF β 1) and osteoprotegerin (OPG) and increased production of receptor activator of nuclear kappa-B ligand (RANKL).^{77–79,262} These cells also produce many cytokines that have been implicated as stimulators of osteoclastic activity including interleukin 1 (IL-1), tumor necrosis factor α (TNF α), interleukin 6 (IL-6), prostaglandin E2 (PGE₂), and interleukin 11 (IL-11).^{77,347,348} In many respects, osteoporosis can be viewed as a breakdown of healthy cellular communication, a breakdown that can be locally reinvigorated using implants with optimized surface parameters.

Implant surface characteristics have proven important for determining successful dental implant outcomes. The positive influence of surface topography on implant osseointegration, achieved through grit-blasting and acid-etching, has been a topic of investigation for several decades.^{29,349,350} Today, microrough surfaces dominate the market as they have been shown to achieve faster bone integration, a higher percentage of bone to implant contact (BIC), and a higher resistance to shear, as determined by removal torque values (RTVs), when compared to smooth implant surfaces.³⁵ Surface nanoroughness¹⁴² and hydrophilicity⁵⁵ have also been shown to be beneficial, particularly when the surface is microstructured. These features provide a surface structure much more analogous to natural bone, thereby influencing the adsorbed protein type, quantity, and conformation as well as downstream control of cellular adhesion,

proliferation, and differentiation. Moreover, when grown on these substrates, cells produce factors that regulate osteoclasts to achieve net new bone formation. It was recently shown that MSCs and osteoblasts grown on microstructured surfaces can regulate osteoclast activity and gene expression to different degrees depending on the properties of the substrate surface.³²⁶ This suggests that small variations in surface properties alone can drastically regulate the fusion of new osteoclasts and the activity of existing osteoclasts.

Much of the research in the field of implantology has been limited to healthy animals and patients. Variations in surface micro/nanoroughness, hydrophilicity, and chemistry may prove important when trying to achieve implant osseointegration in compromised patients. To optimize the use of implant technologies in patients with compromised bone structure and metabolism, a more complete understanding of surface design on osseointegration is needed. The goal of the present study was to determine whether changes in surface micro-/nanostructure and hydrophilicity are sufficient to promote osseointegration in an aged rat with untreated osteoporosis induced by ovariectomy.

Materials and Methods

Implant Preparation

2.5mm diameter, 3.5mm long, 0.8mm pitch, Ti implants were provided by Institut Straumann AG (Basel, Switzerland). Implants were machined from a rod of grade 4 Ti degreased in acetone and processed for 30s in a 55°C 2% ammonium fluoride/2% hydrofluoric acid/10% nitric acid solution. Implants were then blasted with 250 – 500µm corundum and boiled in a mixture of HCl and H₂SO₄. This process was performed in air to generate sandblasted large grit acid etched (SLA) implants. A version of this procedure was performed under nitrogen with subsequent storage in 0.9% saline to generate modified SLA (mSLA) implants. A subset of mSLA implants were aged in saline for 1 month, removed from solution, rinsed in ultrapure water, and repackaged in Al foil to generate SLAnano implants. All implants were γ-irradiated before use.

Implant Characterization

Scanning Electron Microscopy

Scanning electron microscopy (SEM; Hitachi SU-70 FE-SEM, Hitachi, Tokyo, Japan) was used to qualitatively evaluate implant surface structure and roughness. Six images at varying magnifications were captured on implants (n=3) implants per surface modification using 5kV accelerating voltage for a total of 18 images.

Laser Confocal Microscopy

Laser confocal microscopy (LCM, Zeiss LSM 710, Zeiss, Oberkochen, Germany) was used to quantitatively evaluate surface micro-roughness. Measurements on each implant (n=3) were taken over an area of 106.2 μ m x 106.2 μ m with a 20x objective and a scanning pitch of 50nm. A Gaussian high-pass filter with a cutoff wavelength of 100 μ m was used when calculating average surface roughness (S_a) over three scans per implant (total n=9).

X-Ray Photoelectron Spectroscopy (XPS)

Chemical composition of the samples (n=3) was obtained from the sample surfaces by X-Ray Photoelectron Spectroscopy (XPS, Thermo K-Alpha XPS, Thermo Fisher Scientific, Waltham, MA, USA). Spectra were collected using a 500 μ m spot size, using an XR5 gun and Al K α x-ray source at 15kV. Scans were taken with a 20ms dwell time and 1eV step size. Three different locations on each sample (total n=9) were analyzed.

Animals and Surgical Procedures

This study was conducted under approval of the Institutional Animal Care and Use Committee at Virginia Commonwealth University. All experiments were carried out in accordance with approved procedures and reported according to ARRIVE guidelines. All animals were treated humanely per the guidelines outlined in the Guide for the Care and Use of Laboratory Animals by the National Institutes of Health. Animals were single-housed in an individually ventilated, solid-bottomed polysulfone cage and kept at a temperature of 17-28°C

with a humidity of 40-70% and a 12/12 h light/dark cycle.

A schematic detailing the timing of surgical procedures is shown in **Figure 33**. Ovariectomy (OVX) surgery was performed on 25, 8-month-old, virgin, female CD Sprague-Dawley rats (Charles River Laboratories, Wilmington, MA). The OVX induced osteoporotic phenotype developed over the next 6 weeks. All animals had access to water *ad libitum* for the duration of the study; however, OVX animals were pair fed a phytoestrogen-free diet (Advanced Protocol Verified Casein Diet 10 IF, LabDiet, St. Louis, MO, USA) to age matched sham OVX controls. The success of the pair feeding regimen was verified by weekly weighing of all animals for the duration of the study, as described previously.⁸⁵

Once the phenotype developed, SLA (n=10 animals), mSLA (n=10 animals), or SLAnano (n=5 animals) implants were inserted transaxially into the distal metaphyses of each femur under anesthesia. Animals were anesthetized with 5% isoflurane gas inhalation and maintained at 4% isoflurane in O₂ gas inhalation for the duration of the surgical procedure. The hind limbs were prepared by shaving and cleaning using ethanol and chlorohexidine. For each hind leg, an 8mm incision was made over the medial side of the knee and the distal metaphysis was exposed using blunt dissection. A dental handpiece was used to create a 2.2mm diameter and 3.5mm deep hole. Implants were inserted and hand-tightened using a custom-made driver. A stainless-steel cover screw was placed on the end of each implant to prevent bone from growing into the

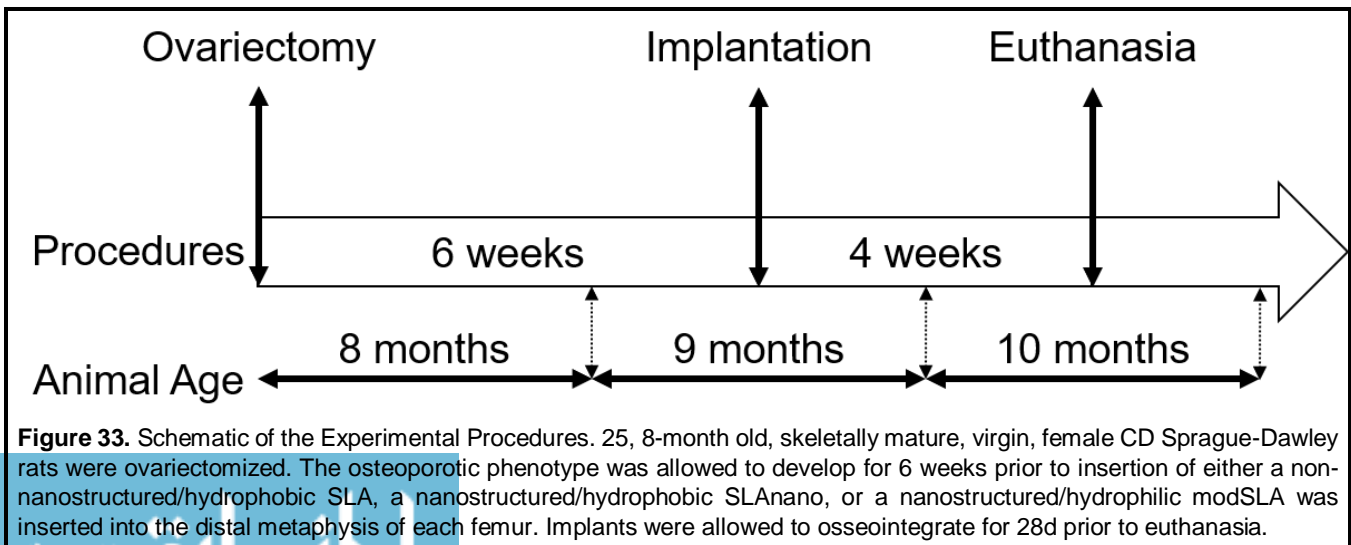


Figure 33. Schematic of the Experimental Procedures. 25, 8-month old, skeletally mature, virgin, female CD Sprague-Dawley rats were ovariectomized. The osteoporotic phenotype was allowed to develop for 6 weeks prior to insertion of either a non-nanostructured/hydrophobic SLA, a nanostructured/hydrophobic SLAnano, or a nanostructured/hydrophilic modSLA was inserted into the distal metaphysis of each femur. Implants were allowed to osseointegrate for 28d prior to euthanasia.

internal threading of the implant. The periosteum and muscle were reapposed and sutured in place using resorbable sutures and the skin was closed with 9mm wound clips. Animals recovered from anesthesia on a water-circulating warming pad and injected subcutaneously with 1mg/kg buprenorphine SR LAB.

28d after the implant surgery rats were euthanized via CO₂ inhalation. The hind limbs from each animal were isolated and prepped for analysis by micro-computed tomography (microCT) and histological analysis (n=5 animals/group). A separate cohort of animals receiving either SLA or mSLA implants were used for removal torque testing (n=5 animals/group). Each limb was treated as a separate sample providing an effective sample size of 10 per implant group for both the removal torque testing and microCT/histological analysis.

Tissue Analysis

MicroCT

MicroCT (SkyScan 1173, Bruker, Kontich, Belgium) was used to assess the peri-implant bone growth and bone-to-implant contact (BIC). Femurs used for microCT were stored and fixed in 10% neutral buffered formalin for at least 24hr prior to imaging. The distal femoral metaphysis was scanned at a resolution of 1120x1120 pixels (image pixel size of 13.66 μ m) over 360° using a 0.25mm brass filter, scanning energies of 120kV and 66 μ A, 420ms exposure time, and 5 x-ray projections acquired every 0.2° and averaged. Using NRecon Software (Bruker), reconstruction of the scanned images was performed using a standard Feldkamp algorithm with a beam hardening correction of 20% and a Gaussian smoothing kernel of 0. After reconstruction, samples were analyzed using CTAn version 1.16.4.1 (Bruker). Bone volume over total volume (BV/TV) was calculated by isolating a uniform volume of interest (VOI) for all samples which contained the distal 3mm of implant and surrounding bone. 3mm was chosen to eliminate any variability arising from the implant not being exactly at bone level for every sample. The implant was then thresholded, the VOI was shrink-wrapped and dilated 2 pixels around the implant and

subtracted from the original VOI. The remaining bone in the VOI was then thresholded and quantified yielding total bone volume (BV) and normalized to the total uniform volume of interest (TV). Bone-to-implant contact (BIC), which quantifies only the bone in direct contact with the implant, was quantified by isolating the distal 3mm of the implant. The implant was thresholded and shrink-wrapped, and the VOI was dilated 10 pixels around the implant and saved as a new volume of interest. In the new VOI, the implant was thresholded, dilated 3 pixels, and subtracted from the VOI. The remaining VOI was then eroded 3 pixels. The remaining bone in the final VOI was thus only in direct contact with the implant (BV) and was normalized to the volume of the implant (TV).

Histology

Following imaging with microCT, samples were placed in fresh 10% neutral buffered formalin and sent to be commercially processed for calcified histological staining (Histion, Everett, WA, USA). Femurs were embedded in methyl methacrylate, sectioned longitudinally relative to the implant and transaxially relative to the femur, and stained with Stevenel's blue and van Gieson. Sections were imaged using bright field light microscopy with an AxioCam MRc5 camera and Axio Observer Z1 and analyzed using ZEN 2012 Blue Edition software (Zeiss).

New peri-implant bone growth was quantified within a uniform rectangular region of interest (ROI) for all samples that was 3.5mm in width by 3.0mm in length for a total of 10.7mm². The ROI was centered on each implant and began 0.3mm beneath its base. The area of all bone within the ROI was quantified yielding BV and normalized to the area of the ROI yielding TV. The area of bone contained within the ROI divided by the area of the ROI was defined as the histological BV/TV. In addition, the perimeter of the implant contained within both the trabecular region and the cortical region of the bone was measured. The trabecular BIC and cortical BIC were determined by dividing the length of bone in direct contact with the implant by the trabecular and cortical perimeter length respectively. The total BIC was calculated by summing both lengths

of contact and dividing by the total perimeter of the implant.

Removal Torque

Removal torque testing was performed on fresh, non-fixed samples using an ElectroForce 3200 Series III test instrument (TA Instruments, New Castle, DE, USA). Because of their asymmetrical shape, femurs were mounted in 1cm diameter flexible polyurethane plastic tubing to ensure no movement of the femur during analysis (Fig. 5A). The tubing was cut into 5cm segments and halved longitudinally to provide access to the implant. Femurs were secured with polyurethane adhesive and allowed to dry overnight prior to testing. The implant on the samples were then fit to a custom-made driver and aligned to the testing machine axis to ensure no initial torque was present on the implant (0Ncm). Torque was then applied to the implants with a rotational speed of 0.1°s^{-1} with an axial displacement of 0.8mm/360° to ensure no compressive load was applied to the sample. Torque vs. degree graphs were generated for each sample and fit to a bilinear model in order to distinguish the toe-region from the linear region using an open-source least squares spline modeling package (SLM - Shape Language Modeling version 1.14) for MATLAB (MathWorks, Natick, MA, USA). The linear region of each graph was then evaluated for the maximum torque, torsional energy (area below linear region), and torsional stiffness (slope of linear region).

Osteoblast Isolation and Biological Response in Vitro

Calvarial osteoblasts were also isolated from the frontal and parietal bones of euthanized rats using an explant technique. After removal of the periosteum and soft tissue, bones were digested for 15min at 37°C with 0.25% trypsin-EDTA (Life Technologies, Carlsbad, CA). Bones were minced into pieces approximately 1mm x 1mm and placed into a 100mm x 20mm Petri dish with Dulbecco's modified Eagle medium (DMEM; Mediatech, Manassas, VA) + 10% fetal bovine serum (FBS) + 1% penicillin-streptomycin (Life Technologies). At confluence, cells were subpassaged and cultured as above. In order to ensure $1\alpha,25$ -dihydroxy vitamin D₃

($1\alpha,25(\text{OH})_2\text{D}_3$; Enzo Biochem, Farmingdale, NY). The osteoblastic phenotype of each of the four groups of isolated cells was confirmed by measuring alkaline phosphatase specific activity and osteocalcin production after treatment of confluent cultures with either 0M or 10^{-8}M $1\alpha,25(\text{OH})_2\text{D}_3$ for 24hrs (Supplementary Fig. 1) on tissue culture polystyrene (TCPS).

Validated rat osteoblasts (rOBs; passage < 4) were separately cultured on TCPS or 15mm Ti SLA, SLAnano or mSLA discs. Discs were prepared from Ti sheets but subjected to the same implant sand-blasting and acid etching procedure as described above. Fabrication of these discs has been described previously.²² Cells were plated at a density of 10,000 cells/cm² and incubated at 37°C in an atmosphere of 5% CO₂ and 100% humidity. Media were changed 24h after plating and every 48h thereafter for 7d. At 7d, cells were incubated with fresh DMEM for 24h. Media were collected and immunoassays were used to measure levels of intact rat osteocalcin (Alfa Aesar, Haverhill, MA) rat/mouse osteopontin (R&D Systems, Minneapolis, MN), mouse osteoprotegerin (R&D Systems), human/mouse/rat BMP2 (PeproTech), mouse receptor activator of nuclear kappa-B ligand (RANKL; R&D Systems), and rat vascular endothelial growth factor (VEGF; R&D Systems).

After collection of media, cell monolayers were washed twice with 0.2ml PBS, lysed in 0.05% Triton X-100, and homogenized by sonication at 40 amplitude using a Vibra-Cell ultrasonicator (Sonics & Materials Inc., Newtown, CT). DNA content in the cell lysate was measured with PicoGreen (Promega, Madison, WI) using a Synergy H1 Hybrid Reader fluorescence detector (BioTek, Winooski, VT) at an excitation of 485 nm and emission of 538 nm. Alkaline phosphatase specific activity [orthophosphoric monoester phosphohydrolase, alkaline; E.C. 3.1.3.1] was assayed in cell lysates by measuring the conversion of *p*-nitrophenylphosphate to *p*-nitrophenol at pH 10.25 and temperature of 37°C. Absorbance was measured at 405nm. Activity was normalized to total protein content in the cell lysates as determined by bicinchoninic acid protein assay kit (Thermo Fisher Scientific, Waltham, MA). Immunoassay data were normalized to DNA

content.

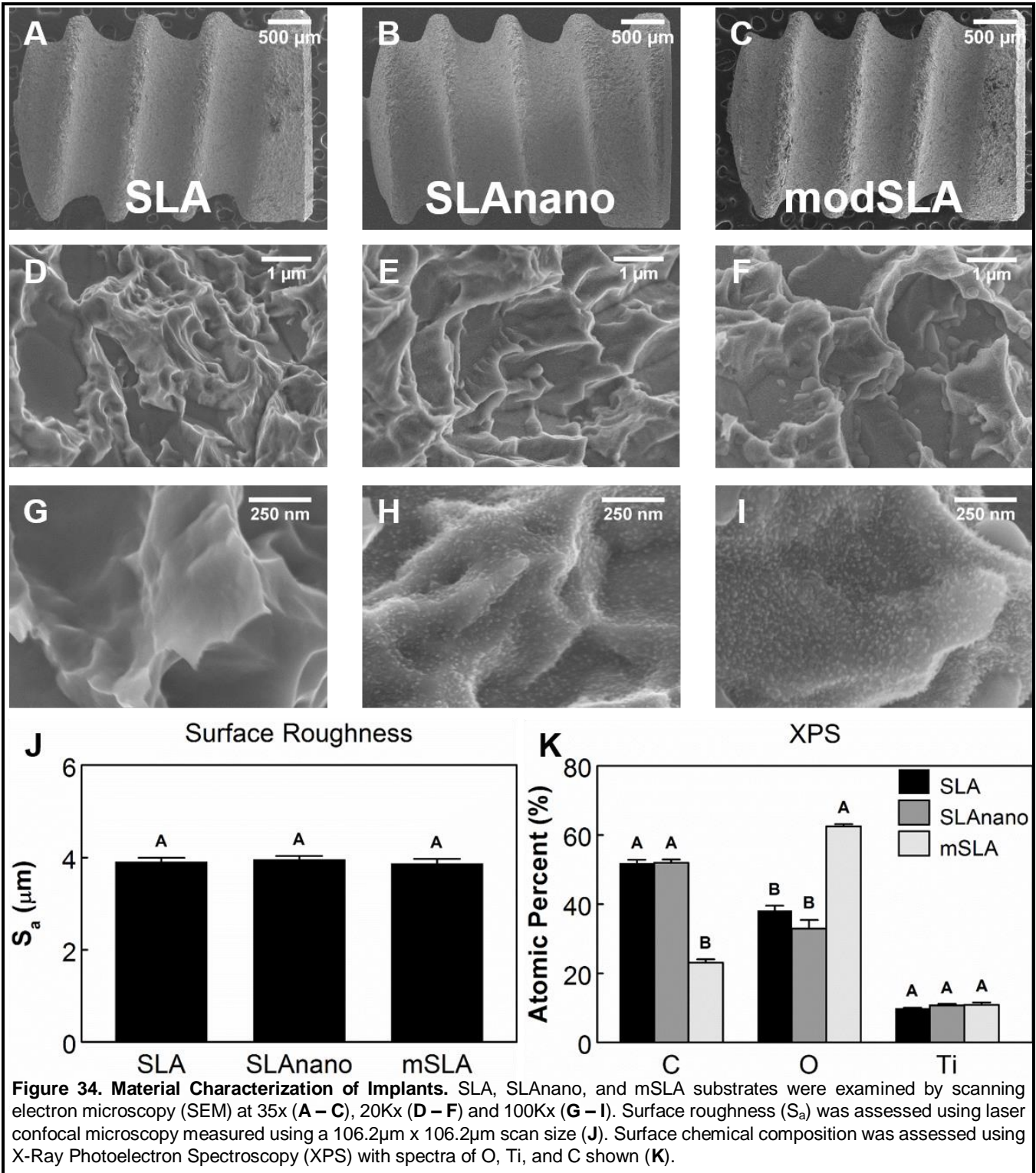
Statistical Analysis

Based on previous studies,^{193,296} in order to detect a 30% mean difference with 20% variance and a type I error rate of 0.05, a two-tailed one-way ANOVA power analysis determined a sample size of 10 per group is necessary to maintain 80% power. In order to ensure that differences in mechanical loading would not affect the results, identical implants were placed in the right and left hind limbs. Since both legs were treated identically, it is safe to assume that movement or loading in one limb will not affect the movement or loading experienced by the other limb. The design of our study permits the assumption that implants from individual limbs can be treated as independent data points rather than dependent. Data are presented as the mean \pm standard error (SE) for each analysis. All cell culture experiments had a sample size of six (n=6) and repeated at least three times to ensure validity of the results. Data shown in the figures are from representative experiments. Except for the removal torque experiment, a one-way analysis of variance was performed with a two-tailed Tukey correction to adjust for multiple comparisons. A t-test was used for the removal torque experiment. P values of <0.05 were considered significant for all statistical analyses and were performed using JMP statistical software (SAS Institute, Cary, NC, USA).

Results

Implant Characterization

Qualitative SEM images (**Fig.34A – I**) revealed that the sandblasting and acid etching procedure maintained the overall threaded macrostructure of the implants (**Fig.34A – C**) while creating similar microtopographies (**Fig.34D – F**). At a higher magnification (**Fig.34G – I**), the presence of nanostructures was observed on SLAnano (**Fig.34H**) and mSLA (**Fig.34I**) implants. Nanostructures were absent from SLA implants (**Fig.34G**). Confocal microscopy confirmed the



similarities in microtopographies, revealing no differences among the implants' mean surface roughness (Fig.34J). XPS (Fig.34K) showed carbon (C), oxygen (O), and titanium (Ti) to be the main atomic components of the SLA, SLAnano, and modSLA implants. No differences in chemical composition was detected between SLA and SLAnano. Compared to mSLA, both SLA

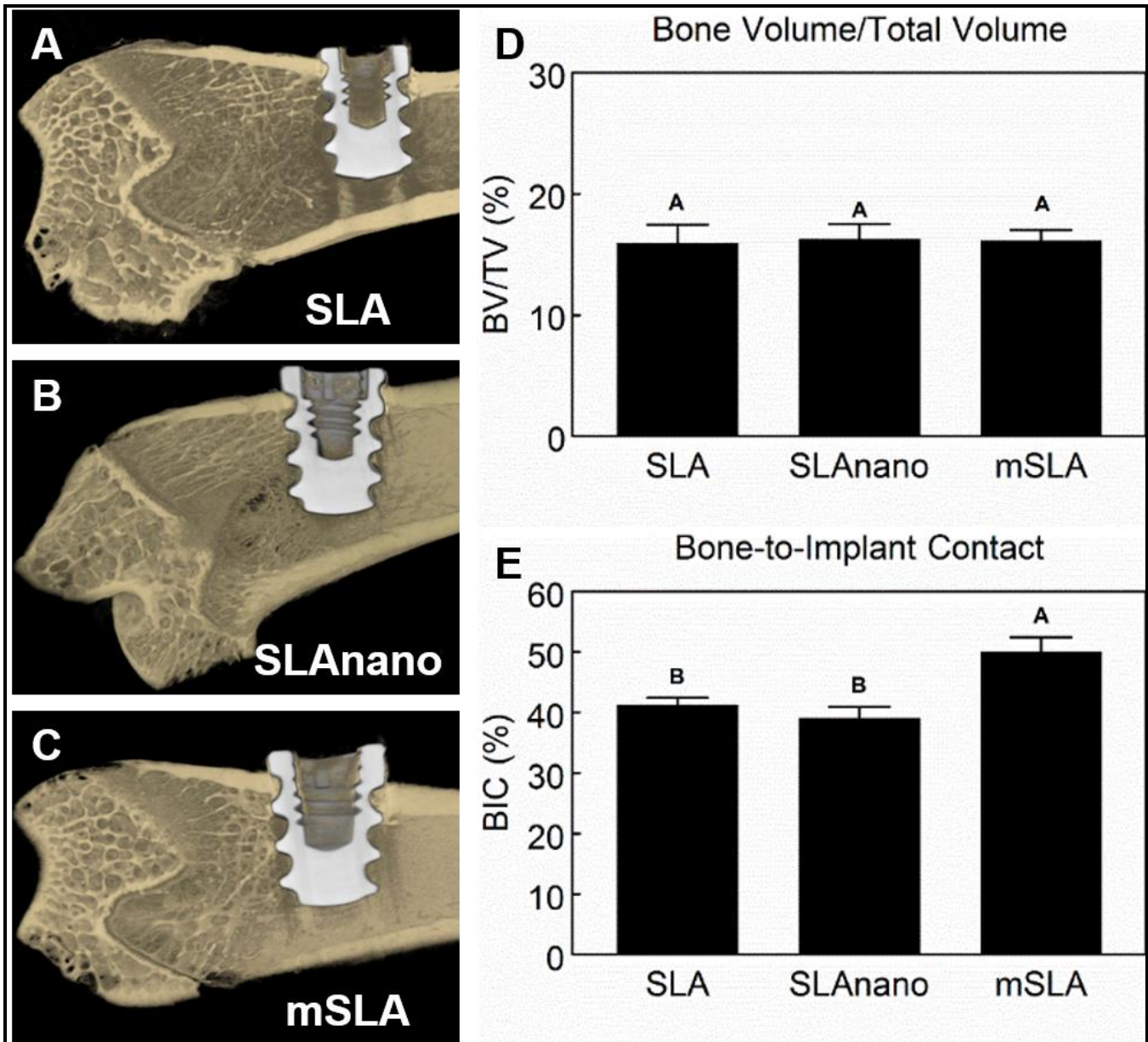
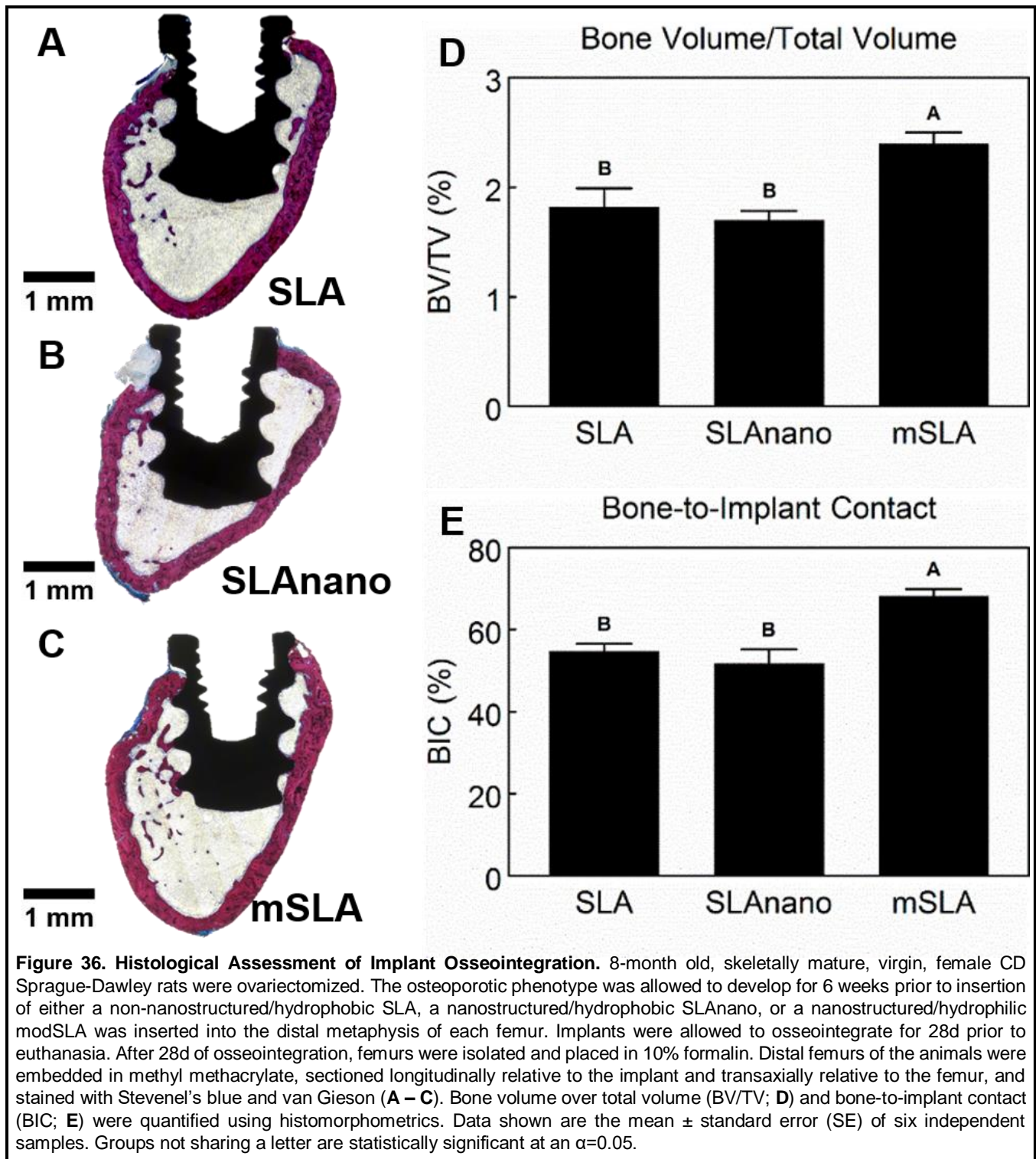


Figure 35. MicroCT Assessment of Implant Osseointegration. 8-month old, skeletally mature, virgin, female CD Sprague-Dawley rats were ovariectomized. The osteoporotic phenotype was allowed to develop for 6 weeks prior to insertion of either a non-nanostructured/hydrophobic SLA, a nanostructured/hydrophobic SLAnano, or a nanostructured/hydrophilic modSLA was inserted into the distal metaphysis of each femur. Implants were allowed to osseointegrate for 28d prior to euthanasia. After 28d of osseointegration, femurs were isolated and placed in 10% formalin. Distal femurs of the animals were analyzed with 3D microCT reconstructions (A – C). Bone volume over total volume (BV/TV; D) and bone-to-implant contact (BIC; E) were quantified from the microCT reconstructions. Data shown are the mean \pm standard error (SE) of ten independent samples. Groups not sharing a letter are statistically significant at an $\alpha=0.05$.

and SLAnano had increased carbon content and decreased oxygen content. Similar titanium content was detected among all three implant surfaces.

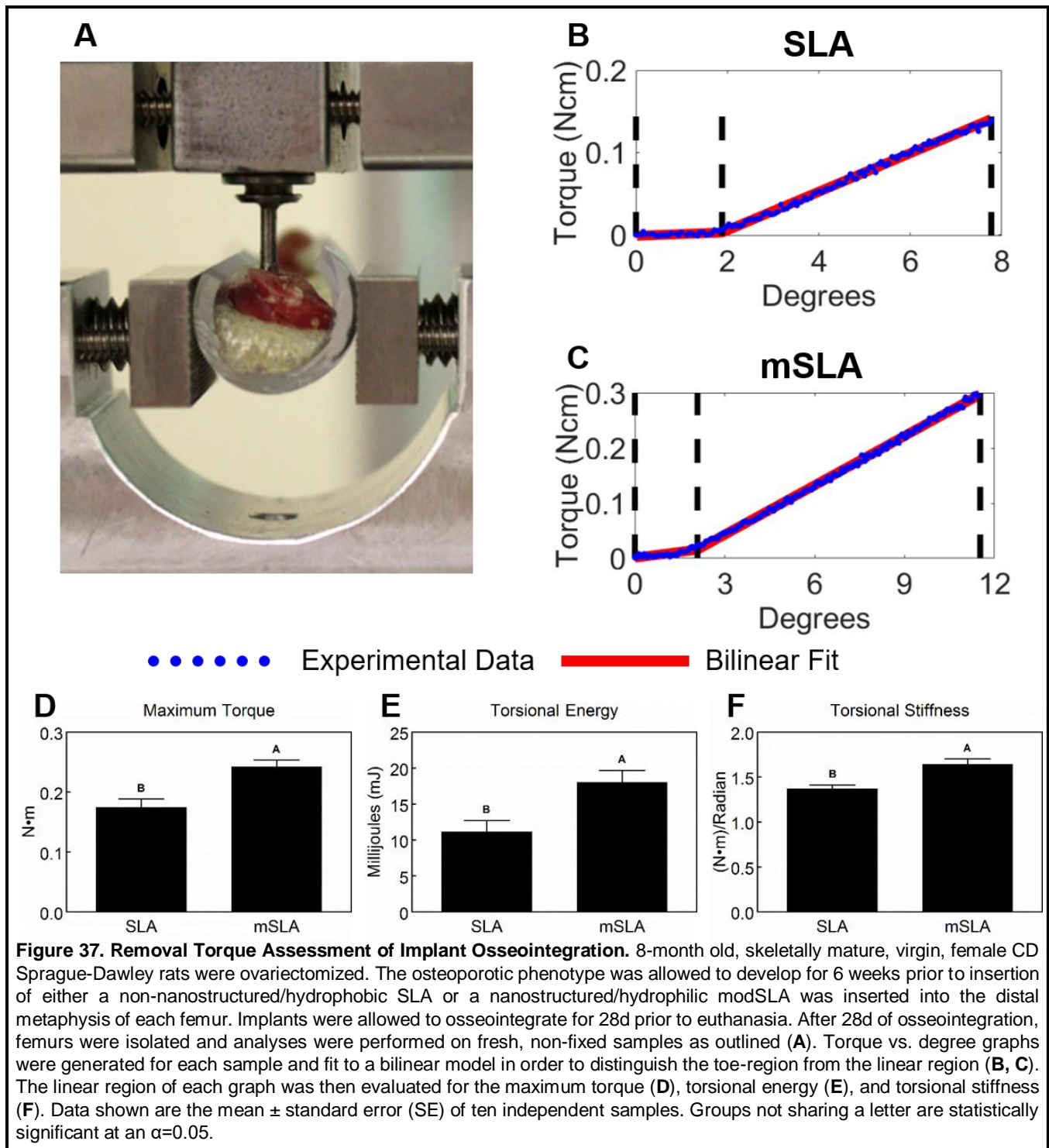
MicroCT and Histology

3D reconstructions of microCT scans (Fig.35A – C) show the implant placement in the distal metaphysis of the femurs. The implants did not contact the growth plate eliminating any potential

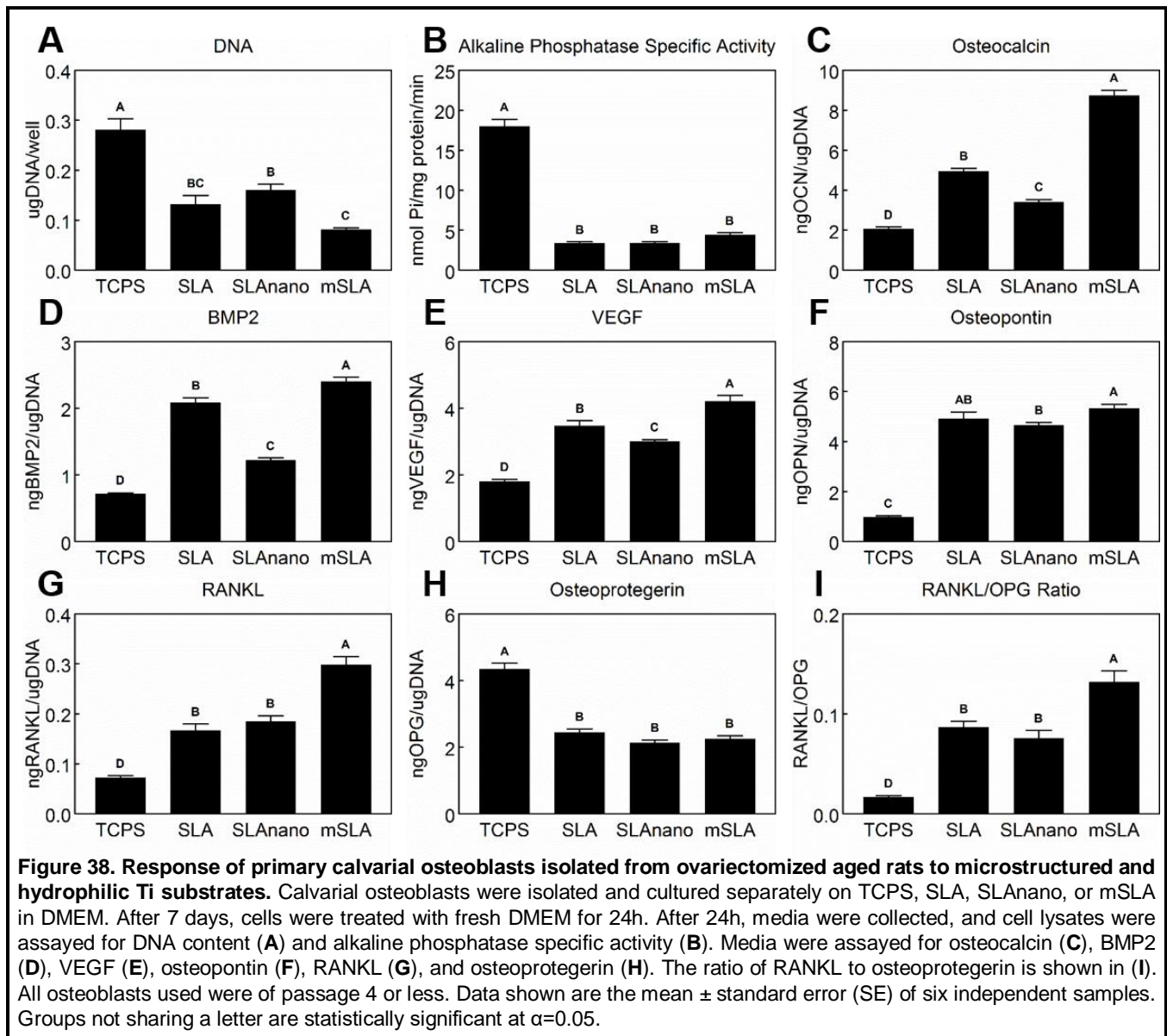


influence on the bone formation in our defined VOI. The BV/TV (**Fig.35D**) was unaffected by the implant type. mSLA promoted increased BIC compared to SLA and SLAnano (**Fig.35E**). Representative histological sections from each group are shown in **Fig.36A – C**. mSLA promoted increased BV/TV (**Fig.36D**) and BIC (**Fig.36E**) compared to SLA and SLAnano.

Removal Torque



Since microCT and histomorphometrics revealed no differences between SLA and SLAnano, removal torque testing was performed on animals receiving either SLA or mSLA. Isolated femurs were secured in polyurethane tubing and aligned to the machine axis in a custom-fabricated sample holder to ensure no movement was created during the test (Fig.37A). Representative torque vs. degree graphs for SLA (Fig.37B) and mSLA (Fig.37C) display the bilinear model (red)



fit to the experimental data (blue). The middle vertical dashed line (black) separates the toe region (left section) and the linear region (right section) as determined by the least squares spline modeling package in MATLAB. The maximum torque (**Fig.37D**), torsional energy (**Fig.37E**), and torsional stiffness (**Fig.37F**) were increased around mSLA implants compared to SLA.

In vitro Cell Response

Addition of 10^{-8} M $1\alpha,25(\text{OH})_2\text{D}_3$ to confluent cultures of rOBs increased osteocalcin and alkaline phosphatase specific activity, confirming their successful isolation and expansion. DNA content (**Fig.38A**) and alkaline phosphatase specific activity (**Fig.38B**) were decreased in SLA cultures compared to TCPS. On microstructured surfaces, DNA content was further reduced in

mSLA cultures compared to SLAnano. No differences in alkaline phosphatase specific activity were detected on microstructured surfaces. rOBs cultured on modified surfaces produced higher quantities of osteocalcin (**Fig.38C**), BMP2 (**Fig.38D**), VEGF (**Fig.38E**), osteopontin (**Fig.38F**), and RANKL (**Fig.38G**) compared to TCPS cultures. Except for osteopontin, mSLA facilitated the greatest production of these factors while SLAnano stimulated the least. Although no differences were detected between mSLA and SLA osteopontin, a greater production was found on mSLA compared to SLAnano. No difference in RANKL production was detected between SLA and SLAnano cultures. Osteoprotegerin production (**Fig.38H**) was decreased to similar levels on modified surfaces compared to TCPS; however, the RANKL/OPG ratio (**Fig.38I**) was increased with the highest levels detected on mSLA.

Discussion

The morbidities associated with an aging population have increased the need for technologies that provide predictable implant osseointegration in dental and orthopaedic sites. Osteoporosis is one such metabolic condition that occurs when excessive bone resorption is not compensated by a concomitant increase in bone formation. The inability of osteoblasts to match the accelerated osteoclastic bone resorption with new bone formation implies a defect in the coupling process. The increased fracture rates³⁵¹ and impaired healing³⁵² associated with osteoporosis have become a significant dental and orthopaedic challenge. Systemic administration of drugs like bisphosphonates or osteoinductive agents like BMPs or parathyroid hormone-related protein (PTHrp) can improve clinical implantation outcomes by increasing bone volume (BV) and bone mineral density (BMD). However, these technologies can be expensive and sometimes require long-term administration. Evidence also indicates their use may have deleterious side effects including osteonecrosis of the jaw and are contraindicated for some applications. Therefore, approaches that do not rely on pharmacologic interventions are needed.

Much of the research regarding the pathophysiology of osteoporosis and mitigating its effects have focused on regulating the hyperactivity of osteoclasts. Impairment of osteoclasts will also cause an inhibitory effect on bone remodeling causing issues where bone turnover is of the utmost importance, such as osseointegration of dental implants. Alternatively, few studies have explored enhancing the osteoanabolic activity of osteoblasts and their progenitors, MSCs. Because of their capacity to self-renew and differentiation into various cell types, treatment strategies aimed at altering the differentiation direction of MSCs or augmenting normal endogenous MSCs could be a potential method for osteoporosis therapy. Specifically, for osteoporosis, this means targeting the altered differentiation potential of MSCs that favors adipogenesis over osteoblastogenesis. Promoting osteoblastic differentiation is not only important for promoting net new bone formation but also for the recruitment of other osteoprogenitor cells via paracrine signaling to hasten the peri-implant healing process. Although the goal of the present study was not concerned with systemic treatment of osteoporosis, the idea of locally mitigating the effects of osteoporosis by targeting MSC and osteoblast differentiation and maturation is pertinent to enhancing implant osseointegration in osteoporotic patients.

In an approach that does not rely on pharmacologic interventions, we have shown that exploitation of the physical surface properties of Ti implants can promote peri-implant bone formation and osseointegration in a model of aged post-menopausal osteoporosis. Moreover, mSLA, a hydrophilic and micro-/nano-structured surface, promoted enhanced osseointegration compared to SLA, a hydrophobic and micro-structured surface, and SLAnano, a hydrophobic micro-/nanostructured surface. Higher BIC values and RTVs were observed in animals receiving mSLA implants. These values were similar to those found in non-compromised animals as previously reported.⁸⁵ Interestingly, increased BV/TV was observed around the mSLA implants as determined by histomorphometrics. The unique mSLA surface is known to promote the

production of factors by cells that act via autocrine/paracrine signaling to induce bone formation locally and distal to the implant,^{61,80} which translates into enhanced contact and distal osteogenesis *in vivo*.¹⁹⁶ Future studies are needed to assess the extent to which mSLA can promote peri-implant bone formation in osteoporotic animals as well as other compromised conditions.

The processing technique used in this study allowed accurate separation between the effects of the nanostructures and the surface hydrophilicity. The sand blasting and acid etching procedure provided a consistent micro-roughness among SLA, SLAnano, and mSLA; however, this process did not induce nanostructure formation. Instead, nanostructure formation was dependent upon the reorganization of the oxide layer facilitated by the aqueous NaCl solution. Similar sized nanostructures were present on SLAnano and mSLA but not SLA. The exact process of nanostructure formation is unknown; however, many studies have fabricated nanostructures on metallic surfaces using a variety of methods involving changes in temperature, pressure, and chemical treatments. X-ray photoelectron spectroscopy (XPS) revealed that aqueous NaCl storage also maintained increased surface oxygen content by preventing carbon contamination on mSLA compared to SLA and SLAnano. Although SLAnano was originally prepared and stored in the same manner as mSLA, removal from NaCl solution was sufficient to reduce the oxygen levels and increase carbon levels to that of SLA. Due to the shape of the implant itself, quantification of the hydrophilicity by contact angle was not possible. However, the contact angle of the 15mm discs subjected to identical surface treatments has been reported previously.²² Additionally, the XPS results revealed a surface composition similar to what was reported on hydrophilic surfaces compared to hydrophobic surfaces.²² These results also confirm our findings reported for the SLA implant confirming batch-to-batch fabrication consistency.⁸⁵

The mechanisms responsible for the enhanced osseointegration observed *in vivo* can be explained by much of our previous *in vitro* work. Estrogen is an osteoprotective hormone, and its deficiency leads to an elevated rate of bone turnover culminating in osteoporosis in females and, in some cases, older males. We showed that female osteoblasts are more sensitive to treatment with 17 β -estradiol (E2) when cultured on microstructured Ti.^{73,75,81} Sensitivity to E2 treatment was also shown to increase when these cells were cultured on SLA and mSLA compared to TCPS or PT. Furthermore, E2 treatment induces the expression of Wnt5a and Wnt11 signaling pathway components. On TCPS, MSC differentiation occurs through the canonical Wnt3A pathway, causing an accumulation of β -catenin in the cytoplasm and its translocation into the nucleus to serve as a transcriptional activator.⁶⁷⁻⁶⁹ Our studies have demonstrated surface mediated MSC differentiation downregulates genes associated with the Wnt3A pathway while upregulating genes of the Wnt11⁷³ and non-canonical calcium-dependent Wnt5a pathway.^{70,71} These data suggest that surface design may be able to compensate for low E2 typical of osteoporosis by stimulating MSC differentiation and osteoblast maturation.

Successful osseointegration not only requires net new bone formation but also involves osteoclast-mediated bone remodeling. Therefore, implants designed for osteoporotic patients should mitigate the effects of the altered communication among the cells responsible for bone remodeling. In osteoporotic patients, MSCs and osteoblasts produce factors favoring osteoclastogenesis unfettered by any regulatory feedback mechanisms. Increased levels of pro-inflammatory IL-6 and decreased levels of TGF β 1 are produced by bone cells isolated from osteoporotic patients compared to healthy patients.^{77-79,262} Interestingly, both E2 treatment and microstructured Ti substrates are known to inhibit IL-6 production while enhancing production of TGF β 1 and OPG.^{75,80,81} It was also shown that conditioned media from MSC cultures grown on microstructured Ti substrates for 7 days inhibit osteoclast activity and this is correlated with surface-dependent production of osteoclast inhibitory factors.³²⁶ In addition to the high

production of negative regulators of osteoclast activity, cells produce high levels of osteocalcin and osteopontin.^{22,53} Osteocalcin has been shown to promote the chemotaxis, adhesion, and spreading of osteoclasts^{86,87} while osteopontin plays a role in anchoring osteoclasts to the mineralized bone matrix.⁸⁸ The sequential production of these factors suggests microstructured Ti facilitates the production of a cascade of factors by MSCs and osteoblasts to mediate osteoclast recruitment while preventing their premature fusion and activity.

Many studies have suggested a favorable effect of a nanostructured surface on osteoblast differentiation and maturation *in vitro* and new bone formation *in vivo*. No positive influence of nanostructures on implant osseointegration in OVX-induced osteoporotic animals was observed in this study. Moreover, the production of osteoblastic factors was impaired in primary osteoblasts when cultured on the hydrophobic/nanostructured SLAnano surface *in vitro*, an effect observed previously in healthy cells. Calvarial osteoblasts isolated from OVX animals displayed decreased osteocalcin, VEGF, BMP2, and osteopontin when cultured on SLAnano. The nanostructure size of the SLAnano surface was previously reported to be ~10nm²² whereas studies that observed positive effects of nanostructures ranged from 40 – 200nm.^{51,142,191} This suggests that osteoblastic differentiation and maturation can be altered by varying the size and shape of the nanostructures. Moreover, the effect of the nanostructures can be recovered and improved through the addition of the hydrophilicity providing the optimum conditions of osteoblastic differentiation and maturation. Interestingly, rOBs on all surfaces displayed decreased productions of OPG and increased productions of RANKL compared to TCPS. Previous studies have shown that aging in humans and rodents leads to an increased osteoblast-specific production of RANKL and decreased osteoprotegerin in osteoblasts,^{78,79} which could be exacerbated by the enhanced maturation that Ti surfaces facilitate in osteoblasts.

Conclusions

Clinical grade Ti was successfully modified to fabricate microrough surfaces exhibiting

hydrophobic or hydrophilic nanostructured surfaces. Moreover, these surfaces were able to osseointegrate in an aged rat model of OVX-induced osteoporosis without pharmacologic intervention. Although modified surfaces were able to osseointegrate, a hydrophilic and micro-/nano-structured mSLA surface had better osseointegration as indicated by higher percent BIC and RTVs. These values are also like what was previously observed in healthy animals receiving SLA implants. *In vitro* production of markers of osteoblastic differentiation and maturation were also greatest on mSLA while a hydrophobic and micro-/nano-structured SLAnano surface delayed the process of osteoblastogenesis. These results suggest that when the appropriate microstructure is present, hydrophilicity may play a greater role in stimulating differentiation of MSCs and osteoprogenitor cells and maturation of osteoblasts than nanostructures. Furthermore, when presented with the optimal surface, similar degrees of osseointegration between healthy and compromised patients can be achieved. Because of these differences observed both *in vitro* and *in vivo*, modified implant surfaces can exert their control over the altered bone remodeling and turnover observed in patients with osteoporosis to stimulate functional osseointegration. This insight is critical to the development of implants that support osseointegration in compromised patients.

Chapter 9. Conclusions and Future Perspectives

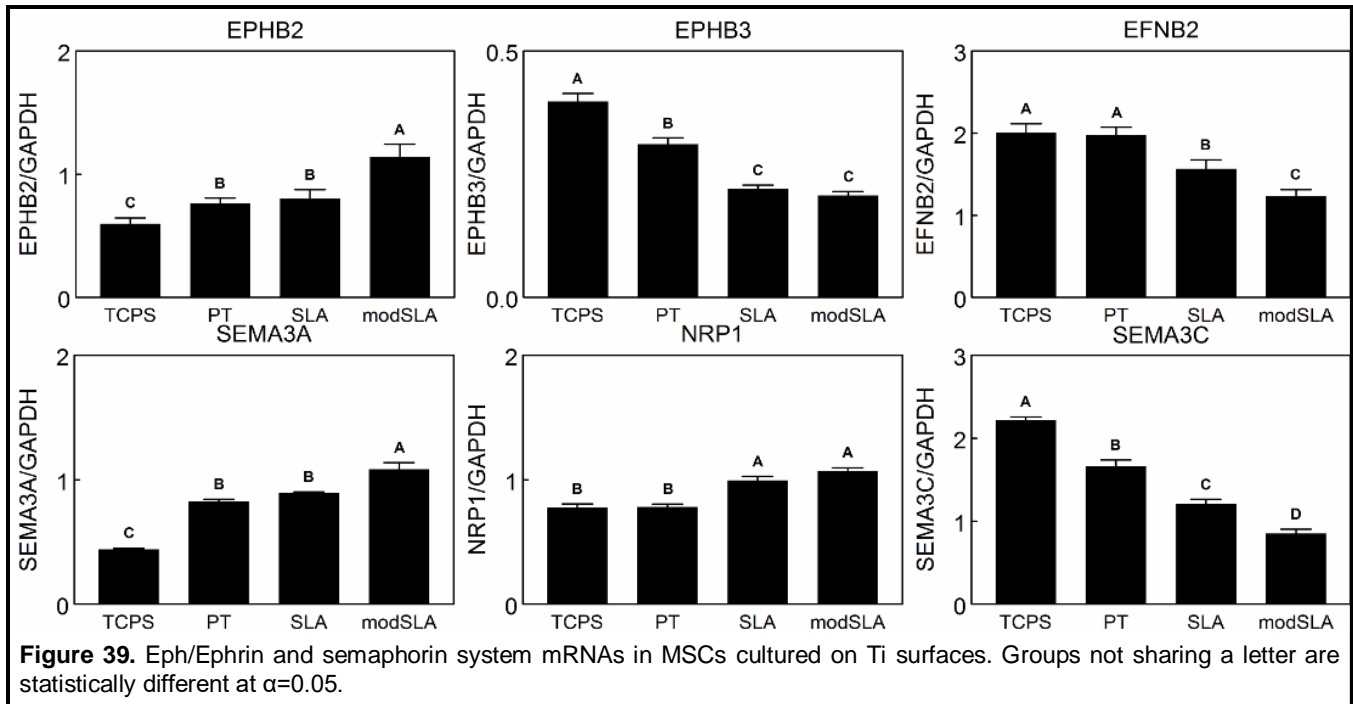
This work has established that microstructured Ti and TiZr surfaces play significant roles in the bone remodeling stage of osseointegration. We have shown that Ti and TiZr can be successfully modified to enhance surface hydrophilicity, create microroughness, and induce nanostructure formation. Although all modified surfaces were able to facilitate a healthy osteoblastic phenotype in both MSCs and NHOsts, nanostructure size of ~11nm may delay the process of osteoblastogenesis. However, the effect of these nanostructures can be recovered with enhanced surface energy (hydrophilicity). This holds true when comparing the *in vitro* response of these cells between Ti to TiZr. Both MSCs and NHOsts responded similarly to both surfaces despite differences in bulk material and variations in surface nanostructure morphology/density. While it is tempting to definitively conclude that surface hydrophilicity overpowers any influence elicited by the surface chemistry (Ti vs. TiZr) or the surface nanoroughness, we are unable due to missing controls. Future studies would benefit from comparing hydrophobic/microrough Ti and TiZr as well as comparing hydrophilic/microrough Ti/TiZr to hydrophilic/microrough/nanorough Ti/TiZr. equivalent.

We also showed that cellular response to surface roughness and hydrophilicity is modulated by nitrogen containing BPs. BPs are commonly used to combat osteoporosis by targeting OCs, slowing the rate and severity of bone resorption providing rationale for their use to enhance osseointegration. Our results indicate their use may have deleterious effects on implant success and patient safety contraindicating their use when implant osseointegration is the desired outcome. Exposure to BPs jeopardizes the pro-osteogenic response osteoblasts have to microstructured surfaces. Since BP treatment was more robust in cells cultured on rough and/or hydrophilic surfaces compared to smooth substrates, this effect may be dependent on cell maturation state, as well as donor sex and age. Moreover, their effects persist *in vivo* and condition osteoblasts to negatively influence their *in vitro* response. Because of their persistent

effects, clinicians may consider implementing a “drug holiday” for patients prescribed BPs, especially those who need a dental and/or orthopaedic implant. Future studies should assess the time it takes for primary osteoblasts to recover from the persistent effects of different BPs.

Clinically, BPs could compromise peri-implant bone formation slowing the rate and quality of implant osseointegration. In order to assess the effects of BPs on osseointegration, an aged rat model with ovariectomized induced osteoporosis was employed. Our results show that osseointegration is decreased in osteoporotic animals compared to age-matched controls. Clinically relevant doses of ibandronate were able to halt the progression of the osteoporotic phenotype. These doses neither increased nor decreased implant osseointegration. However, the *in vitro* response of isolated osteoblasts was impaired, especially in sham ovariectomized animals. Interestingly, cells isolated from untreated ovariectomized animals responded more favorably to microstructured surfaces when compared to cells isolated from healthy controls.

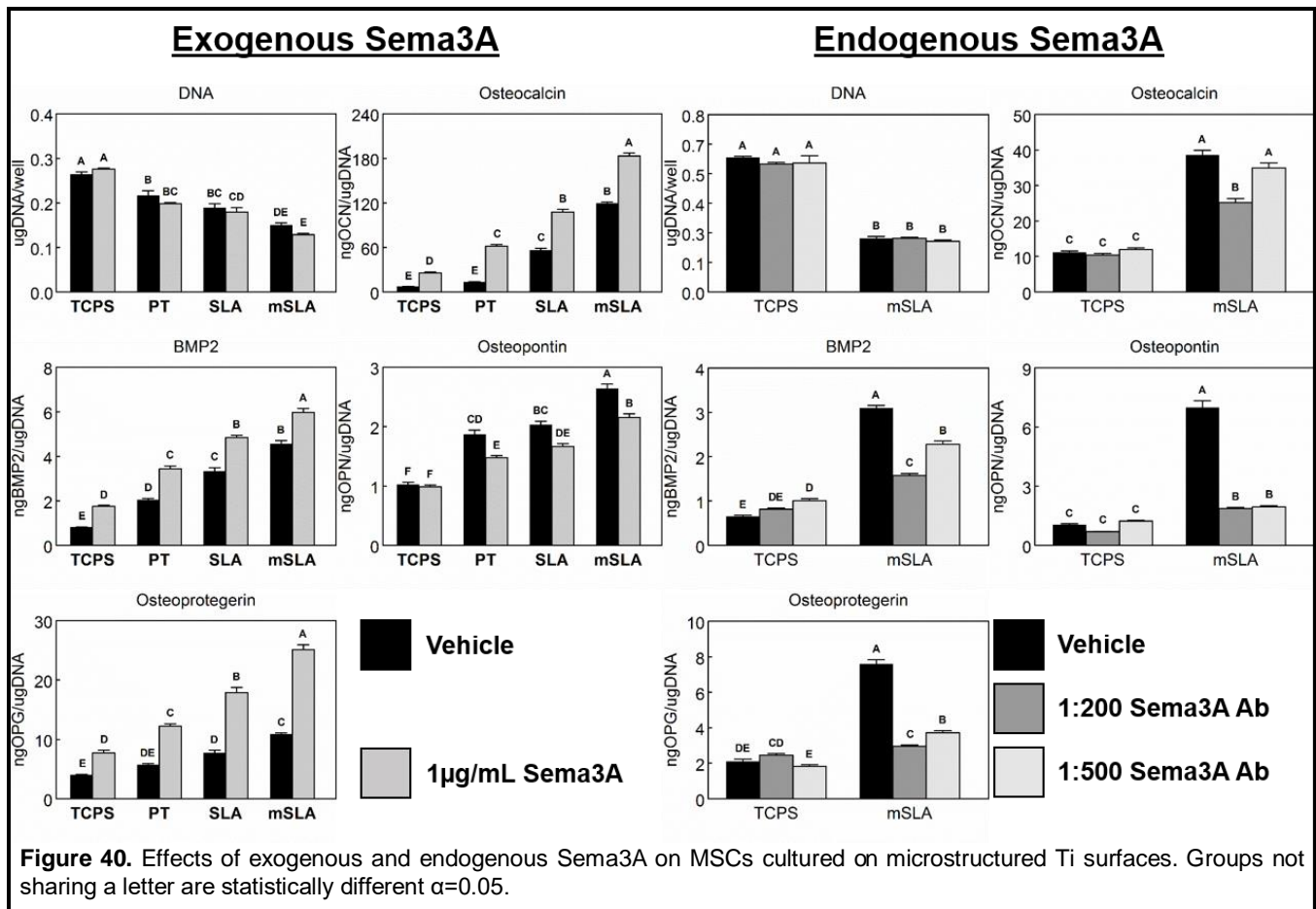
Whether implant surface properties alone were enough to stimulate peri-implant bone formation and osseointegration was assessed using only untreated ovariectomized rats. Clinical grade 4 Ti implants were successfully modified to fabricate microrough surfaces exhibiting hydrophobic or hydrophilic nanostructured surfaces like the grade 2 Ti disks used for *in vitro* studies. Each implant was able to osseointegrate in an aged rat model of OVX-induced osteoporosis without pharmacologic intervention. Unlike what was seen *in vitro*, the hydrophobic nanostructured implant surface did not impair osseointegration. Perhaps after 28d the influence of ~11nm nanostructures cannot be observed and instead reserves its influence over the initial stages. The aspect that was similar to what was observed in healthy MSC and NHOst cultures was the superior influence a hydrophilic and micro-/nano-structured surface had over osseointegration. *In vitro* production of osteoblastic markers from isolated primary cells were perpetuated on this surface as well. These results support the hypothesis that hydrophilicity may exert a greater influence compared to nanostructures. Whether or not it is greater than



microroughness remains to be determined. Regardless, these results suggest that modified implant surfaces exert their control over the altered bone remodeling and turnover observed in patients with osteoporosis to stimulate functional osseointegration.

The question of what to do with this information now presents itself. Current research in the field of dental and orthopaedic implantology tends to focus on the development of novel methods of altering biomaterial surfaces and characterizing their effects on early stage osteogenesis. While these approaches are well-intentioned, it is unlikely that development of an optimal surface design capable of stimulating similar degrees of osseointegration between healthy and osteoporotic patients will manifest itself in this way. Instead, research in the field of dental and orthopaedic implantology should focus on knowledge gaps in bone biology and how implant surface features alter the dynamics of wound healing. Thus, it is of great importance to determine which factors regulate coupling and the influence dental implant surface features have on these mechanisms.

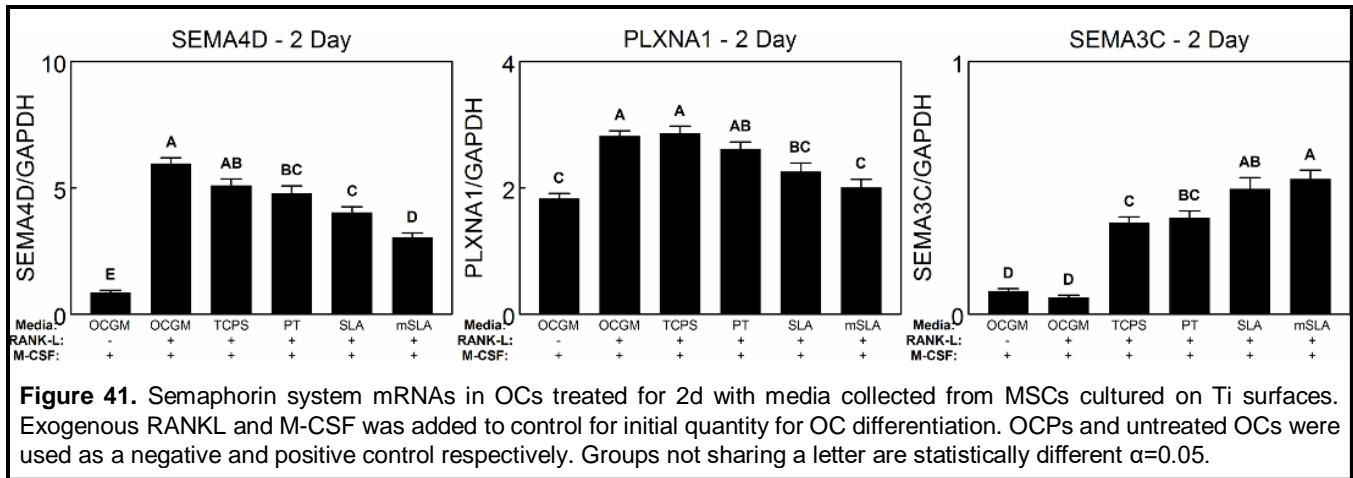
By investigating the extent to which microstructured Ti surfaces modulate the dynamic interplay of multiple cell types, we are innovating the redundancy of contemporary biomaterial surface research. Using a newly developed system that exploits the OsteoLyse Assay Kit, we



have shown that microstructured Ti surfaces indirectly regulate OC activity and gene expression. After surface recognition by integrins, MSC and NHOst protein production is modulated and responsible for the decreased activity of existing OCs and reduced fusion of new OCs. In addition, OC gene expression is selectively regulated suggesting more than one pathway of control may be involved. Of the proteins responsible, the classic coupling mediators, TGF β and OPG, do not contribute to the surface dependent regulation *in vitro*. Efforts should now continue exploring alternative mechanisms capable of regulating bone remodeling.

Two other systems have been identified as important regulators of bone remodeling: 1) Eph/Ephrins and 2) Semaphorins. These two systems aid bone homeostasis and offer an intriguing mechanism for a reciprocal communication of the cell types involved. We have demonstrated that components of these signaling systems are modulated by microstructured Ti surfaces (**Fig.39**). Our research shows mRNAs for EPHB2 and SEMA3A increase on modSLA.

Expression of the SEMA3A receptor, NRP1, is increased on SLA and modSLA. In contrast,



EPHB3, EFNB2, and SEMA3C expression in MSCs decreases in a surface-dependent manner. Addition of exogenous SEMA3A to surface cultured MSCs stimulates their osteoblastic differentiation while addition of a SEMA3A neutralizing antibody slows their osteoblastic differentiation (**Fig.41**). Moreover, conditioned media from MSC cultures stimulates SEMA3C expression in OCs and decreases expression of SEMA4D and PLXNA1 (**Fig.41**). SEMA4D produced by OCs can bind to PLXNB1 on the OB surface to decrease bone formation. Currently, SEMA3C has no known role in regulating bone homeostasis in TCPS culture. Our results suggest that surface-dependent modulation of MSCs and their downstream modulation of osteoclastic activity involve important, novel roles for semaphorin family proteins. Future research should focus on expanding the role semaphorins play in modulating bone remodeling *in vitro* as well as *in vivo*.

A thorough understanding of how cells interact with the physical features of their environments has led to the development of implants that are both biocompatible and bioactive. By targeting the surface of the substrate, major enhancements in the performance of dental and orthopaedic implants have been achieved. Implant surface features are now designed to mimic the inherent surface roughness, surface chemistry, and surface hydrophilicity of native bone. Furthermore, methods to recreate the complex hierarchical features of an osteoclast resorption pit are now widely used to induce combinations of macroscale, microscale, mesoscale, and nanoscale topography. Thus, by mimicking the surface structure present on native bone tissue,

contemporary dental and orthopaedic implants can be designed to achieve rapid and optimal osseointegration. As research into these areas progresses, the future of implantology could see patient-specific implant designs that modulate different pathways, promoting healthy bone formation despite health issues the patient may present.

Vita

Ethan Major Lotz was born on February 4, 1989, in Ocean Springs, Mississippi, and is an American citizen. He graduated from Ocean Springs High School in 2007. He received his Bachelor of Science in Biomedical Engineering from Georgia Institute of Technology, Atlanta, Georgia in 2011. He received a Doctor of Philosophy in Biomedical Engineering from Virginia Commonwealth University, Richmond, Virginia in 2019. As part of his degree, he worked for Institut Straumann AG in Basel, Switzerland between April 2012 and November 2012.

References

- 1 U.S. Department of Health and Human Services, US Department of Health and Human Services. Bone health and osteoporosis: a report of the Surgeon General. *US Heal Hum Serv* 2004;437. <https://doi.org/10.2165/00002018-200932030-00004>.
- 2 Douglass CW, Shih A, Ostry L. Will there be a need for complete dentures in the United States in 2020? *J Prosthet Dent* 2002. <https://doi.org/10.1067/mpr.2002.121203>.
- 3 Papaspyridakos P, Chen C-J, Chuang S-K, Weber H-P, Gallucci GO. A systematic review of biologic and technical complications with fixed implant rehabilitations for edentulous patients. *Int J Oral Maxillofac Implants* 2012.
- 4 Wright NC, Looker AC, Saag KG, Curtis JR, Delzell ES, Randall S, *et al*. The recent prevalence of osteoporosis and low bone mass in the United States based on bone mineral density at the femoral neck or lumbar spine. *J Bone Miner Res* 2014;**29**:2520–6. <https://doi.org/10.1002/jbmr.2269>.
- 5 Brånemark PI, Hansson BO, Adell R, Breine U, Lindström J, Hallén O, *et al*. Osseointegrated implants in the treatment of the edentulous jaw. Experience from a 10-year period. *Scand J Plast Reconstr Surg Suppl* 1977;**16**:1–196. <https://doi.org/10.1007/s11064-007-9532-5>.
- 6 Lang BR, Chiappa AA. Mandibular implants: A new method of attachment. *J Prosthet Dent* 1969;**22**:261–7. [https://doi.org/10.1016/0022-3913\(69\)90255-8](https://doi.org/10.1016/0022-3913(69)90255-8).
- 7 Triplett RG, Frohberg U, Sykaras N, Woody RD. Implant Materials, Design, and Surface Topographies: Their Influence on Osseointegration of Dental Implants. *J Long Term Eff Med Implants* 2003;**13**:18. <https://doi.org/10.1615/jlongtermeffmedimplants.v13.i6.50>.
- 8 Bencharit S, Allen RK, Whitley D. Utilization of Demineralized Bone Matrix to Restore Missing Buccal Bone During Single Implant Placement: Clinical Report. *J Oral Implantol* 2016;**42**:490–7. <https://doi.org/10.1563/aaid-joi-d-16-00054>.

- 9 Irinakis T. Efficacy of Injectable Demineralized Bone Matrix as Graft Material During Sinus Elevation Surgery With Simultaneous Implant Placement in the Posterior Maxilla: Clinical Evaluation of 49 Sinuses. *J Oral Maxillofac Surg* 2011;**69**:134–41. <https://doi.org/10.1016/j.joms.2010.07.028>.
- 10 Bishop GB, Einhorn TA. Current and future clinical applications of bone morphogenetic proteins in orthopaedic trauma surgery. *Int Orthop* 2007;**31**:721–7. <https://doi.org/10.1007/s00264-007-0424-8>.
- 11 Wan M, Cao X. BMP signaling in skeletal development. *Biochem Biophys Res Commun* 2005;**328**:651–7. <https://doi.org/10.1016/j.bbrc.2004.11.067>.
- 12 Bae J-H, Kim Y-K, Myung S-K. Effects of Platelet-Rich Plasma on Sinus Bone Graft: Meta-Analysis. *J Periodontol* 2011;**82**:660–7. <https://doi.org/10.1902/jop.2010.100529>.
- 13 Butterfield KJ, Bennett J, Gronowicz G, Adams D. Effect of platelet-rich plasma with autogenous bone graft for maxillary sinus augmentation in a rabbit model. *J Oral Maxillofac Surg* 2005;**63**:370–6. <https://doi.org/10.1016/j.joms.2004.07.017>.
- 14 Pocaterra A, Caruso S, Bernardi S, Scagnoli L, Continenza MA, Gatto R. Effectiveness of platelet-rich plasma as an adjunctive material to bone graft: a systematic review and meta-analysis of randomized controlled clinical trials. *Int J Oral Maxillofac Surg* 2016;**45**:1027–34. <https://doi.org/10.1016/j.ijom.2016.02.012>.
- 15 DiGiovanni CW, Lin SS, Baumhauer JF, Daniels T, Younger A, Glazebrook M, *et al*. Recombinant Human Platelet-Derived Growth Factor-BB and Beta-Tricalcium Phosphate (rhPDGF-BB/ β -TCP): An Alternative to Autogenous Bone Graft. *J Bone Jt Surgery-American Vol* 2013;**95**:1184–92. <https://doi.org/10.2106/jbjs.k.01422>.
- 16 Nevins M, Nevins ML, Karimbux N, Kim S-W, Schupbach P, Kim DM. The Combination of Purified Recombinant Human Platelet-Derived Growth Factor-BB and Equine Particulate Bone Graft for Periodontal Regeneration. *J Periodontol* 2012;**83**:565–73.

<https://doi.org/10.1902/jop.2011.110298>.

- 17 DEVI R. Clinical Evaluation of Insulin like Growth Factor-I and Vascular Endothelial Growth Factor with Alloplastic Bone Graft Material in the Management of Human Two Wall Intra-Osseous Defects. *J Clin DIAGNOSTIC Res* 2016.
<https://doi.org/10.7860/jcdr/2016/21333.8476>.
- 18 Ueno T, Mizukawa N, Sugahara T. Experimental study of bone formation from autogenous periosteal graft following insulin-like growth factor I administration. *J Cranio-Maxillofacial Surg* 1999;**27**:308–13. <https://doi.org/10.1054/jcms.1999.0077>.
- 19 Rabie ABM, Lu M. Basic fibroblast growth factor up-regulates the expression of vascular endothelial growth factor during healing of allogeneic bone graft. *Arch Oral Biol* 2004;**49**:1025–33. <https://doi.org/10.1016/j.archoralbio.2004.05.012>.
- 20 Alam S, Ueki K, Marukawa K, Ohara T, Hase T, Takazakura D, *et al*. Expression of bone morphogenetic protein 2 and fibroblast growth factor 2 during bone regeneration using different implant materials as an onlay bone graft in rabbit mandibles. *Oral Surgery, Oral Med Oral Pathol Oral Radiol Endodontology* 2007;**103**:16–26.
<https://doi.org/10.1016/j.tripleo.2006.01.019>.
- 21 Nakasa T, Ishida O, Sunagawa T, Nakamae A, Yasunaga Y, Agung M, *et al*. Prefabrication of vascularized bone graft using a combination of fibroblast growth factor-2 and vascular bundle implantation into a novel interconnected porous calcium hydroxyapatite ceramic. *J Biomed Mater Res Part A* 2005;**75A**:350–5.
<https://doi.org/10.1002/jbm.a.30435>.
- 22 Lotz EMM, Olivares-Navarrete R, Berner S, Boyan BDD, Schwartz Z. Osteogenic response of human MSCs and osteoblasts to hydrophilic and hydrophobic nanostructured titanium implant surfaces. *J Biomed Mater Res A* 2016;**104**:3137–48.
<https://doi.org/10.1002/jbm.a.35852>.

- 23 Zhao G, Schwartz Z, Wieland M, Rupp F, Geis-Gerstorfer J, Cochran DL, *et al.* High surface energy enhances cell response to titanium substrate microstructure. *J Biomed Mater Res Part A* 2005;**74A**:49–58. <https://doi.org/10.1002/jbm.a.30320>.
- 24 Minkin C, Jennings JM. Carbonic Anhydrase and Bone Remodeling: Sulfonamide Inhibition of Bone Resorption in Organ Culture. *Science (80-)* 1972;**176**:1031–3. <https://doi.org/10.1126/science.176.4038.1031>.
- 25 Baron R. Cell-mediated extracellular acidification and bone resorption: evidence for a low pH in resorbing lacunae and localization of a 100-kD lysosomal membrane protein at the osteoclast ruffled border. *J Cell Biol* 1985;**101**:2210–22. <https://doi.org/10.1083/jcb.101.6.2210>.
- 26 Everts V, Korper W, Hoeben KA, Jansen IDC, Bromme D, Cleutjens KBJM, *et al.* Osteoclastic bone degradation and the role of different cysteine proteinases and matrix metalloproteinases: Differences between calvaria and long bone. *J Bone Miner Res* 2006;**21**:1399–408. <https://doi.org/10.1359/jbmr.060614>.
- 27 Sakamoto S, Sakamoto M. Biochemical and immunohistochemical studies on collagenase in resorbing bone in tissue culture: A novel hypothesis for the mechanism of bone resorption. *J Periodontal Res* 1982;**17**:523–6. <https://doi.org/10.1111/j.1600-0765.1982.tb02046.x>.
- 28 Puzas JE, Lewis G, Hsu J, Reynolds PR, Rosier RN, OKeefe RJ, *et al.* Osteoblasts preferentially adhere to sites of prior bone resorption. *J Bone Miner Res* 1997;**12**..
- 29 Gittens RA, Olivares-Navarrete R, Schwartz Z, Boyan BD. Implant osseointegration and the role of microroughness and nanostructures: Lessons for spine implants. *Acta Biomater* 2014;**10**:3363–71. <https://doi.org/10.1016/j.actbio.2014.03.037>.
- 30 Zinger O, Zhao G, Schwartz Z, Simpson J, Wieland M, Landolt D, *et al.* Differential regulation of osteoblasts by substrate microstructural features. *Biomaterials*

- 2005;**26**:1837–47. <https://doi.org/10.1016/j.biomaterials.2004.06.035>.
- 31 Zhao G, Zinger O, Schwartz Z, Wieland M, Landolt D, Boyan BD. Osteoblast-like cells are sensitive to submicron-scale surface structure. *Clin Oral Implants Res* 2006;**17**:258–64. <https://doi.org/10.1111/j.1600-0501.2005.01195.x>.
- 32 Teitelbaum SL. Bone resorption by osteoclasts. *Science (80-)* 2000:1504–8. <https://doi.org/10.1126/science.289.5484.1504>.
- 33 Chambers TJ, Revell PA, Fuller K, Athanasou NA. Resorption of bone by isolated rabbit osteoclasts. *Metab Bone Dis Relat Res* 2004. [https://doi.org/10.1016/0221-8747\(84\)90057-2](https://doi.org/10.1016/0221-8747(84)90057-2).
- 34 Arnett TR. Extracellular pH regulates bone cell function. *J Nutr* 2008. <https://doi.org/10.1093/jn/138.2.415S>.
- 35 Bernhard N, Berner S, de Wild M, Wieland M. The binary TiZr Alloy - a newly developed Ti alloy for use in dental implants. *Forum Implant* 2009:30–9.
- 36 Mohammadi S, Wictorin L, Ericson LE, Thomsen P. Cast titanium as implant material. *J Mater Sci Mater Med* 1995;**6**:435–44. <https://doi.org/10.1007/bf00123367>.
- 37 Olefjord I, Hansson S. Surface analysis of four dental implant systems. *Int J Oral Maxillofac Implants* 1993.
- 38 Wennerberg A, Albrektsson T, Andersson B. Design and surface characteristics of 13 commercially available oral implant systems. *Int J Oral Maxillofac Implant* 1993.
- 39 Sing SL, An J, Yeong WY, Wiria FE. Laser and electron-beam powder-bed additive manufacturing of metallic implants: A review on processes, materials and designs. *J Orthop Res* 2015;**34**:369–85. <https://doi.org/10.1002/jor.23075>.
- 40 Brunette DM. Spreading and orientation of epithelial cells on grooved substrata. *Exp Cell Res* 1986;**167**:203–17. [https://doi.org/10.1016/0014-4827\(86\)90217-x](https://doi.org/10.1016/0014-4827(86)90217-x).
- 41 Chehroudi B, Gould TRL, Brunette DM. Effects of a grooved titanium-coated implant

- surface on epithelial cell behavior in vitro and in vivo. *J Biomed Mater Res* 1989. <https://doi.org/10.1002/jbm.820230907>.
- 42 Chehroudi B, Gould TRL, Brunette DM. Titanium-coated micromachined grooves of different dimensions affect epithelial and connective-tissue cells differently in vivo. *J Biomed Mater Res* 1990;**24**:1203–19. <https://doi.org/10.1002/jbm.820240906>.
- 43 Cochran DL, Nummikoski P V., Higginbottom FL, Hermann JS, Makins SR, Buser D. Evaluation of an endosseous titanium implant with a sandblasted and acid-etched surface in the canine mandible: radiographic results. *Clin Oral Implants Res* 1996;**7**:240–52. <https://doi.org/10.1034/j.1600-0501.1996.070306.x>.
- 44 Thomas KA, Cook SD. An evaluation of variables influencing implant fixation by direct bone apposition. *J Biomed Mater Res* 1985;**19**:875–901. <https://doi.org/10.1002/jbm.820190802>.
- 45 Webster TJ, Ergun C, Doremus RH, Siegel RW, Bizios R. Specific proteins mediate enhanced osteoblast adhesion on nanophase ceramics. *J Biomed Mater Res* 2000;**51**:475–83. [https://doi.org/10.1002/1097-4636\(20000905\)51:3<475::aid-jbm23>3.0.co;2-9](https://doi.org/10.1002/1097-4636(20000905)51:3<475::aid-jbm23>3.0.co;2-9).
- 46 Webster T. Enhanced functions of osteoblasts on nanophase ceramics. *Biomaterials* 2000;**21**:1803–10. [https://doi.org/10.1016/s0142-9612\(00\)00075-2](https://doi.org/10.1016/s0142-9612(00)00075-2).
- 47 Webster TJ, Siegel RW, Bizios R. Nanoceramic surface roughness enhances osteoblast and osteoclast functions for improved orthopaedic/dental implant efficacy. *Scr Mater* 2001;**44**:1639–42. [https://doi.org/10.1016/s1359-6462\(01\)00873-9](https://doi.org/10.1016/s1359-6462(01)00873-9).
- 48 Webster TJ, Siegel RW, Bizios R. Osteoblast adhesion on nanophase ceramics. *Biomaterials* 1999;**20**:1221–7. [https://doi.org/10.1016/s0142-9612\(99\)00020-4](https://doi.org/10.1016/s0142-9612(99)00020-4).
- 49 Fung YC, Cowin SC. Biomechanics: Mechanical Properties of Living Tissues, 2nd ed. *J Appl Mech* 1994;**61**:1007. <https://doi.org/10.1115/1.2901550>.

- 50 Jimbo R, Xue Y, Hayashi M, Schwartz-Filho HO, Andersson M, Mustafa K, *et al.* Genetic Responses to Nanostructured Calcium-phosphate-coated Implants. *J Dent Res* 2011;**90**:1422–7. <https://doi.org/10.1177/0022034511422911>.
- 51 Gittens RA, Olivares-Navarrete R, McLachlan T, Cai Y, Hyzy SL, Schneider JM, *et al.* Differential responses of osteoblast lineage cells to nanotopographically-modified, microroughened titanium-aluminum-vanadium alloy surfaces. *Biomaterials* 2012;**33**:8986–94. <https://doi.org/10.1016/j.biomaterials.2012.08.059>.
- 52 Wennerberg A, Svanborg LM, Berner S, Andersson M. Spontaneously formed nanostructures on titanium surfaces. *Clin Oral Implants Res* 2012;**24**:203–9. <https://doi.org/10.1111/j.1600-0501.2012.02429.x>.
- 53 Lotz EMM, Olivares-Navarrete R, Hyzy SLSLSL, Berner S, Schwartz Z, Boyan BDBDD. Comparable responses of osteoblast lineage cells to microstructured hydrophilic titanium-zirconium and microstructured hydrophilic titanium. *Clin Oral Implant Res* 2017;**28**:e51–9. <https://doi.org/10.1111/clr.12855>.
- 54 Dalby MJ, Gadegaard N, Tare R, Andar A, Riehle MO, Herzyk P, *et al.* The control of human mesenchymal cell differentiation using nanoscale symmetry and disorder. *Nat Mater* 2007;**6**:997–1003. <https://doi.org/10.1038/nmat2013>.
- 55 Gittens RARA, Scheideler L, Rupp F, Hyzy SLSLSL, Geis-Gerstorfer J, Schwartz Z, *et al.* A review on the wettability of dental implant surfaces II: Biological and clinical aspects. *Acta Biomater* 2014;**10**:2907–18. <https://doi.org/10.1016/j.actbio.2014.03.032>.
- 56 Bornstein MM, Valderrama P, Jones AA, Wilson TG, Seibl R, Cochran DL. Bone apposition around two different sandblasted and acid-etched titanium implant surfaces: a histomorphometric study in canine mandibles. *Clin Oral Implants Res* 2008;**19**:233–41. <https://doi.org/10.1111/j.1600-0501.2007.01473.x>.
- 57 Eriksson C, Nygren H, Ohlson K. Implantation of hydrophilic and hydrophobic titanium

- discs in rat tibia: cellular reactions on the surfaces during the first 3 weeks in bone. *Biomaterials* 2004;**25**:4759–66. <https://doi.org/10.1016/j.biomaterials.2003.12.006>.
- 58 Huang Q, Lin L, Yang Y, Hu R, Vogler EA, Lin C. Role of trapped air in the formation of cell-and-protein micropatterns on superhydrophobic/superhydrophilic microtemplated surfaces. *Biomaterials* 2012;**33**:8213–20. <https://doi.org/10.1016/j.biomaterials.2012.08.017>.
- 59 Jimbo R, Sawase T, Baba K, Kurogi T, Shibata Y, Atsuta M. Enhanced Initial Cell Responses to Chemically Modified Anodized Titanium. *Clin Implant Dent Relat Res* 2008;**10**:55–61. <https://doi.org/10.1111/j.1708-8208.2007.00061.x>.
- 60 Sawase T, Jimbo R, Baba K, Shibata Y, Ikeda T, Atsuta M. Photo-induced hydrophilicity enhances initial cell behavior and early bone apposition. *Clin Oral Implants Res* 2008;**19**:491–6. <https://doi.org/10.1111/j.1600-0501.2007.01509.x>.
- 61 Olivares-Navarrete R, Hyzy SL, Hutton DL, Erdman CP, Wieland M, Boyan BD, *et al.* Direct and indirect effects of microstructured titanium substrates on the induction of mesenchymal stem cell differentiation towards the osteoblast lineage. *Biomaterials* 2010;**31**:2728–35. <https://doi.org/10.1016/j.biomaterials.2009.12.029>.
- 62 Wilson CJ, Clegg RE, Leavesley DI, Percy MJ. Mediation of Biomaterial–Cell Interactions by Adsorbed Proteins: A Review. *Tissue Eng* 2005;**11**:1–18. <https://doi.org/10.1089/ten.2005.11.1>.
- 63 Wennerberg A, Galli S, Albrektsson T. Current knowledge about the hydrophilic and nanostructured SLActive surface. *Clin Cosmet Investig Dent* 2011:59–67.
- 64 Olivares-Navarrete R, Hyzy SL, Boyan BD, Schwartz Z. Regulation of osteoblast differentiation by acid-etched and/or grit-blasted titanium substrate topography is enhanced by 1,25(OH)₂D₃ in a Sex-Dependent Manner. *Biomed Res Int* 2015. <https://doi.org/10.1155/2015/365014>.

- 65 Braun G, Kohavi D, Amir D, Luna M, Caloss R, Sela J, *et al.* Markers of primary mineralization are correlated with bone-bonding ability of titanium or stainless steel in vivo. *Clin Oral Implants Res* 1995;**6**:1–13. <https://doi.org/10.1034/j.1600-0501.1995.060101.x>.
- 66 Stoumboudi MT, Schwartz Z, Sela J, Goldstein D, Yaffe P, Boyan BD, *et al.* Effect of 17-beta-estradiol on the healing of tibial bone after marrow ablation. *Cells Tissues Organs* 1995. <https://doi.org/10.1159/000147689>.
- 67 Day TF, Guo X, Garrett-Beal L, Yang Y. Wnt/ β -Catenin Signaling in Mesenchymal Progenitors Controls Osteoblast and Chondrocyte Differentiation during Vertebrate Skeletogenesis. *Dev Cell* 2005;**8**:739–50. <https://doi.org/10.1016/j.devcel.2005.03.016>.
- 68 Hill TP, Später D, Taketo MM, Birchmeier W, Hartmann C. Canonical Wnt/ β -catenin signaling prevents osteoblasts from differentiating into chondrocytes. *Dev Cell* 2005;**8**:727–38. <https://doi.org/10.1016/j.devcel.2005.02.013>.
- 69 Rodda SJ. Distinct roles for Hedgehog and canonical Wnt signaling in specification, differentiation and maintenance of osteoblast progenitors. *Development* 2006;**133**:3231–44. <https://doi.org/10.1242/dev.02480>.
- 70 Olivares-Navarrete R, Hyzy SL, Hutton DL, Dunn GR, Appert C, Boyan BD, *et al.* Role of non-canonical Wnt signaling in osteoblast maturation on microstructured titanium surfaces. *Acta Biomater* 2011;**7**:2740–50. <https://doi.org/10.1016/j.actbio.2011.02.030>.
- 71 Olivares-Navarrete R, Hyzy SL, Park JH, Dunn GR, Haithcock DA, Wasilewski CE, *et al.* Mediation of osteogenic differentiation of human mesenchymal stem cells on titanium surfaces by a Wnt-integrin feedback loop. *Biomaterials* 2011;**32**:6399–411. <https://doi.org/10.1016/j.biomaterials.2011.05.036>.
- 72 Boyan BD, Olivares-Navarrete R, Berger MB, Hyzy SL, Schwartz Z. Role of Wnt11 during Osteogenic Differentiation of Human Mesenchymal Stem Cells on Microstructured

- Titanium Surfaces. *Sci Rep* 2018. <https://doi.org/10.1038/s41598-018-26901-8>.
- 73 Dwyer MA, Joseph JD, Wade HE, Eaton ML, Kunder RS, Kazmin D, *et al.* WNT11 expression is induced by estrogen-related receptor α and β -catenin and acts in an autocrine manner to increase cancer cell migration. *Cancer Res* 2010;**70**:9298–308. <https://doi.org/10.1158/0008-5472.CAN-10-0226>.
- 74 Olivares-Navarrete R, Hyzy SL, Chaudhri RA, Zhao G, Boyan BD, Schwartz Z. Sex dependent regulation of osteoblast response to implant surface properties by systemic hormones. *Biol Sex Differ* 2010. <https://doi.org/10.1186/2042-6410-1-4>.
- 75 Lohmann CH, Tandy EM, Sylvia VL, Hell-Vocke AK, Cochran DL, Dean DD, *et al.* Response of normal female human osteoblasts (NHOst) to 17beta-estradiol is modulated by implant surface morphology. *J Biomed Mater Res* 2002;**62**:204–13. <https://doi.org/10.1002/jbm.10290>.
- 76 Boyan BDB, Lossdörfer S, Wang L, Zhao G, Lohmann CH, Cochran DLD, *et al.* Osteoblasts generate an osteogenic microenvironment when grown on surfaces with rough microtopographies. *Eur Cells Mater* 2003;**6**:22–7. <https://doi.org/10.22203/eCM.v006a03>.
- 77 Torricelli P, Fini M, Giavaresi G, Giardino R. Human osteoblast cultures from osteoporotic and healthy bone: Biochemical markers and cytokine expression in basal conditions and in response to 1,25(OH)₂D₃. *Artif Cells Blood Substit Immobil Biotechnol* 2002;**30**:219–27. <https://doi.org/10.1081/BIO-120004341>.
- 78 Cao J, Venton L, Sakata T, Halloran BP. Expression of RANKL and OPG correlates with age-related bone loss in male C57BL/6 mice. *J Bone Min Res* 2003;**18**:270–7. <https://doi.org/10.1359/jbmr.2003.18.2.270>.
- 79 Cao JJ, Wronski TJ, Iwaniec U, Phleger L, Kurimoto P, Boudignon B, *et al.* Aging increases stromal/osteoblastic cell-induced osteoclastogenesis and alters the osteoclast

precursor pool in the mouse. *J Bone Min Res* 2005;**20**:1659–68.

<https://doi.org/10.1359/JBMR.050503>.

- 80 Schwartz Z, Olivares-Navarrete R, Wieland M, Cochran DL, Boyan BD. Mechanisms regulating increased production of osteoprotegerin by osteoblasts cultured on microstructured titanium surfaces. *Biomaterials* 2009;**30**:3390–6.
<https://doi.org/10.1016/j.biomaterials.2009.03.047>.
- 81 Kurebayashi S, Miyashita Y, Hirose T, Kasayama S, Akira S, Kishimoto T. Characterization of mechanisms of interleukin-6 gene repression by estrogen receptor. *J Steroid Biochem Mol Biol* 1997;**60**:11–7. [https://doi.org/10.1016/S0960-0760\(96\)00175-6](https://doi.org/10.1016/S0960-0760(96)00175-6).
- 82 Kieswetter K, Schwartz Z, Hummert TW, Cochran DL, Simpson J, Dean DD, *et al*. Surface roughness modulates the local production of growth factors and cytokines by osteoblast-like MG-63 cells. *J Biomed Mater Res* 1996;**32**:55–63. [https://doi.org/10.1002/\(Sici\)1097-4636\(199609\)32:1<55::Aid-Jbm7>3.0.Co;2-O](https://doi.org/10.1002/(Sici)1097-4636(199609)32:1<55::Aid-Jbm7>3.0.Co;2-O).
- 83 Boyce BF, Xing L. The RANKL/RANK/OPG pathway. *Curr Osteoporos Rep* 2007:98–104. <https://doi.org/10.1007/s11914-007-0024-y>.
- 84 Lohmann CH, Sagun Jr. R, Sylvia VL, Cochran DL, Dean DD, Boyan BD, *et al*. Surface roughness modulates the response of MG63 osteoblast-like cells to 1,25-(OH)(2)D(3) through regulation of phospholipase A(2) activity and activation of protein kinase A. *J Biomed Mater Res* 1999;**47**:139–51.
- 85 Lotz EM, Cohen DJ, Ellis RA, Wayne JS, Schwartz Z, Boyan BD. Ibandronate Treatment Before and After Implant Insertion Impairs Osseointegration in Aged Rats with Ovariectomy Induced Osteoporosis. *JBMR Plus* 2019;**xx**:e10184.
<https://doi.org/10.1002/jbm4.10184>.

- 86 Glowacki J, Rey C, Glimcher MJ, Cox KA, Lian J. A role for osteocalcin in osteoclast

- differentiation. *J Cell Biochem* 1991;**45**:292–302. <https://doi.org/10.1002/jcb.240450312>.
- 87 Ritter NM, Farach-Carson MC, Butler WT, Farach-Carson MC, Butler WT. Evidence for the formation of a complex between osteopontin and osteocalcin. *J Bone Miner Res* 2009;**7**:877–85. <https://doi.org/10.1002/jbmr.5650070804>.
- 88 Reinholt FP, Hultenby K, Oldberg A, Heinegard D. Osteopontin--a possible anchor of osteoclasts to bone. *Proc Natl Acad Sci* 1990;**87**:4473–5. <https://doi.org/10.1073/pnas.87.12.4473>.
- 89 Lohmann CH, Dean DD, Bonewald LF, Schwartz Z, Boyan BD. Nitric oxide and prostaglandin E2 production in response to ultra-high molecular weight polyethylene particles depends on osteoblast maturation state. *J Bone Jt Surg - Ser A* 2002. <https://doi.org/10.2106/00004623-200203000-00012>.
- 90 Soskolne WA, Cohen S, Shapira L, Sennerby L, Wennerberg A. The effect of titanium surface roughness on the adhesion of monocytes and their secretion of TNF-alpha and PGE2. *Clin Oral Implants Res* 2002;**13**:86–93. <https://doi.org/10.1034/j.1600-0501.2002.130111.x>.
- 91 Boyan BD, Lohmann CH, Sisk M, Liu Y, Sylvia VL, Cochran DL, *et al.* Both cyclooxygenase-1 and cyclooxygenase-2 mediate osteoblast response to titanium surface roughness. *J Biomed Mater Res* 2001;**55**:350–9. [https://doi.org/10.1002/1097-4636\(20010605\)55:3<350::aid-jbm1023>3.0.co;2-m](https://doi.org/10.1002/1097-4636(20010605)55:3<350::aid-jbm1023>3.0.co;2-m).
- 92 Sisk MA, Lohmann CH, Cochran DL, Sylvia VL, Simpson JP, Dean DD, *et al.* Inhibition of cyclooxygenase by indomethacin modulates osteoblast response to titanium surface roughness in a time-dependent manner. *Clin Oral Implant Res* 2001;**12**:52–61.
- 93 Olivares-Navarrete R, Hyzy SL, Haithcock DA, Cundiff CA, Schwartz Z, Boyan BD. Coordinated regulation of mesenchymal stem cell differentiation on microstructured titanium surfaces by endogenous bone morphogenetic proteins. *Bone* 2015;**73**:208–16.

<https://doi.org/10.1016/j.bone.2014.12.057>.

- 94 Hyzy SL, Olivares-Navarrete R, Schwartz Z, Boyan BD. BMP2 induces osteoblast apoptosis in a maturation state and noggin-dependent manner. *J Cell Biochem* 2012;**113**:3236–45. <https://doi.org/10.1002/jcb.24201>.
- 95 Wall A, Board T. Bone morphogenetic protein. *Class Pap Orthop* 2014;**362**:465–7. https://doi.org/10.1007/978-1-4471-5451-8_118.
- 96 Gilboa L, Nohe A, Geissendorfer T, Sebald W, Henis YI, Knaus P. Bone Morphogenetic Protein Receptor Complexes on the Surface of Live Cells: A New Oligomerization Mode for Serine/Threonine Kinase Receptors. *Mol Biol Cell* 2013;**11**:1023–35. <https://doi.org/10.1091/mbc.11.3.1023>.
- 97 Van Battum EY, Brignani S, Pasterkamp RJ. Axon guidance proteins in neurological disorders. *Lancet Neurol* 2015. [https://doi.org/10.1016/S1474-4422\(14\)70257-1](https://doi.org/10.1016/S1474-4422(14)70257-1).
- 98 Arese M, Serini G, Bussolino F. Nervous vascular parallels: Axon guidance and beyond. *Int J Dev Biol* 2011. <https://doi.org/10.1387/ijdb.103242ma>.
- 99 Suzuki K, Kumanogoh A, Kikutani H. Semaphorins and their receptors in immune cell interactions. *Nat Immunol* 2008. <https://doi.org/10.1038/ni1553>.
- 100 Pasquale EB. Eph receptor signalling casts a wide net on cell behaviour. *Nat Rev Mol Cell Biol* 2005;**6**:462–75. <https://doi.org/10.1038/nrm1662>.
- 101 Castellani V, Rougon G. Control of semaphorin signaling. *Curr Opin Neurobiol* 2002. [https://doi.org/10.1016/S0959-4388\(02\)00357-4](https://doi.org/10.1016/S0959-4388(02)00357-4).
- 102 Epstein JA, Aghajanian H, Singh MK. Semaphorin signaling in cardiovascular development. *Cell Metab* 2015. <https://doi.org/10.1016/j.cmet.2014.12.015>.
- 103 Jongbloets BC, Pasterkamp RJ. Semaphorin signalling during development. *Development* 2014;**141**:3292–7. <https://doi.org/10.1242/dev.105544>.
- 104 Takamatsu H, Okuno T, Kumanogoh A. Regulation of immune cell responses by

- semaphorins and their receptors. *Cell Mol Immunol* 2010.
<https://doi.org/10.1038/cmi.2009.111>.
- 105 Pasquale EB. Eph-Ephrin Bidirectional Signaling in Physiology and Disease. *Cell* 2008;**133**:38–52. <https://doi.org/10.1016/j.cell.2008.03.011>.
- 106 Zhao C, Irie N, Takada Y, Shimoda K, Miyamoto T, Nishiwaki T, *et al*. Bidirectional ephrinB2-EphB4 signaling controls bone homeostasis. *Cell Metab* 2006;**4**:111–21.
<https://doi.org/10.1016/j.cmet.2006.05.012>.
- 107 Nguyen TM, Arthur A, Hayball JD, Gronthos S. EphB and Ephrin-B Interactions Mediate Human Mesenchymal Stem Cell Suppression of Activated T-Cells. *Stem Cells Dev* 2013;**22**:2751–64. <https://doi.org/10.1089/scd.2012.0676>.
- 108 Arthur A, Zannettino A, Panagopoulos R, Koblar SA, Sims NA, Stylianou C, *et al*. EphB/ephrin-B interactions mediate human MSC attachment, migration and osteochondral differentiation. *Bone* 2011;**48**:533–42.
<https://doi.org/10.1016/j.bone.2010.10.180>.
- 109 Allan EH, Häusler KD, Wei T, Gooi JH, Quinn JMW, Crimeen-Irwin B, *et al*. EphrinB2 regulation by PTH and PTHrP revealed by molecular profiling in differentiating osteoblasts. *J Bone Miner Res* 2008;**23**:1170–81. <https://doi.org/10.1359/jbmr.080324>.
- 110 Verlinden L, Vanderschueren D, Verstuyf A. Semaphorin signaling in bone. *Mol Cell Endocrinol* 2016;**432**:66–74. <https://doi.org/10.1016/j.mce.2015.09.009>.
- 111 Dacquin R, Domenget C, Kumanogoh A, Kikutani H, Jurdic P, Machuca-Gayet I. Control of bone resorption by semaphorin 4D is dependent on ovarian function. *PLoS One* 2011.
<https://doi.org/10.1371/journal.pone.0026627>.
- 112 Negishi-Koga T, Shinohara M, Komatsu N, Bito H, Kodama T, Friedel RH, *et al*. Suppression of bone formation by osteoclastic expression of semaphorin 4D. *Nat Med* 2011;**17**:1473–80. <https://doi.org/10.1038/nm.2489>.

- 113 Zhang Y, Liu B, Ma Y, Jin B. Sema 4D/CD100-plexin B is a multifunctional counter-receptor. *Cell Mol Immunol* 2013. <https://doi.org/10.1038/cmi.2012.65>.
- 114 Zhang Y, Wei L, Miron RJ, Shi B, Bian Z. Anabolic bone formation via a site-specific bone-targeting delivery system by interfering with semaphorin 4d expression. *J Bone Miner Res* 2015;**30**:286–96. <https://doi.org/10.1002/jbmr.2322>.
- 115 Gomez C, Burt-Pichat B, Mallein-Gerin F, Merle B, Delmas PD, Skerry TM, *et al*. Expression of Semaphorin-3A and its receptors in endochondral ossification: Potential role in skeletal development and innervation. *Dev Dyn* 2005;**234**:393–403. <https://doi.org/10.1002/dvdy.20512>.
- 116 Hayashi M, Nakashima T, Taniguchi M, Kodama T, Kumanogoh A, Takayanagi H. Osteoprotection by semaphorin 3A. *Nature* 2012;**485**:69–74. <https://doi.org/10.1038/nature11000>.
- 117 Liu F, Shen W, Qiu H, Hu X, Zhang C, Chu T. Prostate cancer cells induce osteoblastic differentiation via semaphorin 3A. *Prostate* 2015. <https://doi.org/10.1002/pros.22923>.
- 118 Shen WW, Chen WG, Liu FZ, Hu X, Wang HK, Zhang Y, *et al*. Breast cancer cells promote osteoblastic differentiation via Sema 3A signaling pathway in vitro. *Int J Clin Exp Pathol* 2015.
- 119 Liu DM, Lu N, Zhao L, Zhang MJ, Tao B, Xuan Y, *et al*. Serum Sema3A is in a weak positive association with bone formation marker osteocalcin but not related to bone mineral densities in postmenopausal women. *J Clin Endocrinol Metab* 2014. <https://doi.org/10.1210/jc.2014-1443>.
- 120 Oshida Y, Tuna EB, Aktören O, Gençay K. Dental implant systems. *Int J Mol Sci* 2010;**11**:1580–678. <https://doi.org/10.3390/ijms11041580>.
- 121 Brånemark PI, Adell R, Albrektsson T, Lekholm U, Lundkvist S, Rockler B. Osseointegrated titanium fixtures in the treatment of edentulousness. *Biomaterials*

- 1983;4:25–8. <https://doi.org/10.1016/b978-008045154-1.50003-4>.
- 122 Jackson BJ. Small Diameter Implants: Specific Indications and Considerations for the Posterior Mandible: A Case Report. *J Oral Implantol* 2010;**37**:156–64. <https://doi.org/10.1563/aaid-joi-d-09-00142.1>.
- 123 Comfort MB, Chu FCS, Chai J, Wat PYP, Chow TW. A 5-year prospective study on small diameter screw-shaped oral implants. *J Oral Rehabil* 2005;**32**:341–5. <https://doi.org/10.1111/j.1365-2842.2004.01441.x>.
- 124 Degidi M, Piattelli A, Carinci F. Clinical Outcome of Narrow Diameter Implants: A Retrospective Study of 510 Implants. *J Periodontol* 2007;**79**:49–54. <https://doi.org/10.1902/jop.2008.070248>.
- 125 Maló P, De Araújo Nobre M. Implants (3.3mm Diameter) for the Rehabilitation of Edentulous Posterior Regions: A Retrospective Clinical Study with Up to 11 Years of Follow-Up. *Clin Implant Dent Relat Res* 2011;**13**:95–103. <https://doi.org/10.1111/j.1708-8208.2009.00188.x>.
- 126 Romeo E, Lops D, Amorfini L, Chiapasco M, Ghisolfi M, Vogel G. Clinical and radiographic evaluation of small-diameter (3.3-mm) implants followed for 1-7 years: A longitudinal study. *Clin Oral Implants Res* 2006;**17**:139–48. <https://doi.org/10.1111/j.1600-0501.2005.01191.x>.
- 127 Vigolo P, Givani A. Clinical evaluation of single-tooth mini-implant restorations: A five-year retrospective study. *J Prosthet Dent* 2000;**84**:50–4. <https://doi.org/10.1067/mpr.2000.107674>.
- 128 Vigolo P, Givani A, Majzoub Z, Cordioli G. Clinical evaluation of small-diameter implants in single-tooth and multiple-implant restorations: a 7-year retrospective study. *Int J Oral Maxillofac Implants* 2004;**19**:703–9.
- 129 Catalani S, Stea S, Beraudi A, Gilberti ME, Bordini B, Toni A, *et al.* Vanadium release in

whole blood, serum and urine of patients implanted with a titanium alloy hip prosthesis.

Clin Toxicol 2013;**51**:550–6. <https://doi.org/10.3109/15563650.2013.818682>.

- 130 Kasai Y, Iida R, Uchida A. Metal concentrations in the serum and hair of patients with titanium alloy spinal implants. *Spine (Phila Pa 1976)* 2003;**28**:1320–6. <https://doi.org/10.1097/00007632-200306150-00018>.
- 131 Okazaki Y, Gotoh E. Comparison of metal release from various metallic biomaterials in vitro. *Biomaterials* 2005;**26**:11–21. <https://doi.org/10.1016/j.biomaterials.2004.02.005>.
- 132 Hallab NJ, Vermes C, Messina C, Roebuck KA, Glant TT, Jacobs JJ. Concentration- and composition-dependent effects of metal ions on human MG-63 osteoblasts. *J Biomed Mater Res* 2002;**60**:420–33. <https://doi.org/10.1002/jbm.10106>.
- 133 Han CH, Johansson CB, Wennerberg A, Albrektsson T. Quantitative and qualitative investigations of surface enlarged titanium and titanium alloy implants. *Clin Oral Implants Res* 1998;**9**:1–10. <https://doi.org/10.1034/j.1600-0501.1998.090101.x>.
- 134 Khan MA, Williams RL, Williams DF. Conjoint corrosion and wear in titanium alloys. *Biomaterials* 1999;**20**:765–72. [https://doi.org/10.1016/S0142-9612\(98\)00229-4](https://doi.org/10.1016/S0142-9612(98)00229-4).
- 135 Okazaki Y, Rao S, Asao S, Tateishi T, Katsuda S, Furuki Y. Effects of Ti, Al and V Concentrations on Cell Viability. *Mater Trans JIM* 2014;**39**:1053–62. <https://doi.org/10.2320/matertrans1989.39.1053>.
- 136 Stenport VF, Johansson CB. Evaluations of bone tissue integration to pure and alloyed titanium implants. *Clin Implant Dent Relat Res* 2008;**10**:191–9. <https://doi.org/10.1111/j.1708-8208.2007.00077.x>.
- 137 Tintinger GR TAJ. Harmful Interactions of Non-Essential Heavy Metals with Cells of the Innate Immune System. *J Clin Toxicol* 2011;**s3**:. <https://doi.org/10.4172/2161-0495.s3-005>.
- 138 Steinemann SG. Titanium - The material of choice? *Periodontol 2000* 1998;**17**:7–21.

<https://doi.org/10.1111/j.1600-0757.1998.tb00119.x>.

- 139 Zhang YM, Chai F, Hornez JC, Li CL, Zhao YM, Traisnel M, *et al.* The corrosion and biological behaviour of titanium alloys in the presence of human lymphoid cells and MC3T3-E1 osteoblasts. *Biomed Mater* 2009;**4**:. <https://doi.org/10.1088/1748-6041/4/1/015004>.
- 140 Boyan BD, Bonewald LF, Paschalis EP, Lohmann CH, Rosser J, Cochran DL, *et al.* Osteoblast-mediated mineral deposition in culture is dependent on surface microtopography. *Calcif Tissue Int* 2002;**71**:519–29. <https://doi.org/10.1007/s00223-001-1114-y>.
- 141 Chen X, Li Y, Hodgson PD, Wen C. In vitro behavior of human osteoblast-like cells (SaOS2) cultured on surface modified titanium and titanium-zirconium alloy. *Mater Sci Eng C* 2011;**31**:1545–52. <https://doi.org/10.1016/j.msec.2011.07.003>.
- 142 Gittens RA, McLachlan T, Olivares-Navarrete R, Cai Y, Berner S, Tannenbaum R, *et al.* The effects of combined micron-/submicron-scale surface roughness and nanoscale features on cell proliferation and differentiation. *Biomaterials* 2011;**32**:3395–403. <https://doi.org/10.1016/j.biomaterials.2011.01.029>.
- 143 Rupp F, Gittens RA, Scheideler L, Marmur A, Boyan BD, Schwartz Z, *et al.* A review on the wettability of dental implant surfaces I: Theoretical and experimental aspects. *Acta Biomater* 2014:2894–906. <https://doi.org/10.1016/j.actbio.2014.02.040>.
- 144 Rupp F, Scheideier L, Olshanska N, De Wild M, Wieland M, Geis-Gerstorfer J. Enhancing surface free energy and hydrophilicity through chemical modification of microstructured titanium implant surfaces. *J Biomed Mater Res - Part A* 2006;**76**:323–34. <https://doi.org/10.1002/jbm.a.30518>.
- 145 Sista S, Wen C, Hodgson PD, Pande G. The influence of surface energy of titanium-zirconium alloy on osteoblast cell functions in vitro. *J Biomed Mater Res - Part A* 2011;**97**

- A:27–36. <https://doi.org/10.1002/jbm.a.33013>.
- 146 Al-Nawas B, Bragger U, Meijer HJA, Naert I, Persson R, Perucchi A, *et al.* A Double-Blind Randomized Controlled Trial (RCT) of Titanium-13Zirconium versus Titanium Grade IV Small-Diameter Bone Level Implants in Edentulous Mandibles - Results from a 1-Year Observation Period. *Clin Implant Dent Relat Res* 2012;**14**:896–904. <https://doi.org/10.1111/j.1708-8208.2010.00324.x>.
- 147 Barter S, Stone P, Bragger U. A pilot study to evaluate the success and survival rate of titanium-zirconium implants in partially edentulous patients: Results after 24 months of follow-up. *Clin Oral Implants Res* 2012;**23**:873–81. <https://doi.org/10.1111/j.1600-0501.2011.02231.x>.
- 148 Chiapasco M, Casentini P, Zaniboni M, Corsi E, Anello T. Titanium-zirconium alloy narrow-diameter implants (Straumann Roxolid®) for the rehabilitation of horizontally deficient edentulous ridges: Prospective study on 18 consecutive patients. *Clin Oral Implants Res* 2012;**23**:1136–41. <https://doi.org/10.1111/j.1600-0501.2011.02296.x>.
- 149 Gottlow J, Dard M, Kjellson F, Obrecht M, Sennerby L. Evaluation of a New Titanium-Zirconium Dental Implant: A Biomechanical and Histological Comparative Study in the Mini Pig. *Clin Implant Dent Relat Res* 2012;**14**:538–45. <https://doi.org/10.1111/j.1708-8208.2010.00289.x>.
- 150 Saulacic N, Bosshardt DD, Bornstein MM, Berner S, Buser D. Bone apposition to a titanium-zirconium alloy implant, as compared to two other titanium-containing implants. *Eur Cells Mater* 2012;**23**:273–88. <https://doi.org/10.22203/eCM.v023a21>.
- 151 Thoma DS, Jones AA, Dard M, Grize L, Obrecht M, Cochran DL. Tissue Integration of a New Titanium–Zirconium Dental Implant: A Comparative Histologic and Radiographic Study in the Canine. *J Periodontol* 2011;**82**:1453–61. <https://doi.org/10.1902/jop.2010.100737>.

- 152 Olivares-Navarrete R, Hyzy SL, Gittens I RA, Schneider JM, Haithcock DA, Ullrich PF, *et al.* Rough titanium alloys regulate osteoblast production of angiogenic factors. *Spine J* 2013;**13**:1563–70. <https://doi.org/10.1016/j.spinee.2013.03.047>.
- 153 Geblinger D, Addadi L, Geiger B. Nano-topography sensing by osteoclasts. *J Cell Sci* 2010;**123**:1814–1814. <https://doi.org/10.1242/jcs.060954>.
- 154 Yim EKF, Darling EM, Kulangara K, Guilak F, Leong KW. Nanotopography-induced changes in focal adhesions, cytoskeletal organization, and mechanical properties of human mesenchymal stem cells. *Biomaterials* 2010;**31**:1299–306. <https://doi.org/10.1016/j.biomaterials.2009.10.037>.
- 155 Park JH, Wasilewski CE, Almodovar N, Olivares-Navarrete R, Boyan BD, Tannenbaum R, *et al.* The responses to surface wettability gradients induced by chitosan nanofilms on microtextured titanium mediated by specific integrin receptors. *Biomaterials* 2012;**33**:7386–93. <https://doi.org/10.1016/j.biomaterials.2012.06.066>.
- 156 Sjöström T, McNamara LE, Yang L, Dalby MJ, Su B. Novel anodization technique using a block copolymer template for nanopatterning of titanium implant surfaces. *ACS Appl Mater Interfaces* 2012;**4**:6354–61. <https://doi.org/10.1021/am301987e>.
- 157 Lai M, Hermann CD, Cheng A, Olivares-Navarrete R, Gittens RA, Bird MM, *et al.* Role of $\alpha 2\beta 1$ integrins in mediating cell shape on microtextured titanium surfaces. *J Biomed Mater Res Part A* 2014;**103**:564–73. <https://doi.org/10.1002/jbm.a.35185>.
- 158 Hyzy SL, Olivares-Navarrete R, Hutton DL, Tan C, Boyan BD, Schwartz Z. Microstructured titanium regulates interleukin production by osteoblasts, an effect modulated by exogenous BMP-2. *Acta Biomater* 2013;**9**:5821–9. <https://doi.org/10.1016/j.actbio.2012.10.030>.
- 159 Canalis E, Economides AN, Gaggero E. Bone morphogenetic proteins, their antagonists, and the skeleton. *Endocr Rev* 2003:218–35.

<https://doi.org/10.1210/er.2002-0023>.

- 160 Zuo C, Huang Y, Bajis R, Sahih M, Li YP, Dai K, *et al*. Osteoblastogenesis regulation signals in bone remodeling. *Osteoporos Int* 2012;16:53–63.
<https://doi.org/10.1007/s00198-012-1909-x>.
- 161 Olivares-Navarrete R, Raz P, Zhao G, Chen J, Wieland M, Cochran DL, *et al*. Integrin $\alpha 2\beta 1$ plays a critical role in osteoblast response to micron-scale surface structure and surface energy of titanium substrates. *Proc Natl Acad Sci* 2008;105:15767–72.
<https://doi.org/10.1073/pnas.0805420105>.
- 162 Keselowsky BG, Wang L, Schwartz Z, Garcia AJ, Boyan BD. Integrin $\alpha 5$ controls osteoblastic proliferation and differentiation responses to titanium substrates presenting different roughness characteristics in a roughness independent manner. *J Biomed Mater Res - Part A* 2007;80:700–10. <https://doi.org/10.1002/jbm.a.30898>.
- 163 Wang L, Zhao G, Olivares-Navarrete R, Bell BF, Wieland M, Cochran DL, *et al*. Integrin $\beta 1$ silencing in osteoblasts alters substrate-dependent responses to 1,25-dihydroxy vitamin D3. *Biomaterials* 2006;27:3716–25.
<https://doi.org/10.1016/j.biomaterials.2006.02.022>.
- 164 Divya Rani V V., Vinoth-Kumar L, Anitha VC, Manzoor K, Deepthy M, Shantikumar VN. Osteointegration of titanium implant is sensitive to specific nanostructure morphology. *Acta Biomater* 2012;8:1976–89. <https://doi.org/10.1016/j.actbio.2012.01.021>.
- 165 Cochran DL. A Comparison of Endosseous Dental Implant Surfaces. *J Periodontol* 1999;70:1523–39. <https://doi.org/10.1902/jop.1999.70.12.1523>.
- 166 Benic GI, Gallucci GO, Mokti M, Hämmerle CHF, Weber HP, Jung RE. Titanium-zirconium narrow-diameter versus titanium regular-diameter implants for anterior and premolar single crowns: 1-year results of a randomized controlled clinical study. *J Clin Periodontol* 2013;40:1052–61. <https://doi.org/10.1111/jcpe.12156>.

- 167 Kieswetter K, Schwartz Z, Dean DD, Boyan BD. The role of implant surface characteristics in the healing of bone. *Crit Rev Oral Biol Med* 1996;**7**:329–45. <https://doi.org/10.1177/10454411960070040301>.
- 168 Schwartz Z, Boyan BD. Underlying Mechanisms at the Bone-Biomaterial Interface. *J Cell Biochem* 1994;**56**:340–7. [https://doi.org/DOI 10.1002/jcb.240560310](https://doi.org/DOI%2010.1002/jcb.240560310).
- 169 Martin JY, Schwartz Z, Hummert TW, Schraub DM, Simpson J, Lankford J, *et al*. Effect of titanium surface roughness on proliferation, differentiation, and protein synthesis of human osteoblast-like cells (MG63). *J Biomed Mater Res* 1995;**29**:389–401. <https://doi.org/10.1002/jbm.820290314>.
- 170 Raines AL, Olivares-Navarrete R, Wieland M, Cochran DL, Schwartz Z, Boyan BD. Regulation of angiogenesis during osseointegration by titanium surface microstructure and energy. *Biomaterials* 2010;**31**:4909–17. <https://doi.org/10.1016/j.biomaterials.2010.02.071>.
- 171 Zhao G, Raines AL, Wieland M, Schwartz Z, Boyan BD. Requirement for both micron- and submicron scale structure for synergistic responses of osteoblasts to substrate surface energy and topography. *Biomaterials* 2007;**28**:2821–9. <https://doi.org/10.1016/j.biomaterials.2007.02.024>.
- 172 Boyan BD, Schwartz Z, Lohmann CH, Sylvia VL, Cochran DL, Dean DD, *et al*. Pretreatment of bone with osteoclasts affects phenotypic expression of osteoblast-like cells. *J Orthop Res* 2003;**21**:638–47. [https://doi.org/10.1016/S0736-0266\(02\)00261-9](https://doi.org/10.1016/S0736-0266(02)00261-9).
- 173 Sinha RK, Tuan RS. Regulation of human osteoblast integrin expression by orthopedic implant materials. *Bone* 1996;**18**:451–7. [https://doi.org/10.1016/8756-3282\(96\)00044-0](https://doi.org/10.1016/8756-3282(96)00044-0).
- 174 Curtis ASG, Gadegaard N, Dalby MJ, Riehle MO, Wilkinson CDW, Aitchison G. Cells React to Nanoscale Order and Symmetry in Their Surroundings. *IEEE Trans Nanobioscience* 2004;**3**:61–5. <https://doi.org/10.1109/TNB.2004.824276>.

- 175 Rani V V.D., Manzoor K, Menon D, Selvamurugan N, Nair S V. The design of novel nanostructures on titanium by solution chemistry for an improved osteoblast response. *Nanotechnology* 2009;**20**:. <https://doi.org/10.1088/0957-4484/20/19/195101>.
- 176 Khang D, Choi J, Im YM, Kim YJ, Jang JH, Kang SS, *et al*. Role of subnano-, nano- and submicron-surface features on osteoblast differentiation of bone marrow mesenchymal stem cells. *Biomaterials* 2012;**33**:5997–6007. <https://doi.org/10.1016/j.biomaterials.2012.05.005>.
- 177 Sjöström T, Brydone AS, Meek RD, Dalby MJ, Su B, Mcnamara LE, *et al*. Titanium nanofeaturing for enhanced bioactivity of implanted orthopedic and dental devices. *Nanomedicine* 2013;**8**:89–104. <https://doi.org/10.2217/nnm.12.177>.
- 178 Engel E, Michiardi A, Navarro M, Lacroix D, Planell JA. Nanotechnology in regenerative medicine: the materials side. *Trends Biotechnol* 2008;**26**:39–47. <https://doi.org/10.1016/j.tibtech.2007.10.005>.
- 179 Barbucci R, Pasqui D, Wirsén A, Affrossman S, Curtis A, Tetta C. Micro and Nano-Structured Surfaces.
- 180 Fiedler J, Özdemir B, Bartholomä J, Plettl A, Brenner RE, Ziemann P. The effect of substrate surface nanotopography on the behavior of multipotent mesenchymal stromal cells and osteoblasts. *Biomaterials* 2013;**34**:8851–9. <https://doi.org/10.1016/j.biomaterials.2013.08.010>.
- 181 Buser D, Brogini N, Wieland M, Schenk RK, Denzer AJ, Cochran DL, *et al*. Enhanced bone apposition to a chemically modified SLA titanium surface. *J Dent Res* 2004;**83**:529–33. <https://doi.org/10.1177/154405910408300704>.
- 182 Mendonça G, Mendonça DBS, Simões LGP, Araújo AL, Leite ER, Duarte WR, *et al*. The effects of implant surface nanoscale features on osteoblast-specific gene expression. *Biomaterials* 2009;**30**:4053–62. <https://doi.org/10.1016/j.biomaterials.2009.04.010>.

- 183 Wennerberg A, Jimbo R, Stübinger S, Obrecht M, Dard M, Berner S. Nanostructures and hydrophilicity influence osseointegration: A biomechanical study in the rabbit tibia. *Clin Oral Implants Res* 2014;**25**:1041–50. <https://doi.org/10.1111/clr.12213>.
- 184 Park JH, Olivares-Navarrete R, Baier RE, Meyer AE, Tannenbaum R, Boyan BD, *et al.* Effect of cleaning and sterilization on titanium implant surface properties and cellular response. *Acta Biomater* 2012;**8**:1966–75. <https://doi.org/10.1016/j.actbio.2011.11.026>.
- 185 Lavenus S, Berreur M, Trichet V, Pilet P, Louarn G, Layrolle P. Adhesion and osteogenic differentiation of human mesenchymal stem cells on titanium nanopores. *Eur Cells Mater* 2011;**22**:84–96. <https://doi.org/10.22203/eCM.v022a07>.
- 186 Salido M, Vilches JI, Gutiérrez JL, Vilches JI. Actin cytoskeletal organization in human osteoblasts grown on different dental titanium implant surfaces. *Histol Histopathol* 2007;**22**:1355–64.
- 187 Kunzler TP, Drobek T, Schuler M, Spencer ND. Systematic study of osteoblast and fibroblast response to roughness by means of surface-morphology gradients. *Biomaterials* 2007;**28**:2175–82. <https://doi.org/10.1016/j.biomaterials.2007.01.019>.
- 188 Dalby MJ, Gadegaard N, Herzyk P, Sutherland D, Agheli H, Wilkinson CDW, *et al.* Nanomechanotransduction and interphase nuclear organization influence on genomic control. *J Cell Biochem* 2007;**102**:1234–44. <https://doi.org/10.1002/jcb.21354>.
- 189 Baud'huin M, Solban N, Cornwall-Brady M, Sako D, Kawamoto Y, Liharska K, *et al.* A soluble bone morphogenetic protein type IA receptor increases bone mass and bone strength. *Proc Natl Acad Sci* 2012;**109**:12207–12. <https://doi.org/10.1073/pnas.1204929109>.
- 190 Canalis E, Brunet LJ, Parker K, Zanotti S. Conditional inactivation of noggin in the postnatal skeleton causes osteopenia. *Endocrinology* 2012;**153**:1616–26. <https://doi.org/10.1210/en.2011-1604>.

- 191 Gittens RA, Olivares-Navarrete R, Cheng A, Anderson DM, McLachlan T, Stephan I, *et al.* The roles of titanium surface micro/nanotopography and wettability on the differential response of human osteoblast lineage cells. *Acta Biomater* 2013;**9**:6268–77. <https://doi.org/10.1016/j.actbio.2012.12.002>.
- 192 Kopf BS, Ruch S, Berner S, Spencer ND, Maniura-Weber K. The role of nanostructures and hydrophilicity in osseointegration: In-vitro protein-adsorption and blood-interaction studies. *J Biomed Mater Res - Part A* 2015;**103**:2661–72. <https://doi.org/10.1002/jbm.a.35401>.
- 193 Olivares-Navarrete R, Raines AL, Hyzy SL, Park JH, Hutton DL, Cochran DL, *et al.* Osteoblast maturation and new bone formation in response to titanium implant surface features are reduced with age. *J Bone Miner Res* 2012;**27**:1773–83. <https://doi.org/10.1002/jbmr.1628>.
- 194 Olivares-Navarrete R, Hyzy SL, Slosar PJ, Schneider JM, Schwartz Z, Boyan BD. Implant materials generate different peri-implant inflammatory factors: Poly-ether-ether-ketone promotes fibrosis and microtextured titanium promotes osteogenic factors. *Spine (Phila Pa 1976)* 2015;**40**:399–404. <https://doi.org/10.1097/BRS.0000000000000778>.
- 195 Minkin C, Marinho VC. Role of the osteoclast at the bone-implant interface. *Adv Dent Res* 1999;**13**:49–56. <https://doi.org/10.1177/08959374990130011401>.
- 196 Salvi GE, Bosshardt DD, Lang NP, Abrahamsson I, Berglundh T, Lindhe J, *et al.* Temporal sequence of hard and soft tissue healing around titanium dental implants. *Periodontol 2000* 2015;**68**:135–52. <https://doi.org/10.1111/prd.12054>.
- 197 Andrade JD, Hlady V. Protein adsorption and materials biocompatibility: A tutorial review and suggested hypotheses. *Adv. Polym. Sci.* 1986. p. 1–63.
- 198 Marx RE. Platelet-rich plasma: evidence to support its use. *J Oral Maxillofac Surg* 2004;**62**:489–96. <https://doi.org/10.1016/j.joms.2003.12.003>.

- 199 Davies JE. Understanding peri-implant endosseous healing. *J Dent Educ* 2003;**67**:932–49.
- 200 Di Iorio D, Traini T, Degidi M, Caputi S, Neugebauer J, Piattelli A. Quantitative evaluation of the fibrin clot extension on different implant surfaces: An in vitro study. *J Biomed Mater Res - Part B Appl Biomater* 2005;**74**:636–42. <https://doi.org/10.1002/jbm.b.30251>.
- 201 Bruder SP, Fink DJ, Caplan AI. Mesenchymal stem cells in bone development, bone repair, and skeletal regeneration therapy. *J Cell Biochem* 1994;**56**:283–94. <https://doi.org/10.1002/jcb.240560303>.
- 202 Neuss S, Schneider RKM, Tietze L, Knüchel R, Jahnen-Dechent W. Secretion of fibrinolytic enzymes facilitates human mesenchymal stem cell invasion into fibrin clots. *Cells Tissues Organs* 2009;**191**:36–46. <https://doi.org/10.1159/000215579>.
- 203 Kuzyk P, Schemitsch E. The basic science of peri-implant bone healing. *Indian J Orthop* 2011;**45**:108–15. <https://doi.org/10.4103/0019-5413.77129>.
- 204 Berglundh T, Abrahamsson I, Lang NP, Lindhe J. De novo alveolar bone formation adjacent to endosseous implants. *Clin Oral Implants Res* 2003;**14**:251–62.
- 205 Lang NP, Salvi GE, Huynh-Ba G, Ivanovski S, Donos N, Bosshardt DD. Early osseointegration to hydrophilic and hydrophobic implant surfaces in humans. *Clin Oral Implants Res* 2011;**22**:349–56. <https://doi.org/10.1111/j.1600-0501.2011.02172.x>.
- 206 Mulari MTK, Qu Q, Härkönen PL, Väänänen HK. Osteoblast-like cells complete osteoclastic bone resorption and form new mineralized bone matrix in vitro. *Calcif Tissue Int* 2004;**75**:253–61. <https://doi.org/10.1007/s00223-004-0172-3>.
- 207 Udagawa N, Takahashi N, Akatsu T, Tanaka H, Sasaki T, Nishihara T, *et al*. Origin of osteoclasts: mature monocytes and macrophages are capable of differentiating into osteoclasts under a suitable microenvironment prepared by bone marrow-derived stromal cells. *Proc Natl Acad Sci* 2006;**87**:7260–4.

<https://doi.org/10.1073/pnas.87.18.7260>.

- 208 Simonet WS, Lacey DL, Dunstan CR, Kelley M, Chang MS, Lüthy R, *et al*. Osteoprotegerin: A novel secreted protein involved in the regulation of bone density. *Cell* 1997;**89**:309–19. [https://doi.org/10.1016/S0092-8674\(00\)80209-3](https://doi.org/10.1016/S0092-8674(00)80209-3).
- 209 Hotchkiss KM, Reddy GB, Hyzy SL, Schwartz Z, Boyan BD, Olivares-Navarrete R. Titanium surface characteristics, including topography and wettability, alter macrophage activation. *Acta Biomater* 2016;**31**:425–34. <https://doi.org/10.1016/j.actbio.2015.12.003>.
- 210 Hotchkiss KM, Ayad NB, Hyzy SL, Boyan BD, Olivares-Navarrete R. Dental implant surface chemistry and energy alter macrophage activation in vitro. *Clin Oral Implants Res* 2016;**28**:414–23. <https://doi.org/10.1111/clr.12814>.
- 211 Shah FA, Stenlund P, Martinelli A, Thomsen P, Palmquist A. Direct communication between osteocytes and acid-etched titanium implants with a sub-micron topography. *J Mater Sci Mater Med* 2016;**27**:1–9. <https://doi.org/10.1007/s10856-016-5779-1>.
- 212 Shah FA, Wang X, Thomsen P, Grandfield K, Palmquist A. High-Resolution Visualization of the Osteocyte Lacuno-Canalicular Network Juxtaposed to the Surface of Nanotextured Titanium Implants in Human. *ACS Biomater Sci Eng* 2015;**1**:305–13. <https://doi.org/10.1021/ab500127y>.
- 213 Labranche TP, Jesson MI, Radi ZA, Storer CE, Guzova JA, Bonar SL, *et al*. JAK inhibition with tofacitinib suppresses arthritic joint structural damage through decreased RANKL production. *Arthritis Rheum* 2012;**64**:3531–42. <https://doi.org/10.1002/art.34649>.
- 214 Stein NC, Kreuzmann C, Zimmermann SP, Niebergall U, Hellmeyer L, Goettsch C, *et al*. Interleukin-4 and interleukin-13 stimulate the osteoclast inhibitor osteoprotegerin by human endothelial cells through the STAT6 pathway. *J Bone Miner Res* 2008;**23**:750–8. <https://doi.org/10.1359/jbmr.080203>.
- 215 Syversen U, Stunes AK, Gustafsson BI, Obrant KJ, Nordsletten L, Berge R, *et al*.

- Different skeletal effects of the peroxisome proliferator activated receptor (PPAR) α agonist fenofibrate and the PPAR γ agonist pioglitazone. *BMC Endocr Disord* 2009;**9**.
<https://doi.org/10.1186/1472-6823-9-10>.
- 216 Hayase Y, Muguruma Y, Lee MY. Osteoclast development from hematopoietic stem cells: apparent divergence of the osteoclast lineage prior to macrophage commitment. *Exp Hematol* 1997;**25**:19–25.
- 217 Kao WJ, McNally AK, Hiltner A, Anderson JM. Role for interleukin-4 in foreign-body giant cell formation on a poly(etherurethane urea) in vivo. *J Biomed Mater Res* 1995;**29**:1267–75. <https://doi.org/10.1002/jbm.820291014>.
- 218 McNally AK, Anderson JM. Interleukin-4 induces foreign body giant cells from human monocytes/macrophages. Differential lymphokine regulation of macrophage fusion leads to morphological variants of multinucleated giant cells. *Am J Pathol* 1995;**147**:1487–99.
- 219 Duong LT, Lakkakorpi P, Nakamura I, Rodan GA. Integrins and signaling in osteoclast function. *Matrix Biol* 2000:97–105. [https://doi.org/10.1016/S0945-053X\(00\)00051-2](https://doi.org/10.1016/S0945-053X(00)00051-2).
- 220 Gil-Henn H, Destaing O, Sims NA, Aoki K, Alles N, Neff L, *et al*. Defective microtubule-dependent podosome organization in osteoclasts leads to increased bone density in Pyk2^{-/-} mice. *J Cell Biol* 2007;**178**:1053–64. <https://doi.org/10.1083/jcb.200701148>.
- 221 Sims NA, Aoki K, Bogdanovi Z, Maragh M, Okigaki M, Logan S, *et al*. Impaired osteoclast function in Pyk2 knockout mice and cumulative effects in Pyk2/Src double knockout. *J Bone Miner Res* 1999;**14**:S183.
- 222 McHugh KP, Hovalala-Dilke K, Zheng MH, Namba N, Jonathan L, Novack D, *et al*. Mice lacking β 3 integrins are osteosclerotic because of dysfunctional osteoclasts. *J Clin Invest* 2000;**105**:433–40. <https://doi.org/10.1172/JCI8905>.
- 223 Nakamura I, Lipfert L, Rodan GA, Duong LT. Convergence of α β 3 integrin-and macrophage colony stimulating factor-mediated signals on phospholipase Cy in

perfusion osteoclasts. *J Cell Biol* 2001;**152**:361–73.

<https://doi.org/10.1083/jcb.152.2.361>.

- 224 Sanjay A, Houghton A, Neff L, DiDomenico E, Bardelay C, Antoine E, *et al*. Cbl associates with Pyk2 and Src to regulate Src kinase activity, $\alpha\beta 3$ integrin-mediated signaling, cell adhesion, and osteoclast motility. *J Cell Biol* 2001;**152**:181–95.
<https://doi.org/10.1083/jcb.152.1.181>.
- 225 Sly WS, Hu PY. Human Carbonic Anhydrases and Carbonic Anhydrase Deficiencies. *Annu Rev Biochem* 1995;**64**:375–401.
<https://doi.org/10.1146/annurev.bi.64.070195.002111>.
- 226 Fujisaki K, Tanabe N, Suzuki N, Kawato T, Takeichi O, Tsuzukibashi O, *et al*. Receptor activator of NF- κ B ligand induces the expression of carbonic anhydrase II, cathepsin K, and matrix metalloproteinase-9 in osteoclast precursor RAW264.7 cells. *Life Sci* 2007;**80**:1311–8. <https://doi.org/10.1016/j.lfs.2006.12.037>.
- 227 Troen BR. The Regulation of Cathepsin K Gene Expression.
- 228 Bossard MJ, Tomaszek TA, Thompson SK, Amegadzie BY, Hanning CR, Jones C, *et al*. Proteolytic activity of human osteoclast cathepsin K: Expression, purification, activation, and substrate identification. *J Biol Chem* 1996;**271**:12517–24.
<https://doi.org/10.1074/jbc.271.21.12517>.
- 229 Votta BJ, Levy MA, Badger A, Bradbeer J, Dodds RA, James IE, *et al*. Peptide aldehyde inhibitors of cathepsin K inhibit bone resorption both in vitro and in vivo. *J Bone Miner Res* 1997;**12**:1396–406. <https://doi.org/10.1359/jbmr.1997.12.9.1396>.
- 230 Laitala-Leinonen T, Rinne R, Saukko P, Väänänen HK, Rinne A. Cystatin B as an intracellular modulator of bone resorption. *Matrix Biol* 2006;**25**:149–57.
<https://doi.org/10.1016/j.matbio.2005.10.005>.

231 EBELING W, HENNRICH N, KLOCKOW M, METZ H, ORTH HD, LANG H. Proteinase K

from *Tritirachium album* Limber. *Eur J Biochem* 1974;**47**:91–7.

<https://doi.org/10.1111/j.1432-1033.1974.tb03671.x>.

- 232 Russell RGG, Watts NB, Ebetino FH, Rogers MJ. Mechanisms of action of bisphosphonates: similarities and differences and their potential influence on clinical efficacy. *Osteoporos Int* 2008;**19**:733–59. <https://doi.org/10.1007/s00198-007-0540-8>.
- 233 Russell RGG. Bisphosphonates: from bench to bedside. *Ann N Y Acad Sci* 2006;**1068**:367–401. <https://doi.org/10.1196/annals.1346.041>.
- 234 Sato M, Grasser W, Endo N, Akins R, Simmons H, Thompson DD, *et al.* Bisphosphonate action. Alendronate localization in rat bone and effects on osteoclast ultrastructure. *J Clin Invest* 1991;**88**:2095–105. <https://doi.org/10.1172/JCI115539>.
- 235 Plotkin LI, Weinstein RS, Parfitt AM, Roberson PK, Manolagas SC, Bellido T. Prevention of osteocyte and osteoblast apoptosis by bisphosphonates and calcitonin. *J Clin Invest* 1999;**104**:1363–74. <https://doi.org/10.1172/JCI6800>.
- 236 Mathov I, Plotkin LI, Sgarlata CL, Leoni J, Bellido T. Extracellular signal-regulated kinases and calcium channels are involved in the proliferative effect of bisphosphonates on osteoblastic cells in vitro. *J Bone Miner Res* 2001;**16**:2050–6. <https://doi.org/10.1359/jbmr.2001.16.11.2050>.
- 237 Im G II, Qureshi SA, Kenney J, Rubash HE, Shanbhag AS. Osteoblast proliferation and maturation by bisphosphonates. *Biomaterials* 2004;**25**:4105–15. <https://doi.org/10.1016/j.biomaterials.2003.11.024>.
- 238 Kellinsalmi M, Mönkkönen H, Mönkkönen J, Leskelä HV, Parikka V, Hämäläinen M, *et al.* In vitro comparison of clodronate, pamidronate and zoledronic acid effects on rat osteoclasts and human stem cell-derived osteoblasts. *Basic Clin Pharmacol Toxicol* 2005;**97**:382–91. https://doi.org/10.1111/j.1742-7843.2005.pto_176.x.
- 239 Açil Y, Möller B, Niehoff P, Rachko K, Gassling V, Wiltfang J, *et al.* The cytotoxic effects

of three different bisphosphonates in-vitro on human gingival fibroblasts, osteoblasts and osteogenic sarcoma cells. *J Cranio-Maxillofacial Surg* 2012;**40**:e229–35.

<https://doi.org/10.1016/j.jcms.2011.10.024>.

- 240 Idris AI, Rojas J, Greig IR, Van't Hof RJ, Ralston SH. Aminobisphosphonates cause osteoblast apoptosis and inhibit bone nodule formation in vitro. *Calcif Tissue Int* 2008;**82**:191–201. <https://doi.org/10.1007/s00223-008-9104-y>.
- 241 Gasser JA, Kneissel M, Thomsen JS, Mosekilde L. PTH and interactions with bisphosphonates. *J Musculoskelet Neuronal Interact* 2000;**1**:53–6.
- 242 Fournier P, Boissier S, Filleur S, Guglielmi J, Cabon F, Colombel M, *et al*. Bisphosphonates inhibit angiogenesis in vitro and testosterone-stimulated vascular regrowth in the ventral prostate in castrated rats. *Cancer Res* 2002;**62**:6538–44.
- 243 Mashiba T, Hirano T, Turner CH, Forwood MR, Johnston CC, Burr DB. Suppressed Bone Turnover by Bisphosphonates Increases Microdamage Accumulation and Reduces Some Biomechanical Properties in Dog Rib. *J Bone Miner Res* 2010;**15**:613–20. <https://doi.org/10.1359/jbmr.2000.15.4.613>.
- 244 Khosla S, Burr D, Cauley J, Dempster DW, Ebeling PR, Felsenberg D, *et al*. Bisphosphonate-associated osteonecrosis of the jaw: Report of a Task Force of the American Society for Bone and Mineral Research. *J Bone Miner Res* 2007:1479–91. <https://doi.org/10.1359/jbmr.0707onj>.
- 245 Batzer R, Liu Y, Cochran DL, Szmuckler-Moncler S, Dean DD, Boyan BD, *et al*. Prostaglandins mediate the effects of titanium surface roughness on MG63 osteoblast-like cells and alter cell responsiveness to 1 alpha,25-(OH)2D3. *J Biomed Mater Res* 1998;**41**:489–96. [https://doi.org/10.1002/\(SICI\)1097-4636\(19980905\)41:3<489::AID-JBM20>3.0.CO;2-C](https://doi.org/10.1002/(SICI)1097-4636(19980905)41:3<489::AID-JBM20>3.0.CO;2-C).
- 246 Lohmann CH, Bonewald LF, Sisk MA, Sylvia VL, Cochran DL, Dean DD, *et al*.

- Maturation state determines the response of osteogenic cells to surface roughness and 1,25-dihydroxyvitamin D₃. *J Bone Min Res* 2000;**15**:1169–80.
<https://doi.org/10.1359/jbmr.2000.15.6.1169>.
- 247 Boyan BD, Batzer R, Kieswetter K, Liu Y, Cochran DL, Szmuckler-Moncler S, *et al*. Titanium surface roughness alters responsiveness of MG63 osteoblast-like cells to 1 alpha,25-(OH)₂D₃. *J Biomed Mater Res* 1998;**39**:77–85.
[https://doi.org/10.1002/\(sici\)1097-4636\(199801\)39:1<77::aid-jbm10>3.0.co;2-l](https://doi.org/10.1002/(sici)1097-4636(199801)39:1<77::aid-jbm10>3.0.co;2-l).
- 248 Schwartz Z, Lohmann CH, Vocke AK, Sylvia VL, Cochran DL, Dean DD, *et al*. Osteoblast response to titanium surface roughness and 1alpha,25-(OH)₂D₃ is mediated through the mitogen-activated protein kinase (MAPK) pathway. *J Biomed Mater Res* 2001;**56**:417–26. [https://doi.org/10.1002/1097-4636\(20010905\)56:3<417::AID-JBM1111>3.0.CO;2-K](https://doi.org/10.1002/1097-4636(20010905)56:3<417::AID-JBM1111>3.0.CO;2-K).
- 249 Ong JL, Carnes DL, Cardenas HL, Cavin R, Carries D, Cardenas HL, *et al*. Surface roughness of titanium on bone morphogenetic protein-2 treated osteoblast cells in vitro. *Implant Dent* 1997;**6**:19–24. <https://doi.org/10.1097/00008505-199700610-00045>.
- 250 Akatsu T, Murakami T, Nishikawa M, Ono K, Shinomiya N, Tsuda E, *et al*. Osteoclastogenesis inhibitory factor suppresses osteoclast survival by interfering in the interaction of stromal cells with osteoclast. *Biochem Biophys Res Commun* 1998;**250**:229–34.
- 251 von Knoch F, Jaquiere C, Kowalsky M, Schaeren S, Alabre C, Martin I, *et al*. Effects of bisphosphonates on proliferation and osteoblast differentiation of human bone marrow stromal cells. *Biomaterials* 2005;**26**:6941–9.
<https://doi.org/10.1016/j.biomaterials.2005.04.059>.
- 252 Fromigue O, Body JJ, Fromigué O, Body JJ. Bisphosphonates influence the proliferation and the maturation of normal human osteoblasts. *J Endocrinol Invest* 2002;**25**:539–46.

<https://doi.org/10.1007/BF03345497>.

- 253 Sanders JL, Tarjan G, Foster SA, Stern PH. Alendronate/interleukin-1 beta cotreatment increases interleukin-6 in bone and UMR-106 cells: Dose dependence and relationship to the antiresorptive effect of alendronate. *J Bone Miner Res* 1998;**13**:786–92. <https://doi.org/DOI 10.1359/jbmr.1998.13.5.786>.
- 254 Giuliani N, Pedrazzoni M, Passeri G, Girasole G. Bisphosphonates inhibit IL-6 production by human osteoblast-like cells. *Scand J Rheumatol* 1998;**27**:38–41.
- 255 Greiner S, Kadow-Romacker A, Lübberstedt M, Schmidmaier G, Wildemann B. The effect of zoledronic acid incorporated in a poly(D,L-lactide) implant coating on osteoblasts in vitro. *J Biomed Mater Res - Part A* 2007;**80**:769–75. <https://doi.org/10.1002/jbm.a.30950>.
- 256 Yoshinari M, Oda Y, Ueki H, Yokose S. Immobilization of bisphosphonates on surface modified titanium. *Biomaterials* 2001;**22**:709–15. [https://doi.org/10.1016/S0142-9612\(00\)00234-9](https://doi.org/10.1016/S0142-9612(00)00234-9).
- 257 Zheng D, Neoh KG, Kang ET. Immobilization of alendronate on titanium via its different functional groups and the subsequent effects on cell functions. *J Colloid Interface Sci* 2017;**487**:1–11. <https://doi.org/10.1016/j.jcis.2016.10.014>.
- 258 Alqhtani NR, Logan NJ, Meghji S, Leeson R, Brett PM. Low dose effect of bisphosphonates on hMSCs osteogenic response to titanium surface in vitro. *Bone Reports* 2017;**6**:64–9. <https://doi.org/10.1016/j.bonr.2017.02.002>.
- 259 Dunford JE, Thompson K, Coxon FP, Luckman SP, Hahn FM, Poulter CD, *et al*. Structure-Activity Relationships for Inhibition of Farnesyl Diphosphate Synthase in Vitro and Inhibition of Bone Resorption in Vivo by Nitrogen-Containing Bisphosphonates. *J Pharmacol Exp Ther* 2001;**296**:235–42.
- 260 Xie J, Tong A, Kim SC. Patterns of bisphosphonates utilization in patients under age 45

- in a large cohort of commercial insurance beneficiaries in the United States. *PLoS One* 2015;**10**:e0115091. <https://doi.org/10.1371/journal.pone.0115091>.
- 261 Indridason OS, Franzson L, Sigurdsson G. Serum osteoprotegerin and its relationship with bone mineral density and markers of bone turnover. *Osteoporos Int* 2005;**16**:417–23. <https://doi.org/10.1007/s00198-004-1699-x>.
- 262 Corrado A, Neve A, Macchiarola A, Gaudio A, Marucci A, Cantatore FP. RANKL/OPG ratio and DKK-1 expression in primary osteoblastic cultures from osteoarthritic and osteoporotic subjects. *J Rheumatol* 2013;**40**:684–94. <https://doi.org/10.3899/jrheum.120845>.
- 263 Bauss F, Russell RGG. Ibandronate in osteoporosis: preclinical data and rationale for intermittent dosing. *Osteoporos Int* 2004;**15**:423–33. <https://doi.org/10.1007/s00198-004-1612-7>.
- 264 Müller R, Recker RR, Muller R, Recker RR. Bisphosphonate action on bone structure and strength: Preclinical and clinical evidence for ibandronate. *Bone* 2007;**41**:S16–23. <https://doi.org/10.1016/j.bone.2007.08.004>.
- 265 Russell RGG. Ibandronate: Pharmacology and preclinical studies. *Bone* 2006;**38**:S7–12. <https://doi.org/10.1016/j.bone.2006.01.151>.
- 266 Aparicio A, Gardner A, Tu Y, Savage A, Berenson J, Lichtenstein A. In vitro cytoreductive effects on multiple myeloma cells induced by bisphosphonates. *Leukemia* 1998;**12**:220–9. <https://doi.org/DOI 10.1038/sj.leu.2400892>.
- 267 Shipman CM, Rogers MJ, Apperley JF, Russell RGG, Croucher PI. Bisphosphonates induce apoptosis in human myeloma cell lines: a novel anti-tumour activity. *Br J Haematol* 1997;**98**:665–72. <https://doi.org/10.1046/j.1365-2141.1997.2713086.x>.
- 268 Mackie PS, Fisher JL, Zhou H, Choong PFM. Bisphosphonates regulate cell growth and gene expression in the UMR 106-01 clonal rat osteosarcoma cell line. *Br J Cancer*

- 2001;**84**:951–8. <https://doi.org/10.1054/bjoc.2000.1679>.
- 269 Sonnemann J, Eckervogt V, Truckenbrod B, Boos J, Winkelmann W, van Valen F. The bisphosphonate pamidronate is a potent inhibitor of human osteosarcoma cell growth in vitro. *Anticancer Drugs* 2001;**12**:459–65.
- 270 Korpál M, Yan J, Lu X, Xu S, Lerit DA, Kang Y. Imaging transforming growth factor-beta signaling dynamics and therapeutic response in breast cancer bone metastasis. *Nat Med* 2009;**15**:960–6. <https://doi.org/10.1038/nm.1943>.
- 271 Santini D, Vincenzi B, Avvisati G, Dicuonzo G, Battistoni F, Gavasci M, *et al*. Pamidronate induces modifications of circulating angiogenetic factors in cancer patients. *Clin Cancer Res* 2002;**8**:1080–4.
- 272 Vincenzi B, Santini D, Dicuonzo G, Battistoni F, Gavasci M, La Cesa A, *et al*. Zoledronic acid-related angiogenesis modifications and survival in advanced breast cancer patients. *J Interf Cytokine Res* 2005;**25**:144–51. <https://doi.org/10.1089/jir.2005.25.144>.
- 273 Boissier S, Ferreras M, Peyruchaud O, Mignetto S, Ebetino FH, Colombel M, *et al*. Bisphosphonates inhibit breast and prostate carcinoma cell invasion, an early event in the formation of bone metastases. *Cancer Res* 2000;**60**:2949–54.
- 274 Virtanen SS, Vaananen HK, Harkonen PL, Lakkakorpi PT, Väänänen HK, Härkönen PL, *et al*. Alendronate inhibits invasion of PC-3 prostate cancer cells by affecting the mevalonate pathway. *Cancer Res* 2002;**62**:2708–14.
- 275 Jacobs R. Preoperative radiologic planning of implant surgery in compromised patients. *Periodontol 2000* 2003;**33**:12–25. <https://doi.org/10.1046/j.0906-6713.2002.03302.x>.
- 276 Javed F, Ahmed HB, Crespi R, Romanos GE. Role of primary stability for successful osseointegration of dental implants: Factors of influence and evaluation. *Interv Med Appl Sci* 2013;**5**:162–7. <https://doi.org/10.1556/IMAS.5.2013.4.3>.
- 277 Albrektsson T, Johansson C. Osteoinduction, osteoconduction and osseointegration. *Eur*

- Spine J* 2001;**10**:S96–101. <https://doi.org/10.1007/s005860100282>.
- 278 Degidi M, Scarano A, Piattelli M, Perrotti V, Piattelli A. Bone remodeling in immediately loaded and unloaded titanium dental implants: a histologic and histomorphometric study in humans. *J Oral Implantol* 2005;**31**:18–24. <https://doi.org/10.1563/0-717.1>.
- 279 Simpson AH, Murray IR. Osteoporotic Fracture Models. *Curr Osteoporos Rep* 2015:9–15. <https://doi.org/10.1007/s11914-014-0246-8>.
- 280 Tella SH, Gallagher JC. Prevention and treatment of postmenopausal osteoporosis. *J Steroid Biochem Mol Biol* 2014;**142**:. <https://doi.org/10.1016/j.jsbmb.2013.09.008>.
- 281 Plotkin LI, Manolagas SC, Bellido T. Dissociation of the pro-apoptotic effects of bisphosphonates on osteoclasts from their anti-apoptotic effects on osteoblasts/osteocytes with novel analogs. *Bone* 2006;**39**:443–52. <https://doi.org/10.1016/j.bone.2006.02.060>.
- 282 Corrado A, Cantatore FP, Grano M, Colucci S. Neridronate and human osteoblasts in normal, osteoporotic and osteoarthritic subjects. *Clin Rheumatol* 2005;**24**:527–34. <https://doi.org/10.1007/s10067-005-1100-2>.
- 283 Nishikawa M, Akatsu T, Katayama Y, Yasutomo Y, Kado S, Kugai N, *et al*. Bisphosphonates act on osteoblastic cells and inhibit osteoclast formation in mouse marrow cultures. *Bone* 1996;**18**:9–14. [https://doi.org/10.1016/8756-3282\(95\)00426-2](https://doi.org/10.1016/8756-3282(95)00426-2).
- 284 Vitté C, Fleisch H, Guenther HL, Vitte C, Fleisch H, Guenther HL. Bisphosphonates Induce Osteoblasts to Secrete an Inhibitor of Osteoclast-Mediated Resorption. *Endocrinology* 1996;**137**:2324–33. <https://doi.org/10.1210/endo.137.6.8641182>.
- 285 Delmas PD, Vergnaud P, Arlot ME, Pastoureau P, Meunier PJ, Nilssen MHL. The anabolic effect of human PTH (1-34) on bone formation is blunted when bone resorption is inhibited by the bisphosphonate tiludronate-is activated resorption a prerequisite for the in vivo effect of PTH on formation in a remodeling system? *Bone* 1995;**16**:603–10.

[https://doi.org/10.1016/8756-3282\(95\)00113-R](https://doi.org/10.1016/8756-3282(95)00113-R).

- 286 Ettinger B, San Martin J, Crans G, Pavo I. Differential effects of teriparatide on BMD after treatment with raloxifene or alendronate. *J Bone Miner Res* 2004;**19**:745–51. <https://doi.org/10.1359/JBMR.040117>.
- 287 Finkelstein JS, Hayes A, Hunzelman JL, Wyland JJ, Lee H, Neer RM. The Effects of Parathyroid Hormone, Alendronate, or Both in Men with Osteoporosis. *N Engl J Med* 2003;**349**:1216–26. <https://doi.org/10.1056/NEJMoa035725>.
- 288 Samadfam R, Xia Q, Goltzman D. Pretreatment with anticatabolic agents blunts but does not eliminate the skeletal anabolic response to parathyroid hormone in oophorectomized mice. *Endocrinology* 2007;**148**:2778–87. <https://doi.org/10.1210/en.2006-1475>.
- 289 Wood J, Bonjean K, Ruetz S, Bellahcène A, Devy L, Foidart JM, *et al*. Novel antiangiogenic effects of the bisphosphonate compound zoledronic acid. *J Pharmacol Exp Ther* 2002;**302**:1055–61. <https://doi.org/10.1124/jpet.102.035295.opment>.
- 290 Bezzi M, Hasmim M, Bieler G, Dormond O, Rüegg C. Zoledronate sensitizes endothelial cells to tumor necrosis factor-induced programmed cell death: evidence for the suppression of sustained activation of focal adhesion kinase and protein kinase B/Akt. *J Biol Chem* 2003;**278**:43603–14. <https://doi.org/10.1074/jbc.M308114200>.
- 291 Bilezikian JP. Osteonecrosis of the jaw--do bisphosphonates pose a risk? *N Engl J Med* 2006;**355**:2278–81. <https://doi.org/10.1056/NEJMp068157>.
- 292 National Osteoporosis F. *America's Bone Health: The State of Osteoporosis and Low Bone Mass in Our Nation*. 2002.
- 293 American Dental Association. Dental management of patients receiving oral bisphosphonate therapy: Expert panel recommendations. *J Am Dent Assoc* 2006;**137**:1144–50. <https://doi.org/10.14219/jada.archive.2006.0355>.
- 294 Bauss F, Wagner M, Hothorn LH. Total administered dose of ibandronate determines its

- effects on bone mass and architecture in ovariectomized aged rats. *J Rheumatol* 2002;**29**:990–8.
- 295 Park SB, Park SH, Kang YK, Chung CK. The time-dependent effect of ibandronate on bone graft remodeling in an ovariectomized rat spinal arthrodesis model. *Spine J* 2014;**14**:1748–57. <https://doi.org/10.1016/j.spinee.2014.01.042>.
- 296 McMillan J, Kinney RC, Ranly DM, Fatehi-Sedeh S, Schwartz Z, Boyan BD. Osteoinductivity of demineralized bone matrix in immunocompromised mice and rats is decreased by ovariectomy and restored by estrogen replacement. *Bone* 2007;**40**:111–21. <https://doi.org/10.1016/j.bone.2006.07.022>.
- 297 Fu S wen, Zeng G feng, Zong S hui, Zhang Z yong, Zou B, Fang Y, *et al*. Systematic review and meta-analysis of the bone protective effect of phytoestrogens on osteoporosis in ovariectomized rats. *Nutr Res* 2014:467–77. <https://doi.org/10.1016/j.nutres.2014.05.003>.
- 298 Cheung WH, Miclau T, Chow SKH, Yang FF, Alt V. Fracture healing in osteoporotic bone. *Injury* 2016;**47**:S21–6. [https://doi.org/10.1016/S0020-1383\(16\)47004-X](https://doi.org/10.1016/S0020-1383(16)47004-X).
- 299 Giro G. Impact of osteoporosis in dental implants: A systematic review. *World J Orthop* 2015;**6**:311. <https://doi.org/10.5312/wjo.v6.i2.311>.
- 300 Shiota T, Tashiro M, Ohno K, Yamaguchi A. Effect of intermittent parathyroid hormone (1-34) treatment on the bone response after placement of titanium implants into the tibia of ovariectomized rats. *J Oral Maxillofac Surg* 2003;**61**:471–80. <https://doi.org/10.1053/joms.2003.50093>.
- 301 Tokugawa Y, Shiota T, Ohno K, Yamaguchi A. Effects of bisphosphonate on bone reaction after placement of titanium implants in tibiae of ovariectomized rats. *Int J Oral Maxillofac Implants* 2003;**18**:66–74.
- 302 Mendes Duarte P, Neto JBC, Gonçalves PF, Sallum EA, Nociti FH. Estrogen deficiency

- affects bone healing around titanium implants: A histometric study in rats. *Implant Dent* 2003;**12**:340–6. <https://doi.org/10.1097/01.ID.0000099750.26582.4B>.
- 303 Dikicier E, Karaçaylı Ü, Dikicier S, Günaydin Y. Effect of systemic administered zoledronic acid on osseointegration of a titanium implant in ovariectomized rats. *J Cranio-Maxillofacial Surg* 2014;**42**:1106–11. <https://doi.org/10.1016/j.jcms.2014.01.039>.
- 304 Nakamura Y, Hayashi K, Abu-Ali S, Naito M, Fotovati A. Effect of preoperative combined treatment with alendronate and calcitriol on fixation of hydroxyapatite-coated implants in ovariectomized rats. *J Bone Jt Surg - Ser A* 2008;**90**:824–32. <https://doi.org/10.2106/JBJS.G.00635>.
- 305 Duarte PM, de Vasconcelos Gurgel BC, Sallum AW, Filho GRN, Sallum EA, Nociti FH. Alendronate therapy may be effective in the prevention of bone loss around titanium implants inserted in estrogen-deficient rats. *J Periodontol* 2005;**76**:107–14. <https://doi.org/10.1902/jop.2005.76.1.107>.
- 306 Kurth AHA, Eberhardt C, Müller S, Steinacker M, Schwarz M, Bauss F. The bisphosphonate ibandronate improves implant integration in osteopenic ovariectomized rats. *Bone* 2005;**37**:204–10. <https://doi.org/10.1016/j.bone.2004.12.017>.
- 307 Chen BL, Xie DH, Zheng ZM, Lu W, Ning CY, Li YQ, *et al.* Comparison of the effects of alendronate sodium and calcitonin on bone-prosthesis osseointegration in osteoporotic rats. *Osteoporos Int* 2011;**22**:265–70. <https://doi.org/10.1007/s00198-010-1186-5>.
- 308 Narai S, Nagahata S. Effects of alendronate on the removal torque of implants in rats with induced osteoporosis. *Int J Oral Maxillofac Implants* 2003;**18**:218–23.
- 309 Cardemil C, Omar OM, Norlindh B, Wexell CL, Thomsen P. The effects of a systemic single dose of zoledronic acid on post-implantation bone remodelling and inflammation in an ovariectomised rat model. *Biomaterials* 2013;**34**:1546–61. <https://doi.org/10.1016/j.biomaterials.2012.11.003>.

- 310 Chacon GE, Stine EA, Larsen PE, Beck FM, McGlumphy EA. Effect of Alendronate on Endosseous Implant Integration: An In Vivo Study in Rabbits. *J Oral Maxillofac Surg* 2006;**64**:1005–9. <https://doi.org/10.1016/j.joms.2006.01.007>.
- 311 Guimarães MB, Bueno RS, Blaya MBG, Shinkai RSA, Marques LMH. Influence of the local application of sodium alendronate gel on osseointegration of titanium implants. *Int J Oral Maxillofac Surg* 2015;**44**:1423–9. <https://doi.org/10.1016/j.ijom.2015.05.013>.
- 312 Baron R, Tross R, Vignery A. Evidence of sequential remodeling in rat trabecular bone: Morphology, dynamic histomorphometry, and changes during skeletal maturation. *Anat Rec* 1984;**208**:137–45. <https://doi.org/10.1002/ar.1092080114>.
- 313 Erben RG. Trabecular and endocortical bone surfaces in the rat: Modeling or remodeling? *Anat Rec* 1996;**246**:39–46. [https://doi.org/10.1002/\(SICI\)1097-0185\(199609\)246:1<39::AID-AR5>3.0.CO;2-A](https://doi.org/10.1002/(SICI)1097-0185(199609)246:1<39::AID-AR5>3.0.CO;2-A).
- 314 Turner RT, Wakley GK, Hannon KS, Bell NH. Tamoxifen prevents the skeletal effects of ovarian hormone deficiency in rats. *J Bone Miner Res* 1987;**2**:449–56. <https://doi.org/10.1002/jbmr.5650020513>.
- 315 Turner RT, Evans GL, Wakley GK. Reduced chondroclast differentiation results in increased cancellous bone volume in estrogen-treated growing rats. *Endocrinology* 1994;**134**:461–6. <https://doi.org/10.1210/endo.134.1.7506213>.
- 316 Wronski TJ, Lowry PL, Walsh CC, Ignaszewski LA. Skeletal alterations in ovariectomized rats. *Calcif Tissue Int* 1985;**37**:324–8. <https://doi.org/10.1007/BF02554882>.
- 317 Turner RT, Colvard DS, Spelsberg TC. Estrogen inhibition of periosteal bone formation in rat long bones: Down-regulation of gene expression for bone matrix proteins. *Endocrinology* 1990;**127**:1346–651. <https://doi.org/10.1210/endo-127-3-1346>.
- 318 Wronski TJ, Dann LM, Horner SL. Time course of vertebral osteopenia in ovariectomized

- rats. *Bone* 1989;**10**:295–301. [https://doi.org/10.1016/8756-3282\(89\)90067-7](https://doi.org/10.1016/8756-3282(89)90067-7).
- 319 Wronski TJ, Cintrón M, Dann LM. Temporal relationship between bone loss and increased bone turnover in ovariectomized rats. *Calcif Tissue Int* 1988;**43**:179–83. <https://doi.org/10.1007/BF02571317>.
- 320 Turner RT, Maran A, Lotinun S, Hefferan T, Evans GL, Zhang M, *et al.* Animal Models for Osteoporosis. *Rev Endocr Metab Disord* 2001;**2**:117–27. <https://doi.org/10.1023/A:1010067326811>.
- 321 Viera-Negrón YE, Ruan W, Winger JN, Hou X, Sharawy MM, Borke JL. Effect of ovariectomy and alendronate on implant osseointegration in rat maxillary bone. *J Oral Implantol* 2008;**34**:76–82. [https://doi.org/10.1563/1548-1336\(2008\)34\[76:EOOAAO\]2.0.CO;2](https://doi.org/10.1563/1548-1336(2008)34[76:EOOAAO]2.0.CO;2).
- 322 Miller SC, Shupe JG, Redd EH, Miller MA, Omura TH. Changes in bone mineral and bone formation rates during pregnancy and lactation in rats. *Bone* 1986;**7**:283–7. [https://doi.org/10.1016/8756-3282\(86\)90209-7](https://doi.org/10.1016/8756-3282(86)90209-7).
- 323 Francisco JI, Yu Y, Oliver RA, Walsh WR. Relationship between age, skeletal site, and time post-ovariectomy on bone mineral and trabecular microarchitecture in rats. *J Orthop Res* 2011;**29**:189–96. <https://doi.org/10.1002/jor.21217>.
- 324 Wronski TJ, Dann LM, Scott KS, Cintrón M. Long-term effects of ovariectomy and aging on the rat skeleton. *Calcif Tissue Int* 1989;**45**:360–6. <https://doi.org/10.1007/BF02556007>.
- 325 Bauss F, Lalla S, Ende R, Hothorn LA. Effects of treatment with ibandronate on bone mass, architecture, biomechanical properties, and bone concentration of ibandronate in ovariectomized aged rats. *J Rheumatol* 2002;**29**:2200–8. <https://doi.org/0315162X-29-2200> [pii].
- 326 Lotz EMEM, Berger MBMB, Schwartz Z, Boyan BDBD. Regulation of osteoclasts by

- osteoblast lineage cells depends on titanium implant surface properties. *Acta Biomater* 2018;**68**:296–307. <https://doi.org/10.1016/j.actbio.2017.12.039>.
- 327 Lossdorfer S, Schwartz Z, Wang L, Lohmann CH, Turner JD, Wieland M, *et al*. Microrough implant surface topographies increase osteogenesis by reducing osteoclast formation and activity. *J Biomed Mater Res A* 2004;**70**:361–9. <https://doi.org/10.1002/jbm.a.30025>.
- 328 Makhluף HA, Mueller SM, Mizuno S, Glowacki J. Age-related decline in osteoprotegerin expression by human bone marrow cells cultured in three-dimensional collagen sponges. *Biochem Biophys Res Commun* 2000;**268**:669–72. <https://doi.org/10.1006/bbrc.2000.2182>.
- 329 Nations U. *World population Ageing*. vol. United Nat. 2015.
- 330 Felton DA. Edentulism and comorbid factors. *J Prosthodont* 2009;**18**:88–96. <https://doi.org/10.1111/j.1532-849X.2009.00437.x>.
- 331 Xiao W, Li S, Pacios S, Wang Y, Graves DT. Bone Remodeling under Pathological Conditions. *Front Oral Biol* 2015;**18**:17–27. <https://doi.org/10.1159/000351896>.
- 332 Chandran S, John A. Osseointegration of osteoporotic bone implants: Role of stem cells, Silica and Strontium - A concise review. *J Clin Orthop Trauma* 2018. <https://doi.org/10.1016/j.jcot.2018.08.003>.
- 333 Manolagas SC, Parfitt AM. What old means to bone. *Trends Endocrinol Metab* 2010:369–74. <https://doi.org/10.1016/j.tem.2010.01.010>.
- 334 Ahdjoudj S, Fromigué O, Marie PJ. Plasticity and regulation of human bone marrow stromal osteoprogenitor cells: Potential implication in the treatment of age-related bone loss. *Histol Histopathol* 2004:151–8. <https://doi.org/10.14670/HH-19.151>.
- 335 Kassem M, Marie PJ. Senescence-associated intrinsic mechanisms of osteoblast dysfunctions. *Aging Cell* 2011:191–7. <https://doi.org/10.1111/j.1474-9726.2011.00669.x>.

- 336 Marie PJ, Kassem M. Extrinsic mechanisms involved in age-related defective bone formation. *J Clin Endocrinol Metab* 2011;600–9. <https://doi.org/10.1210/jc.2010-2113>.
- 337 Moerman EJ, Teng K, Lipschitz DA, Lecka-Czernik B. Aging activates adipogenic and suppresses osteogenic programs in mesenchymal marrow stroma/stem cells: The role of PPAR- γ 2 transcription factor and TGF- β /BMP signaling pathways. *Aging Cell* 2004;3:379–89. <https://doi.org/10.1111/j.1474-9728.2004.00127.x>.
- 338 Li CJ, Cheng P, Liang MK, Chen YS, Lu Q, Wang JY, *et al.* MicroRNA-188 regulates age-related switch between osteoblast and adipocyte differentiation. *J Clin Invest* 2015;125:1509–22. <https://doi.org/10.1172/JCI77716>.
- 339 Liao L, Yang X, Su X, Hu C, Zhu X, Yang N, *et al.* Redundant miR-3077-5p and miR-705 mediate the shift of mesenchymal stem cell lineage commitment to adipocyte in osteoporosis bone marrow. *Cell Death Dis* 2013;4:. <https://doi.org/10.1038/cddis.2013.130>.
- 340 Yeung DKW, Griffith JF, Antonio GE, Lee FKH, Woo J, Leung PC. Osteoporosis is associated with increased marrow fat content and decreased marrow fat unsaturation: A proton MR spectroscopy study. *J Magn Reson Imaging* 2005;22:279–85. <https://doi.org/10.1002/jmri.20367>.
- 341 Shen W, Chen J, Gantz M, Punyanitya M, Heymsfield SB, Gallagher D, *et al.* MRI-measured pelvic bone marrow adipose tissue is inversely related to DXA-measured bone mineral in younger and older adults. *Eur J Clin Nutr* 2012;66:983–8. <https://doi.org/10.1038/ejcn.2012.35>.
- 342 Rodriguez JP, Montecinos L, Ros S, Reyes P, Martinez J. Mesenchymal stem cells from osteoporotic patients produce a type I collagen-deficient extracellular matrix favoring adipogenic differentiation. *J Cell Biochem* 2000;79:557–65. [https://doi.org/10.1002/1097-4644\(20001215\)79:4<557::AID-JCB40>3.0.CO;2-H](https://doi.org/10.1002/1097-4644(20001215)79:4<557::AID-JCB40>3.0.CO;2-H).

- 343 D'Ippolito G, Schiller PC, Ricordi C, Roos BA, Howard GA. Age-related osteogenic potential of mesenchymal stromal stem cells from human vertebral bone marrow. *J Bone Miner Res* 1999;**14**:1115–22. <https://doi.org/10.1359/jbmr.1999.14.7.1115>.
- 344 Acerbo AS, Kwaczala AT, Yang L, Judex S, Miller LM. Alterations in Collagen and Mineral Nanostructure Observed in Osteoporosis and Pharmaceutical Treatments Using Simultaneous Small- and Wide-Angle X-ray Scattering. *Calcif Tissue Int* 2014;**95**:446–56. <https://doi.org/10.1007/s00223-014-9913-0>.
- 345 Paschalis EP, Shane E, Lyritis G, Skarantavos G, Mendelsohn R, Boskey AL. Bone fragility and collagen cross-links. *J Bone Miner Res* 2004;**19**:2000–4. <https://doi.org/10.1359/JBMR.040820>.
- 346 Viguet-Carrin S, Roux JP, Arlot ME, Merabet Z, Leeming DJ, Byrjalsen I, *et al*. Contribution of the advanced glycation end product pentosidine and of maturation of type I collagen to compressive biomechanical properties of human lumbar vertebrae. *Bone* 2006;**39**:1073–9. <https://doi.org/10.1016/j.bone.2006.05.013>.
- 347 He YQ, Yang H, Shen Y, Zhang JH, Zhang ZG, Liu LL, *et al*. Monotropein attenuates ovariectomy and LPS-induced bone loss in mice and decreases inflammatory impairment on osteoblast through blocking activation of NF- κ B pathway. *Chem Biol Interact* 2018;**291**:128–36. <https://doi.org/10.1016/j.cbi.2018.06.015>.
- 348 Ham JR, Choi RY, Yee ST, Hwang YH, Kim MJ, Lee MK. Methoxsalen supplementation attenuates bone loss and inflammatory response in ovariectomized mice. *Chem Biol Interact* 2017;**278**:135–40. <https://doi.org/10.1016/j.cbi.2017.10.014>.
- 349 Boyan BDB, Lotz EMEM, Schwartz Z. Roughness and Hydrophilicity as Osteogenic Biomimetic Surface Properties. *Tissue Eng Part A* 2017;**23**:ten.TEA.2017.0048. <https://doi.org/10.1089/ten.TEA.2017.0048>.
- 350 Rupp F, Liang L, Geis-Gerstorfer J, Scheideler L, Hüttig F. Surface characteristics of

dental implants: A review. *Dent Mater* 2018;40–57.

<https://doi.org/10.1016/j.dental.2017.09.007>.

351 Schneider E, Goldhahn J, Burckhardt P. The Challenge: Fracture Treatment in Osteoporotic Bone.

352 Merheb J, Temmerman A, Rasmusson L, Kübler A, Thor A, Quirynen M. Influence of Skeletal and Local Bone Density on Dental Implant Stability in Patients with Osteoporosis. *Clin Implant Dent Relat Res* 2016;**18**:253–60.

<https://doi.org/10.1111/cid.12290>.